Synthesis and properties of branched poly(ethylene oxybenzoate)s

Anderson, Ian Christopher

Synthesis and properties of branched poly(ethylene oxybenzoate)s

Ian Christopher Anderson

A thesis submitted for the degree of Doctor of Philosophy at the University of Durham

March 2000

Abstract

Synthesis and properties of branched poly(ethylene oxybenzoate)s

Ian C. Anderson, Ph. D. Thesis, March 2000

The synthesis and properties meta and para poly(ethylene oxybenzoate)s, two semi-crystalline polymers, are reported. It is found that by copolymerising equimolar quantities of meta and para monomers amorphous polymers are produced which are significantly more soluble than their respective homopolymers. The effects of introducing an AB_2 branching agent (**A**) into *p*-PEOB are also considered. It is found that the relationship between Tg and molecular weight does not vary significantly with the extent of branching. Using the data obtained from DSC experiments, a linear relationship between the melting temperature and the branching composition of *p*-PEOB is reported up to a critical value of **12.5mole%** of **A**, above which materials are amorphous and chloroform soluble. A general technique for measuring number average molecular weight of branched materials, using ^{1}H NMR end group counting, is described. This is used successfully in the analysis of *p*-PEOB copolymers with less than 15mole% branching. Molecular weights of the amorphous materials, i.e. with extents of branching in excess of 12.5mole%, are measured using conventional GPC with respect to linear polystyrene equivalents. Relationships between the extent of branching, log Mw and log [η] in chloroform, appear to be linear for amorphous copolymers with branching compositions of between 20mole% and 100mole%. A detailed analysis of carbonyl signals in ^{13}C NMR spectra of these materials is reported, which provides evidence that the copolymerisations are statistical and not selective.

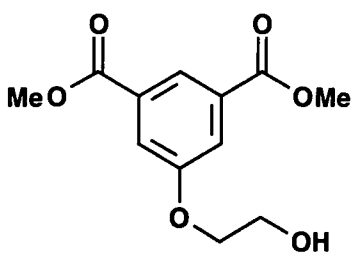

A

Acknowledgements

I would like to thank my supervisor Professor W. J. Feast for his wisdom and assistance over the last three years and gratefully acknowledge the input of my industrial supervisor Dr. W. A. MacDonald. I am also extremely grateful to the support staff at the University of Durham: Dr. Alan M. Kenwright, Julia Say, Catherine F. Heffernan, Ian H. McKeag for their contributions to the NMR work included in this thesis; Ray Hart and Gordon Haswell for their glass blowing talents; Dave Hunter for his invaluable assistance in the high pressure laboratory and finally but by no means least Gordon Forrest, Andrew Bosanko and Douglas Carswell for running the GPC and DSC services.

Without the reassurance of my friends and family I am sure that I would never have made it this far. So, for their encouragement and support I offer my heartfelt thanks. I am especially grateful to my parents for whom I owe the largest debt of thanks. As a small token of my gratitude I would like to dedicate this thesis in their honour.

Memorandum

The work reported in this thesis was carried out at the Interdisciplinary Research Centre in Polymer Science and Technology at the University of Durham between September 1996 and September 1999. The work has not been submitted for any other degree and is the original work of the author except where acknowledged by an appropriate reference.

Financial Support

I gratefully acknowledge the funding provided by the EPSRC, ICI and Du Pont.

Table of Contents

Chapter 1

Introduction and Background

1.1 Introduction

This thesis describes the author's work on the synthesis and characterisation of linear and branched polyesters related to poly(ethylene terephthalate) (PET), a commercially important material. The systems investigated are meta poly(ethylene oxybenzoate) (***m*-PEOB**), para poly(ethylene oxybenzoate) (***p*-PEOB**) and copolymers of meta and para poly(ethylene oxybenzoate) in equimolar ratios. The effects of incorporating ethylene oxyisophthalate branching units **A** into *p*-PEOB are also investigated in detail. The thesis is divided into seven chapters. In this chapter the theoretical background to the synthesis of branched polymers is discussed together with some illustrative examples. In Chapter 2, the synthesis of monomers and polymers is described. The linear semi-crystalline homopolyesters and the amorphous copolyesters produced in this study are described in Chapter 3. In Chapter 4, the analysis of the semi-crystalline branched copolymers is described, while Chapter 5 is concerned with the analysis of the amorphous branched copolymers. The determination of molecular weight in these systems, using ^{1}H NMR end group, is described in Chapter 6 with an overall summary of the outcomes of this work and suggestions for further work in Chapter 7.

1.2 Growth Mechanisms

The mechanisms by which polymer chains grow maybe divided into two general types; step and chain growth processes. Step growth processes are characterised by the slow growth of molecular weight, the requirement for high conversion for high molecular weight and the use of one reaction type only. By contrast chain growth polymerisations can give high molecular weight products in the early stages of reaction; relying on several types of reaction, usually including initiation (formation of the active species), propagation (growth of the molecular chain) and termination. The polymerisations discussed in this thesis all proceed *via* step growth mechanisms which therefore merit further discussion.

Many monomers may be polymerised using step growth routes, however, not all can be taken to high molecular weight. This is due to hindrances that prevent the growth of the polymer chain. Indeed, any side reaction or contamination that results in the formation, or presence, of monofunctional units will limit the extent of reaction. If high molecular weights are to be obtained it is

essential that an exact stoichiometric balance between the concentration of reacting functionalities is ensured.

1.3 Bifunctional Polycondensation Reactions

Flory[1] was the first to apply rigorous statistical treatments to the polycondensation reactions of bifunctional monomers. He analysed the general schemes known as AB and AA/BB polymerisations, in which A and B functional groups can only react with each other.

$$x\ \text{A-B} \longrightarrow \text{A-B(A-B)}_{(x-2)}\ \text{A-B}$$

$$x/2\ \text{A-A} + x/2\ \text{B-B} \longrightarrow \text{A-A(B-BA-A)}_{(x-2)/2}\text{B-B}$$

where x is the total number of bifunctional molecules incorporated into the polymer.

When x, the number of incorporated monomer units is an even integer, the resultant structures are as shown above. However, when x is odd, it is possible for AA/BB polymers to adopt two structural arrangements as shown.

$$(x+1)/2\ \text{A-A} + (x-1)/2\ \text{B-B} \longrightarrow \text{A-A(B-BA-A)}_{(x-3)/2}\text{B-BA-A}$$

$$(x-1)/2\ \text{A-A} + (x+1)/2\ \text{B-B} \longrightarrow \text{B-BA-A(B-BA-A)}_{(x-3)/2}\text{B-B}$$

Flory's theoretical treatment of bifunctional condensation polymers, relied upon several fundamental assumptions. The first assumed that functional group reactivity was independent of polymer chain length; the second assumed that polymer growth proceeded in the absence of side reactions and cyclisation. In practice however, side reactions do occur and cyclisation is a feature of all polycondensations. In spite of its limitations, Flory's treatment offered unique insight into the size distribution of linear step-growth polymers. The main features of the argument are presented below.

Assuming a fixed 1:1 stoichiometry of reactive functional groups the expression for the extent of reaction or conversion, $\boldsymbol{p}$, in an AB type polymerisation may be defined as shown in Equation 1.1;

$$p = (N_0\text{-}N)/N_0 \qquad \text{Eq. 1.1}$$

where N_0 is the original number of monomer molecules and N is the number of molecules at a specified time.

As the concentrations of both A and B groups are equivalent, p is also the probability that an A or B functionality has reacted. The number average degree of polymerisation for this system, χ_n, may be defined as the ratio of monomer molecules measured at the start of the reaction to the total number of molecules at any given time t, see Equation 1.2.

$$\chi_n = N_0/N = 1/(1-p) \qquad \text{Eq. 1.2}$$

A more general form of the equation was described by Carothers[2] for multifunctional systems and is shown as Equation 1.3.

$$\chi_n = 2/(2-pf) \qquad \text{Eq. 1.3}$$

Where f is the average functionality of all the monomers in the polymerising system1; p is the fraction of functional groups consumed.

This equation reveals that high extents of reaction (p>0.98) are essential if high molecular weight polymers are to be obtained; the point is illustrated graphically in Figure 1.1. Although the Carothers equation predicts number average degrees of polymerisation from extents of reaction, p, it tells us nothing about the weight distribution of the polymer. To obtain this information we must consider Flory's statistical treatment of AB step growth polymers.

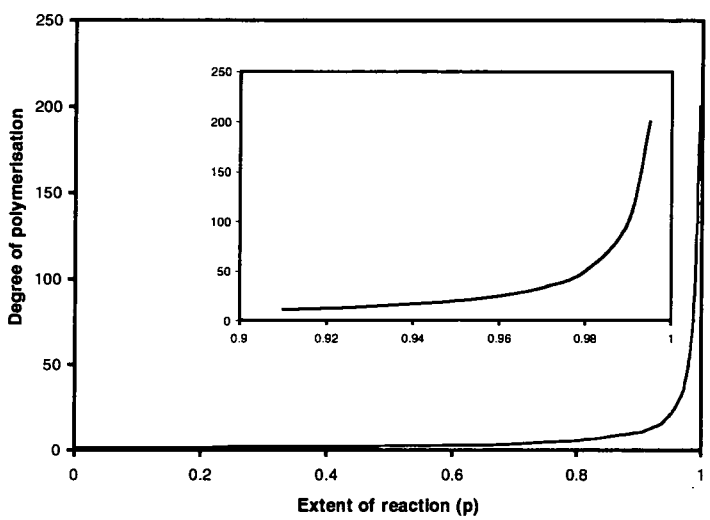

Fig. 1.1 Theoretical extent of reaction *vs.* degree of polymerisation for an AB bifunctional step growth polymer.

Consider an AB polymer consisting of (x-2) repeat units. The probability (N'_x) of finding an A group attached to this x-mer is equal to the probability of finding x-1 reacted 'B' groups and one unreacted end group. As defined previously, the probability of finding a reacted 'B' group is the extent of reaction, p; see Equation 1.2. Thus, the probability that (x-1) 'B' groups have reacted must be the product of (x-1) extents of reaction, $p^{(x-1)}$. When multiplied by (1-p), the probability of finding an unreacted 'B' group, we obtain the mole fraction of x-mer in the polymer; Equation 1.4.

$$N'_x = p^{(x-1)}(1-p) \qquad \text{Eq. 1.4}$$

When N is the total number of molecules in the system, the number of x-mers (N_x) may be given as;

$$N_x = N.N'_x \qquad \text{Eq. 1.5}$$

If N is substituted for $N_0(1-p)$ and N'_x is substituted by the expression described in Equation 1.4 we obtain Equation 1.6.

$$N_x = N_0\, p^{(x-1)}\,(1-p)^2 \qquad \text{Eq. 1.6}$$

Consequently, if the difference between the weight of an end group and the repeat unit of the polymer is ignored, the weight fraction of x-mer may be written;

$$W_x = x\, N_x / N_0 \qquad \text{Eq. 1.7}$$

Substituting with equation 1.6 leads to the expression;

$$W_x = x\, p^{(x-1)}\,(1-p)^2 \qquad \text{Eq. 1.8}$$

Equations 1.6 and 1.8 can be used to plot mole and weight fractions of polymer molecules against their degrees of polymerisation; Figures 1.2 and 1.3.

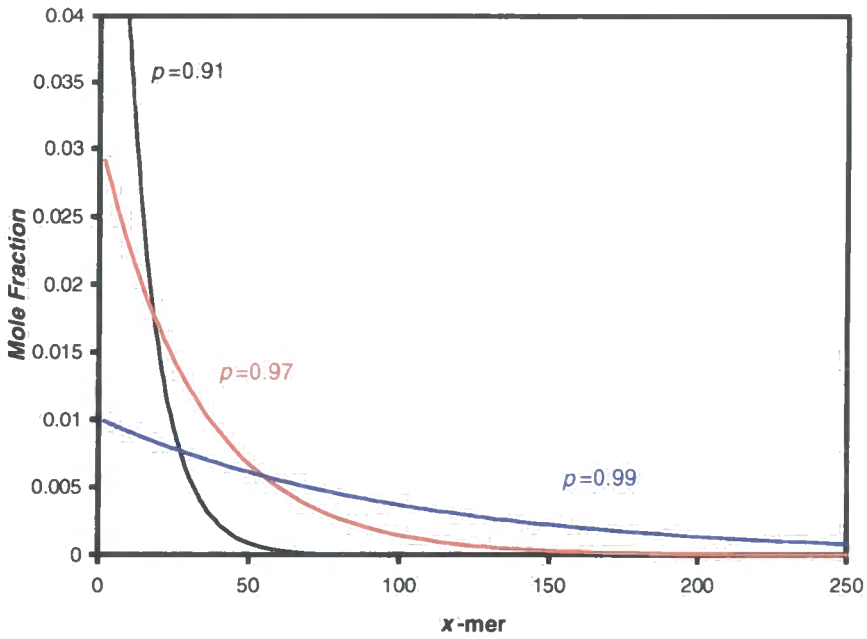

Fig. 1.2 Mole fraction distribution of AB step growth polymers at high extents of reaction.

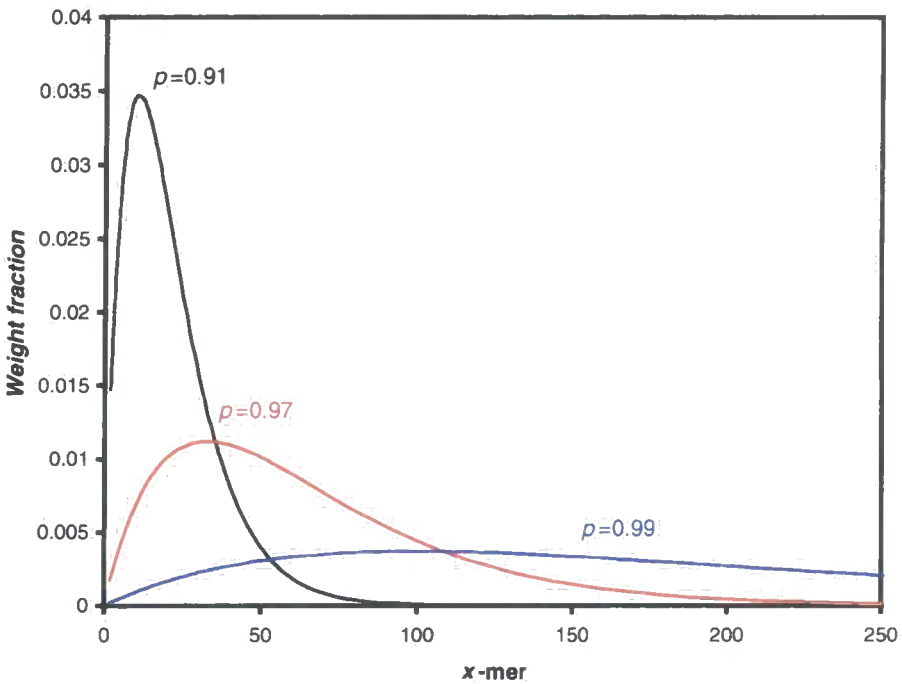

Fig. 1.3 Weight fraction distribution of AB step growth polymers at high extents of reaction.

A polymer sample almost invariably consists of a distribution of structures and masses. Three molecular weight averages; number, weight and z-average are defined by the following equations: [3]

$$M_n = \Sigma M_x N_x / \Sigma N_x \qquad \text{Eq. 1.9}$$

$$M_w = \Sigma M_x^{\,2} N_x / \Sigma M_x N_x \qquad \text{Eq. 1.10}$$

$$M_z = \Sigma M_x^{\,3} N_x / \Sigma M_x^{\,2} N_x \qquad \text{Eq. 1.11}$$

Different experimental techniques give the different molecular weight averages; measurements of colligative properties give Mn, light scattering gives Mw; and sedimentation gives Mw and Mz. It is possible with modern GPC measurements to obtain all three averages with one experiment.

Flory[1] used a series of substitutions and summations to evaluate these molecular weight averages in terms of the extent of reaction, p, for an AB polymerisation adopting a most probable distribution.

$$M_n = M_0/(1-p) \qquad \text{Eq. 1.12}$$

$$M_w = M_0\,(1+p)/(1-p) \qquad \text{Eq. 1.13}$$

$$M_z = M_0\,(1+4p+p^2)/(1-p^2) \qquad \text{Eq. 1.14}$$

where M_0 is the molecular weight of one segment.

The polydispersity of any given polymeric system is defined as the ratio Mw : Mn. Using Equations 1.12 and 1.13, Flory evaluated the polydispersity of an AB step growth polymer to be $(1+p)$. Thus, it followed straightforwardly that, at one hundred percent conversion the polydispersity reaches a theoretical maximum value of two.

1.4 Polycondensations of multifunctional $AB_{(f-1)}$ molecules

In 1952 Flory[4] published a statistical treatment of branched polymers, constructed from $AB_{(f-1)}$ units. Such systems were of interest because, in the absence of side reactions, they would produce branched topologies which were free from cross-links. As in the treatment of AB systems, Flory assumed that molecules do not cyclise. Furthermore, the reactivity of B groups was assumed to be independent of the extent of reaction and their position within the molecule.

The extent of reaction, expressed as a fraction of A groups or foci consumed, p_a, has limits of zero and one. Although identical numbers of A and B groups must be consumed during a polymerisation, the fraction of reacted B groups will depend on the monomer functionality, **f**, as defined in Equation 1.15.

$$p_b = p_a/(f\text{-}1) = \alpha \qquad \text{Eq. 1.15}$$

Several other parameters defined by Flory in his original paper are also presented here. The number average degree of polymerisation, χ_n, for a polymer consisting of $AB_{(f-1)}$ units is similar to the basic definition expressed in Equation 1.2 for an AB polymer.

$$\chi_n = 1/(1-p_a) \text{ or } 1/[1-\alpha(f-1)] \qquad \text{Eq. 1.16}$$

The probability, α, that a functional B group has reacted, is equivalent to p_b, the fraction of B groups consumed. From equation 1.15 it is clear that α approaches a maximum value of 1/(f-1) when p_a=1. Thus, for an AB_2 polymer at 100% conversion, only half of the B groups will have been consumed.

It can be shown that the probability of finding an unreacted A at the focus of a molecule consisting of (x-1) reacted B groups and fx-2x+1 unreacted B groups is P_x, defined in Equation 1.17.

$$P_x = \alpha^{(x-1)} (1-\alpha)^{(fx-2x+1)} \qquad \text{Eq. 1.17}$$

Assuming that every B group is distinguishable from every other and molecules are not cyclised, there are w_x possible ways to arrange monomer residues in the polymer, as described by Equation 1.18. By multiplying this value by the probability, P_x, defined in Equation 1.17, we obtain the mole fraction of x-mer present (N_x).

$$w_x = (fx\text{-}x)!/(fx\text{-}2x+1)!\,x! \qquad \text{Eq. 1.18}$$

$$N_x = w_x\, \alpha^{(x-1)} (1-\alpha)^{(fx-2x+1)} \qquad \text{Eq. 1.19}$$

Flory described the mole fraction of x-mer present using an alternative expression, as shown in Equation 1.20.

$$N_x = [(1-\alpha)/\alpha]\, w_x\, \beta^x \qquad \text{Eq. 1.20}$$

$$\beta = \alpha\,(1-\alpha)^{f-2} \qquad \text{Eq. 1.21}$$

By evaluating complex summations, Flory arrived at the weight fraction, W_x, and weight average degree of polymerisation, χ_w, shown in Equations 1.22 and 1.23, respectively.

$$W_x = [(1-\alpha)/\alpha]\, [1-\alpha^2(f-1)]\, x\, w_x\, \beta^x \qquad \text{Eq. 1.22}$$

$$\chi_w = [1-\alpha^2(f-1)]/[1-\alpha(f-1)]^2 \qquad \text{Eq. 1.23}$$

A comparison between Flory's statistical analyses reveals several distinct differences between the predictions made for AB polymers and those made for hyperbranched $AB_{(f-1)}$ systems. Polydispersity, χ_w/χ_n, is determined by dividing Equation 1.23 by 1.16 as given by $[1-\alpha^2(f-1)]/[1-\alpha(f-1)]$. For AB_2 polymerisations where f=3 and α reaches a maximum 0.5, the analysis predicts that polydispersity tends to infinity at high conversion, see Figure 1.4. It is also evident that in the case of $AB_{(f-1)}$ polymers, for any polymer sample, monomeric species dominate in terms of both number and weight; see Figures 1.5 and 1.6. The general relationship between mole fraction and DP is similar to that for linear polymers; Figure 1.5. However, linear AB polymers are characterised by a maximum in the plot of weight fraction *vs.* molecular size and are theoretically limited to polydispersities of two, contrasting with the situation for AB_2 polymers as shown in Figure 1.6.

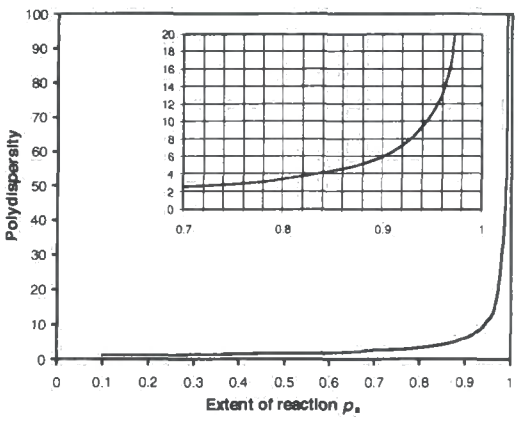

Fig. 1.4 Plot showing extent of reaction against theoretical polydispersity of an AB_2 polymer.

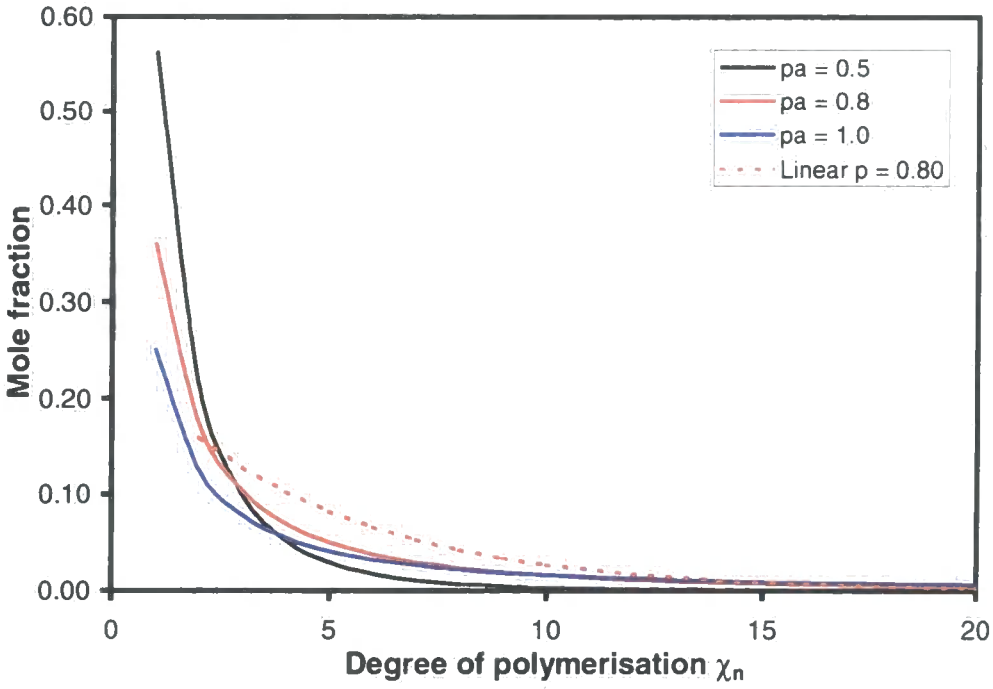

Fig. 1.5 Theoretical mole fraction distribution of a statistical AB_2 step growth polymer compared to an equivalent AB polymer.

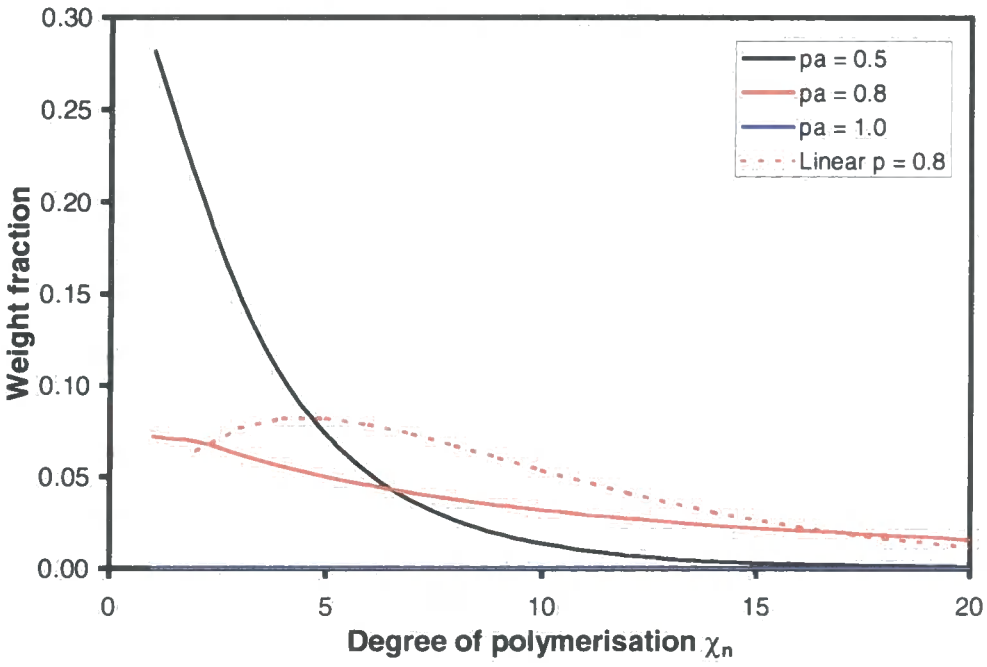

Fig. 1.6 Theoretical weight fraction distribution of a statistical AB_2 step growth polymer compared to an equivalent AB polymer. (Curve for $p_a = 1$ is the line y = 0)

1.5 Co-condensations of AB and $AB_{(f-1)}$ Functional Molecules

In the same publication as the analysis of $AB_{(f-1)}$ polymers, Flory[4] applied a statistical treatment to $AB/AB_{(f-1)}$ copolymers. Equations for the statistical distribution of molecules were expressed in terms of two quantities, n, the number of branching units and l, the number of linear units. However, as Flory considered the resultant formulae to be "too cumbersome to be of much practical use", we shall not consider them further. In an alternative approach, he disregards bifunctional units to significantly reduce the complexity of the problem. The structural distribution is then determined in terms of one parameter, n, the number of branching units.

The probability α, was defined as the probability that a B group, belonging to a branch unit, would lead *via* a series of zero or more AB residues to a second branching group, Equation 1.24.

$$\alpha = p_b \rho/[1-p_b(1-\rho)] \qquad \text{Eq. 1.24}$$

where ρ is the mole fraction of branching units.

A second branching factor, α', was used as the probability that a molecule would possess at least one branching unit; Equation 1.25.

$$\alpha' = \alpha/p_b \qquad \text{Eq. 1.25}$$

As the mole fraction of linear molecules, N_0, is the probability that a polymer chain will not contain any branching functionality it may be written as Equation 1.26.

$$N_0 = 1-\alpha' \qquad \text{Eq. 1.26}$$

The mole fraction of *n*-mer, N_n, was calculated by using the same method as for the pure $AB_{(f-1)}$ analogue. The result of this analysis is shown in Equation 1.27.

$$N_n = (\alpha'/\alpha)\,(1-\alpha)\,w_n\,\beta^n \qquad \text{Eq. 1.27}$$

The variable β is defined in Equation 1.21.

Flory predicted that, for a statistical copolymer, the average length of a linear chain segment would be independent of the number of incorporated branching units, *n*. Consequently, the average weight of a molecule should be proportional to the number of linear chains, or incorporated branching units, *n*. He evaluated that the copolymer weight fractions would be expressed by Equations 1.28 and 1.29; differentiating between linear structures (W_0) and those with *n* incorporated branching units (W_n).

$$W_0 = (1-\alpha') \; [1-\alpha(f-1)]/[1+(\alpha'-\alpha)(f-1)] \qquad \text{Eq. 1.28}$$

$$W_n = (\alpha'/\alpha)(1-\alpha)(fn-n+1) \; [1-\alpha(f-1)] \; w_n \, \beta^n \, / \, [1+(\alpha'-\alpha)(f-1)] \qquad \text{Eq. 1.29}$$

The resultant distributions are complex but are illustrated in Figures 1.7 to 1.10 for copolymers with 50mole% and 80mole% branching at four extents of reaction, $p_a = 0.25, 0.5, 0.8, 0.95$.

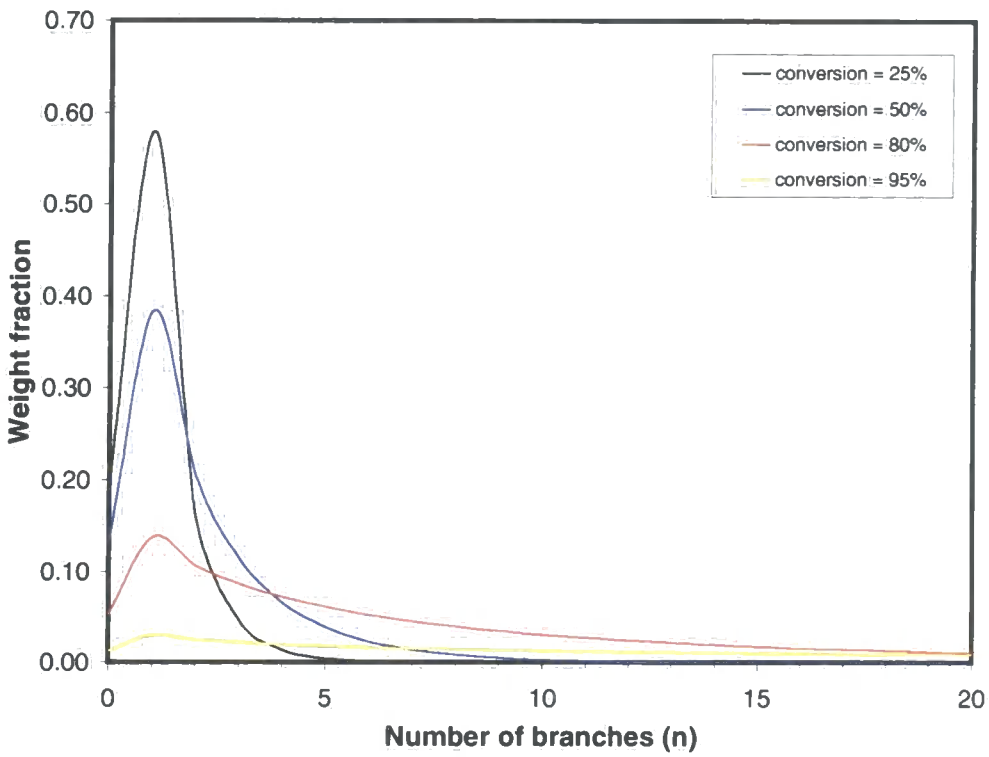

Fig. 1.7 Theoretical weight fraction distribution of an AB/AB$_2$ step growth copolymer (50:50) at several extents of reaction.

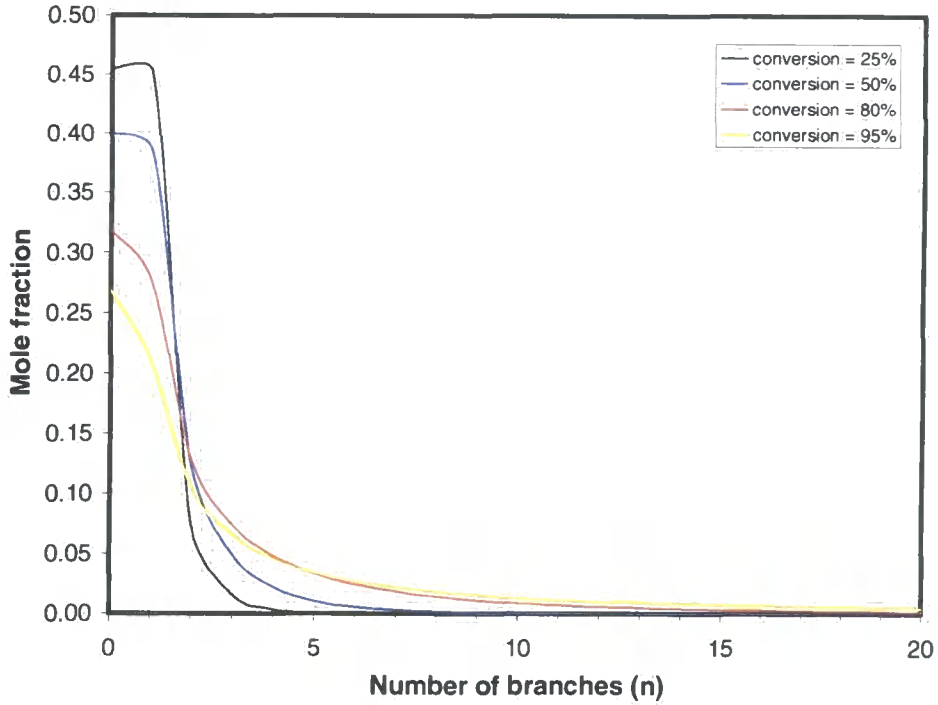

Fig. 1.8 Theoretical mole fraction distribution of an AB/AB$_2$ step growth copolymer (50:50) at several extents of reaction.

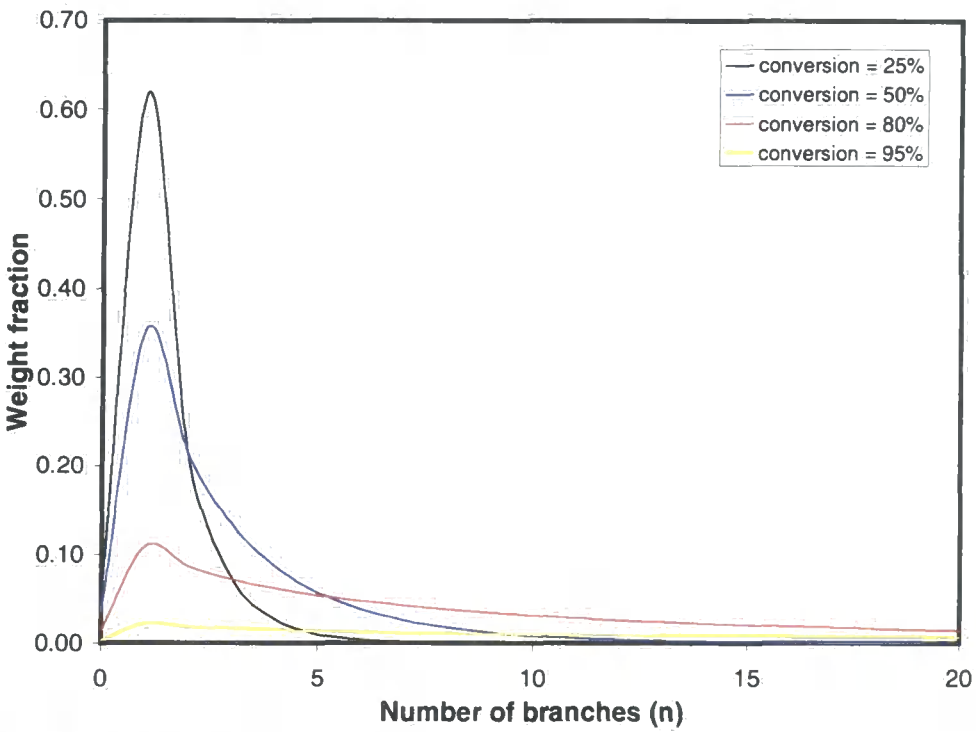

Fig. 1.9 Theoretical weight fraction distribution of an AB/AB$_2$ step growth copolymer (20:80) at several extents of reaction.

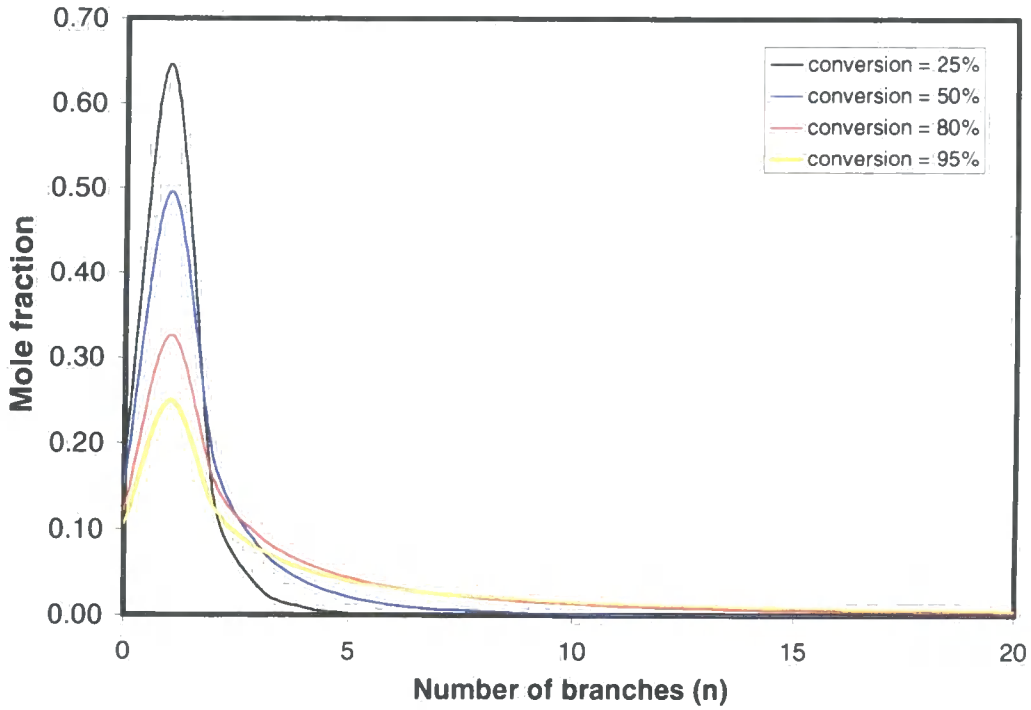

Fig. 1.10 Theoretical mole fraction distribution of an AB/AB_2 step growth copolymer (20:80) at several extents of reaction.

1.6 Linear, Hyperbranched and Dendritic Macromolecules

Traditionally, the efforts of polymer researchers have concentrated on the development of synthetic linear systems. In comparison to branched polymers, linear materials are easier to characterise and offer properties which are, on the whole, better suited to commercial applications. The interest in branched systems spans many decades, however, it is only in the last twenty years that significant advances have been made in this area.

In solution, linear polymers approximate to random coil structures with two chain ends; in the solid state the situation is complicated by crystallisation. However, the properties of these materials are dominated by functional groups in the polymer backbone and, at high molecular weights, by the effects of chain entanglements. The contribution from chain ends to the properties of these materials is negligible. By contrast, hyperbranched and dendritic systems are very different.

Originally described by Flory[4], in his theoretical treatment of $AB_{(f-1)}$ homopolymers, the 'hyperbranched' macromolecules synthesised to date have been almost exclusively AB_2 systems. These polymers consist of statistically distributed branching units which are subdivided into three general types; fully reacted

branching residues (green), partially reacted units (black) and end groups, (blue); as shown in Figure 1.11. In the absence of intramolecular cyclisation, hyperbranched molecules carry one focal A group indicated in red.

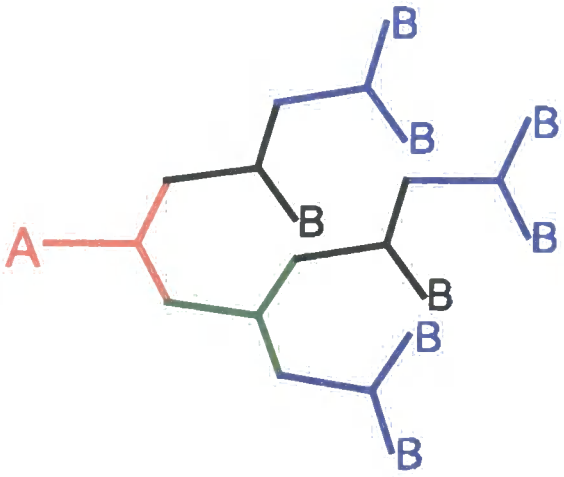

Fig. 1.11 Diagram showing the various types of structural units found in 'hyperbranched' systems.

Although hyperbranched and dendritic macromolecules have some structural similarities, there are significant differences between their reported properties and methods of synthesis. Dendrimers are assembled using iterative stepwise procedures to produce structures that are often claimed to be monodisperse. These novel architectures are characterised in terms of a generation number, which corresponds to the number of layers of fully reacted branching units; Figure 1.12. As each additional generation doubles the number of groups at the periphery, relatively few layers are required to build up large numbers of end groups. Dendrimers may be core terminated; this has the effect of further increasing the number of end groups and modifying the solution properties of the material.

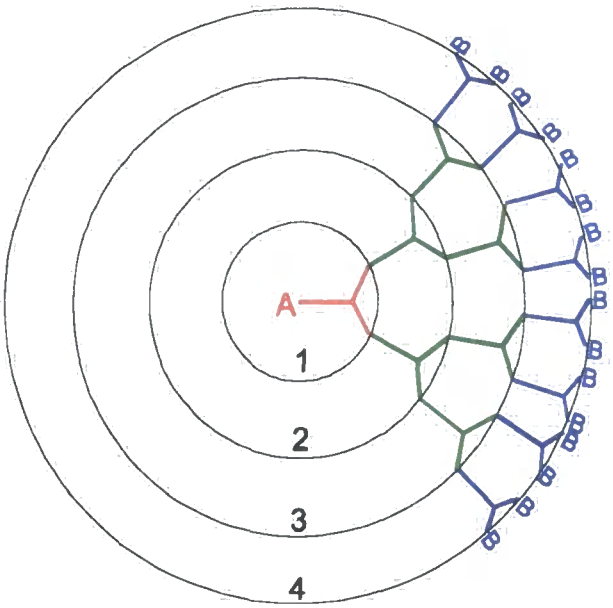

Fig. 1.12 Diagram showing a perfectly branched 4TH generation dendritic wedge.

In contrast, hyperbranched polymers are synthesised *via* 'one-pot' reactions. These structures are generated statistically and contain many 'branching defects'. Defects produce vast numbers of structural isomers, which lead to broad distributions in structure as well as molecular weight. Consequently, the unambiguous characterisation of these materials is difficult and problematic. A fundamental feature of both hyperbranched and dendritic systems is the large number of end groups. Unlike linear polymers, the numerous chain ends of branched materials are anticipated to play a significant role in the determination of polymer behaviour.

1.7 A comparison between the properties of linear, hyperbranched and dendritic macromolecules[5]

Hawker, Fréchet and Wooley[5] have compared the physical properties of linear, hyperbranched and dendritic polymers based on 3,5-dihydroxybenzoic acid (**A**,**B**) and compared these polymers with poly(3-oxybenzoate) **C**.

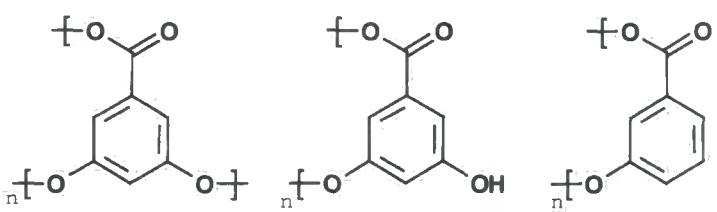

The linear polymer **B** was synthesised because the large numbers of end groups made for a more accurate comparison with hyperbranched and dendritic analogues. Analysis of the glass transition temperatures of linear, hyperbranched and dendritic polymers based on **A** and **B**, revealed that they were essentially the same. Properties were reported as follows: a fourth generation core terminated dendrimer with phenolic end groups had a Tg of 210°C, the hyperbranched polymer of unspecified molecular weight was found to have a Tg of 197°C and the linear analogue **B**, also of unspecified molecular weight, had a Tg of 204°C. By comparison, the glass transition temperature of poly(3-oxybenzoate) **C**, although not reported in their publication, is 157°C.[6] The thermal degradation of all three phenolic terminated architectures was reported to be identical within experimental error. Furthermore, the glass transition temperatures of benzylether terminated polymers were also reported. A Tg of 73°C was found for the dendritic polyester and a Tg of 78°C for the corresponding linear analogue. These findings led the authors to conclude that Tg and decomposition temperatures were independent of molecular architecture but influenced significantly by the nature of the chain ends.

The solubilities of these materials in acetone were also reported. The phenolic terminated dendrimer had a solubility of 1.05g ml^{-1} whilst the hyperbranched polymer had a solubility of 0.7g ml^{-1} and less than 0.02g of the linear analogue would dissolve per millilitre of acetone. By comparison poly(3-oxybenzoate) **C**, was found to be completely insoluble in acetone leading the authors to conclude that the high solubility of dendrimers and hyperbranched macromolecules was the result of their highly branched architectures and large numbers of end groups.

An area where the properties of dendritic macromolecules have been shown to differ radically from both linear and hyperbranched systems is in their viscosity behaviour. The general solution behaviours of linear, hyperbranched and dendritic polymers are summarised in Figure 1.13. It is widely accepted that the viscosity of linear polymers increases with molecular weight in accordance with the Mark-Houwink equation; $[\eta]=KM^a$. Dendrimers, on the other hand, do not obey this relationship. A plot of log(intrinsic viscosity) against generation number for core terminated 'tridendrons' reveals a characteristic bell shaped curve with a maximum at about generation 3. A maximum in the intrinsic viscosity of monodendrons is

also observed but this occurs, typically, between generations 4 and 5. The unique solution behaviour of dendritic macromolecules is explained by considering the shape of the molecule. The surface area of a dendrimer increases as the square of the radius ($A=4\pi r^2$) whilst the mass of end groups doubles for each generation and therefore increases exponentially. This characteristic behaviour has been reported by Frechet et al for polyether dendrimers,[8] and by Tomalia et al for poly(amidoamine), or PAMAM dendrimers.[9]

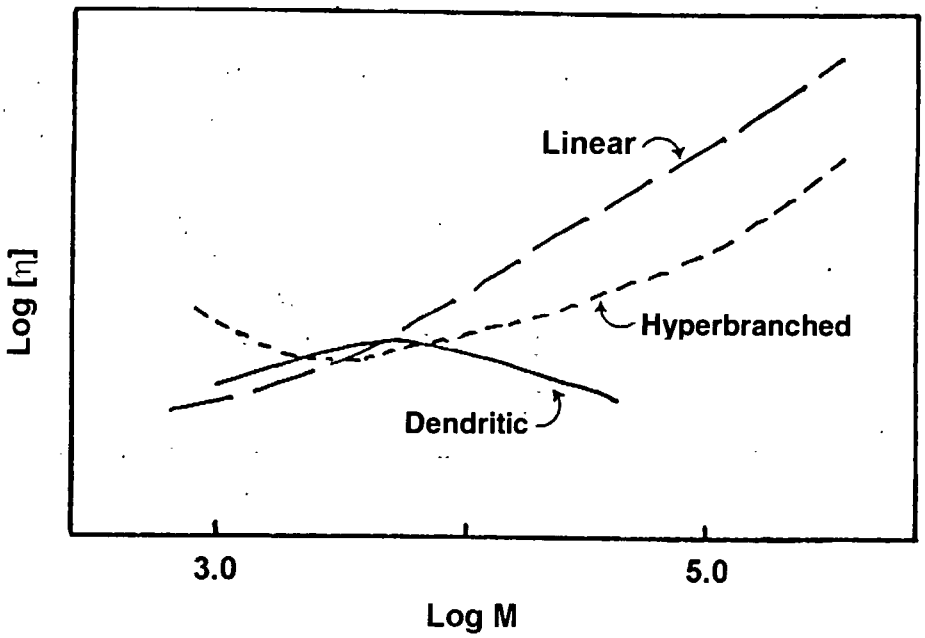

Fig. 1.13 Typical solution viscosity *vs.* log(molecular weight) behaviour for linear, hyperbranched and dendritic systems.[7]

The molecular weight relationship observed for hyperbranched polymers more closely resembles linear systems than dendritic. However, the 'hyperbranched' analogue of Tomalia's PAMAM dendrimer, synthesised by Hobson and Feast,[10] is reported as displaying dendritic solution behaviour. However, the polymer was not reported as being statistical but perfectly branched, i.e. with a degree of branching (DB) close to 1. By contrast, statistically branched homopolymers have a DB of 0.5 at one hundred percent conversion. The degree of branching (DB) was defined by Frey et al[11] as being 2D/(2D+L); where D = the number of fully reacted or 'dendritic' units and L is the number of partially reacted or 'linear' units. It is used to compare the number of growth directions in the polymer with the theoretical maximum.

In the remaining sections of this chapter three common commercial polymers are discussed.

1.8 Branching in polyethylene[12]

Polyethylene (PE), with the structure shown below, is conceptually the most simple of all synthetic polymers. However, the various methods used in the preparation of commercial PE yield materials with structures and properties that are very different.

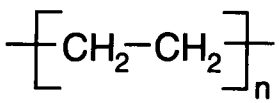

Unsubstituted linear polyethylene achieves the highest density 0.96-0.97 g cm^{-3} and melting point, 135°C of any PE architecture. This is due to the high crystalline content of the material, typically 70-90%. However, most polyethylene polymers incorporate branching to some extent. A brief synopsis of three general grades of commercial PE polymer is provided in the following paragraphs; highlighting the differences in production techniques, properties and structure.

Low density polyethylene (LDPE)

Commercial LDPE produced by the original ICI high pressure/high temperature route can be manipulated to give a wide variety of products and properties. The controlled variation of pressure during the polymerisation is used to influence the extent of long and short chain branching and ultimately to control the properties of the resultant material. Commercial LDPE is synthesised at pressures of around 40,000psi and contains, typically, 4 long chains and 15-30 alkyl substituents per 1000 carbon atoms. Long chain branching, a characteristic feature of LDPE polymers results in the formation of branched segments which may be as long as the backbone itself. Increasing the reaction pressure to 90,000psi significantly reduces the extent of branching. Resultant polyethylene materials are then essentially linear with typically 0.6 long chain branches and 0.8 alkyl substituents per 1000 carbon atoms. However, the extreme conditions required to achieve this reduction in branching content are not feasible commercially.

The properties of commercially available LDPE are highly dependent on the density and crystallinity of the material which are themselves strongly influenced by the extent of branching. Owing to their high amorphous content, LDPE polymers possess remarkable toughness and high impact strength. Their flexibility, ease of processing, transparency, chemical resistance, low permeability to water and outstanding electrical properties make them ideal for applications such as packaging and cable coatings. However, LDPE materials are subject to slow deformation under constant stress, called 'creep'. Consequently, they are not used for structural applications.

High Density Polyethylene (HDPE)

One of the most important advances in PE synthesis was the discovery in the 1950s by Ziegler and coworkers, that ethylene would polymerise at ambient temperature and atmospheric pressure in the presence of an alkyl aluminium compound and a transition metal halide. They found that the product of this reaction was essentially linear and highly crystalline. Commercial HDPE has less than 7 branch points per 1000 carbon atoms, typically, and these are all short chain defects (alkyl substituents).

The Phillips catalyst, developed at the same time as Ziegler's, utilises a chromium trioxide catalyst which is supported on silica. It relies on moderate pressures to be effective but produces HDPE with fewer branching defects than the Ziegler route. Between these two catalysts, they account for almost all production of commercial grade HDPE.

Linear Low Density Polyethylene (LLDPE)

LLDPE is a copolymer of PE with typically 8-10% of an α-olefin, such as but-1-ene, pent-1-ene, hex-1-ene or oct-1-ene. By varying the type and extent of comonomer incorporation, it is possible to control the number of short chain branches in the resultant material. LLDPE has superior impact strength to LDPE, improved toughness and a lower brittle temperature.

Effects of Branching in Polyethylene

Long chain branching exerts a strong influence over melt viscosity and the relationship with shear rate. Indeed, under practical extrusion conditions, i.e. high shear, the melt viscosity of branched LDPE is much lower than that of unbranched LLDPE; Figure 1.14. Consequently, the former can be extruded at a lower temperature and a higher rate with an overall decrease in energy consumption.

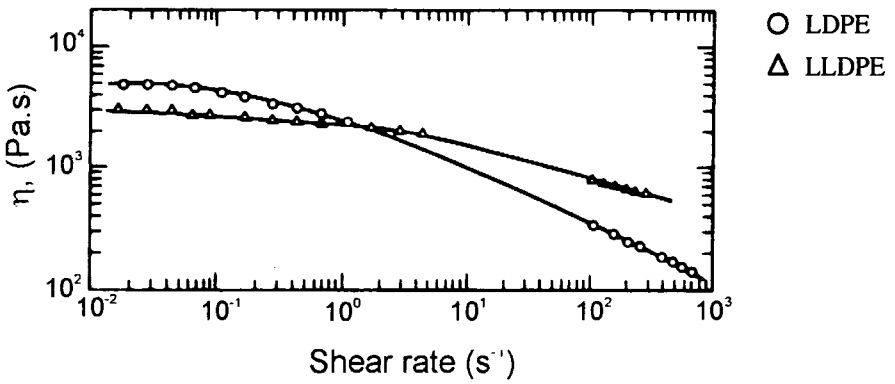

Fig. 1.14 Polyethylene melt viscosity η *vs.* shear rate at 220°C.[12]

An increase in the dimensions of a polyethylene melt occur after it has been forced under pressure through the dye of an extruder. This effect, called die swell, increases with long chain branching and molecular weight. It also increases with shear rate up to a critical value above which melt fracture occurs; polymer melt is then extruded with a rough uneven surface called 'shark skin'. Melt fracture is itself subject to influence from long chain branching, occurring less readily for LDPE than for LLDPE.

In solution, the highly branched structures of LDPE are less extended, i.e. more compacted, than their linear analogues with equivalent molecular weights. Consequently, lower viscosities are observed for branched LDPE polymers. A plot of log[η] *vs.* log Mn reveals a linear relationship for LLDPE polymers, which agrees with the Mark-Houwink equation $[\eta]=KM^a$. However, LDPE solution behaviour deviates from the linear analogue to approach a plateau value at high molecular weights; Figure 1.15. Indeed, the decrease in [η] as compared with linear PE can be used a measure of the extent of long chain branching in these systems.

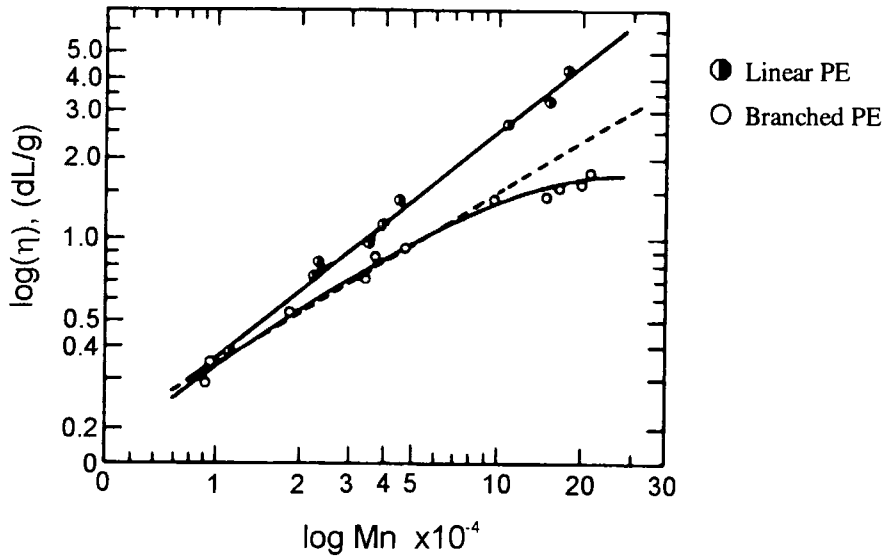

Fig. 1.15 Relationships between intrinsic viscosity [η] and Mn for fractions of linear and branched polyethylene.[12]

As alkyl side chains are excluded from the crystal lattice, short chain branching is the main controlling influence of crystallinity, density and associated properties in PE polymers. In LDPE, alkyl branches are created primarily through a free radical backbiting mechanism. However, in LLDPE short chain branches are purposefully introduced *via* a controlled copolymerisation of α-olefins and ethylene. This offers the advantage of being able to easily modify the properties of PE materials through changes in the monomer feed stock.

1.8 Branching in Polystyrene

It is known that copolymerisations of styrene and divinyl benzene, prepared *via* free radical chain growth mechanisms, result in cross-linked polystyrene gels. However, an investigation by Oun[13] revealed that copolymers of styrene with 0.9% by weight of DVB units, acting as tetrafunctional branch points, were soluble in methyl ethyl ketone and THF. Fractionated samples were analysed using light scattering techniques and the branching and expansion factors calculated from light scattering data. However, the analyses of these data did not show good agreement with theory.

The main problem associated with introducing branch points into linear polymers is gelation. Flory[14] and Stockmayer[15] both considered the theoretical

basis for gelation in what were coined 'three-dimensional' polymerisations. They both concluded that the gel point could only be reached at a specific extent of reaction, dependent on both the branching functionality and the percentage composition of branching units in the monomer feed. Consequently, branching with multifunctional A_x or B_x molecules is limited to low extents of branching and low molecular weights. The addition of a monofunctional chain terminating agents can be used to prevent the onset of gelation to produce soluble, highly functionalised molecules.[16,17]

Considerable interest in the synthesis and characterisation of hyperbranched macromolecules has been shown over the last decade. Like dendrimers they are highly functionalised but lack the symmetry and structural regularity obtained from dendritic macromolecules. The main advantage of hyperbranched polymers over dendrimers is their ease of synthesis. Indeed, it is possible to obtain soluble hyperbranched polymers *via* a 'one-pot' reaction that possess some of the qualities and characteristics of dendrimers without the need for laborious protection, deprotection reaction sequences. However, in many cases these systems lack the properties of perfect dendritic structures.

Although less well researched, the incorporation of AB_2 branching units into an AB linear polymer provides a means of obtaining soluble, highly functionalised polymers without gelation. This was demonstrated for copolymers of polystyrene by Matyjaszewski et al[18] using an atom transfer radical polymerisation of commercially available *p*-(chloromethyl)styrene (CMS) in the presence of Cu(I) and 2,2'-bipyridyl (bpy). The synthesis of hyperbranched CMS was also reported.

In the synthesis described by Matyjaszewski, the CMS monomer was considered to be an AB_2 molecule which was capable of creating a soluble hyperbranched polymer as illustrated in Figure 1.16. In the ATRP mechanism, CMS is acting as both monomer and initiator. The chlorine atom is homolytically cleaved at the benzylic position by Cu(I) to form a benzyl radical and Cu(II)Cl. This radical is capable of initiating polymerisation through the double bond of a second monomer molecule. The propagating chain may be deactivated by Cu(II)Cl at any point during the reaction and then reactivated again at a later time by Cu(I). The ATRP mechanism behaves in a manner that is similar to step growth, where molecules of any given number of units, x, may react with the focal group of another molecule, with y incorporated units. The broad polydispersities observed in

these systems are consistent with this type of mechanism. Propagation of the polymer chains creates pendant *p*-benzyl chloride units; any number of which may be active at any one time, dependent on concentration of Cu in the reaction. An increase in the number of radical ions will lead eventually to 'bimolecular coupling', or intramolecular cyclisation, to yield a cross-linked intractable gel. Indeed, cross-linking was reported by the author for reactions with greater than 10mole% Cu after 30 minutes.

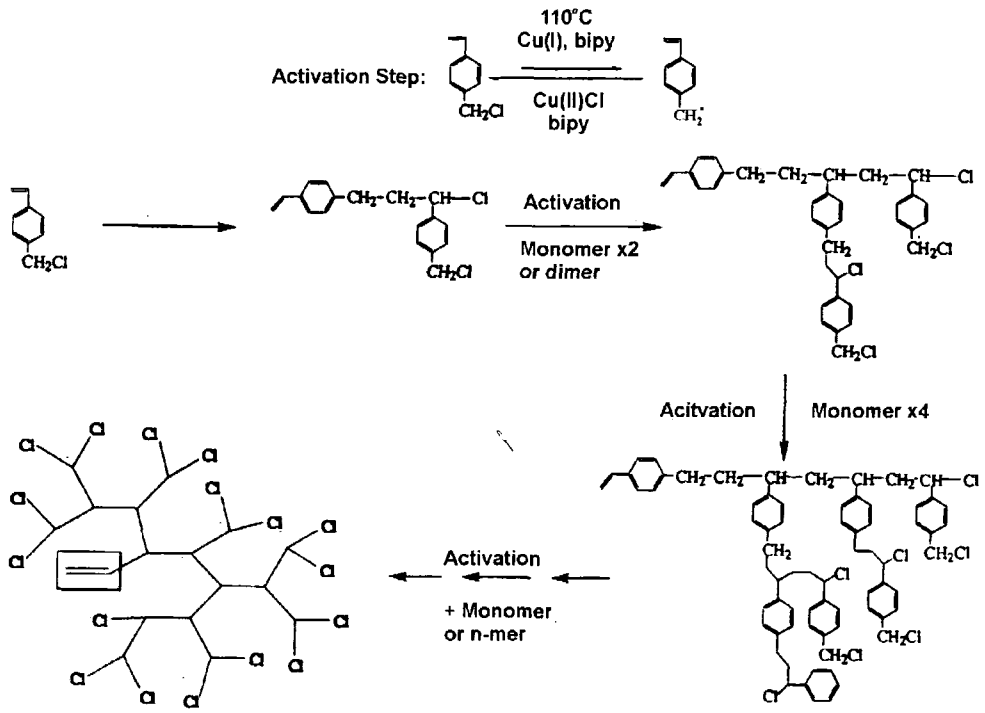

Fig. 1.16 Formation of a hyperbranched polymer by Atom Transfer Radical polymerisation of CMS.[18]

Matyjaszewski showed using Mark-Houwink plots, Figure 1.17, that the solution viscosity of a 2mole% branched PS copolymer was lower than the corresponding linear analogue of the same molecular weight. Furthermore, the observed relationship was linear between molecular weights of 10^3 and 10^6. Clearly, a range of branched polystyrenes with various compositions could be synthesised without the formation of intractable cross-linked gels, providing that a suitable concentration of initiator is selected.

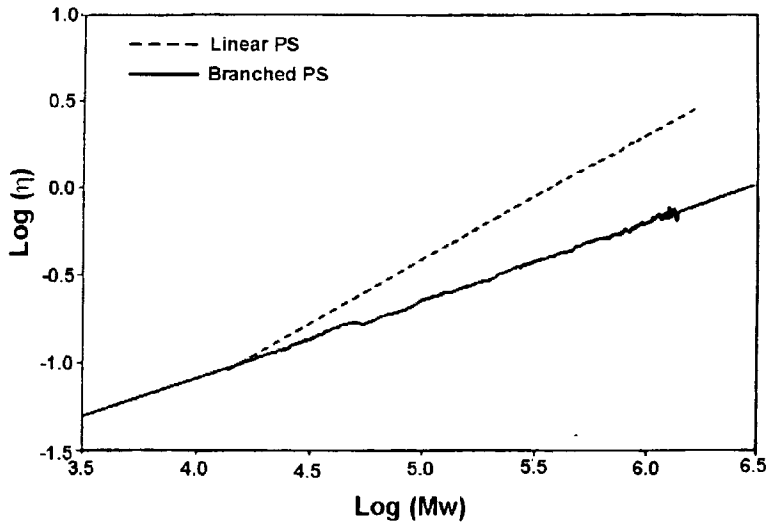

Fig. 1.17 Mark-Houwink plots showing Log(Mw) as determined by light scattering against log(intrinsic viscosity) for linear and 2mole% branched polystyrene.[18]

1.9 Poly(ethylene terephthalate)[19]

Poly(ethylene terephthalate) (PET), Figure 1.18, was discovered in the UK in the early 1940s following the pioneering work of Carothers.[20] Introduced commercially in 1953 as a textile fibre, its volume of production and range of products has increased dramatically over the last fifty years. In 1970 the world-wide film production of PET was *ca.* 500 tons. This grew to more than 500,000 tons in 1985 and was predicted to grow at an annual rate of 14% per annum. At this time, fibre production exceeded film manufacture by a staggering 5.6 million tons.

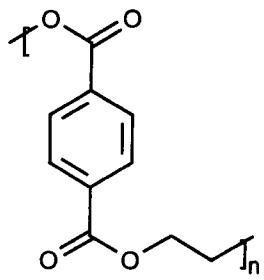

Fig. 1.18 Poly(ethylene terephthalate) PET.

So, what is PET and why is it so commercially successful? PET is classified as an engineering material because of its excellent thermal, mechanical, optical and electrical properties. It has excellent mechanical properties when oriented and has

consequently found its way into fibres, films and blow moulded products. Indeed, its high strength, rigidity and good surface hardness make it ideal for many engineering applications. PET is a relatively inexpensive material and its success as a commercial material can be attributed to its 'cost effective' properties.

The basic manufacturing process for PET is identical for all products including fibres, films, filaments and bottles; products differing only in their processing, handling and addition of additives. The synthesis of PET from dimethyl terephthalate (DMT) is essentially a two step process. The first step involves the transesterification of DMT and ethylene glycol; Figure 1.19. A 2.1:1 mixture of ethylene glycol and dimethyl terephthalate is charged into a reactor and heated slowly. A catalyst, almost always a metal acetate, is added to the reactor below 430K. Dimers and trimers of PET are formed between 430K and 470K and are accompanied by the rapid evolution of methanol. After this initial surge of reactivity the temperature is slowly increased to 530K and held until 95% of the methanol has been collected. The reactor is then heated by a further 10K to 540K to drive the reaction to completion.

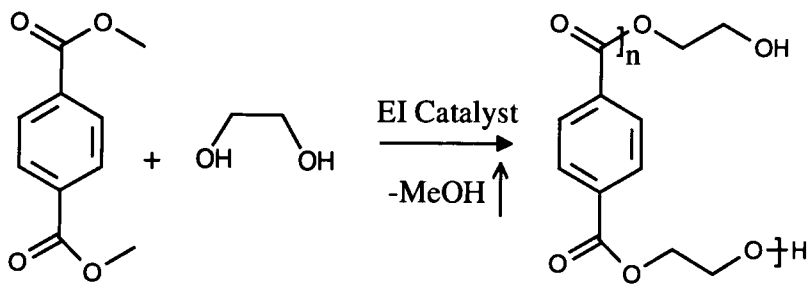

Fig. 1.19 PET synthesis step 1: Ester Interchange.

Oligomers, formed during the first stage are fed to the main polymerisation reactor. It is important that this first stage is driven to completion as the presence of methyl ester chain ends, acting as chain terminating agents, limit the molecular weight of the resultant polymer in the second stage of the synthesis. Polymerisation occurs when the oligomers of PET are heated to 560K in the presence of a suitable polycondensation (PC) catalyst. Glycol is eliminated during the reaction and is distilled from the reactor under vacuum, see Figure 1.20. The reactor is maintained at 560K until the desired Mn is reached; determined by monitoring the power requirement of the stirrer as it agitates the polymer melt.

Some catalysts include acetates of antimony, calcium, magnesium and manganese although zinc acetate is one of the most commonly used. Polycondensation catalysts typically used are antimony trioxide, germanium dioxide or titanium tetrabutoxide. Catalysts that are soluble in glycol can be precipitated as phosphate or phosphites with the addition of triphenylphosphine (TPP) to prevent polymer degradation during processing.

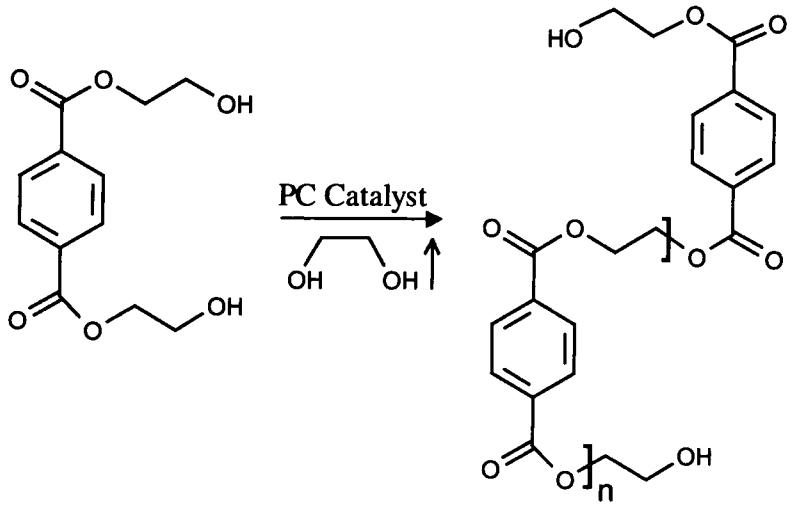

Fig. 1.20 PET synthesis step 2: Polycondensation.

The structure shown in Figure 1.20 does not represent PET in its entirety. This is because PET polymers contain *ca.* 1.5mole% of cyclic material, the majority of which is cyclic trimer. In addition, a side reaction of ethylene glycol during the polymerisation of PET results in the formation of *ca.* 2-5mole% diglycol and traces of triglycol units in the polymer. These are present as copolymerised units in the chain and lower the melting temperature of the polymer by *ca.* 2.2°C.

The glass transition temperature of PET has been measured between 70-120°C and is dependent on the technique of measurement, the rate of measurement and the extent of crystallinity in the polymer. PET is also known to exhibit multiple endothermic transitions. After crystallising, there is a morphological rearrangement of less perfectly formed crystallites into more organised arrangements close to the melt temperature. This has been confirmed by measurements using electron microscopy and small angle neutron scattering. The equilibrium melt temperature of PET has been determined as 290°C.

PET with a weight average of ~35,000 is manufactured for oriented films and fibres. However, for injection moulding higher molecular weight materials

(Mw~80,000) are required to avoid brittle mouldings. The compatibility of PET with many different types of filler, polymer additives and modifying agents is one of the principal reasons why there has been such a large market expansion of injection-moulded polyester products since its introduction in 1966. There are a wide range of additives that can be used, a few of which include, glass fibre, glass beads, calcium carbonate, carbon powder, flame retardants, impact modifiers, antistatic agents, uv stabilisers and so on. These enhance the properties of the material and expand the range of available products and applications. Meanwhile, manufacturers continue to search for cheaper, more efficient methods of production and processing of PET, in their relentless attempts to lower the costs associated with its manufacture.

In the remainder of this thesis, a study of linear and branched polyesters with structures similar to that of PET is described

1.10 References

1. Flory P.J., *J. Am. Chem. Soc.*, **58**, (1936), 1877
2. Carothers W.H., *Trans. Faraday Soc.*, **32**, (1936), 39
3. Lansing, Kraemer, *J. Am. Chem. Soc.*, **56**, (1934), 912
4. Flory P.J., *J. Am. Chem. Soc.*, **74**, (1952), 2718
5. Wooley K.L., Hawker C.J., Fréchet J.M.J., *Polymer*, **35(21)**, (1994), 4489
6. Hricheldorf H.R., Zang Q., Schwarz G., *Polymer*, **23**, (1982), 1821
7. Hawker C.J., Fréchet J.M.J., *ACS Symp.*, **Chapter 7**, (1996), 132
8. Wooley K.L., Hawker C.J., Fréchet J.M.J., Turner S.R., Rubinstein M., Mourey T.H., *Macromolecules*, **25**, (1992), 2401
9. Tomalia D.A., Naylor A.M., Goddard W.A., *Angew. Chem. Int. Ed. Engl.*, **29**, (1990), 138
10. Hobson L.J., Feast W.J., *Chem. Comm.*, **21**, (1997), 2067
11. Hölter D., Burgath A., Frey H., *Acta Polymer*, **48**, (1997), 30
12. Encyclopedia of Polymer Science, 2nd Ed., Vol. 6, Wiley & Sons (1985), 412-429
13. Oun A.M., *Polymer Int.*, **29**, (1992), 307
14. Flory P.J., *J. Am. Chem. Soc.*, **63**, (1941), 3083
15. Stockmayer W.H., *J. Chem. Phys.*, **11(2)**, (1943), 45

16. Ruxanadra F.R., Shanks R.A., Battcharya S.N., *Polym. Int.*, **42**, (1997), 267
17. Manaresi P., Munari A., Pilati F., *Polymer*, **27**, (1986), 955
18. Gaynor S.G., Edelman S., Matyjaszewski K., *Macromolecules*, **29**, (1996), 1079
19. Encyclopedia of Polymer Science, 2nd Ed., Vol. 12, Wiley & Sons (1985), 19-250
20. Carothers W.H., Hill J.W., *J. Am. Chem. Soc.*, **54**, (1932), 1579

Chapter 2

Monomer Synthesis and Polymerisations

2.1 Introduction

Our investigation into the effects of branching in linear polyesters required the following monomers.

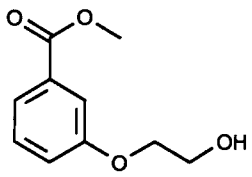

1

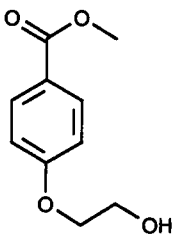

2

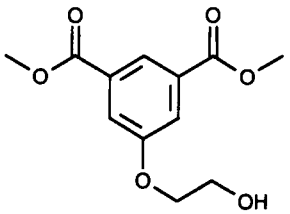

3

These were the two bifunctional linear monomers, methyl 3-(2-hydroxyethoxy) benzoate (**1**) and methyl 4-(2-hydroxyethoxy)benzoate (**2**), and the branching agent, dimethyl 5-(2-hydroxyethoxy)isophthalate (**3**), depicted above.

Two general strategies, developed previously for the synthesis of monomer **3**, were considered for molecules **1** and **2**. A two step strategy, which exploits an initial esterification and a base catalysed ring opening of ethylene oxide is shown in Scheme 2.1. An alternative four-step strategy is shown in Scheme 2.2, which utilises acetate protection/deprotection as indicated in the diagram.

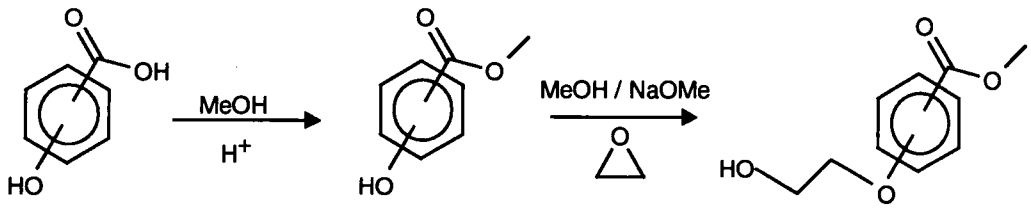

Scheme 2.1 General synthetic strategy (I) to aromatic hydroxyethoxyesters.

The route outlined in Scheme 2.1 was the quickest and most efficient synthesis, allowing monomer production on a two hundred gram scale. However, there were limitations for this process. Firstly, specialised reactors capable of withstanding operating pressures of up to 200psi were required. This made the use of autoclaves mandatory and limited the scale of production to the size and availability of these

vessels. Secondly, ethylene oxide, a low boiling, highly flammable gas is a hazardous chemical. Therefore, in acknowledgement of health and safety requirements, vacuum line techniques were used to manipulate the gas and prevent airborne contamination.

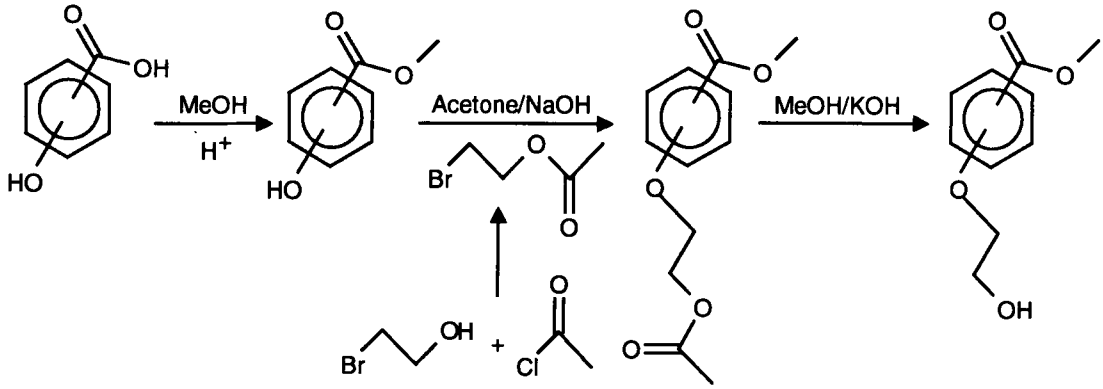

Scheme 2.2 General synthetic strategy (II) to aromatic hydroxyethoxyesters.

The route shown in scheme 2.2 was lower yielding and more labour intensive than the strategy described previously. Other problems included, physical constraints i.e., the size and weight of the glassware, and our failure to obtain methyl 3-(2-hydroxyethoxy)benzoate *via* this approach, even though the para and the 3,5-derivatives were successfully produced using this route. There seems to be no steric or electronic rationalisation for this failure. In conclusion, Scheme 2.1 was the most advantageous, providing savings in both time and material costs whilst maintaining the required versatility.

The method of polymerisation was adapted from a technique developed by Stainton[1], Parker and Keeney in Durham, details of which are provided later in this chapter.

Titanium tetrabutoxide is a tried and tested transesterification catalyst for the production of PET. Although extremely effective in increasing rates of reaction, as compared to catalyst free polymerisations, it is rarely used commercially. This is due to the formation of a highly coloured impurity that renders the catalyst unsuitable for applications where optical purity is required. However, titanium tetrabutoxide is a readily available liquid which is easily manipulated and metered into the reaction vessel. This makes it suitable for use in this work.

Experimental procedures are described in the following sections, complete with product characterisation data obtained during the course of this study. Copies of the original experimental data (IR, ^{1}H and ^{13}C NMR spectra) are included in the appendices.

2.2 Experimental

2.2.1. General

Organic reagents, purchased from Aldrich Chemical Co. and Lancaster Synthesis Ltd., were used without further purification. Infrared spectra, recorded using a Perkin-Elmer 1600 series FTIR spectrometer, were obtained for all pure reaction products. Melting points were obtained using an electrothermal IA9200 series digital melting point apparatus and ^{1}H, ^{13}C NMR spectra recorded on a Varian VXR 400 NMR spectrometer at 400.0MHz (^{1}H) and 100.6MHz (^{13}C) or a Varian Gemini at 200MHz (^{1}H) and 50.2MHz (^{13}C). The solvent system chosen for NMR analysis of polycrystalline materials was a mixture of deuterated chloroform and a minimum quantity of trifluoroacetic acid, the composition being determined by dropwise addition of the acid. Amorphous materials were analysed in solutions of pure deuterated chloroform and mixtures of deuterated chloroform and trifluoroacetic acid. NMR spectra of linear *m*-poly(ethylene oxybenzoate) were also obtained for solutions in DMSO-d_6 at 95°C.

Size exclusion chromatography (SEC) was performed on solutions of the amorphous copolymer systems using three columns of 5μm PL gel with 100Å, 10^3Å and 10^5Å pore sizes, a Waters differential refractometer detector ERC7515A and chloroform as eluent. Columns were calibrated using polystyrene standards supplied by Polymer Labs. In addition, copolymers with 80mole% branching were analysed using THF eluent, three mixed bed 10μm gel columns and a triple detector consisting of a Viscotek LD600 right angle light scattering detector and a combined Viscotek model 200 differential refractometer and viscometer.

Elemental analyses, CHN, were performed using an Exeter Analytical Elemental Analyser CE-440 and mass spectra were recorded on a Micromass Autospec.

A Schott automatic viscometer, consisting of a thermostat CT1650, water bath CT62/2M, piston burette Visco-Doser AVS 20 and data recorder AVS 350, was used to determine the intrinsic viscosities of amorphous copolymeric materials in chloroform. However, the poor solubility of crystalline materials prevented a comparative study. Thermogravimetric analyses were performed using a Rheometrics Ltd. TG760 thermobalance. TG traces were recorded under a nitrogen atmosphere, using a heating rate of 10°C min^{-1}. Decomposition temperatures were recorded as the temperature of 2% weight loss. Differential scanning calorimetry was carried out using either a Perkin-Elmer DSC 7 or a Perkin-Elmer Pyris-1 DSC.

2.2.2 Synthesis

The codes shown in bold script indicate the location of the raw data within the appendices; thus, **A01-2** indicates that the ^{13}C NMR spectrum (A01–2) of compound 01 (A01-2) is to be found in appendix A (A01-2).

2.2.2a Dimethyl 5-hydroxyisophthalate (A01)

5-Hydroxyisophthalic acid (200g, 1.1mol), and anhydrous methanol (2L) were charged into a 5L flange flask, equipped with a stirrer, gas inlet, gas outlet and a water cooled reflux condenser. The gas inlet was connected to a 225g cylinder of anhydrous $HCl_{(g)}$ and the outlet to a NaOH(aq) scrubbing tower. Anhydrous $HCl_{(g)}$ (25g, 0.7mol) was then bubbled through the solution and the reaction mixture stirred under reflux for 24 hours. On cooling to room temperature, white needle like crystals of crude dimethyl 5-hydroxyisophthalate formed in the acidic methanol. The solution was cooled to 0°C, increasing the rate of crystallisation and improving the overall product yield.

Crystals, collected by filtration, were washed with copious quantities of water and recrystallised from hot $MeOH/H_2O$. Product was then collected by filtration, washed with aliquots of 10% methanol/water solution and dried under vacuum to give dimethyl 5-hydroxyisophthalate **(A01)** as a white powdery solid (193.9g, 0.92mol, 84%); m.p. 158°C (lit[2] 158-159°C); found C, 57.30%; H, 4.85%; $MH^+_{(MS,\ CI)}$, 211; $C_{10}H_{10}O_5$ requires C, 57.14%; H, 4.80%; M, 210. ^1H NMR **(A01-1)** ($CDCl_3$, 400MHz, δ) 1.60 (s, broad, 1H, phenolic O<u>H</u>), 3.88 (s, 6H, OC<u>H</u>$_3$), 7.69 (s, 2H, aromatic C-<u>H</u>),

8.19 (s, 1H, aromatic C-H); ^{13}C NMR **(A01-2)** ($CDCl_3$, 100MHz, δ) 52.5 ($O\underline{C}H_3$), 120.8; 123.0 (aromatic C-H), 131.9 (aromatic $\underline{C}$-$COOCH_3$), 156.0 (aromatic C-O), 166.2 ($\underline{C}$=O); IR **(A01-3)** (KBr disc, cm^{-1}) 3360 (broad, H-bonded O-H stretch), 3012 (w, aryl-H C-H stretch), 2962 (w, saturated C-H stretch), 1706 (s, aromatic ester C=O stretch), 756 (s, aryl-H C-H out of plane vibration).

2.2.2b Dimethyl 5-(2-hydroxyethoxy)isophthalate (A02)

Dimethyl 5-hydroxyisophthalate (185g, 0.88mol), sodium methoxide (12g, 0.22mol) and dry analar methanol (1.2L) were charged into a 2L autoclave. Ethylene oxide (58g, 1.3mol) was vacuum transferred into the autoclave and the reaction vessel pressurised with nitrogen to 100psi. The contents of the reactor were stirred for six hours at 100°C during which period the pressure rose to a maximum of 180psi before returning to its initial value. The autoclave was then allowed to cool to room temperature. After venting to a $NaOH_{(aq)}$ scrubbing tower, the reaction mixture was concentrated under reduced pressure and poured into a large excess of water. The crude precipitated product was recovered by filtration, washed with water, recrystallised from hot $MeOH/H_2O$ and dried under vacuum to give dimethyl 5-(2-hydroxyethoxy)isophthalate **(A02)** as a white crystalline solid (83g, 0.33mol, 68%), m.p. 113°C-114°C (lit[3] 112-112.5°C); found C, 56.60%; H, 5.60%; $MH^+_{(MS,\ CI)}$, 255; $C_{12}H_{14}O_6$ requires C, 56.68%; H, 5.55%; M, 254. ^{1}H NMR **(A02-1)** ($CDCl_3$, 400MHz, δ) 2.10 (s, broad, 1H, O<u>H</u>), 3.94 (s, 6H, $OC\underline{H}_3$), 4.00 (t, 2H, ^{1}J~4Hz, $CH_2C\underline{H}_2OH$), 4.17 (t, 2H, ^{1}J~4Hz, $C\underline{H}_2CH_2OH$), 7.77 (s, 2H, aromatic C-H), 8.29 (s, 1H, aromatic C-H); ^{13}C NMR **(A02-2)** ($CDCl_3$, 100MHz, δ) 52.5 ($O\underline{C}H_3$), 61.2 ($\underline{C}H_2OH$), 69.8 ($\underline{C}H_2CH_2OH$), 119.8; 123.3 (aromatic $\underline{C}$-H), 131.8 (aromatic $\underline{C}$-$COOCH_3$), 151.7 (aromatic $\underline{C}$-O), 166.0 ($\underline{C}$=O); IR **(A02-3)** (KBr disc, cm^{-1}) 3330 (s, broad, O-H stretch), 2952 (m, saturated C-H stretch), 1728 (s, aromatic ester C=O stretch), 1596 (s, aryl C=C stretch).

2.2.2c Methyl 4-(2-hydroxyethoxy)benzoate: method 1 (A03)

Methyl 4-hydroxybenzoate (200g, 1.3mol), sodium methoxide (16.2g, 0.30mol) and dry analar methanol (1.2L) were charged into a 2L autoclave. Ethylene oxide (58g, 1.3mol) was vacuum transferred into the autoclave and the reaction vessel pressurised with nitrogen to 100psi. The contents of the autoclave were stirred for 6 hours at 100°C and then allowed to cool to room temperature. After venting to a $NaOH_{(aq)}$ scrubbing tower, methanol was removed under vacuum. The crude product was then dissolved in dichloromethane and washed with water and brine. After separation and removal of the solvent under reduced pressure, the product was recrystallised from hot toluene, collected by filtration and dried under vacuum to give methyl 4-(2-hydroxyethoxy)benzoate (**A03**) as a white crystalline solid (193g, 0.98mol, 75%), m.p. 68-69°C (lit[4] 65-68°C); found C, 61.15%; H, 6.21%; $MH^+_{(MS,\ CI)}$, 197; $C_{10}H_{12}O_4$ requires C, 61.28%; H, 6.13%; M, 196. ^{1}H NMR (**A03-1**) ($CDCl_3$, 400MHz, δ) 2.01 (t, 1H, ^{1}J=6.2Hz, O<u>H</u>), 3.89 (s, 3H, O<u>CH</u>$_3$), 4.00 (m, 2H, CH_2<u>CH_2</u>OH), 4.14 (t, H, ^{1}J=4.2Hz, <u>CH_2</u>CH_2OH), 6.93 (d, 2H, ^{1}J=8.8Hz, aromatic C-<u>H</u>), 7.99 (d, 2H, ^{1}J=9.2Hz, aromatic C-<u>H</u>); ^{13}C NMR (**A03-2**) ($CDCl_3$, 100MHz, δ) 51.9 (O<u>C</u>H_3), 61.3 (<u>C</u>H_2OH), 69.3 (<u>C</u>$H_2$$CH_2$OH), 114.1; 131.7 (aromatic <u>C</u>-H), 123.0 (aromatic <u>C</u>-$COOCH_3$), 162.3 (aromatic <u>C</u>-O), 166.8 (<u>C</u>=O); IR (**A03-3**) (KBr disc, cm^{-1}) 3425 (s, broad, O-H stretch), 2931 (w, saturated C-H stretch), 1719 (m, aromatic ester C=O stretch), 1609 (s, aryl C=C stretch).

2.2.2d Methyl 4-(2-acetoxyethoxy)benzoate (A04)

Methyl 4-hydroxybenzoate (162g, 1.06mol), anhydrous potassium carbonate (146.1g, 1.06mol), bromoethylacetate (230.6g, 1.38mol) and dry analar acetone (1.5L), were charged into a 5L flange flask fitted with a reflux condenser. The reaction mixture was stirred under reflux for three days and allowed to cool to room temperature. The crude reaction mixture was concentrated under reduced pressure, poured into excess water, extracted into dichloromethane, shaken with 0.5mol $NaOH_{(aq)}$ solution (3x1L) and washed with brine. After removing the dichloromethane solvent under reduced pressure, the product was recrystallised from hot toluene, collected by filtration and dried under vacuum to give methyl 4-(2-acetoxyethoxy)benzoate (**A04**) as

a white crystalline solid (58g, 0.24mol, 23%), m.p. 84°C; found C, 60.75%; H, 5.95%; $MH^+_{(MS, CI)}$, 239; $C_{10}H_{12}O_4$ requires C, 60.52%; H, 5.88%; M, 238. ^{1}H NMR **(A04-1)** ($CDCl_3$, 400MHz, δ) 2.11 (s, 3H, OAc), 3.89 (s, 3H, $OC\underline{H}_3$), 4.22 (t, 2H, ^{1}J~5Hz, $CH_2C\underline{H}_2OAc$), 4.44 (t, 2H, ^{1}J~5Hz, $C\underline{H}_2CH_2OAc$), 6.93 (d, 2H, ^{1}J=8.8Hz, aromatic C-H), 7.99 (d, 2H, ^{1}J=8.8Hz, aromatic C-H); ^{13}C NMR **(A04-2)** ($CDCl_3$, 100MHz, δ) 20.9 (acetate $OCOC\underline{H}_3$), 51.9 (ester $COOC\underline{H}_3$), 61.0 ($\underline{C}H_2OH$), 66.0 ($\underline{C}H_2CH_2OH$), 114.1; 131.6 (aromatic C-H), 123.1 (aromatic $\underline{C}$-$COOCH_3$), 162.1 (aromatic $\underline{C}$-O), 166.7 (ester $\underline{C}$=O), 171.0 (ester $\underline{C}$=O); IR **(A04-3)** (KBr disc, cm^{-1}) 3407 (H_2O, O-H stretch), 2946 (w, saturated C-H stretch), 1744 (s, aliphatic C=O stretch), 1714 (s, aromatic C=O stretch).

2.2.2e Methyl 4-(2-hydroxyethoxy)benzoate: method 2 (A03)

Methyl 4-(2-acetoxyethoxy)benzoate (57.6g, 0.24mol), potassium hydroxide (0.76g, 0.013mol) and dry analar methanol (0.6L), were charged into a 2L flange flask fitted with a water cooled condenser. The reaction mixture was then stirred at room temperature for forty-eight hours, concentrated under reduced pressure and poured into excess water. The crude product was extracted into dichloromethane and the resulting solution washed with brine. After removing the solvent under reduced pressure the product, recrystallised from hot toluene, was collected by filtration and dried under vacuum to give methyl 4-(2-hydroxyethoxy)benzoate **(A03)** as a white crystalline solid (35g, 0.13mol, 74%), m.p. 66-68°C (lit[4] 65-68°C); found C, 61.25%; H, 6.14%; $MH^+_{(MS, CI)}$, 197; $C_{10}H_{12}O_4$ requires C, 61.28%; H, 6.13%; M, 196. ^{1}H NMR **(A03-1)**, ^{13}C NMR **(A03-2)** and IR **(A03-3)** spectra were identical with those of samples produced by method 1.

2.2.2f Methyl 3-(2-hydroxyethoxy)benzoate (A05)

Methyl 3-hydroxybenzoate (150g, 1.035mol), sodium methoxide (12.95g, 0.237mol) and dry analar methanol (0.6L) were charged into a 2L autoclave. Ethylene oxide (69g, 1.66mol, 1.6eq) was vacuum transferred into the autoclave and the reaction vessel pressurised with nitrogen to 100psi. The reaction mixture was stirred for 6 hours at 100°C and then allowed to cool to room temperature. After venting to a $NaOH_{(aq)}$

scrubbing tower, the solvent was removed under reduced pressure. The crude product was dissolved in dichloromethane, washed with water and brine, and the solvent removed under reduced pressure. The crude product, an orange oil, was then purified by column chromatography on silica gel (Aldrich, mesh 70-230); eluent (9:1) dichloromethane/ethyl acetate. Appropriate fractions, analysed by thin layer chromatography, were combined and the solvent removed under reduced pressure. The product was dried under vacuum to give methyl 3-(2-hydroxyethoxy)benzoate **(A05)** as a pale yellow oil (64g, 0.33mol, 33%), found C, 61.30%; H, 6.00%; $MH^+_{(MS, CI)}$, 197; $C_{10}H_{12}O_4$ requires C, 61.28%; H, 6.13%; M, 196. ^{1}H NMR **(A05-1)** ($CDCl_3$, 400MHz, δ) 2.21 (s, broad, 1H, O<u>H</u>), 3.90 (s, 3H, OC<u>H</u>$_3$), 3.97 (t, 2H, ^{1}J~4Hz, $CH_2C\underline{H}_2OH$), 4.13 (t, 2H, ^{1}J~4Hz, $C\underline{H}_2CH_2OH$), 7.15 (m, 2H, aromatic C-<u>H</u>), 7.34 (m, 1H, aromatic C-<u>H</u>), 7.56 (m, 1H, aromatic C-<u>H</u>), 7.65 (m, 1H, aromatic C-<u>H</u>); ^{13}C NMR **(A05-2)** ($CDCl_3$, 100MHz, δ) 52.2 (O<u>C</u>H$_3$), 61.3 (<u>C</u>H$_2$OH), 69.4 (<u>C</u>H$_2$CH$_2$OH), 114.6; 119.9; 122.4; 129.4 (aromatic <u>C</u>-H), 131.4 (aromatic <u>C</u>-COOCH$_3$), 162.3 (aromatic <u>C</u>-O), 166.8 (<u>C</u>=O); IR **(A05-3)** (KBr disc, cm^{-1}) 3445 (s, broad, O-H stretch), 2951 (m, saturated C-H stretch), 1717 (m, aromatic ester C=O stretch), 1585 (s, aryl C=C stretch).

2.2.3 Polymerisation

Residual traces of water react with titanium tetrabutoxide, the chosen transesterification catalyst, to form hydroxy titanate species with no catalytic activity. Consequently, in an attempt to exclude moisture from the reactor, glassware was routinely flamed and cooled under dry nitrogen before use.

Twenty-gram batches of monomer were dried under vacuum and added to the reaction vessel. Titanium tetrabutoxide, a thick viscous liquid, was then added in the ratio 1mg:1g (catalyst:monomer) using a microlitre syringe. The density of titanium butoxide (1g cm^{-3}) gave catalyst mole percentages of between 0.05 and 0.07, depending on the ratio of di- to trifunctional monomers used.

Upon reassembly, the reactor was heated to 150°C using an oil bath. Molten monomers were then mixed by a two paddle stirrer, designed to ensure good mixing in both the vertical and horizontal directions. The temperature of the polymerisation vessel was increased to 240°C at a rate of 10°C min^{-1} and maintained throughout the

reaction. Methanol, an unwanted side-product, was removed by sweeping the polymerisation vessel with a slow stream of dry nitrogen. This helped to drive the equilibrium to high conversion and minimise the effects of oxidative degradation.

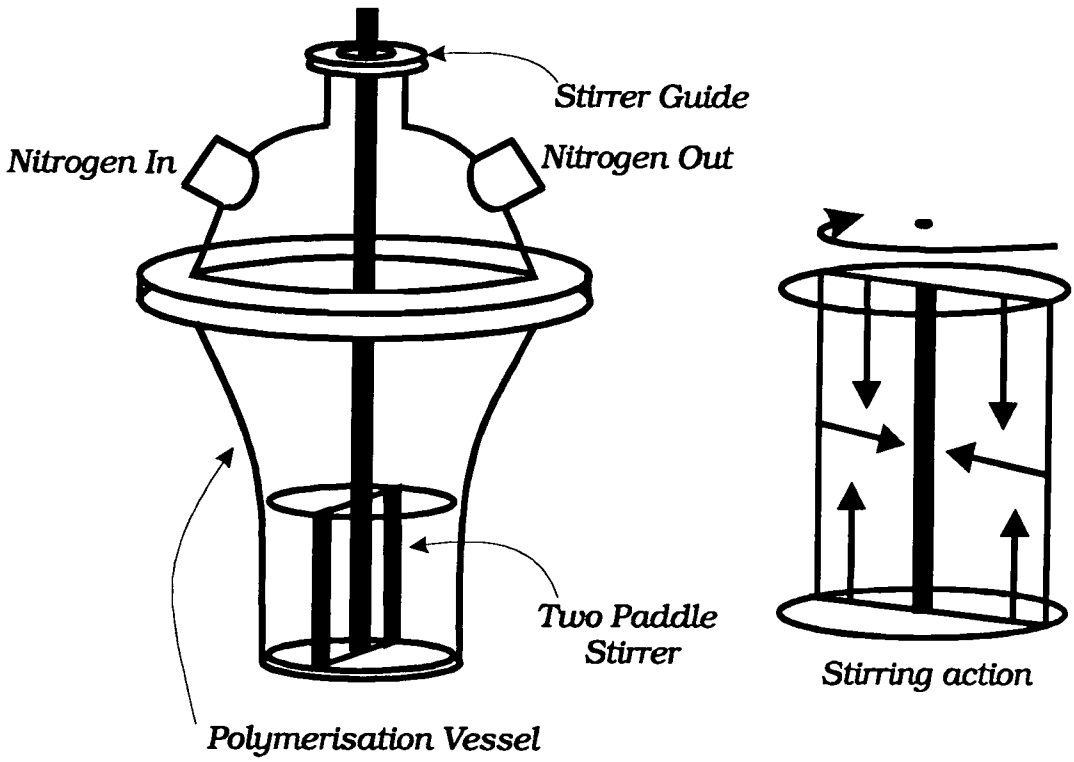

Fig. 2.1 Polymerisation apparatus.

Polymer samples were extracted at intervals of 15, 30 or 60 minutes, depending on the experiment, and analysed using several characterisation techniques. Details of these analyses are given in the relevant sections of this thesis. After obtaining the required samples, the remaining polymer was recovered by solvent extraction. A diamond wheel was used to cut away the bottom half of polymerisation vessel containing the surplus polymer. This section of glass was then broken into manageable pieces using a hammer and the polymer extracted with hot solvent, in a Soxhlet apparatus, over a period of several days; the period of extraction varying with the experiment. Chloroform was used to dissolve the amorphous materials. However, the addition of up to 10% w/w trifluoroacetic acid was required to dissolve the semi-

crystalline polymers. Extracted polymers were reprecipitated into methanol, recovered by filtration and dried under vacuum to a constant weight.

As made samples were isolated as hard solids, which varied in colour from straw yellow at low DP, through orange, to brown at higher molecular weights. However, the coloured impurity remained in solution after reprecipitation and the final recovered materials were white.

2.2.4 Polymer Characterisation

2.2.4.1 IR Spectroscopic Analyses

IR spectra were recorded using conventional KBr discs, which were prepared by grinding the polymer with dry analar KBr and pressing at 10 tons load. The following abbreviations are used in Table 2.1:- ***(a)*** (w, aryl-H C-H stretch), ***(b)*** (w, saturated C-H stretch), ***(c)*** (s, aromatic ester C=O stretch), ***(d)*** (s, aryl-H C-H out of plane vibration), ***(e)*** (s, aryl C=C stretch). Spectra are recorded in the appendices, as indicated in the Table.

Polymer designation: p = *p*-poly(ethylene oxybenzoate) (*p*-PEOB)
m = *m*-poly(ethylene oxybenzoate) (*m*-PEOB)
b = poly(ethylene 5-oxyisophthalate) (5-PEOI)

Polymer Description	Appendix	Comment	*a*	*b*	*c*	*d*	*e*
p	B01-1	Homopolymer	3076	2953	1716	-	1607
m	B02-1	Homopolymer	3072	2959	1717	-	1585
50:50 (m:p)	B03-1	Copolymer	3074	2954	1715	-	1606
b	B04-1	Homopolymer	3088	2953	1725	756	1596
80:20 (b:p)	B05-1	80% Branched	3084	2952	1722	754	1605
60:40 (b:p)	B06-1	60% Branched	3084	2952	1721	754	1606
40:60 (b:p)	B07-1	40% Branched	-	2952	1719	-	1606

continued overleaf

20:80 (b:p)	B08-1	20% Branched	-	-	1717	-	1606
15:75 (b:p)	B09-1	15% Branched	-	-	1713	-	1607
10:90 (b:p)	B10-1	10% Branched	-	-	1718	-	1606
4:96 (b:p)	B11-1	4% Branched	-	2958	1715	-	1606
3:97 (b:p)	B12-1	3% Branched	-	2951	1714	-	1606
2:98 (b:p)	B13-1	2% Branched	-	2952	1711	-	1606
1:99 (b:p)	B14-1	1% Branched	-	2952	1713	-	1606

Table 2.1 IR spectroscopic characterisation.

2.2.4.2 ^{1}H NMR Spectroscopy ($CDCl_3$/TFA)

Assignments of ^{1}H NMR spectra, obtained in $CDCl_3$/TFA solution at 400MHz, are summarised below. This data is recorded as a matter of record and will be analysed and discussed at relevant points in the thesis. Copies of the original data are recorded in the appendices, as indicated in bold script.

***p*-PEOB (B01-2)**, 3.96 (s, variable, $OC\underline{H}_3$), 4.40 (s, 2H, ether-$C\underline{H}_2$), 4.73 (s, 2H, ester-$C\underline{H}_2$), 6.99 (pseudo d, 2H, ^{1}J~8.6Hz, aromatic C-$\underline{H}$), 8.02 (pseudo d, 2H, ^{1}J~8.6Hz, aromatic C-$\underline{H}$); ***m*-PEOB (B02-2)**, 3.97 (s, variable, $OC\underline{H}_3$), 4.37 (s, 2H, ether-$C\underline{H}_2$), 4.72 (s, 2H, ester-$C\underline{H}_2$), 7.17 (m, 1H, aromatic C-$\underline{H}$), 7.36 (m, 1H, aromatic C-$\underline{H}$), 7.59 (s, 1H, aromatic C-$\underline{H}$), 7.66 (m, 1H, aromatic C$\underline{H}$); **5-PEOI (B04-2)**, 3.94 (s, 3H, $OC\underline{H}_3$), 4.40 (s, 2H, ether-$C\underline{H}_2$), 4.72 (s, 2H, ester-$C\underline{H}_2$), 7.79 (s, 2H, aromatic C-$\underline{H}$), 8.26 (s, 1H, aromatic C-$\underline{H}$); **80mole% branched *p*-PEOB (B05-2)**, 3.94 (s, 6.1H, $OC\underline{H}_3$), 4.39 (s, 4.4H, ether-$C\underline{H}_2$), 4.71 (s, 4.6H, ester-$C\underline{H}_2$), 6.93 (s, 1.0H, aromatic C-$\underline{H}$), 7.79 (s, 3.8H, aromatic C-$\underline{H}$), 7.98 (s, 1.0H, aromatic C-$\underline{H}$), 8.27 (s, 2.0H, aromatic C-$\underline{H}$); **60mole% branched *p*-PEOB (B06-2)**, 3.92 (s, variable, $OC\underline{H}_3$), 4.37 (s, 3.1H, ether-$C\underline{H}_2$), 4.69 (s, 3.1H, ester-$C\underline{H}_2$), 6.93 (s, 1.4H, aromatic C-$\underline{H}$), 7.77 (s, 2.0H, aromatic C-$\underline{H}$), 7.97 (s, 1.4H, aromatic C-$\underline{H}$), 8.27 (s, 1.0H, aromatic C-$\underline{H}$); **40mole% branched *p*-PEOB (B07-2)**, 3.96 (s, variable, $OC\underline{H}_3$), 4.38 (s, 4.6H, ether-$C\underline{H}_2$), 4.72 (s, 4.7H, ester-$C\underline{H}_2$), 6.95 (s, 3.0H, aromatic C-$\underline{H}$), 7.81 (s, 2.0H, aromatic C-$\underline{H}$), 7.99 (s, 3.0H, aromatic C-$\underline{H}$), 8.30 (s, 1.0H, aromatic C-$\underline{H}$); **20mole% branched *p*-PEOB (B08-2)**, 3.96 (s, variable, $OC\underline{H}_3$), 4.37 (s, 11.1H, ether-$C\underline{H}_2$), 4.71 (s, 11.2H,

ester-C$\underline{H}_2$), 6.96 (s, 9.6H, aromatic C-$\underline{H}$), 7.82 (s, 2.5H, aromatic C-$\underline{H}$), 8.00 (s, 9.2H, aromatic C-$\underline{H}$), 8.31 (s, 1.0H, aromatic C-$\underline{H}$); **15mole% branched *p*-PEOB (B09-2)**, 3.95 (s, variable, OC$\underline{H}_3$), 4.34 (s, 12.7H, ether-C$\underline{H}_2$), 4.70 (s, 13.7H, ester-C$\underline{H}_2$), 6.96 (s, 13.8H, aromatic C-$\underline{H}$), 7.81 (s, 2.1H, aromatic C-$\underline{H}$), 8.00 (s, 13.4H, aromatic C-$\underline{H}$), 8.32 (s, 1.0H, aromatic C-$\underline{H}$); **12.5mole% branched *p*-PEOB (B09-b-2)**, 3.95 (s, variable, OC$\underline{H}_3$), 4.34 (s, 12.7H, ether-C$\underline{H}_2$), 4.70 (s, 13.7H, ester-C$\underline{H}_2$), 6.96 (s, 13.8H, aromatic C-$\underline{H}$), 7.81 (s, 2.1H, aromatic C-$\underline{H}$), 8.00 (s, 13.4H, aromatic C-$\underline{H}$), 8.32 (s, 1.0H, aromatic C-$\underline{H}$); **10mole% branched *p*-PEOB (B10-2)**, 3.94 (s, variable, OC$\underline{H}_3$), 4.37 (s, 18.9H, ether-C$\underline{H}_2$), 4.69 (s, 19.1H, ester-C$\underline{H}_2$), 6.96 (pseudo d, 17.0H, ^{1}J~8.2Hz, aromatic C-$\underline{H}$), 7.81 (s, 2.0H, aromatic C-$\underline{H}$), 8.00 (pseudo d, 17.3H, ^{1}J~8.2Hz, aromatic C-$\underline{H}$); **4mole% branched *p*-PEOB (B11-2)**, 3.96 (s, variable, OC$\underline{H}_3$), 4.37 (s, 41.1H, ether-C$\underline{H}_2$), 4.70 (s, 41.6H, ester-C$\underline{H}_2$), 6.97 (pseudo d, 41.1H, ^{1}J~8.2Hz, aromatic C-$\underline{H}$), 7.81 (s, 2.1H, aromatic C-$\underline{H}$), 8.00 (pseudo d, 41.1H, ^{1}J~8.2Hz, aromatic C-$\underline{H}$), 8.32 (s, 1.0H, aromatic C-$\underline{H}$); **3mole% branched *p*-PEOB (B12-2)**, 3.95 (s, variable, OC$\underline{H}_3$), 4.38 (s, 48.5H, ether-C$\underline{H}_2$), 4.71 (s, 49.5H, ester-C$\underline{H}_2$), 6.97 (pseudo d, 48.5H, ^{1}J~8.8Hz, aromatic C-$\underline{H}$), 7.81 (s, 2.0H, aromatic C-$\underline{H}$), 8.01 (pseudo d, 48.0H, ^{1}J~8.8Hz, aromatic C-$\underline{H}$), 8.32 (s, 0.8H, aromatic C-$\underline{H}$); **2mole% branched *p*-PEOB (B13-2)**, 3.95 (s, variable, OC$\underline{H}_3$), 4.38 (s, 62.0H, ether-C$\underline{H}_2$), 4.71 (s, 62.0H, ester-C$\underline{H}_2$), 6.97 (pseudo d, 72.5H, ^{1}J~8.2Hz, aromatic C-$\underline{H}$), 7.83 (s, 2.0H, aromatic C-$\underline{H}$), 8.01 (pseudo d, 71.0H, ^{1}J~8.2Hz, aromatic C-$\underline{H}$), 8.32 (s, 1.0H, aromatic C-$\underline{H}$); **1mole% branched *p*-PEOB (B14-2)**, 3.96 (s, variable, OC$\underline{H}_3$), 4.38 (s, 134.0H, ether-C$\underline{H}_2$), 4.71 (s, 134.0H, ester-C$\underline{H}_2$), 6.97 (pseudo d, 140.0H, ^{1}J~8.6Hz, aromatic C-$\underline{H}$), 7.83 (s, 2.0H, aromatic C-$\underline{H}$), 8.01 (pseudo d, 142.0H, ^{1}J~8.6Hz, aromatic C-$\underline{H}$), 8.32 (s, 1.0H, aromatic C-$\underline{H}$).

2.2.4.3 ^{1}H NMR Spectroscopy ($CDCl_3$)

Assignments of ^{1}H NMR spectra, obtained in $CDCl_3$ solution at 400MHz, are summarised overleaf. Copies of the original data are recorded in the appendices, as indicated.

5-PEOI (B04-3), 3.89 (s, 1.6H, OC$\underline{H}_3$), 4.37 (s, 1.9H, ether-C$\underline{H}_2$), 4.68 (s, 2H, ester-C$\underline{H}_2$), 7.74 (s, 2H, aromatic C-$\underline{H}$), 8.24 (s, 0.8H, aromatic C-$\underline{H}$);

80mole% branched *p*-PEOB (B05-3), 3.90 (s, 6.4H, $OC\underline{H}_3$), 4.37 (s, 4.9H, ether-$C\underline{H}_2$), 4.69 (s, 5.2H, ester-$C\underline{H}_2$), 6.92 (s, 1.0H, aromatic C-H), 7.76 (s, 4.2H, aromatic C-H), 7.97 (s, 1.1H, aromatic C-H), 8.26 (s, 2.1H, aromatic C-H); **60mole% branched *p*-PEOB (B06-3)**, 3.89 (s, variable, $OC\underline{H}_3$), 4.35 (s, 3.5H, ether-$C\underline{H}_2$), 4.67 (s, 3.6H, ester-$C\underline{H}_2$), 6.91 (s, 1.5H, aromatic C-H), 7.76 (s, 2.2H, aromatic C-H), 7.97 (s, 1.4H, aromatic C-H), 8.26 (s, 1.0H, aromatic C-H); **40mole% branched *p*-PEOB (B07-3)**, 3.91 (s, variable, $OC\underline{H}_3$), 3.93 (s, variable, $OC\underline{H}_3$), 3.98 (s, variable, $C\underline{H}_2OH$, monomer), 4.13 (s, variable, $ArOC\underline{H}_2$, monomer), 4.36 (s, 4.5H, ether-$C\underline{H}_2$), 4.69 (d, 4.6H, ^1J=15.6Hz, ester-$C\underline{H}_2$), 6.96 (s, 3.1H, aromatic C-H), 7.79 (s, 2.1H, aromatic C-H), 8.01 (s, 3.1H, aromatic C-H), 8.31 (s, 1.0H, aromatic C-H); **20mole% branched *p*-PEOB (B08-3)**, 3.88 (s, variable, $OC\underline{H}_3$), 4.33 (s, 10.5H, ether-$C\underline{H}_2$), 4.64 (s, 10.4H, ester-$C\underline{H}_2$), 6.93 (s, 8.4H, aromatic C-H), 7.78 (s, 2.3H, aromatic C-H), 7.99 (s, 8.2H, aromatic C-H), 8.29 (s, 1.0H, aromatic C-H); **15mole% branched *p*-PEOB (B09-3)**, 3.89 (s, variable, $OC\underline{H}_3$), 3.93 (s, variable, $OC\underline{H}_3$), 3.99 (s, variable, $C\underline{H}_2OH$, monomer), 4.14 (s, variable, $ArOC\underline{H}_2$, monomer), 4.34 (s, 11.0H, ether-$C\underline{H}_2$), 4.65 (s, 11.5H, ester-$C\underline{H}_2$), 6.94 (s, 11.0H, aromatic C-H), 7.79 (s, 1.8H, aromatic C-H), 8.00 (s, 10.8H, aromatic C-H), 8.31 (s, 1.0H, aromatic C-H).

2.2.4.4 ^{13}C NMR Spectroscopy ($CDCl_3$/TFA)

Assignments of ^{13}C NMR spectra, obtained in $CDCl_3$/TFA solution at 100MHz, are summarised below. Copies of the original data are recorded in the appendices, as indicated.

TFA; 110.2; 113.0; 115.9; 118.7 ($\underline{C}F_3$, ^1J=280Hz), 159.6; 160.0; 160.4; 160.9 (TFA $\underline{C}$=O, ^2J=40Hz)

***p*-PEOB (B01-4)**, 64.0; 66.0 (alkyl-$\underline{C}H_2$), 114.6; 132.3 (aromatic $\underline{C}$-H), 121.5 (aromatic $\underline{C}$-$COOCH_2$-), 163.1 (aromatic $\underline{C}$-O), 168.7 ($\underline{C}$=O); ***m*-PEOB (B02-4)**, 64.1; 65.9 (alkyl-$\underline{C}H_2$), 115.1; 121.0; 122.; 129.7 (aromatic $\underline{C}$-H), 130.2 (aromatic $\underline{C}$-$COOCH_2$-), 158.2 (aromatic $\underline{C}$-O), 168.1 ($\underline{C}$=O); **5-PEOI (B04-4)**, 53.1 ($COO\underline{C}H_3$), 64.0; 66.5 (alkyl-$\underline{C}H_2$), 120.6; 123.9 (aromatic $\underline{C}$-H), 131.5; 131.8 (aromatic $\underline{C}$-$COOCH_2$-), 158.8 (aromatic $\underline{C}$-O), 166.2; 167.0 ($\underline{C}$=O); **80mole% branched *p*-PEOB (B05-4)**, 52.9; 53.2 ($COO\underline{C}H_3$), 63.7; 64.1; 65.7; 65.9; 66.1; 66.5; 66.7 (alkyl-$\underline{C}H_2$),

114.6; 120.6; 132.2; 132.3 (aromatic C-H), 123.9; 131.5; 131.7 (aromatic C-$COOCH_2$), 158.8; 158.9; 162.8; 162.9 (aromatic C-O), 166.2; 167.1 (C=O); **60mole% branched *p*-PEOB (B06-4)**, 52.8; 53.1 ($COOCH_3$), 63.6; 64.0; 65.2; 65.8; 65.9; 66.1; 66.3; 66.6; 66.7 (alkyl-CH_2), 114.6; 120.6; 123.9; 132.2; 132.3 (aromatic C-H), 122.3; 122.6; 131.6; 131.8 (aromatic C-$COOCH_2$-), 158.8; 158.9; 162.8; 162.9; 163.0 (aromatic C-O), 166.1; 167.0; 167.5; 168.6 (C=O); **40mole% branched *p*-PEOB (B07-4)**, 52.6; 52.9 ($COOCH_3$), 61.4; 63.3; 63.8; 65.0; 65.6; 65.8; 66.0; 66.3; 66.5; 68.4 (alkyl-CH_2), 114.3; 120.3; 123.7; 132.2; 132.3 (aromatic C-H), 122.0; 122.3; 131.6; 131.8 (aromatic C-$COOCH_2$-), 158.5; 158.6; 162.5; 162.6; 162.8 (aromatic C-O), 165.8; 166.7; 167.3; 168.3 (C=O); **20mole% branched *p*-PEOB (B08-4)**, 52.7; 53.0 ($COOCH_3$), 61.6; 63.5; 63.9; 65.2; 65.9; 66.1; 66.3; 66.6; 66.8; 68.8 (alkyl-CH_2), 114.6; 120.5; 120.6; 123.9; 124.0; 132.1; 132.2 (aromatic C-H), 122.3; 122.4; 122.7; 131.6; 131.9 (C-$COOCH_2$-), 158.8; 158.9; 162.7; 162.8; 163.0 (aromatic C-O), 166.0; 166.8; 167.3; 168.3 (C=O); **15mole% branched *p*-PEOB (B09-4)**, 53.1 ($COOCH_3$), 63.8; 64.2; 66.0; 66.2 (alkyl-CH_2), 114.4; 132.0; 132.2 (aromatic C-H), 121.6; 131.1 (aromatic C-$COOCH_2$-), 163.0 (aromatic C-O), 168.4 (C=O); **12.5mole% branched *p*-PEOB (B09-b-4)**, 53.0 ($COOCH_3$), 63.8; 64.1; 65.8; 66.0 (alkyl-CH_2), 114.4; 132.0; 132.2 (aromatic C-H), 121.7; 131.2 (aromatic C-$COOCH_2$-), 162.8; 163.0 (aromatic C-O), 166.6, 168.0 (C=O); **10mole% branched *p*-PEOB (B10-4)**, 52.8 ($COOCH_3$), 63.6; 65.3; 65.9; 66.3 (alkyl-CH_2), 114.6; 120.4, 132.2; 132.3 (aromatic C-H), 122.2 (aromatic C-$COOCH_2$-), 162.9; 163.0 (aromatic C-O), 166.2; 167.6 (C=O); **4mole% branched *p*-PEOB (B11-4)**, 53.1 ($COOCH_3$), 64.0; 65.1; 65.8; 66.0 (alkyl-CH_2), 114.5; 132.2; 132.3 (aromatic C-H), 121.5; 121.8 (aromatic C-$COOCH_2$-), 163.1 (aromatic C-O), 168.6 (C=O); **3mole% branched *p*-PEOB (B12-4)**, 53.0 ($COOCH_3$), 63.8; 65.1; 65.7; 66.0 (alkyl-CH_2), 114.5; 132.1; 132.2 (aromatic C-H), 121.6 (aromatic C-$COOCH_2$-), 162.8; 163.0 (aromatic C-O), 168.3 (C=O); **1mole% branched *p*-PEOB (B14-4)**, 53.2 ($COOCH_3$), 63.9; 65.3; 65.9; 66.2 (alkyl-CH_2), 114.7; 132.4 (aromatic C-H), 121.9 (aromatic C-$COOCH_2$-), 163.2 (aromatic C-O), 168.4 (C=O).

2.2.4.5 ^{13}C NMR Spectroscopy ($CDCl_3$)

Assignments of ^{13}C NMR spectra, obtained in $CDCl_3$ solution at 100MHz, are summarised below. Copies of the original data are recorded in the appendices, as indicated.

5-PEOI (B04-5), 52.3 (C-$COOCH_2$-), 63.3; 66.2 (alkyl-CH_2), 119.7; 119.9; 123.3 (aromatic C-H), 131.3; 131.7 (aromatic C-$COOCH_2$-), 158.4 (aromatic C-O), 165.1, 165.7 (C=O); **80mole% branched *p*-PEOB (B05-5)**, 52.1; 52.7 (C-$COOCH_2$-), 63.1; 63.7; 66.1; 66.6; 66.9 (alkyl-CH_2), 114.4; 120.1; 120.3; 123.7; 132.1 (aromatic C-H), 120.1; 131.7; 131.8 (aromatic C-$COOCH_2$-), 158.7; 162.3; 162.6 (aromatic C-O), 165.5; 166.1 (C=O); **60mole% branched *p*-PEOB (B06-5)**, 52.1; 52.7 (C-$COOCH_2$-), 61.4; 63.1; 63.7; 66.1; 66.4; 66.6; 66.9 (alkyl-CH_2), 114.4; 122.8; 123.3; 123.7; 123.9; 132.1 (aromatic C-H), 120.1; 120.3; 131.5; 131.7 (aromatic C-$COOCH_2$-), 158.7; 158.9; 162.4; 162.6; 162.7 (aromatic C-O), 165.5; 166.2; 166.9 (C=O); **40mole% branched *p*-PEOB (B07-5)**, 51.9; 52.4 (C-$COOCH_2$-), 61.4; 62.7; 63.4; 65.8; 66.1; 66.3; 66.6; 69.2; 70.0 (alkyl-CH_2), 114.1; 120.0; 123.4; 131.8 (aromatic C-H), 122.5; 123.0; 131.5; 131.6 (aromatic C-$COOCH_2$-), 158.5; 158.6; 162.2; 162.3; 162.5 (aromatic C-O), 165.3; 166.0; 166.9 (C=O); **20mole% branched *p*-PEOB (B08-5)**, 52.2; 52.7 (C-$COOCH_2$-), 61.5; 63.0; 63.7; 66.1; 66.4; 66.6; 66.9; 69.6; (alkyl-CH_2), 114.5; 120.5; 123.9; 131.9 (aromatic C-H), 122.8; 123.2.; 132.1; 131.6 (aromatic C-$COOCH_2$-), 162.7 (aromatic C-O), 165.6; 166.3; 167.0 (C=O).

2.2.4.6 ^{1}H NMR Spectroscopy (DMSO-d_6)

Assignments of ^{1}H NMR spectra obtained in DMSO-d_6 solution at 400MHz and 95°C are summarised below. Copies of the original data are recorded in the appendices, as indicated.

***p*-PEOB (B01-6)**, 3.77 (s, monomer, alcohol-CH_2), 3.79 (s, variable, OCH_3), 4.07 (s, monomer, ether-CH_2), 4.33 (s, 2H, ether-CH_2), 4.55 (s, 2H, ester-CH_2), 7.04 (s, 2H, aromatic C-H), 7.86 (s, 2H, aromatic C-H); ***m*-PEOB (B02-6)**, 3.71 (s, monomer, alcohol-CH_2), 3.82 (s, variable, OCH_3), 4.03 (s, monomer, ether-CH_2), 4.36 (s, 2H, ether-CH_2), 4.57 (s, 2H, ester-CH_2), 7.21 (s, 1H, aromatic C-H), 7.36 (s, 1H, aromatic C-H), 7.49 (m, 2H, aromatic C-H).

2.2.4.7 ^{13}C NMR Spectroscopy (DMSO-d_6)

The assignment of the ^{13}C NMR spectrum obtained in DMSO-d_6 solution at 100MHz and 95°C is summarised below. A copy of the original data is recorded in the appendix, as indicated.

***m*-PEOB (B02-7)**, 62.9; 66.0 (alkyl-$\underline{C}H_2$), 114.9; 119.6; 121.4; 129.3 (aromatic $\underline{C}$-H), 130.7 (aromatic $\underline{C}$-$COOCH_3$), 158.0 (aromatic $\underline{C}$-O), 164.9 ($\underline{C}$=O).

2.3 References

1. Stainton N.M., PhD Thesis, University of Durham, 1994
2. Yoshino T., Nagata Y., Itoh E., Hashimoto T., Terashima S., *Tetrahedron*, **53(30)**, (1997), 10239
3. Feast W.J., Stainton N.M., *J. Mater. Chem.*, **5(3)**, (1995), 405
4. Patent, *Chem. Abs.*, **72**, 90052

Chapter 3

Linear polymers of meta and para poly(ethylene oxybenzoate)

3.1 Introduction to linear polyesters and history of *p*-PEOB

p-Poly(ethylene oxybenzoate), *p*-PEOB, is similar in some aspects of structure and properties to poly(ethylene terephthalate), PET. Discovered by Whinfield et al[1] in 1946, *p*-PEOB did not find commercial application for another two decades due to difficulties in achieving high molecular weight and reproducible properties. The research and development efforts of the Kokoku Rayon and Pulp Company, in 1956, generated significant industrial interest and paved the way to the eventual commercial production of *p*-PEOB in 1967.[2] Mitsubishi Chemical Industries assisted the development of raw material manufacture throughout 1958, solving many of the problems associated with industrial-scale monomer synthesis. However, it was the expertise of the Daiwa Spinning Company in 1962, which was instrumental in the development of textile manufacturing techniques. A partnership of these three companies, under the name Polyesterether Development Company, became responsible for the production and marketing of 'A-Bell', a commercial grade *p*-PEOB fibre.[3] In the early seventies, commercial production was moved to a company called 'A-Tell';[4] a joint venture between Unitika, itself an amalgamation of Nichibo and Nippon Rayon, and Mitsubishi Chemical Industries.

Early successes saw fibre production rise steadily and in 1974 150 tons per month were being spun for use, primarily, as filament yarn. However, a subsequent rise in production costs of *p*-hydroxybenzoic acid, the principal raw material in the synthesis of *p*-PEOB, and the fall in costs of rival materials such as PET, led to the eventual collapse of the *p*-PEOB textile market. The requirement for chemically resistant canvas and filter materials in paper mills sustained *p*-PEOB production for a while longer. However, with significantly diminished capacity the cessation of commercial production was inevitable.

The manufacturing process, as developed by the Polyesterether Development Company, for large-scale *p*-PEOB production[2] is summarised in Figure 3.1. The principal raw material, *p*-hydroxybenzoic acid, is obtained by the Kolbe-Schmidt reaction between potassium-phenolate and carbon dioxide. This is further reacted with ethylene oxide, in aqueous solution, to yield 4-(2-hydroxyethoxy)benzoic acid. After refining and drying, the product is dissolved in methanol and esterified in the presence

of an acidic catalyst. Monomer is then isolated by vacuum distillation and, under the conditions of high vacuum and in the presence of a catalyst, polymer is produced by intensive stirring at 250-260°C. Methanol is removed by distillation as it is formed and heating continues until high polymer is obtained.

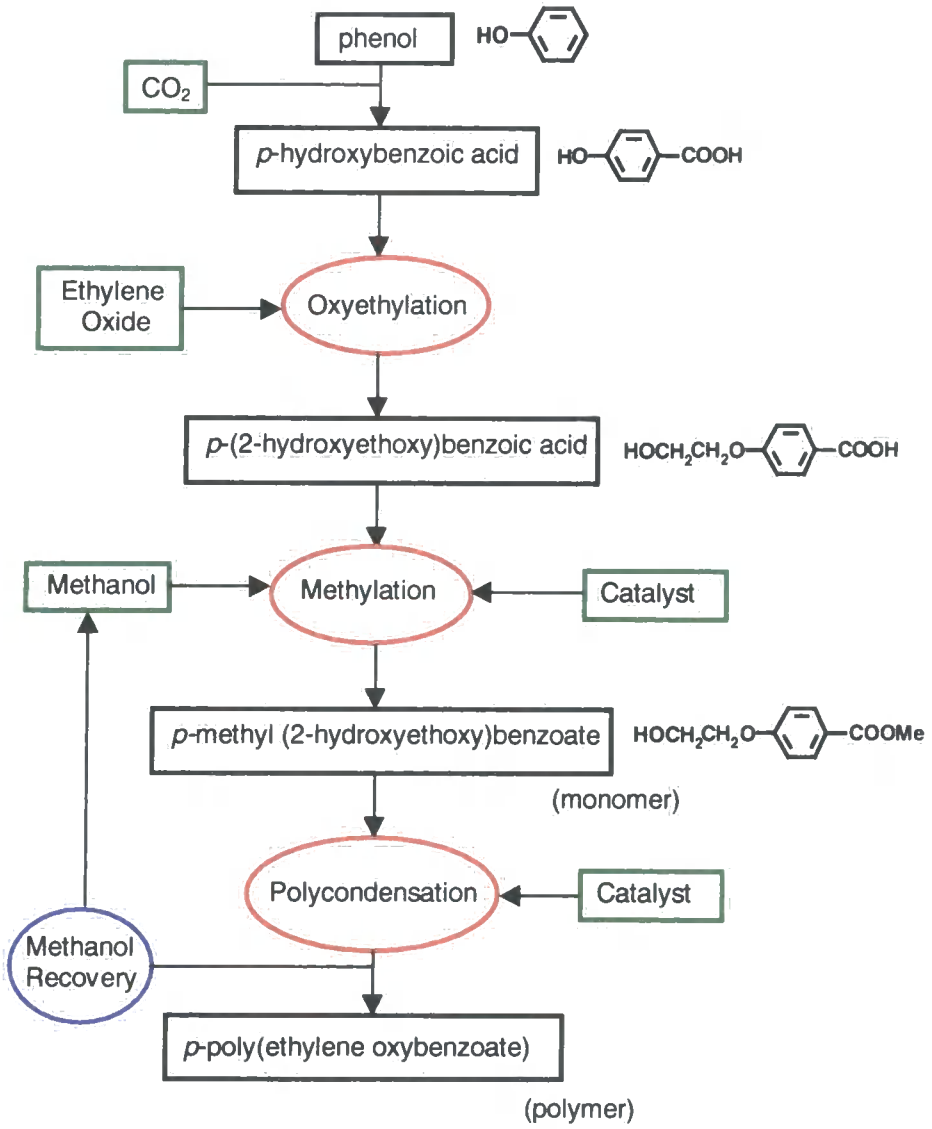

Fig. 3.1 *p*-PEOB: The manufacturing process as developed by the Polyesterether Development Company.[2]

The crystalline structure of *p*-PEOB, as studied by Korematzu et al,[5] was found to consist of two crystalline forms, designated as α and β. Transformations between these crystalline forms were reported by the author, as outlined in Figure 3.3.

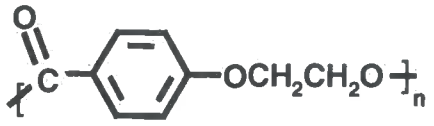

Fig. 3.2 The *p*-PEOB repeat unit.

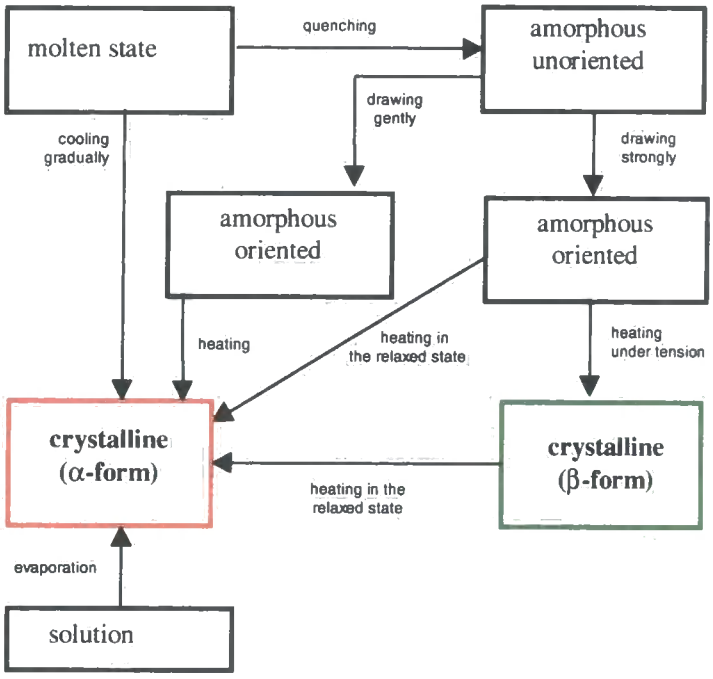

Fig. 3.3 Methods of crystalline transformation described by Korematzu.[5]

Drawn fibres, heat treated under tension and thermally stabilised in the relaxed state were reported as having a fibre period of 15.4Å, determined by X-ray diffraction, and to exist almost exclusively in the α–crystalline form. By contrast, *p*-PEOB fibres drawn and heat treated under tension revealed complicated patterns of α-crystallites superposed over a second crystalline form. This second pattern, called the β-crystal, was postulated to correspond to a straightened 'zig-zag' configuration with a fibre period of 19.0Å in contrast to the α-form, which was assigned the more coiled and contracted 'cis' arrangement.

Both α and β crystallites coexist in the 'as made' material, the ratio of each being controlled by thermal and mechanical treatment of the polymer. A relative increase in β-crystallinity is achieved by drawing and heating under tension, however,

the α-form dominates in the relaxed state, i.e. when no mechanical work has been undertaken.

The following figures, abstracted from two related publications,[2, 4] summarise aspects of *p*-PEOB behavior in relation to some better-known materials.

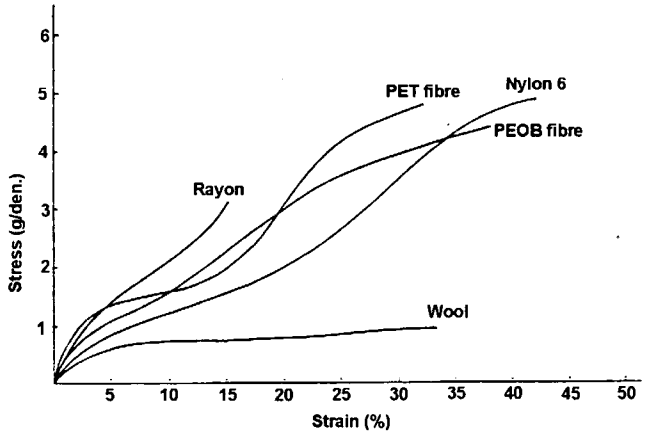

Fig. 3.4 Stress-strain curves.[2]

Stress-strain curves of some common fibres, including *p*-PEOB, are shown in Figure 3.4. In the elastic recovery region, below 5% strain, the Youngs modulus of *p*-PEOB appears midway between PET and Nylon 6. Values of 500-900 kg/mm^2 for *p*-PEOB are similar to those reported for the Youngs modulus of silk (650-1200 kg/mm^2).

Fibres of *p*-PEOB were reported as having remarkable elasticity. In comparison to PET, *p*-PEOB was found to be more elastic when stretched excessively or repeatedly and showed least permanent deformation, see Figure 3.5; evidence perhaps, for why *p*-PEOB was so well suited for use in fitted fabrics. In addition, its resistance to alkali and acid, combined with strong weathering resistance, made the use of *p*-PEOB fibres possible for both industrial and commercial fabrics; see Figure 3.6. Even after prolonged exposure to UV radiation, *p*-PEOB fibres did not discolour, become brittle or lose significant mechanical strength; Figure 3.7.

The effect upon relative tenacity of fibres exposed to air at various temperatures is shown in Figure 3.8. In this respect, *p*-PEOB showed very little deterioration over

the temperature range indicated. However, irreversible changes occur at the molecular level at 150°C, which result in the loss of the material's soft delicate touch. Consequently, special care must be taken not to exceed this temperature whilst ironing. Nevertheless, the fabric's natural resistance to creasing meant that it rarely required ironing.

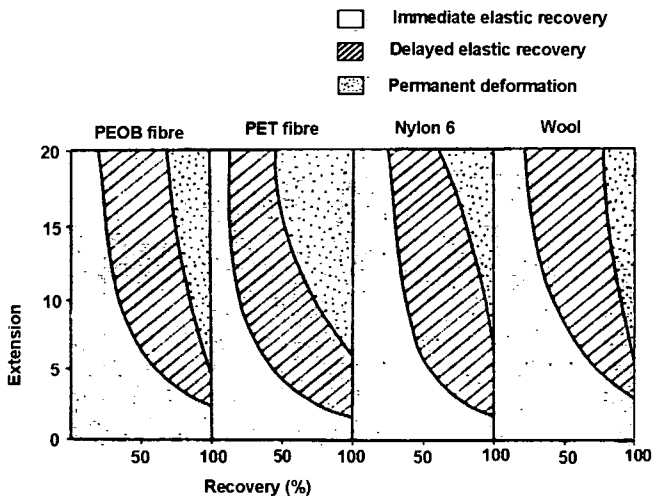

Fig. 3.5 Elastic recovery as a function of extension.[2]

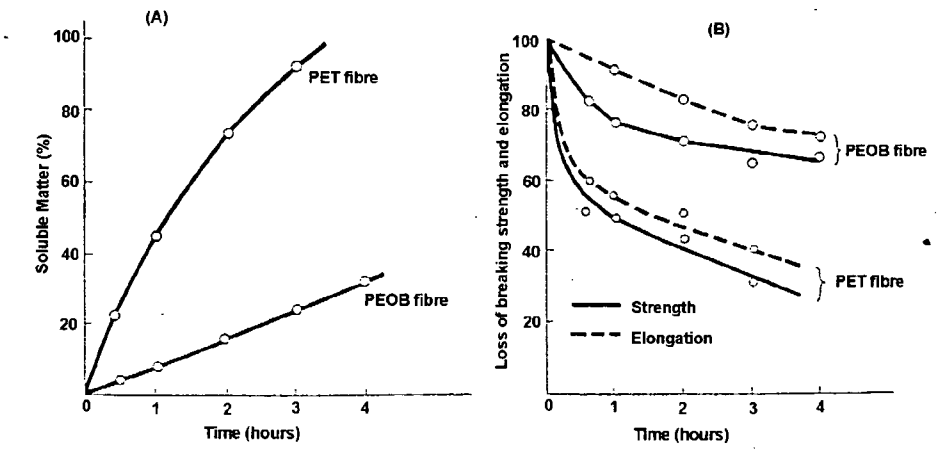

Fig. 3.6 Effects of exposing p-PEOB and PET to boiling 20% NaOH(aq).[2]

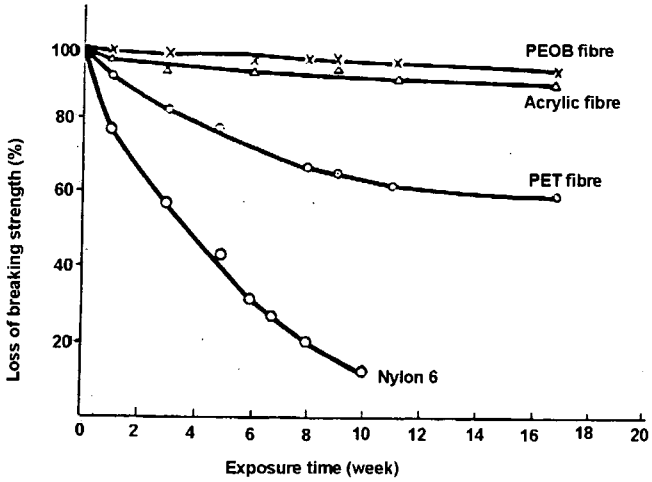

Fig. 3.7 Effects of prolonged exposure to UV radiation.[2]

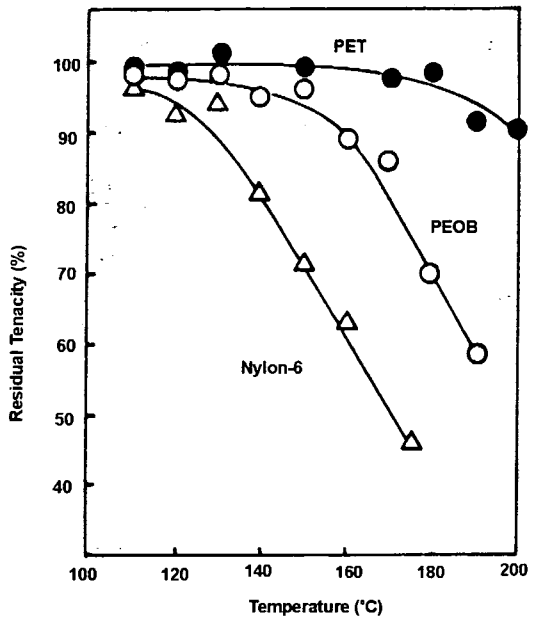

Fig. 3.8 Tenacity measured as a function of temperature.[4]

p-PEOB was reputed to have many other advantages, e.g. boiling it in water converted the material into a high-density crepe like fabric. This was not easily achieved with PET. Fibres were resistant to abrasion, not highly hygroscopic or prone to large electrostatic build-up. Furthermore, they possessed excellent wash and wear characteristics and were more easily dyed than PET fibres, indicated in Figure 3.9.

Under identical conditions, *p*-PEOB fibres would require only 15 minutes at 100°C to reach the same extent of dye adsorption as PET fibres after five hours.

p-PEOB was also suited to use in blends; complementing materials by adding durability and functionality. Many beautifully spun fabrics demonstrating excellent performance, especially in dyeing and finishing, were produced by blending *p*-PEOB with wool, cotton and rayon.

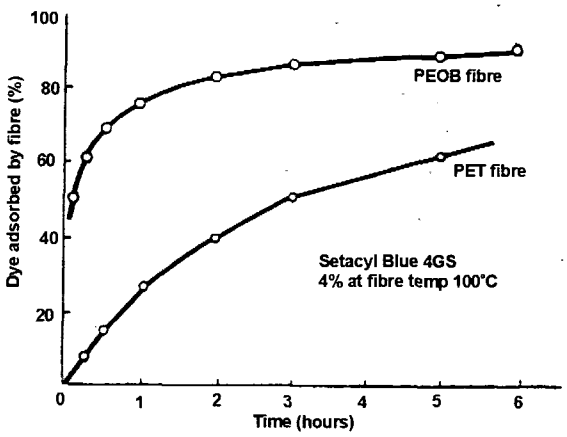

Fig. 3.9 Dyeability.[2]

Data abstracted from the aforementioned publications have been used to compare *p*-PEOB film with commercial grade PET. Although somewhat dated, the information reveals several differences between the mechanical properties of the two materials. *p*-PEOB exhibits significantly greater heat shrinkage than does PET, greater elongation and reduced tensile strength. However, in terms of impact strength *p*-PEOB is superior. Mechanical properties of 25μm thick biaxially drawn films of PET and *p*-PEOB are listed in Table 3.1.

	p-PEOB	PET
Tensile strength (kg/mm^2) [200mm/min]	18	22
Elongation at break (%) [200mm/min]	127	113
Thermal shrinkage (%) [in hot air, 150°C x 24h]	3.8	2.8
Missile impact strength (kg cm)	31	25
Light transmittance (%) [560nm]	92	89

Table 3.1 General characteristics of 25μm film.[4]

Gas	*p*-PEOB [ml m^{-2} h^{-1} atm^{-1}]	PET [ml m^{-2} h^{-1} atm^{-1}]
Nitrogen	0.10	0.56
Oxygen	3.49	2.90
Carbon dioxide	7.43	12.7

Table 3.2 Gas permeability of a 25μm film.[4]

Blow-moulded PET bottles and biaxially drawn films find extensive use in the packaging industry. However, although PET is one of the few materials exploited commercially in the containment of carbonated drinks, to lower carbon dioxide permeability to acceptable levels requires a considerable thickness of film. A special grade of PET material is manufactured for this purpose. Results collected in Table 3.2 indicate that the permeability of *p*-PEOB to carbon dioxide and nitrogen is significantly lower than PET. Consequently, thinner films of *p*-PEOB would suffice to provide the same level of containment. However, as *p*-PEOB is no longer commercially available it is unlikely to ever be developed for use in the packaging industry.

The threat to molecular weight and mechanical properties of PET from hydrolysis is significant. Consequently, to lessen the effects of hydrolysis, PET is routinely dried before processing. By contrast, *p*-PEOB is reported to be more resistant to the effects of hydrolysis. Figure 3.10 shows the changes in intrinsic viscosity of moulded films of approximately 400μm thickness, as measured in *o*-chlorophenol at 25°C, after soaking in boiling water over a period of days.

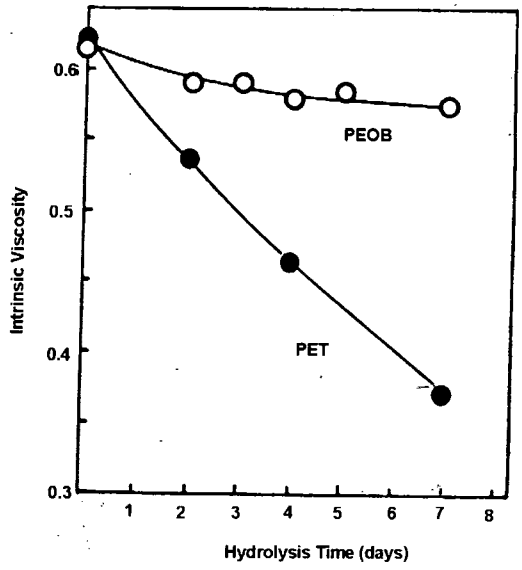

Fig. 3.10 Hydrolysis of film, thickness 400μm, in boiling water.[4] (*o*-chlorophenol @ 25°C)

The results indicate a marked deterioration in the PET sample over a period of three days, whereas after eight days, *p*-PEOB shows only marginal deterioration.

3.2 Molecular weight determination

3.2.1 Background

High field NMR spectroscopy has been used to provide structural and molecular weight information about linear and branched *p*-PEOB materials. Initial experiments showed that a few percent by volume, of TFA in $CDCl_3$, was sufficient to solubilise semi-crystalline polymers. Furthermore, as the quantity of acid required was relatively small, non-deuterated TFA was used as the NMR cosolvent.

Many crystalline polyesters, including PET and *p*-PEOB, show poor solubility in common organic solvents. As a consequence, investigators have resorted to using halogenated solvents, in spite of the hazards involved. Solvents such as chlorinated-phenols, strong organic acids such as trifluoroacetic acid (TFA) and dichloroacetic acid (DCA), and the powerful but toxic hexafluoroisopropanol (HFIP) are all included in

this list. Due to biological and environmental hazards, rigorous protocols must be adopted when handling, using or disposing of solutions containing any of the above.

In the absence of intramolecular cyclisation, unreacted end groups may be used to determine number average molecular weight, provided they can be differentiated from other groups in the polymer. NMR spectroscopy is one technique, which is able to make this distinction. Information given below and in Section 3.2.2 explains how ^{1}H NMR end group counting has been applied to the homopolymers of para and meta poly(ethylene oxybenzoate).

The peaks used to calculate the number average molecular weight of *p*-PEOB were the methyl ester end group (e) and methylene CH_2 groups (c) and (d), as indicated in Figure 3.11. In addition, the peaks used to calculate the number average molecular weight of *m*-PEOB samples are shown in Figure 3.12. These were, the methyl ester end group (g) and methylene CH_2 groups (e) and (f). The calculation of molecular weight is discussed in detail in Section 3.2.2.

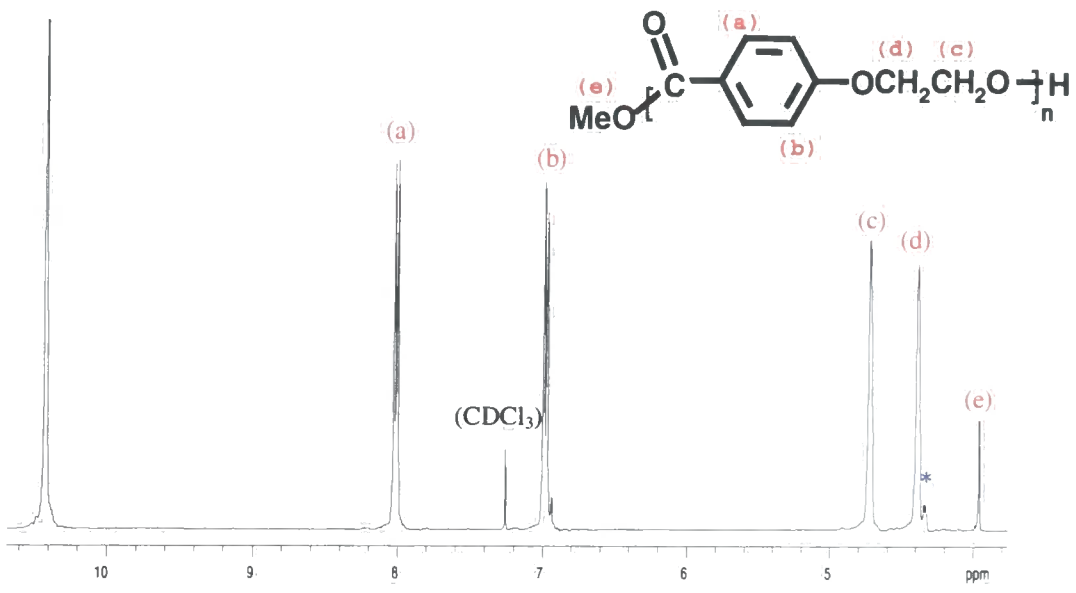

Fig. 3.11 400MHz ^{1}H NMR spectrum of *p*-PEOB ($CDCl_3$/ TFA, 400MHz, δ).

* –CH_2 groups (monomer – TFA capped)

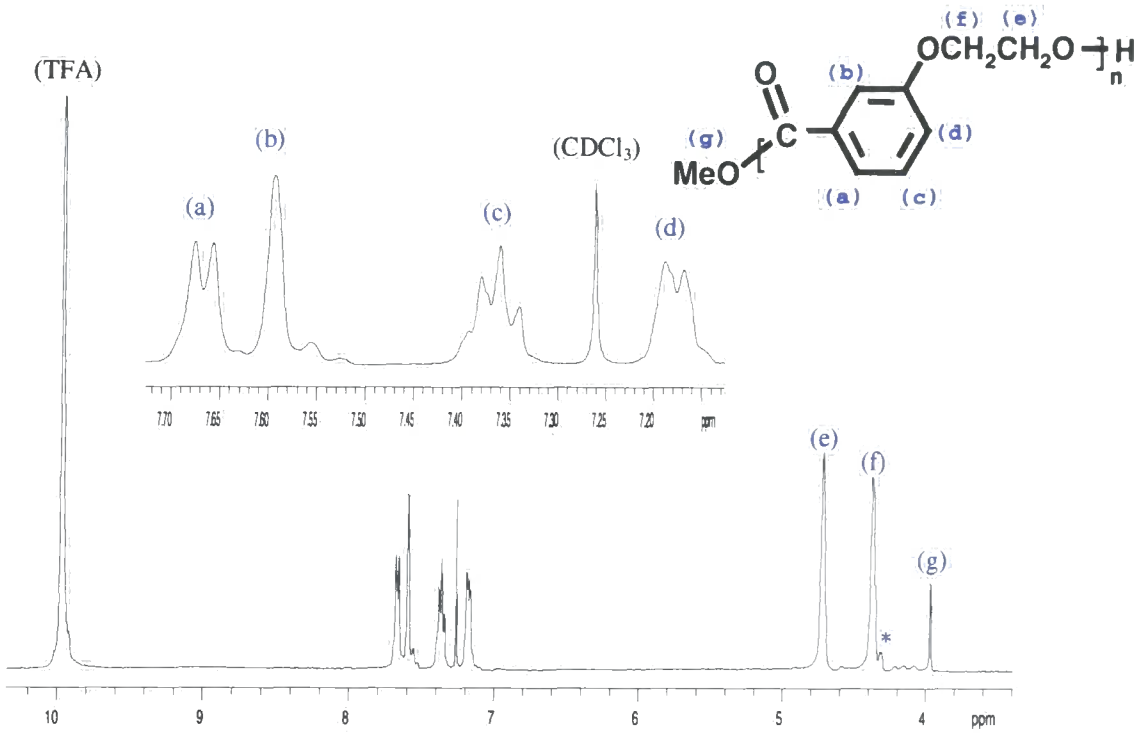

Fig. 3.12 400MHz ^{1}H NMR spectrum of *m*-PEOB ($CDCl_3$/ TFA, 400MHz, δ).

* $-CH_2$ groups (monomer – TFA capped)

3.2.2 Mn Calculations

Number average molecular weights of linear PEOB homopolymers were calculated as shown here for the para isomer. However, the same general principles also apply to samples of *m*-PEOB.

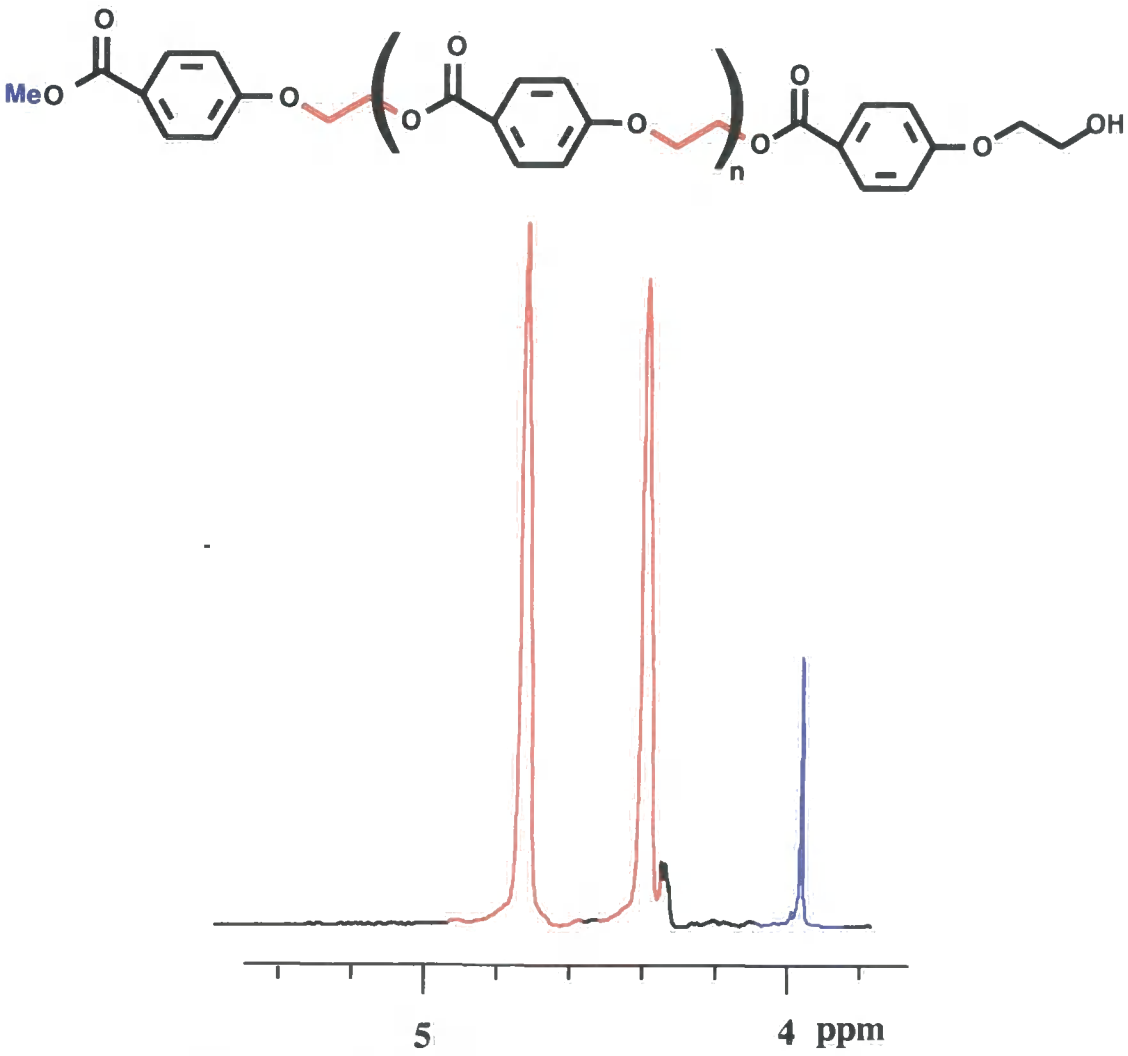

Fig. 3.13 400MHz ^{1}H NMR spectrum of *p*-PEOB (4.2ppm-5.4ppm).

Figure 3.13 shows an expanded region of a 400MHz ^{1}H NMR spectrum of a typical *p*-PEOB sample. The signal strength of methylene groups, identified in red, provides a measure of the average number of repeat units present in the polymer backbone, relative to that of the methyl ester group (blue).

Assuming the absence of intramolecular cyclisation, the equation, relating signal intensities to average degree of polymerisation, can be written:

$$\overline{DP} = [{}^{I}CH_2 / {}^{I}CH_3] \times [3/2]$$

Where ${}^{I}CH_2$ = integrated signal intensity, as measured for a CH_2 group.

${}^{I}CH_3$ = integrated signal intensity, as measured for the methyl ester moiety.

Referring to Figure 3.13, the NMR spectrum reveals two CH_2 peaks, both of which have been used to generate number average molecular weights. Values generally agreed to within 3% or less but in some cases, particularly at higher molecular weights, the error could be as much as 10%. Although Mn values quoted in Tables 3.3 and 3.6 are an average of these two calculations, the assumption of no cyclisation means that the number average molecular weight may be over estimated.

3.3 Analysis of *p*-PEOB samples using Differential Scanning Calorimetry

Differential Scanning Calorimetry (DSC) proved to be a useful tool in assessing the effects of branching (Chapters 4 and 5). However, without a detailed analysis of linear *p*-PEOB as a reference material, results obtained from branched copolymers could only be qualitatively interpreted. A typical DSC trace for a sample of linear *p*-PEOB is shown in Figure 3.14. The diagram reveals four distinct thermal events, a glass transition, two crystallisation exotherms and a melting endotherm. Using the instrument software, we were able to measure enthalpy changes and to determine peak and onset temperatures for each process.

Seven 5g samples of linear *p*-PEOB were synthesised to study the effects of changing molecular weight on the thermal properties of the material. Approximately, half of each sample was analysed 'as made' and the remainder examined after reprecipitation and drying.

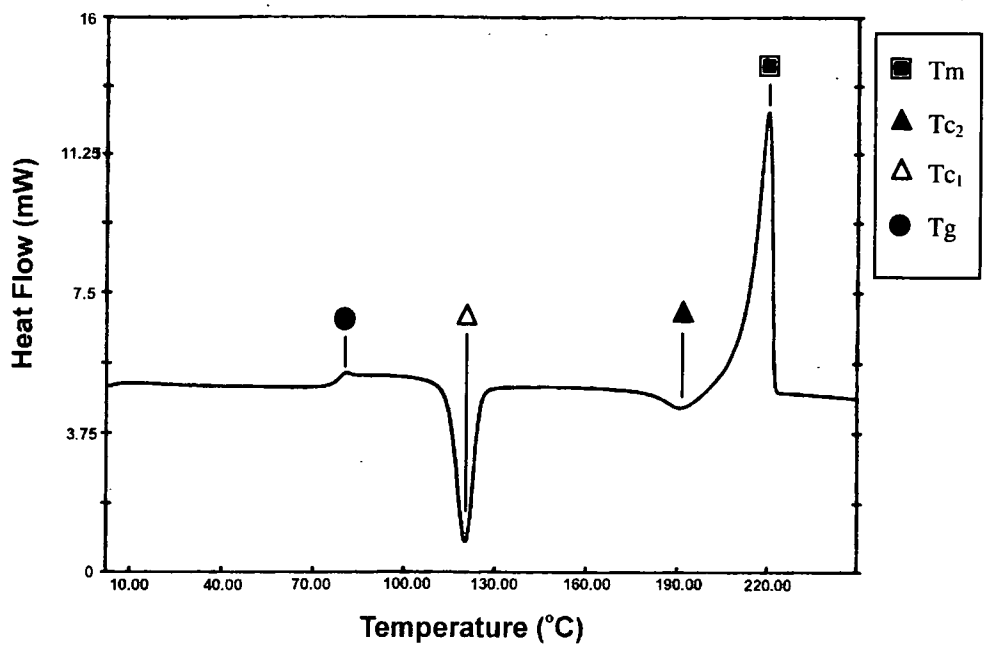

Fig. 3.14 Typical DSC trace of a *p*-PEOB sample after quenching, recorded at a heating rate of 10°C min^{-1}.

After establishing by thermogravimetric analysis that 2% weight loss occurred at 320°C, this temperature was used as the upper limit during DSC analysis. This ensured minimal sample degradation and reduced the risk of instrument damage from corrosive volatile materials.

Reproducibility and standardisation of sample analyses was achieved by adopting the heating and cooling protocols indicated in the diagram below.

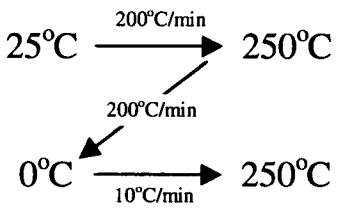

Samples of 5-10mg were heated from room temperature to 250°C and held at that temperature for one minute to ensure a uniform layer of polymer in the cell and good thermal contact. Samples were then cooled rapidly from the melt and the DSC trace recorded at a heating rate of 10°C min^{-1}. Transition temperatures and enthalpy measurements were analysed using the instrument software and the results collected in Table 3.3.

Sample	Mn*	Tg	ΔCp	Tc_1**	ΔH_{Tc_1}	Tc_2**	ΔH_{Tc_2}	Tm**	ΔH_{Tm}
1	4,600	343.3	0.4	387.5	-35.4	456.1	-6.3	490.3	65.8
1p	4,800	-	-	378.3	-30.1	458.9	-7.9	489.2	66.2
2	21,100	351.0	0.3	393.2	-25.9	463.4	-4.6	492.8	49.7
2p	-	348.9	0.4	390.4	-33.6	462.2	-5.4	492.2	57.6
3	32,300	352.2	0.3	391.6	-25.1	462.5	-5.5	492.6	60.0
3p	21,100	348.3	0.3	391.8	-22.5	463.9	-5.8	492.7	59.6
4	27,600	350.6	0.4	393.8	-28.1	463.3	-5.9	493.0	58.3
4p	28,100	348.7	0.4	391.2	-37.1	462.0	-5.1	492.1	60.1
5	22,900	351.2	0.3	395.8	-21.9	465.1	-4.7	491.9	52.6
5p	32,300	350.0	0.4	393.7	-32.7	463.4	-3.6	491.6	54.7
6	119,800	352.5	0.4	401.1	-30.6	465.5	-4.6	492.1	52.1
6p	24,100	349.5	0.4	395.5	-36.2	461.3	-4.9	490.3	57.3
7	11,600	348.9	0.2	390.0	-10.4	466.1	-7.6	493.5	63.1
7p	19,800	349.0	0.4	393.3	-38.0	461.7	-6.3	492.3	57.8

Table 3.3 Molecular weights and results of thermal analyses for *p*-PEOB samples.

p – reprecipitated and dried * Mn, as determined by ^{1}H NMR ** Peak values indicated Temperature /K, Enthalpy /Jg^{-1}, Tg taken as the midpoint of the transition.

Excluding the analyses of samples 1 and 1p, the effects of reprecipitation on the thermal characteristics of linear *p*-PEOB have been evaluated as an average of six experiments. Results are collected in Table 3.4 along with the standard deviations.

$\Delta Tg = -1.5 \pm 1.0\ ^{\circ}C$	
$\Delta Tc_1 = -1.6 \pm 3.0\ ^{\circ}C$	$\Delta(\Delta H_{Tc_1}) = +9.7 \pm 9.9\ Jg^{-1}$
$\Delta Tc_2 = -1.9 \pm 2.2\ ^{\circ}C$	$\Delta(\Delta H_{Tc_2}) = -0.3 \pm 0.9\ Jg^{-1}$
$\Delta Tm = -0.8 \pm 0.7\ ^{\circ}C$	$\Delta(\Delta H_{Tm}) = +1.9 \pm 4.6\ Jg^{-1}$

Table 3.4 Changes in transition temperatures and enthalpies accompanying the reprecipitation of linear *p*-PEOB.

As is apparent from Table 3.4, the changes in thermal characteristics between as-made and reprecipitated samples were insignificant for all transitions, with the possible exception of Tg. Surprisingly, the removal of monomer through reprecipitation, detected by ^{1}H NMR measurements, resulted in a very small lowering of Tg. This effect can be attributed to traces of trapped solvent in the polymer.

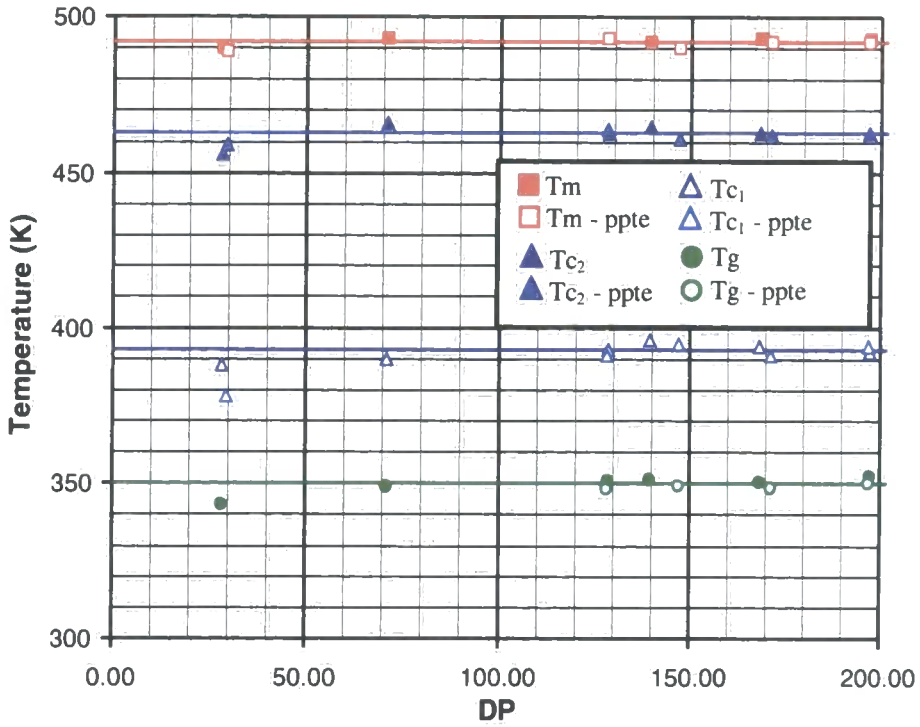

Fig. 3.15 Plot of transition temperatures against degree of polymerisation for *p*-PEOB samples.

Figure 3.15 shows transition temperatures, as measured for *p*-PEOB samples, plotted as a function of degree of polymerisation, calculated by ^{1}H NMR spectroscopy. It is evident from the plot that thermal transitions of *p*-PEOB reach a plateau at between 30 and 70 repeat units. Furthermore, linear regression analyses of these data, excluding the first two data points, gives the plateau values and associated standard deviations as recorded in Table 3.5. These averages are shown on Figure 3.15 as a series of horizontal lines, colour coded according to their respective transition; green for Tg, blue for crystallisation and red for melting.

T_g = 350.1 ± 1.4 K (77.1°C)	ΔC_p = +0.35 ± 0.07 Jg^{-1}
T_{c_1} = 393.3 ± 3.1 K (120.3°C)	ΔH_{Tc1} = -28.5 ± 8.0 Jg^{-1}
T_{c_2} = 463.2 ± 1.5 K (190.2°C)	ΔH_{Tc2} = -5.3 ± 1.0 Jg^{-1}
T_m = 492.3 ± 0.9 K (219.3°C)	ΔH_{Tm} = +56.9 ± 3.9 Jg^{-1}

Table 3.5 Averaged plateau values for thermal transitions in *p*-PEOB.

For samples to be free of crystallinity prior to analysis, the sum of the exothermic transitions should equal that of endothermic transitions, recorded during the DSC heating cycle. In practice, 23.1±8.9 Jg^{-1} of excess endothermic enthalpy was measured per analysis, indicating that crystallisation must have occurred during the rapid (200°C min^{-1}) cooling stage.

In addition, Tc was found to be largely independent of molecular weight. This was not expected on the basis of reported PET behaviour. However, it is possible to speculate as to why this might be. Firstly, there is no reason, *a priori*, why the relationship between the crystallisation temperature (Tc) of *p*-PEOB and number average molecular weight should be analogous to that established for PET. Secondly, inaccuracies in the measurements of number average molecular weight, using ^1H NMR spectroscopy, may have distorted the relationship. Figure 3.16 illustrates how the accuracy of end group counting diminishes with increased molecular weight. Clearly, as can be seen from the diagram, when the methyl signal decreases to about 1% of the methylene signal (0.3 units), the estimated error is approximately ±40%.

Several measurements were obtained for samples of linear *p*-PEOB to test the reproducibility of Mn determination using ^1H NMR spectroscopy, the results of which are presented in Table 3.6. Inhomogeneous sampling cannot be ruled out as a possible cause for the scatter of data as different samples were used for each of the three measurements. However, these data emphasise the difficulties in obtaining accurate molecular weight information using NMR end group counting.

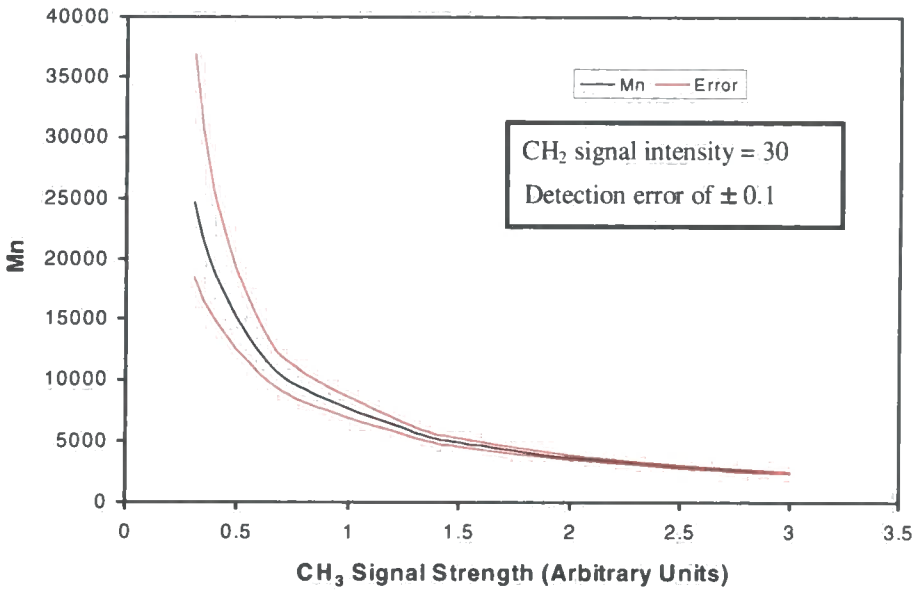

Fig. 3.16 Theoretical plot, showing the effect of diminishing CH_3 signal intensity on the accuracy of Mn determination.

Sample	Mn (1)	Mn (2)	Mn (3)	Average	±
1p	4,800	4,600	4,600	4,700	2.8%
3p	21,100	8,300	18,600	16,000	42.6%
4p	28,100	24,700	27,900	26,900	7.2%
5	22,900	26,600	22,700	24,000	9.1%
5p	32,300	17,900	21,400	23,900	31.4%
6p	24,100	100,500	43,900	56,200	70.6%

Table 3.6 Duplicate Mn calculations based on ^{1}H NMR end group counting.

When analysing thermal transitions for a material, peak and onset temperatures may provide complementary information. Figure 3.17 shows the melt and crystallisation temperatures of *p*-PEOB plotted against the degree of polymerisation, as measured by NMR spectroscopy. It reveals that the trends in peak and onset data are similar.

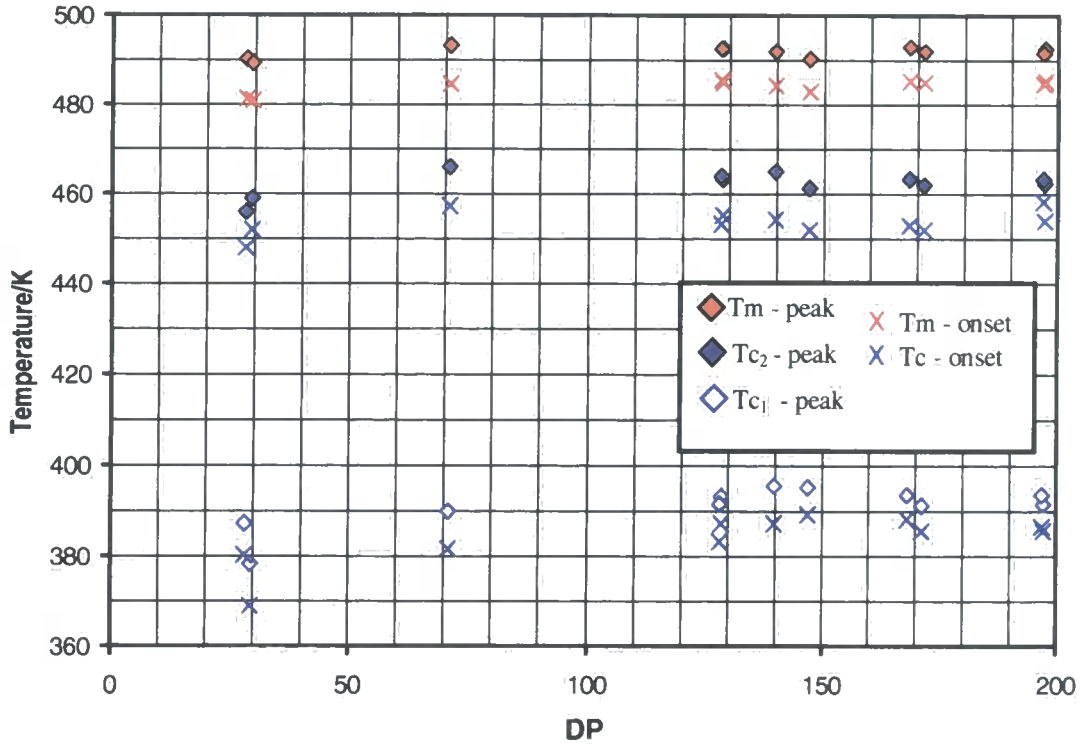

Fig. 3.17 Peak and onset data for *p*-PEOB, showing melting and crystallisation transitions plotted against degree of polymerisation, as measured by ^{1}H NMR.

Tc_1 = 386.5 ± 2.5 K (113.5°C)
Tc_2 = 453.3 ± 3.6 K (180.3°C)
Tm = 484.8 ± 0.7 K (211.8°C)

Table 3.7 *p*-PEOB onset values.

ΔTc_1 = 6.8 ± 0.3 K
ΔTc_2 = 9.9 ± 3.1 K
ΔTm = 7.5 ± 0.5 K

Table 3.8 (peak – onset) data for *p*-PEOB.

Statistical analyses of the onset data, presented in Figure 3.17, are summarised in Table 3.7. Furthermore, comparisons between peak and onset data are quoted in Table 3.8. The fact that there is little change in the difference between peak and onset

temperatures for the various transitions, across the range of sample DPs, implies that this is a fairly well behaved polymerisation and that the recorded parameters reflect real plateau values for this material.

3.4 Analysis of low molecular weight *p*-oligo(ethylene oxybenzoate)

As was shown in the previous section, all thermal transitions reach plateau values at chain lengths in excess of DP 70. However, the characterisation of short chain materials is of interest in studying how *p*-PEOB material properties develop as a function of DP. Indeed, the behaviour of oligomers may be relevant to understanding the influence of chain segment lengths on the properties of branched copolymers; the main interest of this thesis. To this end, thermal characteristics of low DP *p*-PEOB oligomers have been examined.

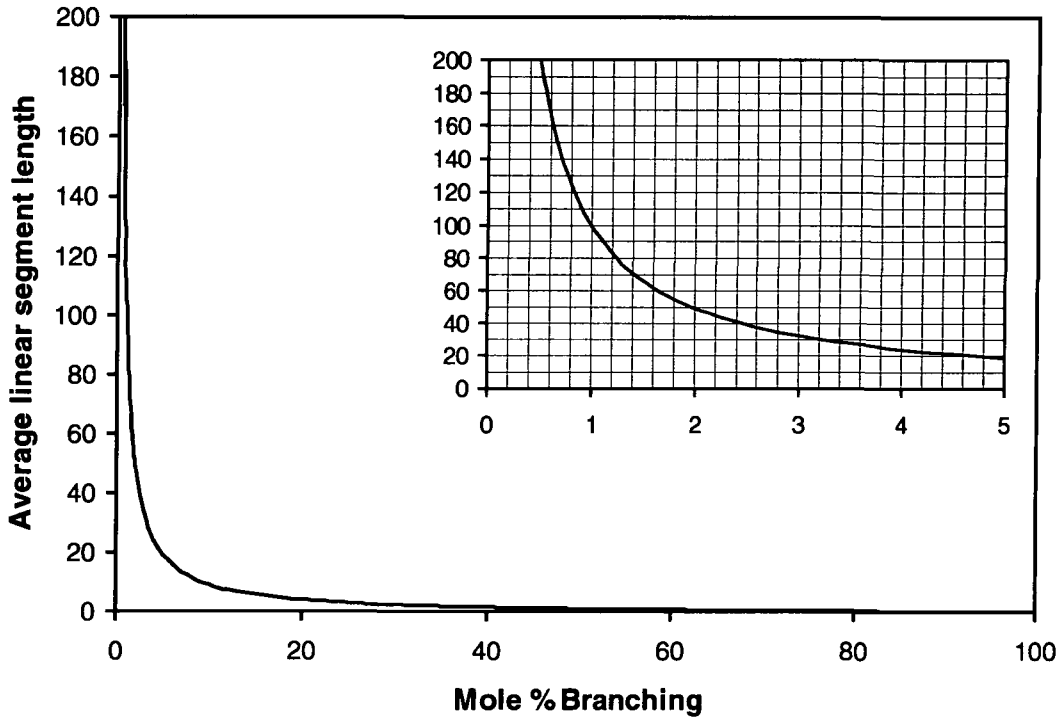

Fig. 3.18 Plot of average linear chain length against percentage branching for a statistically distributed copolymer at 100% conversion.

Figure 3.18 illustrates how the average linear chain length varies as a function of branching composition. The critical chain length of linear *p*-PEOB, i.e. the point at which the transition temperatures reach their plateau values, was established at between thirty and seventy repeat units in Section 3.3. The cross-referencing of these values with percentage branching in Figure 3.18 reveals the 'critical branching density' of branched *p*-PEOB to be between 1.4% and 3.2%, i.e. the branching content required to reduce the average linear segment length to the critical value.

The polymerisation technique, described in Chapter 2, was adapted to provide a slower rate of polymerisation. Indeed, the increase in the sampling rate and the lowering of polymerisation temperature allowed samples with DPs of between 2 and 42 to be extracted over a twelve hour period. These samples were then analysed using ^{1}H and ^{13}C NMR, TGA and DSC, the results of which are discussed in subsequent paragraphs.

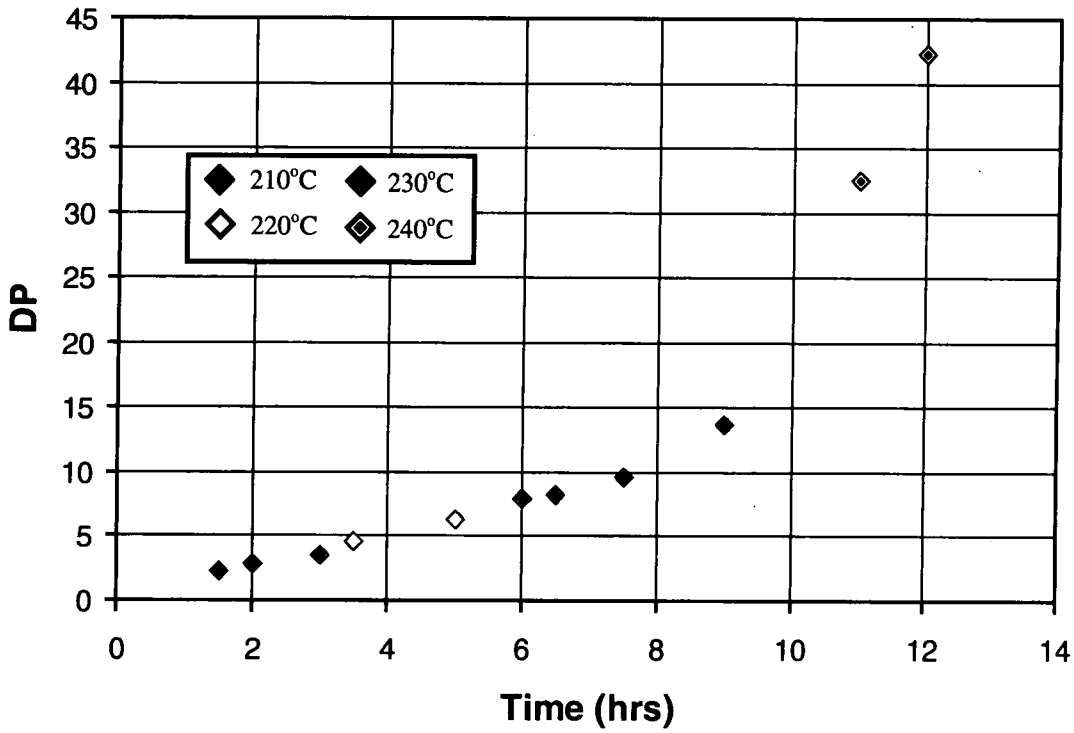

Fig. 3.19 Plot of degree of polymerisation, as measured by NMR, against reaction time (reaction temperatures are coloured coded).

The reactor was initially heated to 210°C after which, the temperature was increased in steps of 10°C at 2½, 5 and 10½ hours. However, no significant increase in the rate of polymerisation was observed until the reactor temperature had reached 240°C.

In a step growth polymerisation, the most numerous species are always low DP oligomers and monomers. Consequently, as the effects of monomer on the thermal characteristics of low DP samples of *p*-PEOB were unknown, it was necessary to determine the extent to which this might influence the results. To this end, monomer was extracted from several low DP *p*-PEOB samples using hot chloroform and Soxhlet apparatus, and identified using thin layer chromatography. Although, in many cases the bulk of the sample was dissolved during extraction, samples of sufficient mass were dried and analysed alongside 'as made' materials; see Figure 3.20.

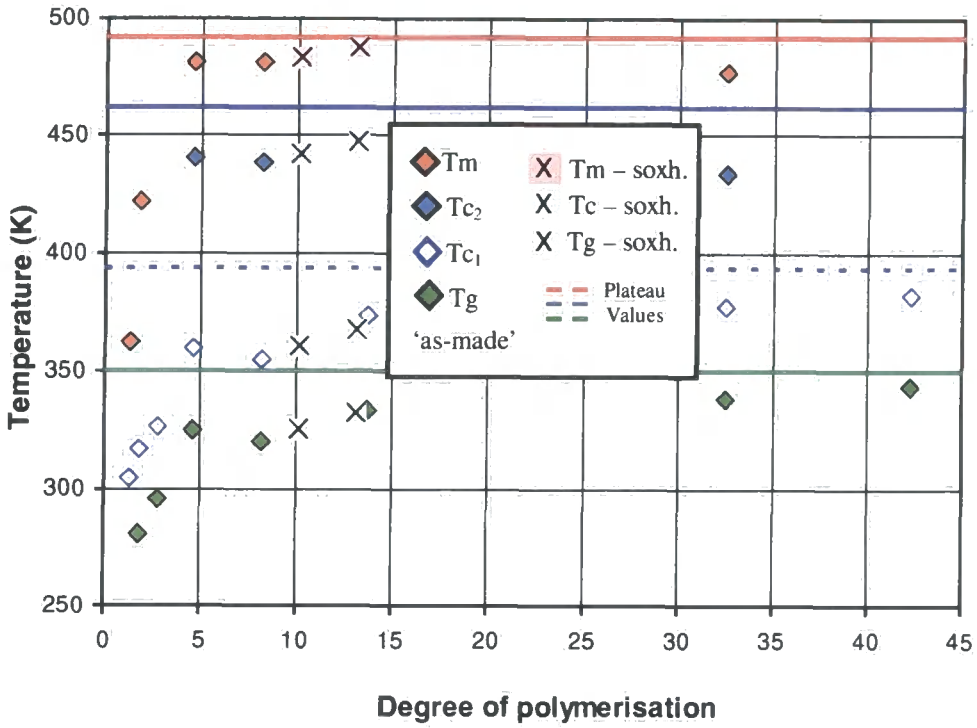

Fig. 3.20 Thermal properties of low DP oligomers of linear *p*-PEOB.

The temperature of 2% weight loss for some 'as-made' samples was beneath the expected melt temperature. Consequently, in order to obtain good thermal contact, the sample, sealed inside a DSC pan was heated to 240°C and then quenched in liquid

nitrogen before placing in the DSC apparatus. A heating run was then recorded at 10°C min^{-1} to within 5°C of the 2% weight loss temperature.

Melt, crystallisation and glass transition data, obtained for the oligomers of *p*-PEOB, are plotted against molecular weight in Figure 3.20. Above DP 10, a slow increase in the transition temperatures of this material is observed, with increasing molecular weight, toward their plateau values. In contrast, a rapid 'fall-off' occurs for samples below DP 10 and the cessation of secondary crystallisation is observed in samples of DP 4 or less.

3.4.1 Tg data analysis

For many common amorphous polymers the plot of log(chain-length), measured in chain atoms, or bonds, against the glass transition temperature, reveals three characteristic regions. The first of these occurs at or above the critical chain length, x_c, which varies between 90 for very flexible polymers such as poly(dimethyl siloxane) and 600 for more rigid polymers such as poly(α-methyl styrene). At this point, Tg tends to an asymptotic value, designated Tg(∞). The empirical relationship between Tg(∞) and x_c is reported in Equation 3.1.[6]

$$Tg(\infty) = 372.6 \log x_c - 595 \qquad \text{Eq. 3.1}$$

Below the critical chain length, x_c, the dependence of the glass transition temperature on the molar mass of the polymer may be described by the Bueche relationship, as shown in Equation 3.2.

$$Tg = Tg(\infty) - (K/Mn) \qquad \text{Eq. 3.2}$$

$$K = 2\rho N_A \theta / \alpha_f$$

Where ρ is the polymer density, N_A is Avagadro's constant, θ is the free volume contribution of one chain end, α_f is the free volume expansivity and Mn is the number average molecular weight of the polymer.

In the region where the rate of decrease in the glass transition temperature with decreasing molecular weight accelerates, Equation 3.2 is not valid. This transition usually occurs in polymers of 10 or 20 bond lengths and marks the point above which, polymers begin to adopt gaussian coil conformations.

These characteristic regions, shown in Figure 3.21 for three amorphous polymers, have been observed for *p*-PEOB in this work, even though it is a semi-crystalline material.

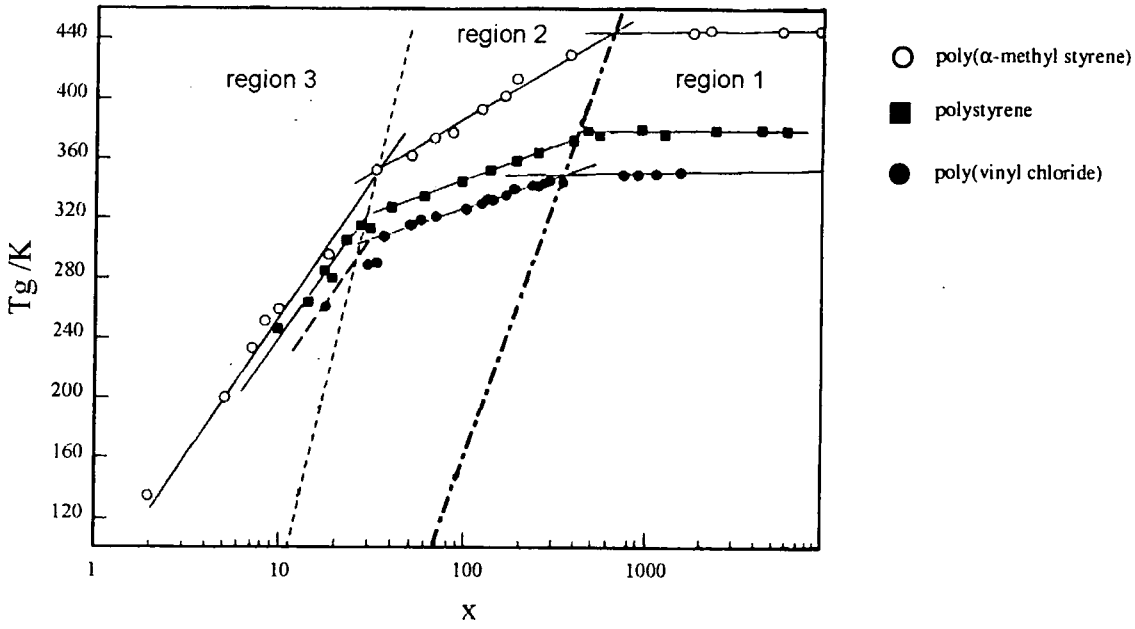

Fig. 3.21 Plot showing glass transition temperatures varying as a function of log x.[6]

The glass transition data, shown in Figure 3.20 for the oligomers of *p*-PEOB, reveal that the Tg plateau (350K) is approached at about DP 45, which equates to a chain length of approximately 360 bonds. The substitution of Tg into Equation 3.1 leads to the prediction that the plateau will be reached at a chain length (x_c) of 340 bonds. This is in good agreement with the measured DP. Correlation with the Beuche relationship (Eq. 3.3), using a least squares fitting procedure, reveals a correlation coefficient of 0.979 for the plot of glass transition temperature against reciprocal DP;

Figure 3.22. Finally, the transition into region 3 occurs at about DP 4 (approximately 32 bond lengths), which is in agreement with the predicted value.

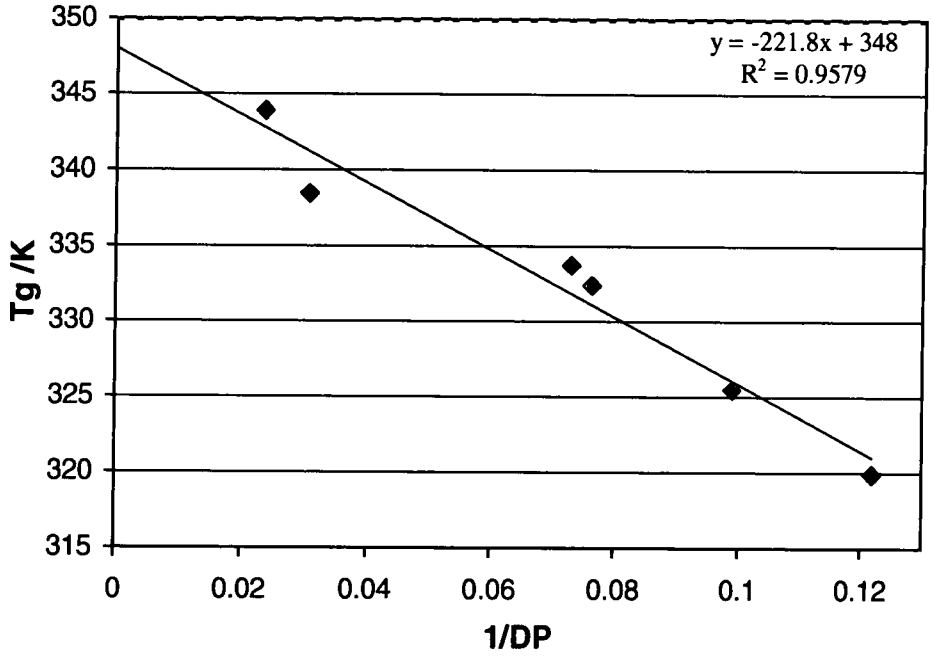

Fig. 3.22 The glass transition temperatures of *p*-PEOB plotted as a function of reciprocal DP.

Thus, although we know that the material is a semi-crystalline thermoplastic, the analysis of Tg data for this polyester is in good agreement with generalisations established for amorphous polymers[6]. However, Tg values were determined for samples quenched from the melt, which contained a relatively low proportion of crystallinity. Consequently, their observed correlation with amorphous polymer behaviour is not too surprising.

3.5 Effects of diglycolation

Under the conditions of industrial PET production, the incorporation of diethylene glycol units (DEG or 2,2'-oxydiethanol) is unavoidable. Moreover, the extent of copolymerisation influences the properties of the polymer; a 30°C decrease in the melt temperature and a reduction in Tg and density of PET being reported for the deliberate addition of 15mole% DEG.[7] Although Seganov et al[7] found no evidence to

show the onset of crystallisation was affected by diethylene glycol incorporation, using aminolysis, they were able to prove that a proportion of DEG units were incorporated into the crystal lattice.[8]

In contrast, the diethylene glycol content of *p*-PEOB, as used in this work, was controlled by the careful purification of monomer. Traces of the diglycol impurity, methyl 4-(5'-hydroxy-3'-oxapentoxy)benzoate (**4**), produced by a second addition of ethylene oxide, were removed by recrystallising the monomer from toluene. Changes in the characteristic properties of the polymer would result from the failure to eliminate this impurity from the feed. This is illustrated by some of our earlier work, where the polymerisation of contaminated monomer resulted in the incorporation of this defect.

The impurity was separated from a batch of crude monomer by silica gel chromatography (Aldrich, mesh 70-230), using dichloromethane/ethyl acetate (8:2) as eluent. The solvent was removed from a fraction rich in impurity **4**, and the product identified by mass, ^{1}H and ^{13}C NMR spectroscopy. The NMR spectra, in Figures 3.23 and 3.24, show that this compound is not pure. Nevertheless, mass spectroscopy showed the correct molecular ion for compound **4** ($MH^{+}_{(MS, CI)}$, 241, required M, 240). The determination of structure then followed straightforwardly from the assignments of ^{1}H and ^{13}C NMR spectra, as summarised overleaf.

For the copolymer prepared from monomers **2** and **4**, the ^{1}H NMR spectrum revealed a DP of approximately 50 and a 9.4±0.8mole% incorporation of diethylene glycol units. By contrast, polymers prepared from pure monomer **2**, under identical conditions, i.e. heated at 240°C for 6 hours, would have an approximate DP of 120, or higher. Whether or not the presence of DEG units was responsible for this apparent decrease in molecular weight was not investigated due to time constraints. However, differential scanning calorimetry (DSC) was used to assess the changes in thermal characteristics of *p*-PEOB resulting from the incorporation of **4**.

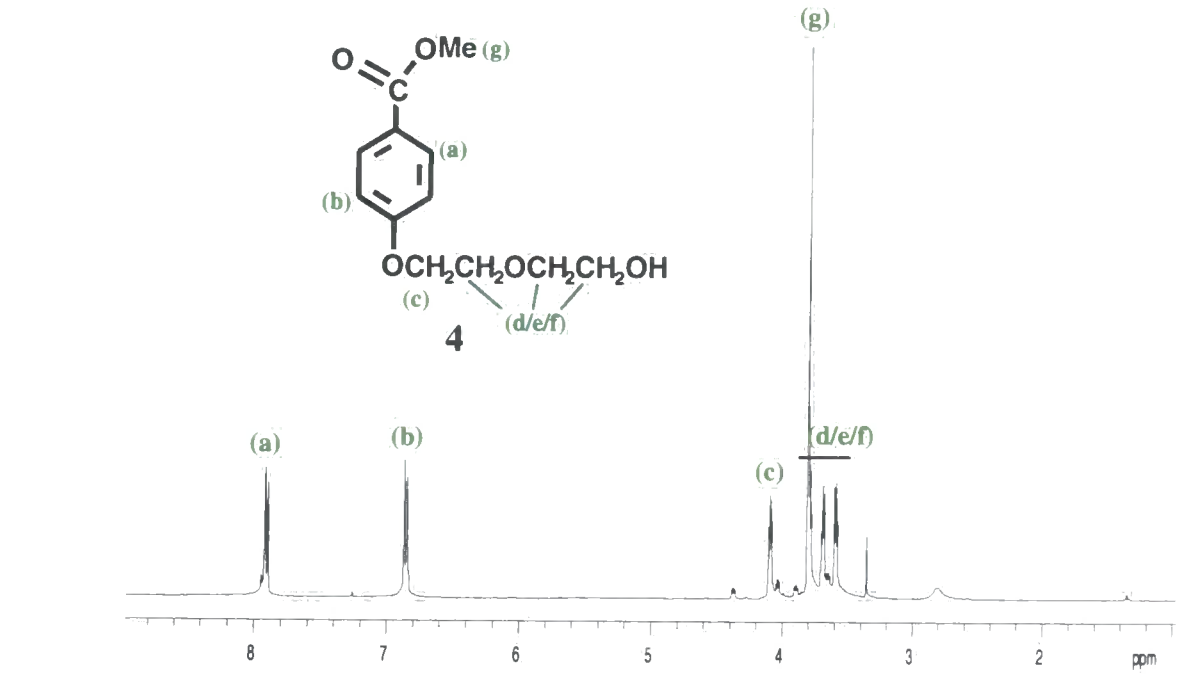

Fig. 3.23 400MHz ^{1}H NMR spectrum methyl 4-(5'-hydroxy-3'-oxapentoxy)benzoate (4).

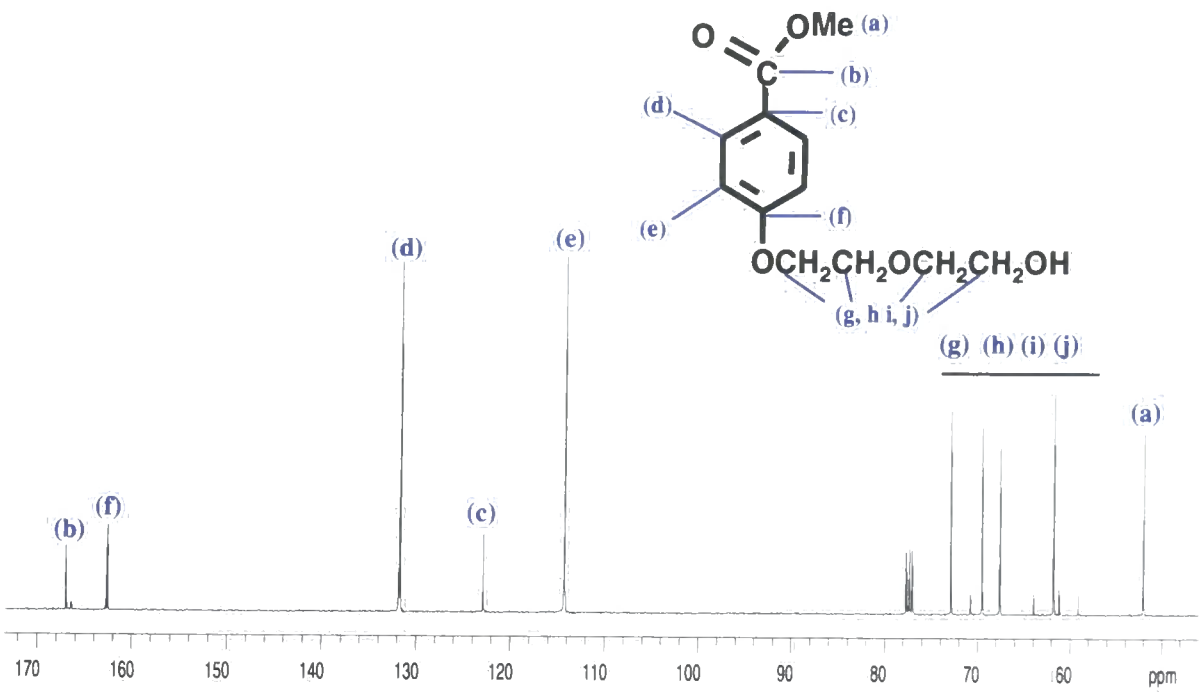

Fig. 3.24 400MHz ^{13}C NMR spectrum of methyl 4-(5'-hydroxy-3'-oxapentoxy)benzoate (4).

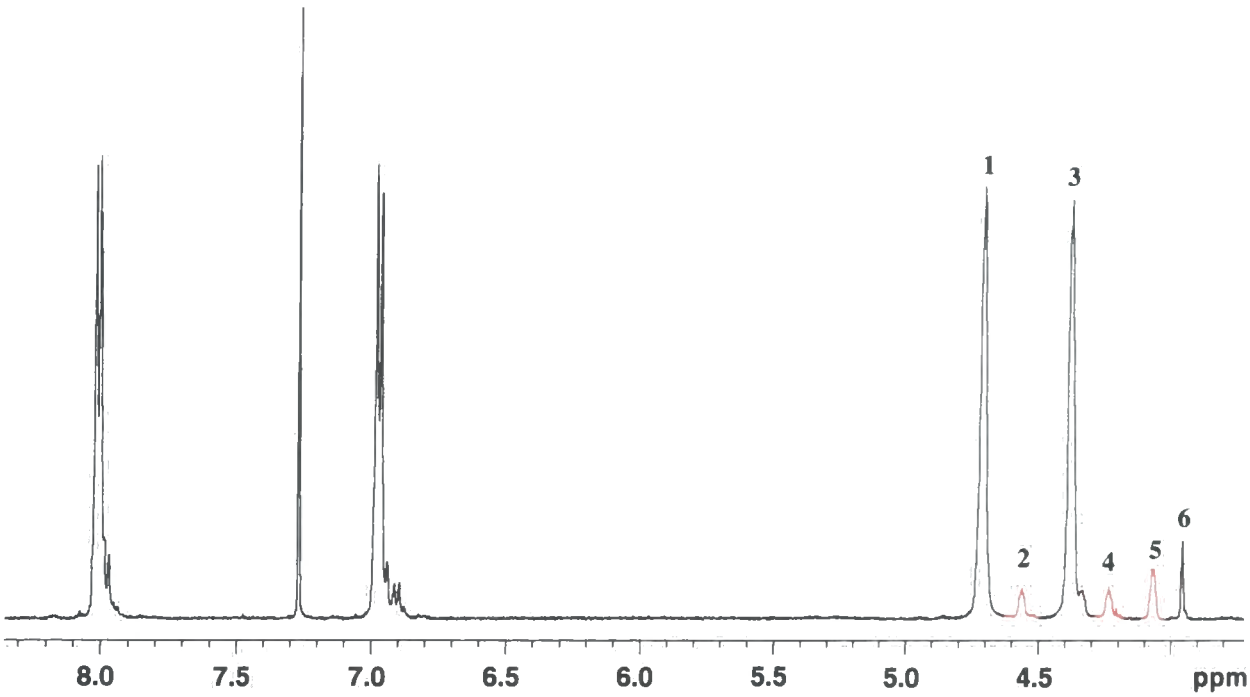

Fig. 3.25 400MHz ^{1}H NMR spectrum of the *p*-PEOB copolymer of with *ca.* 10mole% DEG.

The assignment of the ^{1}H NMR spectrum, as shown for the DEG copolymer, in Figure 3.25, is as follows: (δ); 3.93 (s, COOMe), **4.02** (m, DEG), **4.22** (m, DEG), 4.35 (s, 2H, ArOC$\underline{H}_2$CH_2O), **4.52** (m, DEG), 4.67 (s, ArOCH_2C$\underline{H}_2$O), 6.95 (pseudo d, J=8.8Hz, Ar-H), 7.99 (pseudo d, 2H, J=8.8Hz, Ar-H). The signals due to DEG units are identified in red with an intensity ratio of 2:1:1, as required.

A second experiment was undertaken to establish whether DEG units were formed *via* structural rearrangement or side reactions in *p*-PEOB during polymerisation. Eleven samples were extracted from a copolymerisation of a 9:1 mixture of monomers **2** and **4** at half-hour intervals and analysed by ^{1}H NMR. Peaks in the DEG and EG methylene region of the NMR spectrum, labelled one through six in Figure 3.25, were used to establish whether the DEG content of the polymer increased with reaction time. The intensity of peak 1, associated with EG units, was normalised to 100% and the relative intensities of the other peaks calculated and plotted in Figure 3.26. Each coloured bar represents a sample extracted at a half hourly interval.

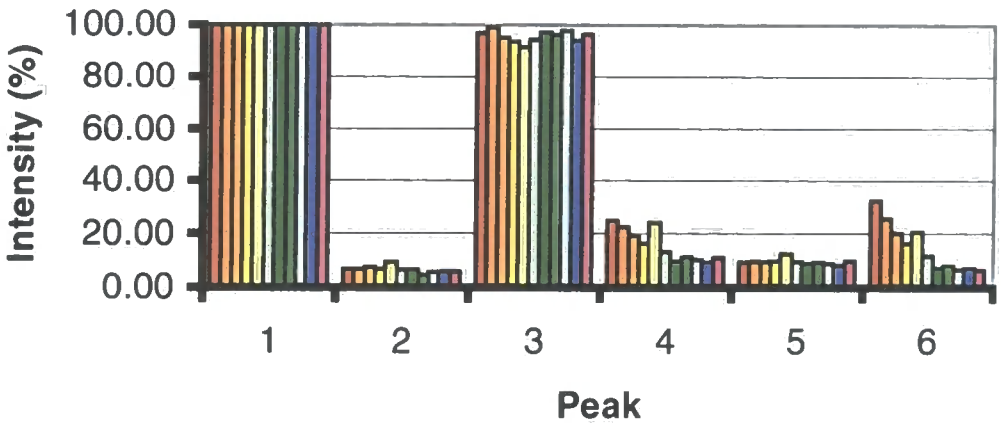

Fig. 3.26 Peak intensities of DEG containing *p*-PEOB polymer monitored over 5½ hours.

Legend: *p*-PEOB CH_2 groups – peaks 1 and 3, DEG CH_2 groups – peaks 2, 4*, 5, methyl ester end group – peak 6, (Monomer) CH_2 groups – peak 4*.

* peak four was not resolved into constituent parts.

After five and a half hours at 240°C there was no observed increase in the intensity of peaks associated with DEG. The only measurable changes were in the signal intensities of monomer **2** and the methyl ester end groups of the polymer, which both decreased. In conclusion, Figure 3.26 shows the extent of DEG incorporation to be solely dependent on the amount of contaminant introduced into the monomer feed.

3.6 *meta*-Poly(ethylene oxybenzoate) *m*-PEOB

In looking to design and develop tailor made materials, encompassing a balance of properties, scientists have sought a better understanding of structure-property relationships. The high melt temperatures of aromatic polyesters, as compared to their low melting aliphatic analogues, were not adequately explained until 1950.[10] Increased melt temperatures were attributed initially to strong interchain attractions but were shown later to be a consequence of increased chain rigidity resulting from the incorporation of para linked phenylene groups. Until 1959, no systematic study of the effects of substituting para phenylene linkages with meta isomers had been undertaken,

although, some work had been published prior to this by Hill, Walker and Bunn.[11,12] In 1959, Conix and Kerpel[13] published their study of the effects of replacing para linked phenylene groups, in aromatic polyesters, with meta equivalents. A series of isomeric homopolymers synthesised from isophthalic acid, terephthalic acid and a range of glycols with various spacer lengths were analysed. A summary of their findings is provided in Figure 3.27 and Table 3.10.

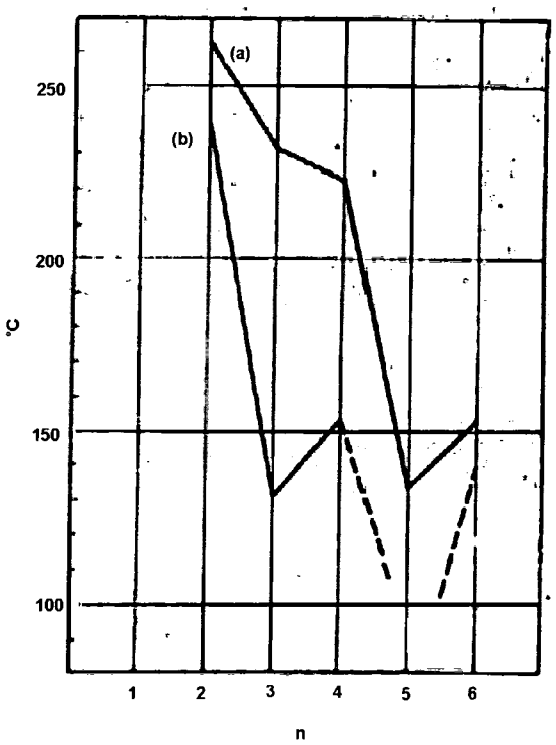

Fig. 3.27 Crystalline melting points of polyphthalates: (a) polymethylene terephthalates; (b) polymethylene isophthalates; n = number of carbon atoms in the glycol residue.[13]

The authors reported that the isophthalate isomer of PET melted over a broad temperature range, softening at 160°C to become a viscous liquid at about 200°C. Furthermore, birefringent spherulites were observed, 'floating' in the amorphous liquid, which disappeared at the crystalline melting point of the material (240°C).

Glycol (n)	Tm (isophthalate)	Tm (terephthalate)	Δ(Tm)
2	240°C	264°C	24°C
3	132°C	230°C	98°C
4	152°C	223°C	71°C
5	-	134°C	-
6	140°C	152°C	12°C

Table 3.10 Melting point summary of the polymethylene terephthalate and isophthalate polymers studied by Conix and Kerpel.[13]

In this Section, the properties of *m*-PEOB as synthesised for this work are compared with those of *p*-PEOB. In addition, the work of Conix and Kerpel provides a useful reference for the comparison of these polymers with their PET analogues.

Eight 5g samples of linear *m*-PEOB were synthesised to study the effects of molecular weight on the thermal characteristics of the material. Approximately, half of each sample was analysed 'as made' and the remainder examined after reprecipitation and drying. As with the investigation of *p*-PEOB, the 2% weight loss temperature (320°C) was established by thermogravimetric analysis. Samples were then analysed by DSC below this temperature, to limit sample degradation and prevent instrument damage. Reproducibility and standardisation between samples, was achieved by adopting the heating and cooling protocols indicated below.

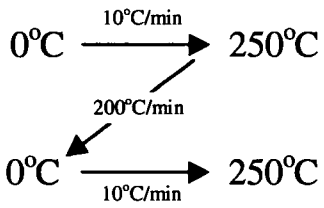

3.6.1 DSC Analysis

Figure 3.28 shows typical DSC traces obtained for various stages of the analysis. The first trace, indicated by a solid black line, corresponds to the initial heating cycle. The second, denoted by a dashed line, shows analysis after quenching. Indeed, in the majority of cases, the thermal characteristics of samples were assessed

before and after quenching. The results of these analyses are plotted against molecular weight, as measured by ^{1}H NMR, in Figures 3.29 and 3.30. Furthermore, average values for transition temperatures and associated enthalpy changes were evaluated and are reported in Tables 3.11 and 3.12.

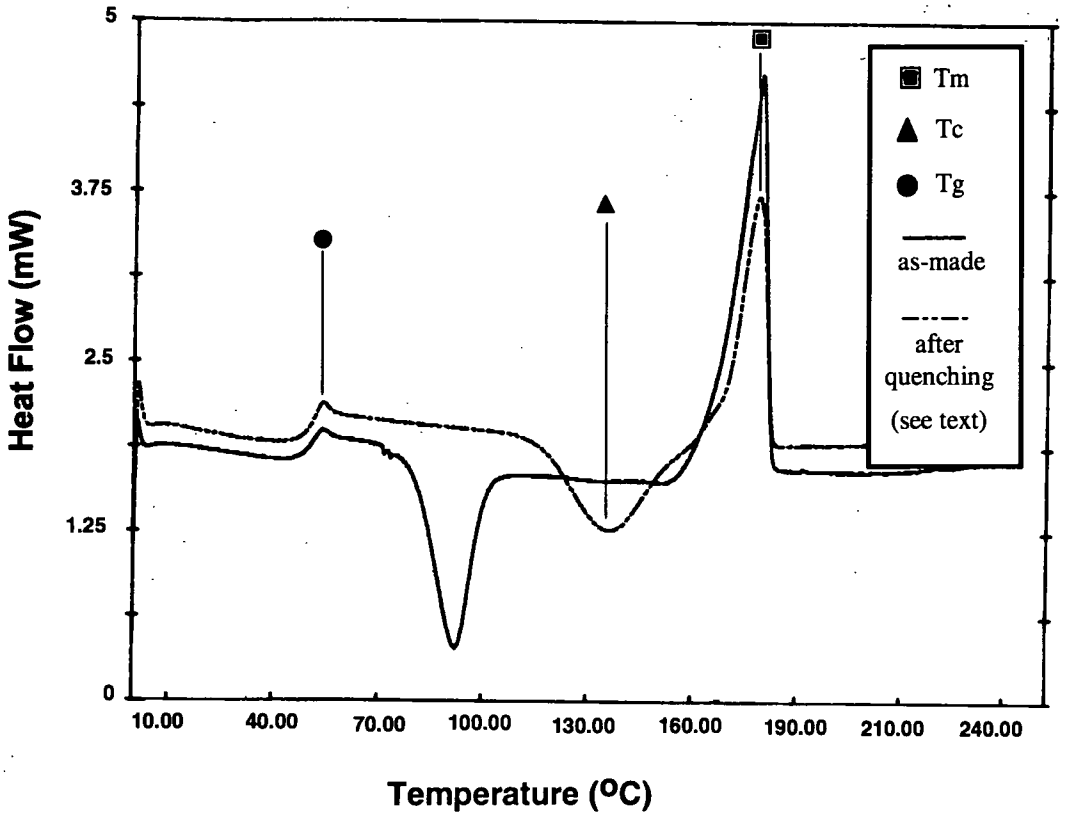

Fig. 3.28 Typical DSC traces for 'as made' and quenched *m*-PEOB.

Tg = 326.1 ± 2.3 K (53.1°C)	$\Delta Cp = +0.26 \pm 0.09\ Jg^{-1}$
Tc = 373.2 ± 15.8 K (100.2°C)	$\Delta H_{Tc} = -22.2 \pm 9.2\ Jg^{-1}$
Tm = 451.5 ± 1.7 K (178.5°C)	$\Delta H_{Tm} = +48.8 \pm 11.9\ Jg^{-1}$
	$\Delta H_{Tm} + \Delta H_{Tc} = 29.4 \pm 13.9\ Jg^{-1}$

Table 3.11 Plateau values for thermal transitions in *m*-PEOB, determined from data obtained during the initial scan.

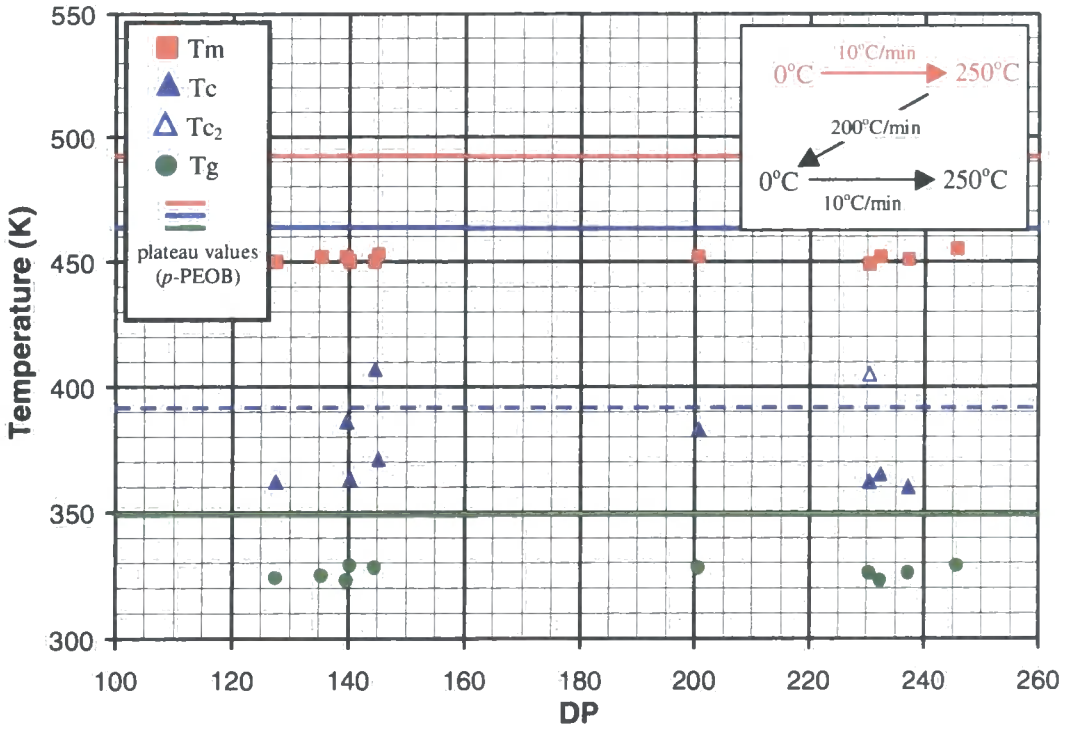

Fig. 3.29 Plot of thermal transitions for *m*-PEOB against degree of polymerisation – data recorded during the initial scan.

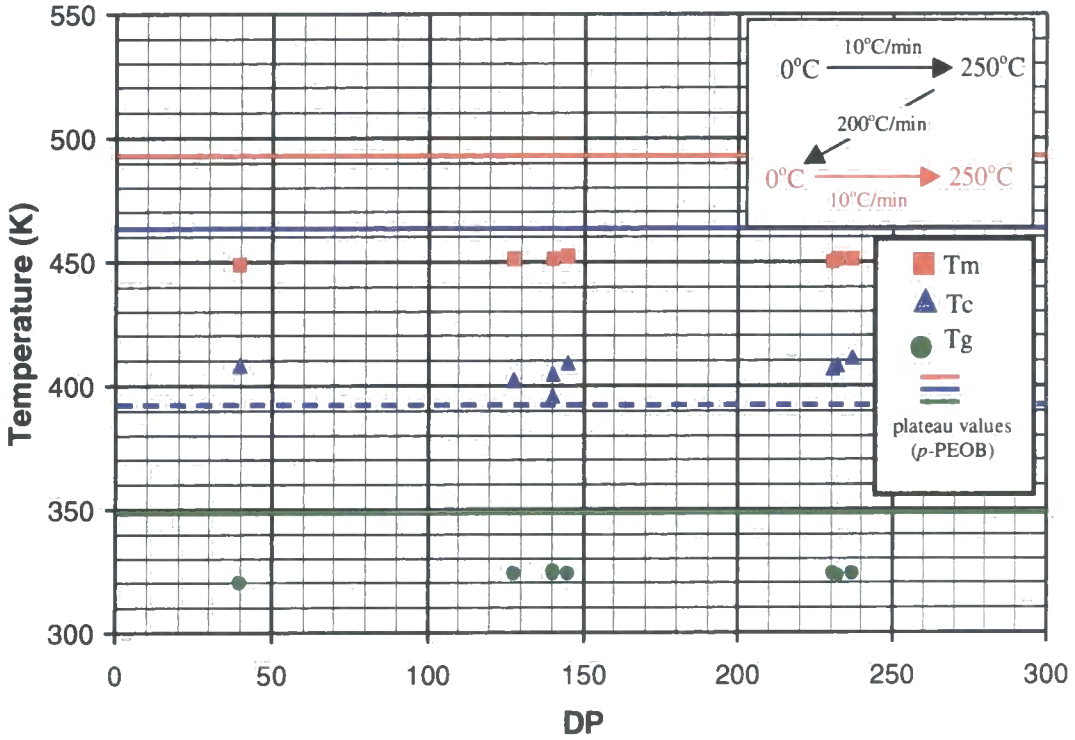

Fig. 3.30 Plot of thermal transitions for *m*-PEOB against degree of polymerisation – data recorded after quenching.

For comparison, the thermal plateau values of *p*-PEOB are represented in Figures 3.29 and 3.30 by coloured horizontal lines, as indicated in the legend.

Tg = 324.0 ± 0.6 K (51.0°C)	$\Delta Cp = +0.37 \pm 0.03\ Jg^{-1}$
Tc = 405.8 ± 4.8 K (132.8°C)	$\Delta H_{Tc} = -30.3 \pm 14.1\ Jg^{-1}$
Tm = 450.8 ± 0.9 K (177.8°C)	$\Delta H_{Tm} = +30.8 \pm 14.8\ Jg^{-1}$
	$\Delta H_{Tm} - \Delta H_{Tc} = 0.5 \pm 1.6\ Jg^{-1}$

Table 3.12 Plateau values for thermal transitions in *m*-PEOB, determined from data obtained after quenching.

Comparing the data between Tables 3.11 and 3.12, greater reproducibility is revealed in the glass transition after quenching, although no significant difference between actual values is evident. On the other hand, measurements of peak crystallisation temperatures, obtained before and after quenching, differed by 32.6±20.6°C. However, the variation in thermal history of the samples may account for these discrepancies. Indeed, the 70% reduction in data-scatter, observed after quenching, emphasises the fact that thermal history is an important determinant of behaviour in this polymer. By contrast, the melt temperature of *m*-PEOB appeared to be independent of thermal history, i.e. the same result was obtained regardless of whether samples were quenched or not.

Comparison between the enthalpies of fusion and crystallisation, in *m*-PEOB, emphasised the importance of quenching. There was no apparent difference between the magnitudes of exothermic and endothermic transitions for the samples quenched prior to analysis. By contrast, 'as made' materials, analysed by DSC, were shown to have 29.4±13.9 Jg^{-1} of excess endothermic enthalpy.

Samples of meta and para poly(ethylene oxybenzoate) polymers were both cooled from the melt at 200°C min^{-1} and analysed by DSC. Residual crystallinities of 23.1±8.9 Jg^{-1} were recorded for the para isomer, in contrast to samples of *m*-PEOB, which were amorphous. We conclude therefore, that *p*-PEOB has a faster rate of crystallisation than the meta analogue.

Onset temperatures associated with melting and crystallisation transitions were determined using DSC. The data are collected in Table 3.13. In addition, comparisons between peak and onset temperatures were evaluated and recorded in Table 3.14.

Tc = 387.5 ± 2.9 K (114.5°C)
Tm = 441.1 ± 0.6 K (168.1°C)

Table 3.13 *m*-PEOB onset values.

ΔTc = 18.0 ± 2.4 K
ΔTm = 10.0 ± 0.3 K

Table 3.14 *m*-PEOB (peak - onset) values.

Differences between peak and onset values measured between *m*-PEOB and *p*-PEOB (ΔTc_1=6.8±0.3K, ΔTc_2=9.91±3.1K, ΔTm=7.5±0.5K), reveal a broader temperature range in the meta isomer, over which melting and crystallisation transitions occur.

ΔTg = -25.8 ± 1.8 °C	$\Delta(\Delta Cp) = +0.02 \pm 0.11\ Jg^{-1}$
ΔTc = +12.3 ± 7.0 °C	$\Delta(\Delta H_{Tc}) = +3.5 \pm 23.1\ Jg^{-1}$
ΔTm = -41.5 ± 1.7 °C	$\Delta(\Delta H_{Tm}) = +26.1 \pm 10.5\ Jg^{-1}$

Table 3.15 Effects on polymer thermal transitions (peak values) of changing para to meta linked ethylene oxybenzoate units. ($Tc = Tc_1$)

Replacement of para by meta linked ethylene oxybenzoate units resulted in changes in the thermal characteristics as reported in Table 3.15. The marked reduction in the glass transition, observed when para linked phenylene units were replaced by their meta linked analogues, is probably due to the increased free volume and disorder created by a 'kinked' polymer chain. Polymers can be characterised in terms of the ratio Tg:Tm, which lies between 0.5 and 0.8 in 80% of known polymeric materials.

Interestingly, the relationship between the melting point and glass transition of both ethylene oxybenzoate polyesters is almost identical. The Tg:Tm ratios of *m*-PEOB and *p*-PEOB being 0.72 and 0.71, respectively. The reduction in the ease with which *m*-PEOB crystallises, and the lowering of the melt temperature with respect to the para isomer can be explained qualitatively. Meta linked phenylene units produce non-symmetrical distributions of mass about their axis of rotation. Consequently, more space and energy are required to rotate these groups into a configuration required for the crystal lattice. The outcome is a reduction in the rate of crystallisation, in comparison with the para isomer.

Many factors influence the structure of a crystal lattice; including the shape, symmetry, chain mobility and group interactions of the polymer. Indeed, there are no grounds to presume that the isomers of para and meta-poly(ethylene oxybenzoate) will adopt similar crystal structures. Changes in entropy associated with melting have been calculated for the isomers of PEOB and recorded in Table 3.16. A lower entropy of fusion is observed for *m*-PEOB, albeit with significant uncertainty, which indicates that different modes of crystallisation must exist for isomers of PEOB.

	$\Delta H_{Tm}/Jg^{-1}$	Tm /K	$\Delta S_{Tm}/Jg^{-1}K^{-1}$
p-PEOB	56.9 ± 3.9	492.3 ± 0.8	0.116 ± 0.008
m-PEOB	30.8 ± 14.8	450.8 ± 0.9	0.068 ± 0.033

Table 3.16 Entropies and enthalpies of fusion shown with their respective melt plateau temperatures, as recorded for meta and para PEOB.

The melt temperatures of polyethylene terephthalate and polyethylene isophthalate were measured, by Conix and Kerpel,[13] at 264°C and 240°C, respectively, a difference of 24°C. In comparing the melt temperatures of para and meta isomers of PEOB we find a difference of approximately 40°C; with differences between the melt temperatures of PET and *p*-PEOB of 45°C. Difficulties in crystallising samples of glycol-isophthalates, observed by Conix and Kerpel, and the broad melting range of polyethylene isophthalate, in particular, were not observed for *m*-PEOB. Clearly, as

illustrated, the absence of one carbonyl group from the repeat unit of the polymer has implications for the behaviour of oxybenzoate polymers, as compared to their phthalate analogues.

3.7 Meta and para poly(ethylene oxybenzoate) copolymers

The effects of copolymerising two isomeric forms of ethylene oxybenzoate were investigated. Ten grams of an equimolar mixture of meta and para methyl (2-hydroxyethoxy)benzoate (monomers **1** and **2**) were mixed intimately and heated to 240°C in the presence of titanium tetrabutoxide, a transesterification catalyst. Samples of polymer were extracted at thirty-minute intervals during the first two hours of the reaction and then at intervals of one hour, subsequently. Details of the synthesis are recorded in Chapter 2.

The number average molecular weight of each sample was determined by ^{1}H NMR end group counting. Measurements revealed that in comparison to the homopolymers, the rate of copolymer formation was lower than expected. After eight hours the copolymer Mn had reached 4800 (DP=29), as compared to 20,000 (DP=122), typically obtained for para or meta PEOB, under identical conditions. The copolymer was soluble in chloroform and dichloromethane, allowing the determination of molecular weights by gel permeation chromatography; see Figure 3.31 and 3.32.

The number average molecular weight, as measured by GPC using a polystyrene calibration, increased linearly with reaction time, Figure 3.31 and were greater than the values determined by ^{1}H NMR spectroscopy. The increase in Mw, as determined by GPC, was more rapid than for Mn, see Figure 3.32, which gave rise to an increase in polydispersity (Mw/Mn) from 2.1 to 3.9 over the seven hour reaction period. Theory predicts that for step-growth AB polymerisations, the polydispersity will equal a maximum value of two at one hundred percent conversion. This effect therefore requires consideration. It is possible that the observed increase in polydispersity may be an artefact; e.g. a poor baseline from the output of the refractive index detector, or peak broadening due to column inefficiencies. However, the GPC software used was reputedly accurate to ±10%, which may be a contributory factor,

also. On the other hand, chemical explanations, i.e. low levels of competing reactions such as branching and cyclisation, may also exist to explain this apparent discrepancy.

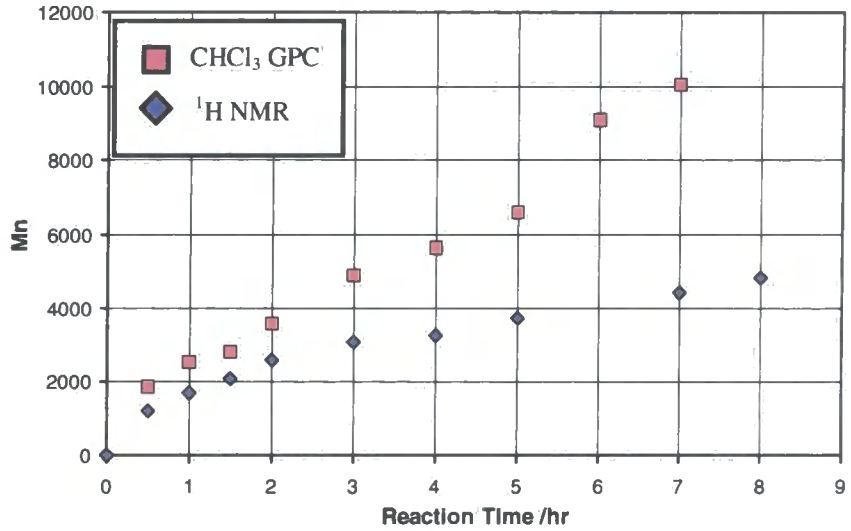

Fig. 3.31 Number average molecular weight of copolymer samples synthesised from an equimolar mixture of 1 and 2 measured by ^{1}H NMR ($CDCl_3$) and GPC ($CHCl_3$, 5μm gel columns of 100Å, 10^3Å, 10^5Å pore size, PS standards), plotted against reaction time.

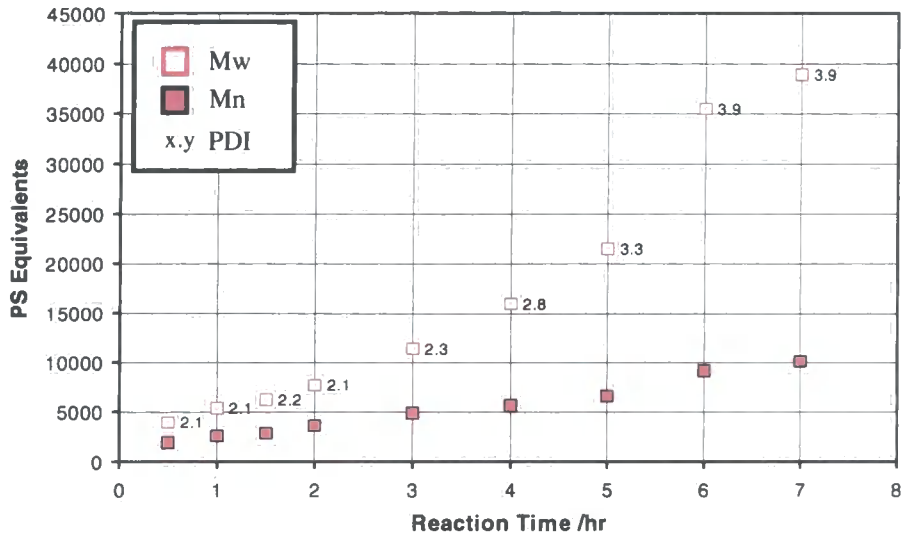

Fig. 3.32 Plot of reaction time *vs.* Mn and Mw measured by GPC ($CHCl_3$, 5μm gel columns of 100Å, 10^3Å, 10^5Å pore size, PS standards) for copolymer samples synthesised from an equimolar mixture of 1 and 2.

Figure 3.33 shows the RI detector response curve plotted against elution time for a typical PEOB copolymer with an equimolar ratio of meta and para linked units. It clearly indicates that the weight distribution is monomodal, as is consistent with other linear step growth polymerisation reactions.

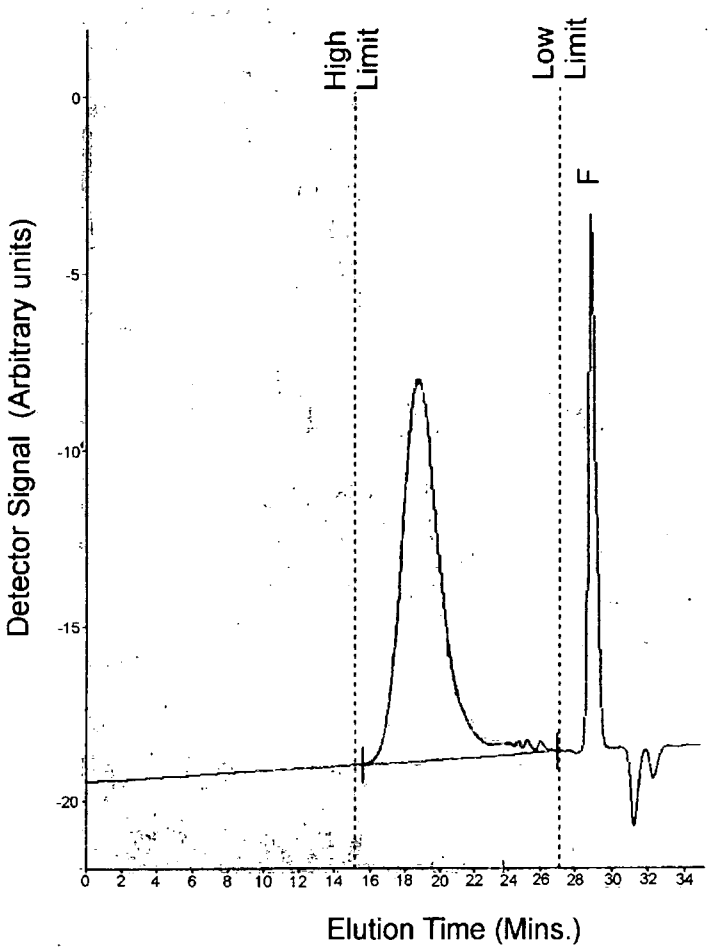

Fig. 3.33 RI detector trace of a PEOB copolymer synthesised from an equimolar ratio of 1 and 2 and separated using GPC ($CHCl_3$ GPC, 5μm gel columns of 100Å, 10^3Å, 10^5Å pore size).

The chloroform soluble samples of the equimolar meta:para PEOB copolymer were analysed by viscometry, using a Schott automatic viscometer. After determining the t_0 value for chloroform, polymer solution was introduced into an Ubbelhode-0c viscometer tube for analysis. The auto-doser was programmed to deliver 25cm^3 of chloroform, in steps of 5cm^3 and, after each dilution, to allow a period of equilibration

before data acquisition. Seven measurements were taken per dilution, from which, reduced and inherent viscosities were calculated and plotted against concentration. The limiting viscosity number, a measure of influence of an isolated polymer molecule on solution viscosity, was evaluated by extrapolating the measured values to zero concentration. Although limiting viscosity numbers, or intrinsic viscosities, are specific to polymer structure, molecular weight and solvent they may be related to molecular weight using the Mark-Houwink relationship, Equation 3.4.

$$[\eta] = KM^{\alpha} \qquad \text{Eq. 3.4}$$

In this expression, the exponent α is a function of polymer shape and solvent quality. The constant K, a function of molecular 'stiffness', is related to bond rotation energies. For a randomly coiled linear polymer in a theta solvent, the limiting viscosity number $[\eta]$, is predicted to behave as a function of the square root of the molecular weight, that is when α=0.5. In thermodynamically better solvents, the α exponent will increase, brought about by the expansion of the polymer molecule due to better polymer-solvent interactions. However, the value of α does not usually exceed 0.8 for linear polymers in thermodynamically good solvents. It is important to note that α is also a determinant of shape. In theory, a value of zero is predicted for hard spheres, which approaches unity for random coils. At the extreme, a value of two is predicted for rigid rods.

Although viscosity average molecular weights are stipulated, in practice, they are difficult to measure. The similarity with weight average molecular weight makes the use of Mw in Equation 3.4 a viable alternative. However, as the GPC calibration used linear polystyrene standards there is uncertainty as to the 'real' values of Mw. Nevertheless, the good correlation between log$[\eta]$ and log(Mw) (linear regression coefficient of 0.999), in Figure 3.34, suggests that this copolymer is displaying normal solution behaviour, as associated with linear polymers. These attempts to determine molecular weight by conventional solution measurements lead us to the conclusion that we have genuine linear polymers.

In the absence of other analyses, ^{1}H NMR spectroscopy would be expected to give the more accurate number average molecular weight. However, as was demonstrated in Section 3.3, the reproducibility of NMR measurements could only be relied upon at low values of Mn.

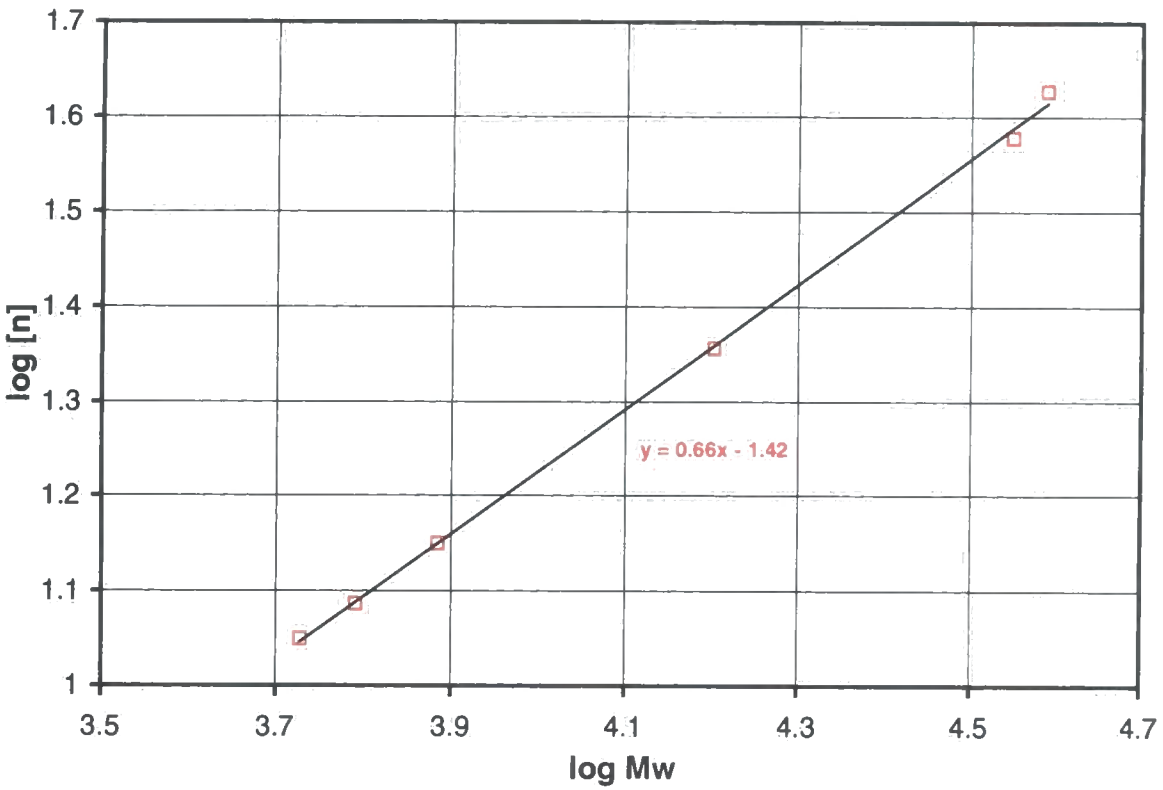

Fig. 3.34 Mark-Houwink plot, showing log Mw measured by GPC (in $CHCl_3$) against the log of limiting viscosity number ($CHCl_3$, ml g^{-1}) for 50:50 para:meta copolymers of poly(ethylene oxybenzoate).

3.7.1 DSC Analysis

DSC analysis of the PEOB copolymer synthesised from an equimolar ratio of monomers **1** and **2**, revealed a glass transition but no evidence of crystallisation. This is consistent with the material being an amorphous, random copolymer. Figure 3.35 shows a typical DSC trace, heated at 10°C min^{-1}.

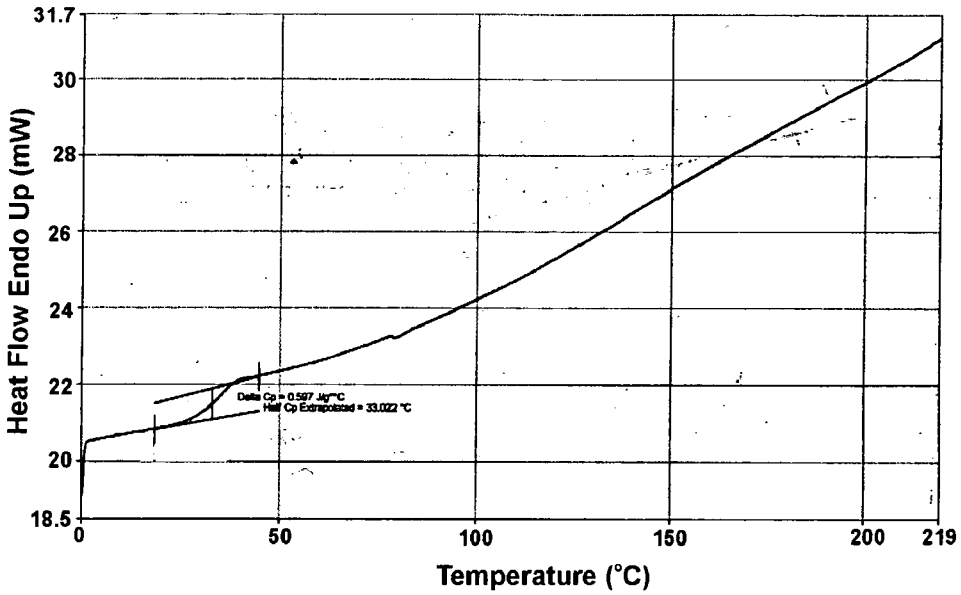

Fig. 3.35 Typical DSC trace of poly(ethylene oxybenzoate) copolymer synthesised from an equimolar ratio of 1 and 2.

Copolymer samples were analysed by DSC and the observed glass transition temperatures plotted against number average molecular weights, as determined by ^1H NMR spectroscopy (see Figure 3.36). For comparison purposes, the plateau values of the Tgs of both para and meta homopolymers are indicated on the plot. The glass transition temperature of the amorphous copolymer increases with molecular weight over the range indicated. Although, clearly higher than that of the meta homopolymer, the plateau value could not be determined due to a lack of sufficiently high molecular weight material. However, the shape of the curve suggests a plateau value halfway between the homopolymers.

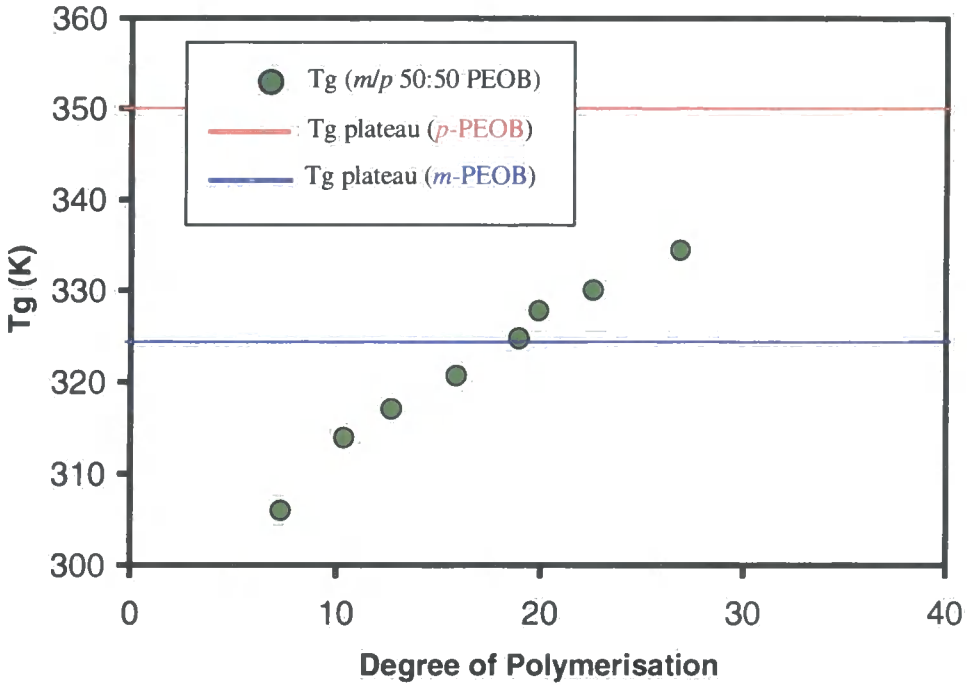

Fig. 3.36 Plot of glass transition against degree of polymerisation, as measured by ^{1}H NMR spectroscopy for the 50:50 meta/para PEOB copolymer.

It is evident from the analysis of PEOB that its solubility is inextricably linked to the crystallinity and structural regularity of the polymer. Indeed, an equimolar mixture of meta and para ethylene oxybenzoate units in PEOB resulted in a dramatic increase in solubility, which accompanied the breakdown of molecular order within the system. However, the extent of disruption caused by varying the ratio of para and meta isomers was not investigated due to time constraints.

3.8 References

1. Cook J.G., Dickson J.T., Lowe A.R., Whinfield J.R., B.P. **604985**, I.C.I. Ltd., (1946)
2. Nagasawa F., Nuiya M., *Japan Chemical Quarterly*, **3**, (1967), 46-49
3. Rashbrook R.B., The chemistry and technology of polyester polymer, I.C.I. Ltd., **PLU/16/2955/C**, (1971)
4. Mihara K., *Die Angew. Makromol. Chem.*, **40/41**, (1974), 41-55

5. Korematsu M., Kuriyama S., Nippon Kagaku Zasshi, **81**, (1960), 852
6. J.M.G. Cowie, *Polymers: Chemistry & Physics of Modern Materials*, 2nd Edition Blackie Academic, pages 270-271
7. Fakirov S., Schultz J.M., Seganov I., *J. Appl. Polym. Sci.*, **32**, (1986), 3371-3392
8. Fakirov S., Seganov I., Prangowa L., *Makromol. Chem.*, **184**, (1984), 807-819
9. Guzman J., Fatov J.G., *Eur. Polym. J.*, **14**, (1978), 943
10. Evans R.D., *J. Am. Chem. Soc.*, **72**, (1950), 2018
11. Hill R., Walker E.E., *J. Polym. Sci.*, **3**, (1948), 619
12. Bunn C.W., *Appl. Phys.*, **25**, (1954), 820
13. Conix A., Van Kerpel R., *J. Polym. Sci.*, **40**, (1959), 521-532

Chapter 4

Crystalline Copolymers of Branched
p-Poly(ethylene oxybenzoate)

4.1 Intoduction

4.1.1 General considerations concerning branched polymers prepared via step-growth routes

Linear polymers can be produced by chain or step growth processes. However, in this work we are concerned with only step growth syntheses, which give rise to linear materials using reactions termed as AB or AA/BB polymerisations. The polyesterification reaction of a monomer containing both acid and alcohol functionalities is an example of the AB process, whereas the polyesterification of a diol with a diacid is an example of an AA/BB process. In this section, the consequences of introducing polyfunctional branching agents into AB and AA/BB polymerisations are considered.

Poly(ethylene oxybenzoate) and poly(ethylene terephthalate) have some structural similarities. However, *p*-PEOB is synthesised using an 'AB' step-growth

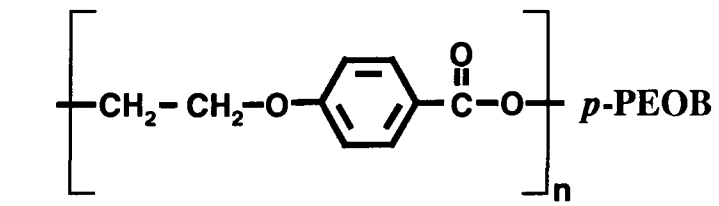

p-PEOB

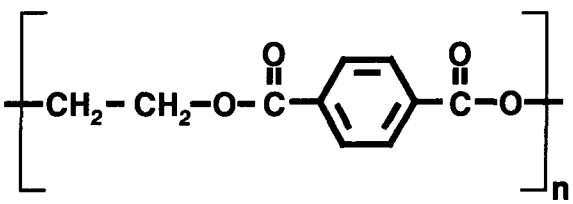

PET

polymerisation in contrast to PET, which is produced *via* the 'AA/BB' route. In the case of an AB polymer, in the absence of cyclisation, there is always one 'A' group and one 'B' group at the chain termini. For AA/BB systems, chains with odd numbers of monomer units may have either two 'A' or two 'B' termini. Chains with an even number of monomers will have one 'A' and one 'B' at the termini, as per the AB polymer; see Chapter 1. This has implications for the introduction of polyfunctional branching units.

In the copolymerisation of trifunctional A_3 or B_3 molecules with AB linear units, only one branching unit can be incorporated per polymer molecule. The branching agent acting as a core, or tether, ties together several linear chains to create a 'star polymer'. Control of molecular weight is achieved by the manipulation of monomer feed, i.e. the ratio of branched to linear monomers. By increasing the proportion of core molecules the lengths of resultant linear chains are reduced; the additive acting as a chain growth controller.

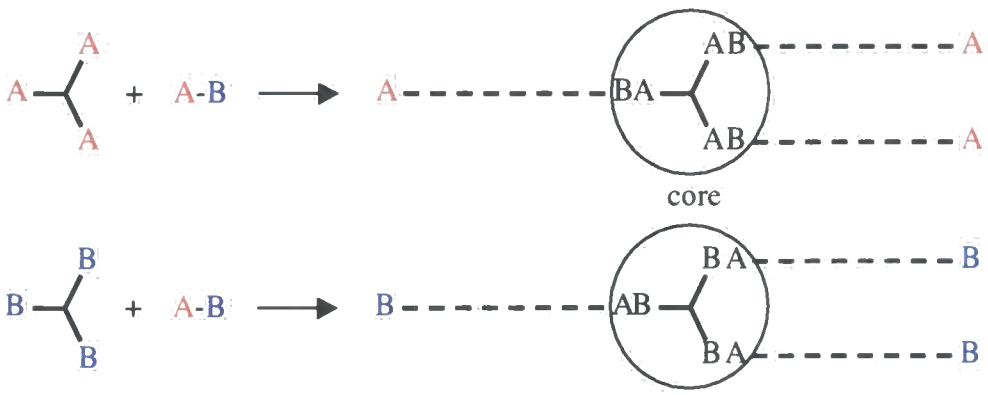

Fig. 4.1 Formation of stars *via* AB/A_3 or B_3 copolymerisation.

However, a different outcome is realised if A_3 or B_3 trifunctional molecules are polymerised with AA/BB linear units. As the limit of one branch per macromolecule is no longer mandatory, the number of incorporated branching units can be controlled by the monomer feed and the extent of reaction. However, these 'multiplybranched' macromolecules will eventually form insoluble three-dimensional networks or gels, see Figure 4.2.

In the absence of cyclisation, copolymerisations of AB linear units with AB_2 monomers produce structures which have a solitary 'A' group, called the focus, and unreacted B groups equal to the number of incorporated branching units plus one. The average linear chain length, or segment length, is determined by the ratio of AB to AB_2 monomers in the feed but the molecular weight is controlled, ultimately, by the extent of reaction. Unlike branched AA/BB systems, AB/AB_2 copolymers are free from

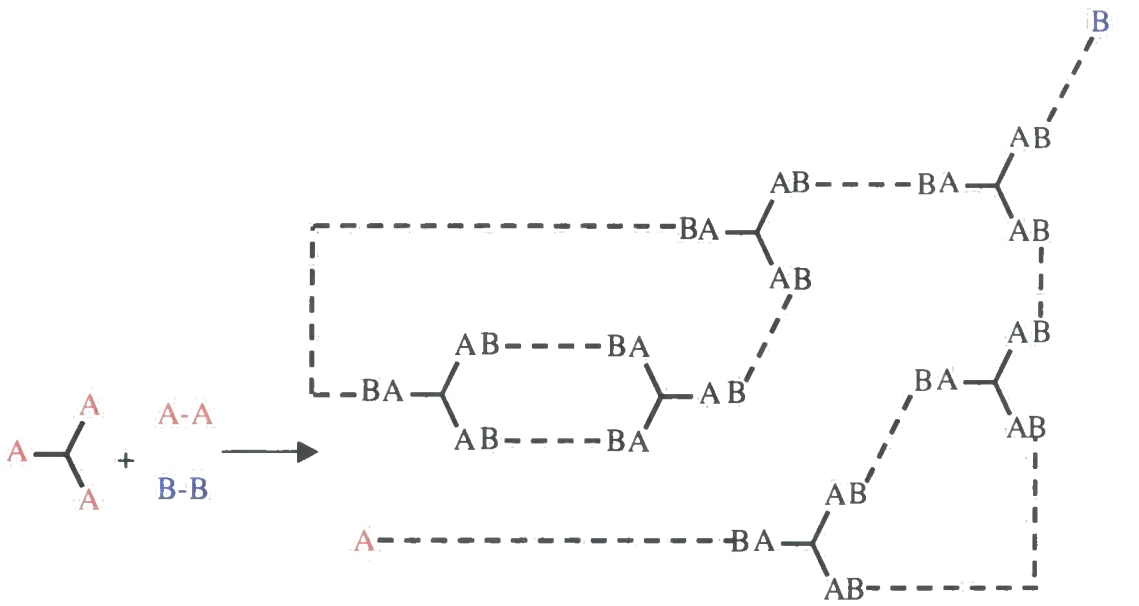

Fig. 4.2 Formation of gels *via* AA/BB/A_3 copolymerisation.

cross-links and are generally more soluble than their corresponding linear analogues. However, the incorporation of fully or partially reacted branching units dramatically increases the number of structural isomers, the polydispersity and the difficulty in characterising the polymer in detail. As with all polymers, without isolating structurally pure samples by means of designed synthesis, fractionation or chromatography, only 'averaged' structures can be determined.

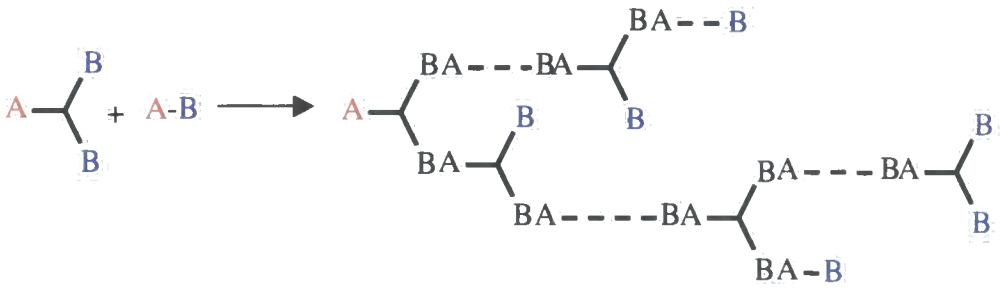

Fig. 4.3 Formation of soluble branched copolymers *via* AB/AB_2 copolymerisation reactions.

Different circumstances prevail when AA/BB monomers are polymerised in the presence of an AB_2 branching agent. Polymers grow outwards, in all directions, from a central AB_2 core and not, as in the previous example, from a focal point. Further

complexity and structural diversity is created because, as with the linear analogues, end groups may be, either 'A' or 'B'. Consequently, cross-linking will lead eventually to insoluble three-dimensional networks, see Figure 4.4.

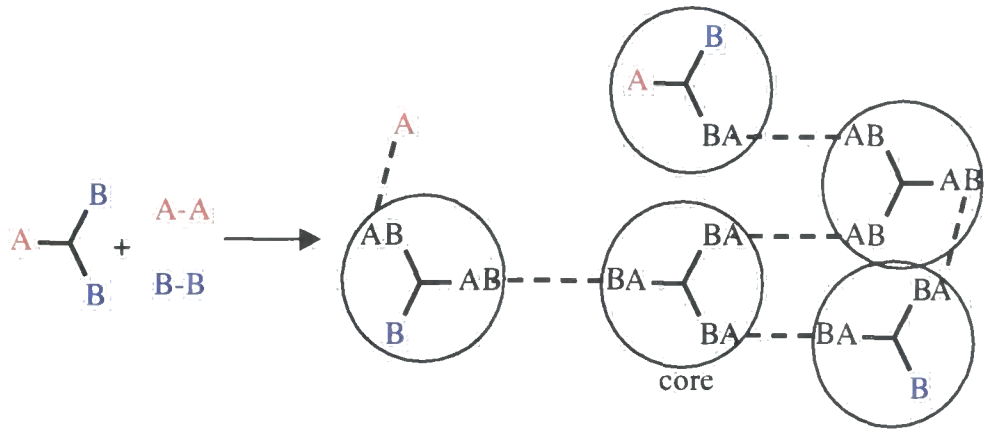

Fig. 4.4 Network formation *via* AA/BB/AB_2 copolymerisation.

It is evident from these general considerations that the inclusion of any A_3, B_3 or AB_2 branching agent in an AA/BB polymerisation will lead eventually to gelation, if the concentration of polyfunctional molecules is above a low threshold value. In contrast, AB/AB_2, AB/A_3 and AB/B_3 systems allow control over the levels of branching to produce cross-link free topologies.

4.1.2 Previous studies

Few investigations into the effects of branching in linear polymers have been reported. One of the principal reasons for this is the difficulty associated with characterising the resultant materials; gelation being the single most problematic aspect of branching AA/BB systems. Consequently, until now, efforts have focussed primarily on the modification of commercially available materials, which include polystyrene,[1-2] PET,[3-5] PBT[6] and its isomer poly(butylene isophthalate).[7,8]

Flory[9] published his theoretical treatment of AB/AB_2 copolymers in 1952. Using statistical analysis to enumerate possible configurations of linear and branched units in the copolymer, he predicted the most probable size distribution. However, it was to be another thirty years before the first report of an AB/AB_2 copolymer was published by Kricheldorf et al[10].

Poly(3-oxybenzoate) as first described by Schiff[11] in 1882, was reinvestigated in 1959 by Gilkey and Caldwell[12] and reported as having unremarkable properties. In 1982 Kricheldorf modified poly(3-oxybenzoate) using 3,5-bistrimethylsiloxy benzoyl chloride to generate the first synthetic AB/AB_2 copolymer. It was to be a further eight years before Kim and Webster[13] synthesised the first 'pure' synthetic AB_2 hyperbranched polymer, a branched polyphenylene derivative. The following paragraphs give a brief synopsis of Kricheldorf's work toward branched poly(3-oxybenzoate), which is relevant to the present study.

The early work of Kricheldorf et al[11] established synthetic methodology for the production of high molecular weight poly(3-oxybenzoate) based on the bulk polymerisation of 3-trimethylsiloxy benzoyl chloride. The copolymerisation of 3-trimethylsiloxy benzoyl chloride and 3,5-bistrimethylsiloxy benzoyl chloride was reported to produce branched polyesters, which were free of cross-links, regardless of conversion and branching content.

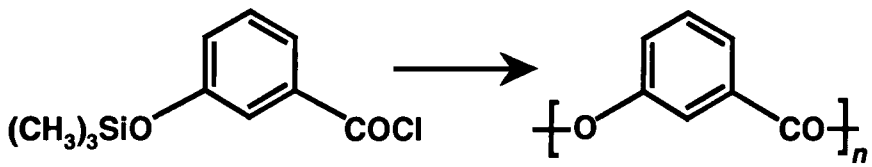

Fig. 4.5 Synthesis of poly(3-oxybenzoate).

Direct spectroscopic evidence for branching was provided by ^{13}C NMR, based on the identification of sequences of linear and branched units in the carbonyl region of the spectrum. Molecular weight data were obtained for chloroform soluble copolymers using vapour pressure osmometry and, for a limited number of samples, using gel permeation chromatography. Moreover, no evidence for microgels was observed by GPC, as weight distributions were monomodal. An interesting and unexpected feature of branched poly(3-oxybenzoate) was the apparent linear relationship between the yield of crystallisable polymer, isothermally crystallised from pyridine and benzene (1:1), and the extent of branching; however, this was not reported in detail. Finally, thermogravimetric analysis in air revealed that the incorporation of branching units did not significantly affect thermal stability, as linear and branched materials gave the same TG trace.

In a later publication, Kricheldorf et al[14] compared the effects of branching units and end groups on the thermal properties of poly(3-oxybenzoate). Glass transition temperatures of the branched copoly(3-oxybenzoate)s were shown to be dependent on both the number and type of end groups; Figure 4.6. Furthermore, a distinct minimum in the glass transition temperature was observed for the copolymer bearing acetate end groups and with 10mole% branching units. In Figure 4.6, data set 'A' had diesterol branches and diacid end groups; 'B' had diolester branches and diphenol end groups and 'C' had diolester branches and acetate end groups.

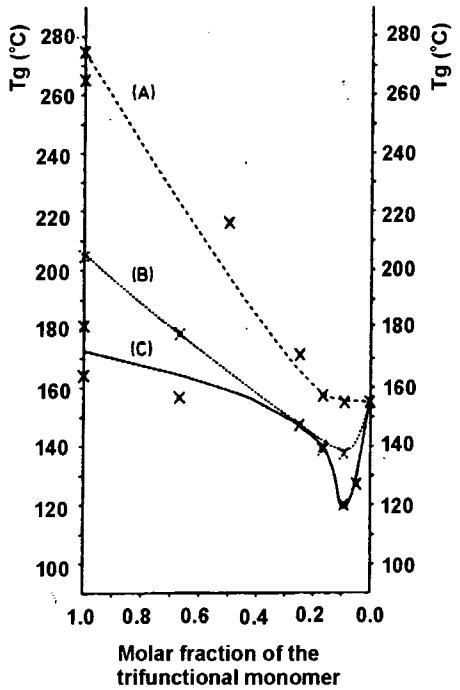

Fig. 4.6 Glass transition vs. molar fraction of branching agent in AB_2/AB aromatic polyesters (see text).

4.2 Results and Discussion

4.2.1 Branched *p*-poly(ethylene oxybenzoate)

Branched *p*-PEOBs of various molecular weights were synthesised from methyl 4-(2-hydroxyethoxy)benzoate (**2**) and dimethyl 5-(2-hydroxyethoxy)isophthalate (**3**) using a bulk polymerisation technique, described in Chapter 2.

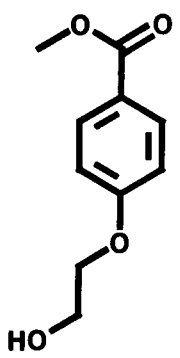

2

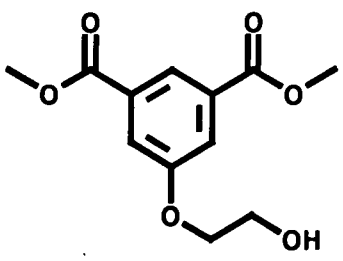

3

Eleven copolymers with 1mole%, 2mole%, 3mole%, 5mole%, 10mole%, 12.5mole%, 15mole%, 20mole%, 40mole%, 60mole% and 80mole% branching were synthesised. The set of polymers was then divided into two subgroups based on morphology and solubility. Copolymers with 12.5mole% branching or less were crystalline, chloroform-insoluble materials, in contrast to copolymers possessing more than 12.5mole%, which were amorphous and soluble in chloroform. Results obtained for the crystalline copolymers are discussed in this chapter; the amorphous copolymer results are discussed in Chapter 5.

4.2.2 Determination of copolymer composition using ^{1}H NMR spectroscopy

Analysis of the aromatic signals in the ^{1}H NMR spectra (6-9ppm) of the various copolymer samples was used to establish the branching content. Branching units possess three aromatic protons; two (C) coincident at **7.79ppm**, the remaining proton (A) at **8.26ppm**. Linear units have four aromatic protons, as two pairs of two, (D) at **6.99ppm** and (B) at **8.02ppm**, see Figure 4.7. The multiplicity in this region of the spectrum means that the integrated relative intensities of several pairs of signals can be

used to compute the branch:linear incorporation ratio. Ideally, all of the calculations should produce the same value but in practice, errors in determining signal integrations mean that this is not so. In every case, the four computations were evaluated and an average taken. Table 4.1 shows the collection of data for crystalline copolymers with the accompanying standard deviations.

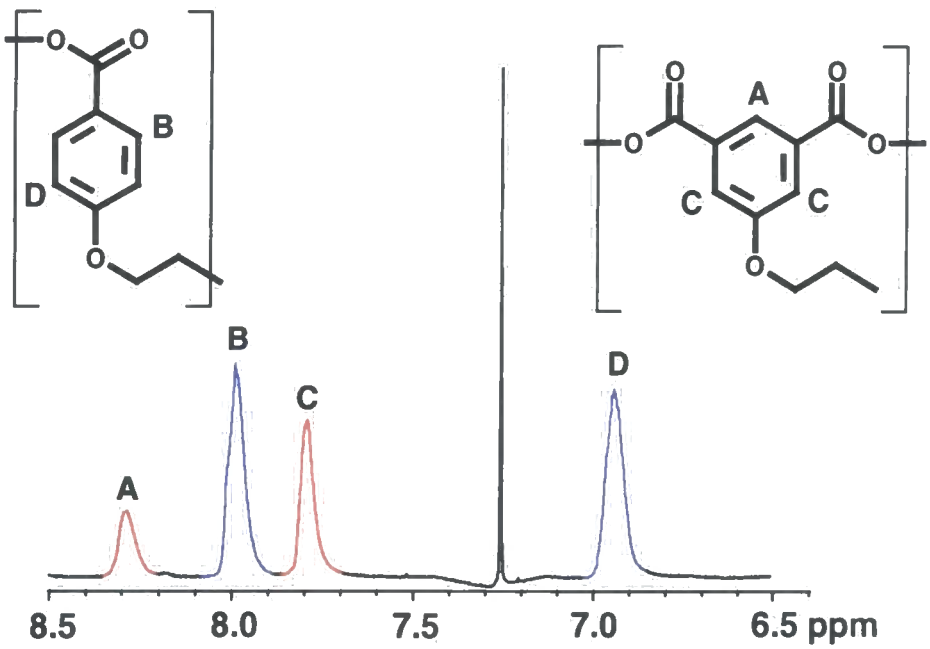

Fig. 4.7 ^{1}H NMR spectrum showing the aromatic region (6.5-8.5ppm) of the 40% branched PEOB copolymer. ($CDCl_3$/TFA)

Methyl 4-(2-hydroxyethoxy)benzoate (**2**), having a lower melting point and molecular mass than the AB_2 monomer (**3**) is expected to be the more volatile component. Indeed, a greater loss of **2** from the reaction mixture by evaporation would lead to higher branching ratios than anticipated, based on the weight of monomers in the feed. However, there appears to be no systematic trend in the difference between calculated and experimentally determined AB_2 incorporation.

NMR evaluations of percentage incorporation of branching units are in general agreement with the values determined by weighing. However, from inspecting Table 4.1, it is apparent that there are discrepancies between the branching compositions, as determined using the NMR technique. A poor signal to noise ratio

might account for the discrepancies at low branching ratios but it cannot realistically explain the errors observed for copolymers with 10mole% branching or more. It is likely that the observed differences reflect the errors inherent in the method.

Weighed* [mole%]	C/(C+B) [mole%]	C/(C+D) [mole%]	2A/(2A+B) [mole%]	2A/(2A+D) [mole%]	Average** [mole%]
1%	1.7 ± 0.5	1.6 ± 0.5	0.5 ± 0.2	0.5 ± 0.3	1.3 ± 0.6
2%	2.6 ± 0.5	2.6 ± 0.5	1.0 ± 0.5	1.0 ± 0.5	1.8 ± 0.3
3%	2.8 ± 0.5	2.8 ± 0.5	1.3 ± 0.6	1.3 ± 0.6	2.2 ± 0.7
4%	3.4 ± 0.4	3.4 ± 0.4	1.5 ± 0.2	1.5 ± 0.2	2.7 ± 0.6
10%	10.2 ± 0.5	9.9 ± 0.4	12.7 ± 0.6	12.7 ± 0.6	11.2 ± 0.5
12.5%	13.4 ± 0.3	13.1 ± 0.3	10.1 ± 1.6	10.0 ± 1.5	11.7 ± 0.8

Table 4.1 Percentage branching of poly(ethylene oxybenzoate) samples as calculated by ^{1}H NMR spectroscopy. ($CDCl_3$/TFA)

* Percentage branching, as calculated from monomer feed; ** Average percentage branching calculated from the NMR data; A, B, C and D correspond to signal intensities of peaks, labelled in Figure 4.7. The individual values in the table were determined by analysis of samples removed from the polymerisation at different times.

Evidence for the chemical incorporation of branching units is also provided by ^{1}H NMR. The reprecipitation and subsequent reanalysis of the 4mole% branched *p*-PEOB copolymer revealed an increase in the branching composition; Table 4.2. By contrast, the sample of 10mole% branched *p*-PEOB revealed a decrease in branching content. However, the fact that signals A-D are still present after reprecipitation, in addition to the reduction in crystalline content with increasing extents of branching are strong indicators that genuine AB_2/AB copolymers have been synthesised.

Weighed* [mole%]	C/(C+B) [mole%]	C/(C+D) [mole%]	2A/(2A+B) [mole%]	2A/(2A+D) [mole%]	Average** [mole%]
4%	3.4 ± 0.4	3.4 ± 0.4	1.5 ± 0.2	1.5 ± 0.2	2.7 ± 0.6
4% (p)	4.5	4.6	4.1	4.2	4.4
10%	10.2 ± 0.5	9.9 ± 0.4	12.7 ± 0.6	12.7 ± 0.6	11.2 ± 0.5
10% (p)	11.1	11.0	7.8	7.7	9.4

Table 4.2 Percentage branching as determined by ^{1}H NMR spectroscopy of 'as made' and reprecipitated copoly(ethylene oxybenzoate)s. ($CDCl_3$/TFA)

* Percentage branching, as calculated from monomer feed; ** Average percentage branching calculated from the NMR data; (p) Sample reprecipitated into methanol, filtered and dried before analysis.

4.2.3 ^{13}C NMR spectroscopy

Minor changes in the ^{13}C NMR spectra of *p*-PEOB were observed with the introduction of 10mole% branching, which became more apparent at higher branching ratios. The most significant changes occurred in the carbonyl region 155-175ppm. In the spectrum of 12.5mole% branched *p*-PEOB, the signal at 168.0ppm, Figure 4.8, correlates reasonably well with the carbonyl signal in linear *p*-PEOB chains at 168.7ppm, indicated in red. In addition, the low intensity signal (blue) at 166.6ppm is consistent with the chemical shifts of carbonyl groups present in branching units. Indeed, the pure hyperbranched polymer has two signals in this region of the ^{13}C NMR spectrum, at 166.2ppm and 167.0ppm, which are attributed to reacted and unreacted ester functionalities, respectively, see Section 5.3. It seems likely that the solitary signal, present in the spectra of copolymer samples with 10mole% and 12.5mole%, is being generated by fully reacted branching units.

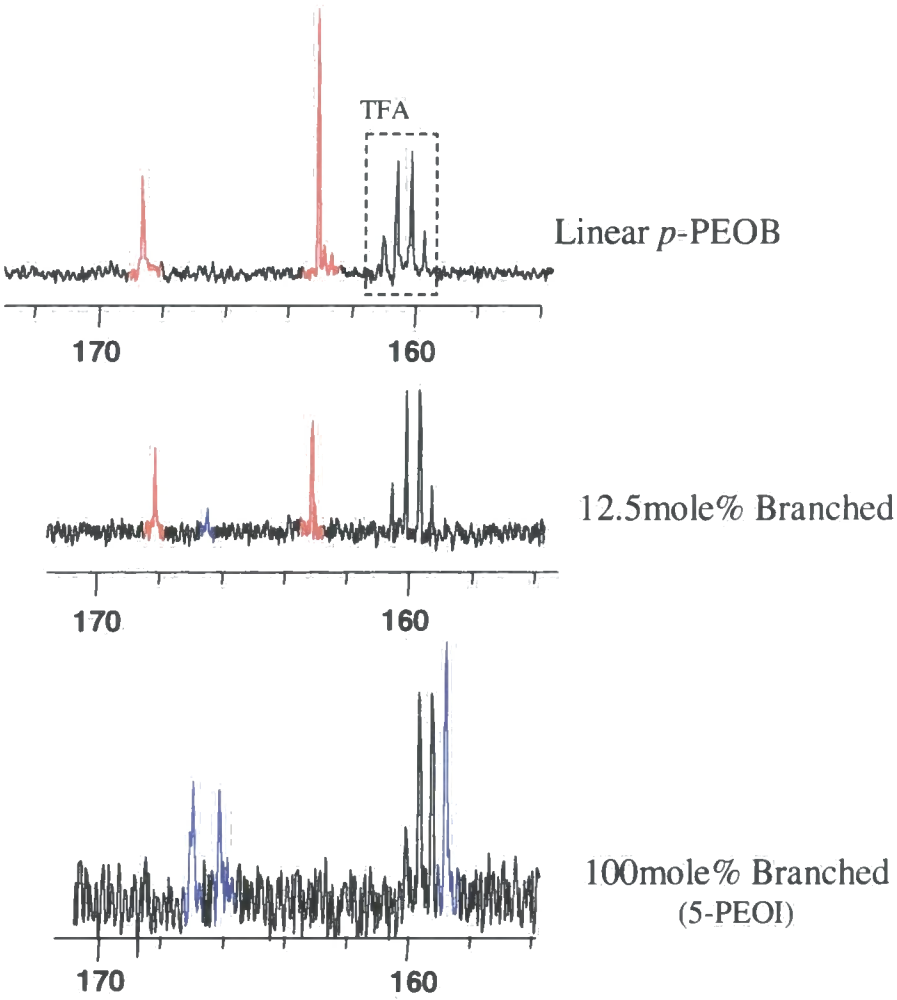

Fig. 4.8 ^{13}C NMR spectra (155-175ppm).

4.2.4 I.R. spectroscopic analysis

The infrared spectra of a series of crystalline copolymers with varying extents of AB_2 monomer incorporation are printed in Figure 4.9.

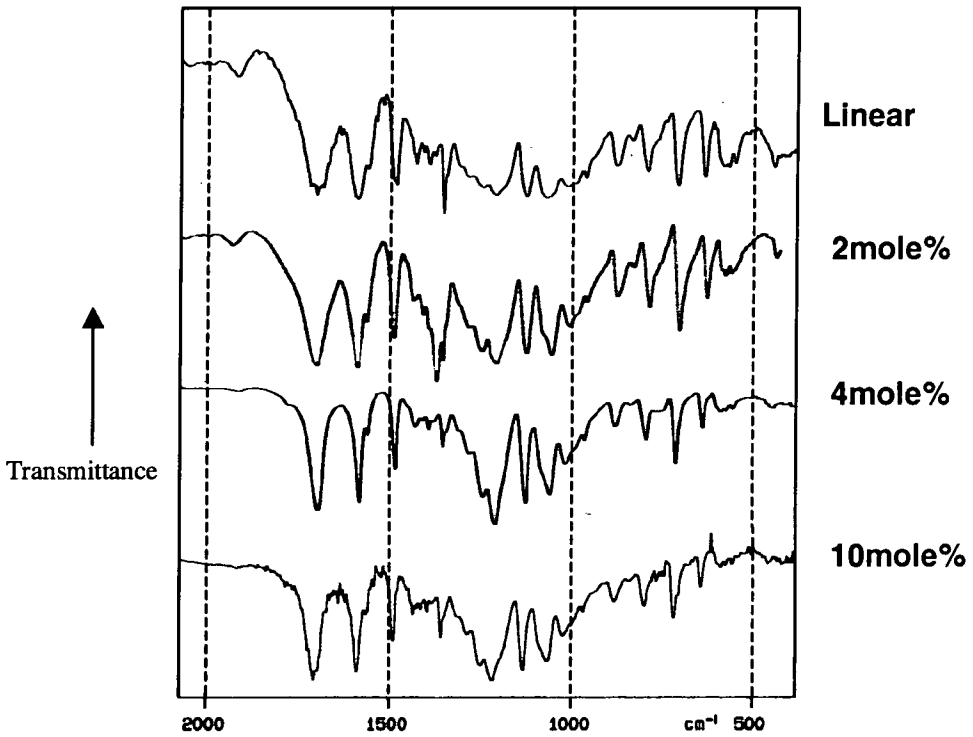

Fig. 4.9 Infrared spectra of linear and branched *p*-PEOB.

The spectra are similar except for subtle changes. However, these changes are more easily seen with the introduction of 15mole%+, as will be presented and discussed in Chapter 5. The similarity of the spectra is consistent with the structure of these polymers.

4.2.5 DSC analysis

The copolymer decomposition temperatures were determined as 2% weight loss, using thermogravimetric analysis. In the absence of monomer, decomposition temperatures of 320°C were measured consistantly. Furthermore, the incorporation of AB_2 branching agent did not appear to affect the decomposition temperature of the copolymer. Samples were analysed by differential scanning calorimetry below the decomposition temperature to avoid excessive degradation and deposition of materials

within the instrument sample capsule. Reproducibility and standardisation of recording conditions was achieved by adopting the following protocols for the heating and cooling stages, as indicated in the diagram.

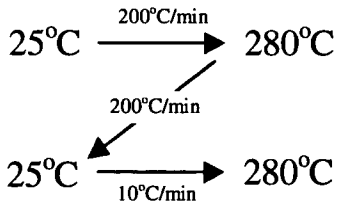

DSC analysis

Figure 4.10 shows a typical DSC trace of a 4% branched *p*-PEOB copolymer. Clearly, as can be seen from the figure, the four basic transitions present in the homopolymer are also observed in copolymers with low percentage branching. Thermal transitions have been measured an analysed with respect to branching composition and molecular weight and are presented and discussed in subsequent sections.

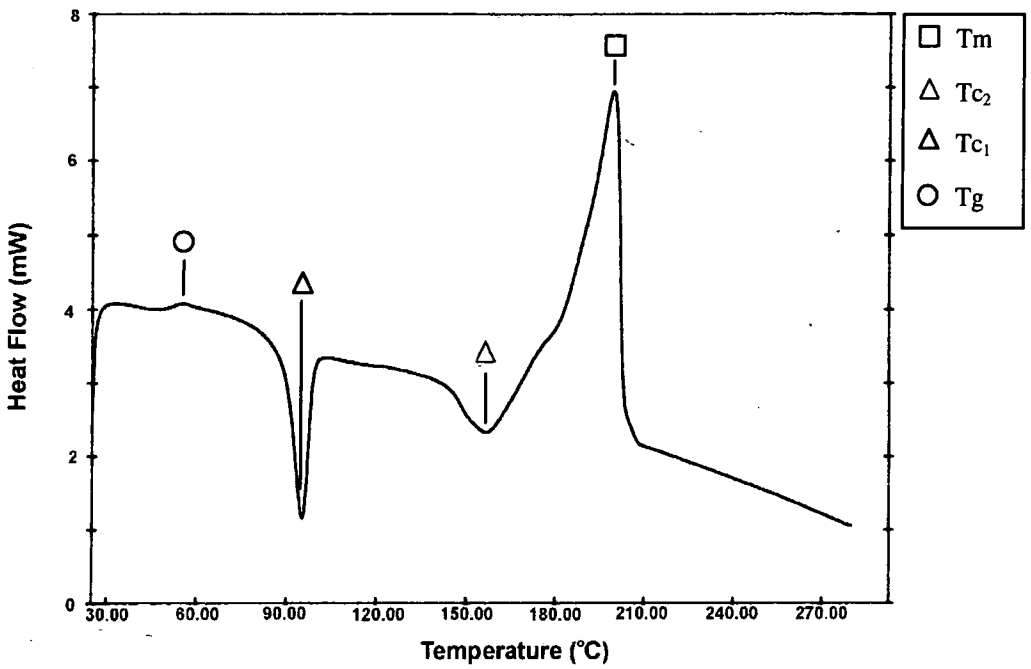

Fig. 4.10 Typical DSC trace of a 4mole% branched *p*-PEOB copolymer.

4.2.5(i) The glass transition

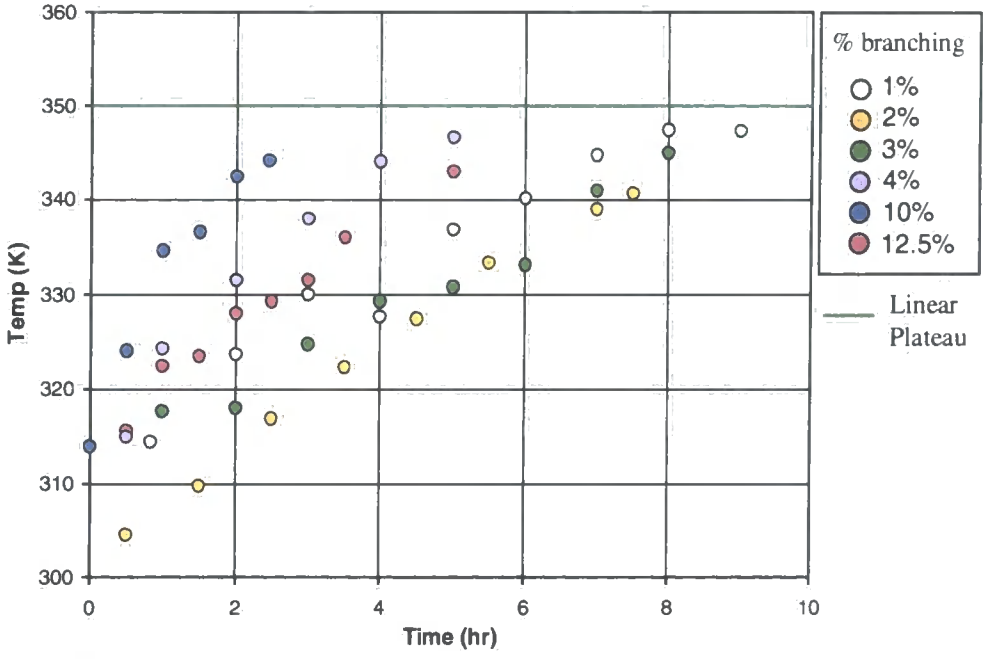

Fig. 4.11 Glass transition temperatures, as plotted for *p*-PEOB copolymers with 1mole%-12.5mole% branching against reaction time.

Figure 4.11 shows the glass transition temperatures, measured by DSC for *p*-PEOB copolymers with various extents of branching, plotted against reaction time. The figure reveals a steady increase in the glass transition temperature with reaction time, toward the linear plateau value of 350K (77°C). However, apart from the general trend indicated in the diagram there appears to be no direct correlation between the branching composition, Tg and the polymerisation time.

Number average molecular weights were determined using ^{1}H NMR end group counting, as described in Chapter 6 of this thesis. When the glass transition temperatures are plotted against Mn, a clear-cut trend is revealed, which appears to be unaffected by the copolymer branching composition, Figure 4.12. The glass transition temperatures of linear *p*-PEOB oligomers, as previously recorded in Section 3.4, are also shown. Clearly, the thermal behaviours of low DP linear oligomers and crystalline branched copolymers of *p*-PEOB are identical, with respect to Mn. The data also demonstrate that the end group counting method, developed to determine the number

average molecular weight of *p*-PEOB copolymers, is effective for the range of DPs and branching compositions analysed here (see Chapter 6).

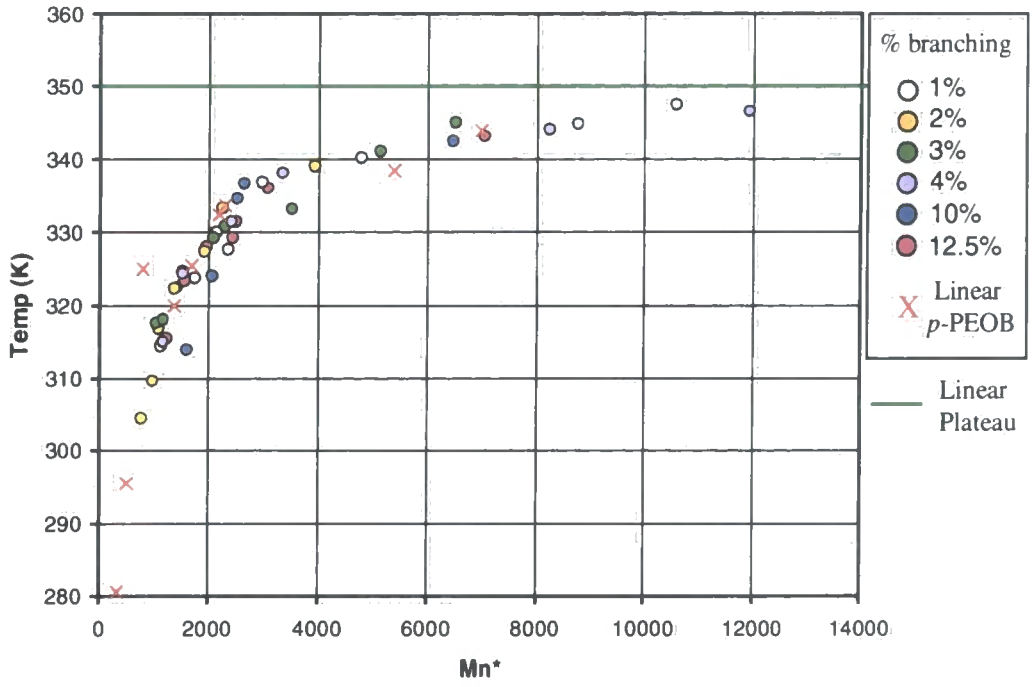

Fig. 4.12 Glass transition temperatures plotted against Mn, for *p*-PEOB homopolymers and copolymers with 1mole% to 12.5mole% branching.

* Mn as determined by ^{1}H NMR spectroscopy.

4.2.5(ii) Crystallisation

The extent to which *p*-PEOB is sensitive to the effects of branching is revealed by analysis of crystallinity in the polymer. Even relatively small amounts of AB_2 incorporation (1-4mole%) give rise to measurable increases in the crystallisation temperature, Figure 4.13.

A reduction in the crystallisation temperature (Tc_1) of *p*-PEOB linear oligomers was observed with decreasing DP, as shown in Figure 4.13; indicating that lower molecular weight samples were more easily organised into crystallisable configurations. The introduction of polyfunctional units into the polymer reduces the average linear segment length between branch points, as discussed in Section 3.4. If these segments were to behave as free independent *p*-PEOB chains then the temperature of crystallisation would decrease, as observed for the homopolymer.

However, clearly this does not happen. The reorganisation of linear segments into crystallisable configurations is made progressively more difficult with increasing extents of branching, as illustrated in Figure 4.13; greater deviation from linear behaviour being observed for samples of higher molecular weight and higher extents of branching.

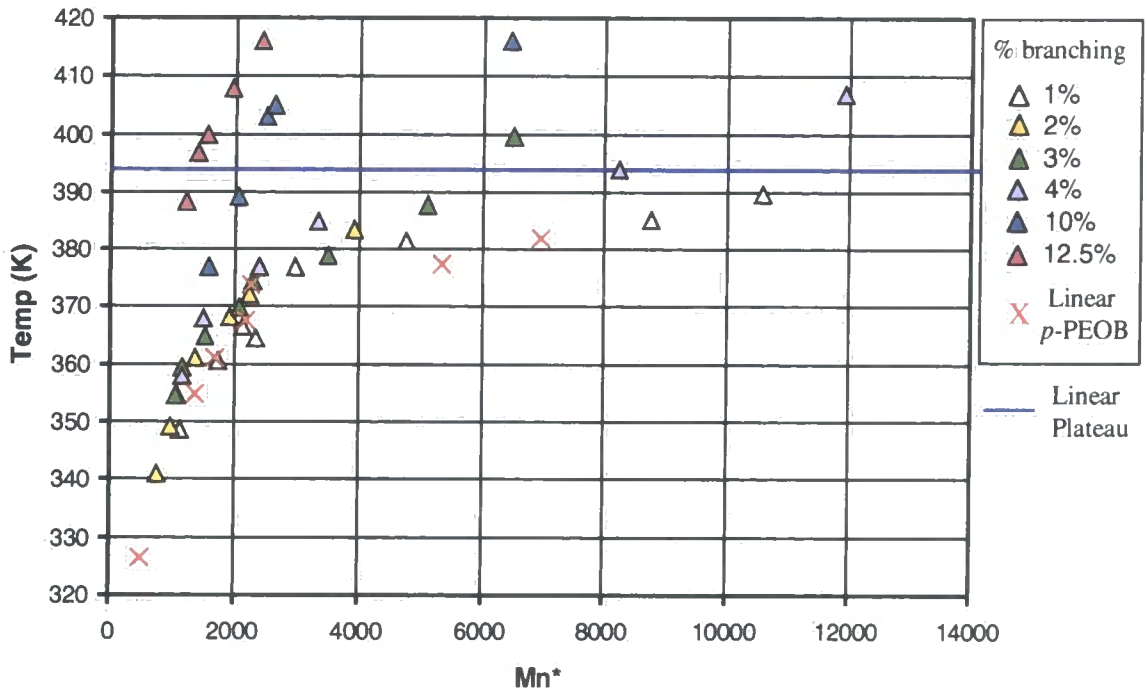

Fig. 4.13 Peak crystallisation temperatures plotted against Mn, for *p*-PEOB homopolymers and copolymers with 1mole% to 12.5mole% branching.

* Mn as measured by ^{1}H NMR spectroscopy

The relative effect of branching on the crystallisation of *p*-PEOB has been determined using the data presented in Figure 4.13. At a sufficiently high molecular weight, a copolymer with 1mole% branching will have, on average, 99 linear units between every branch point. Thus, for this statistical copolymer a number average molecular weight of 16400 is required for an average of one incorporated branch point per molecule. Likewise, for copolymers with 2mole%, 3mole%, 4mole%, 10mole% and 12.5mole% branching, number average molecular weights of 8200, 5500, 4100, 1700 and 1400 are required, respectively, to obtain structures with an average of one branch point. The effect of branching is then determined by cross-referencing these

calculated masses with the crystallisation data recorded in Figure 4.13. A 37°C increase in the crystallisation transition Tc_1 is observed for the copolymer with 12.5mole% branching. Furthermore, increases of 22°C, 9°C and 10°C are observed for copolymers with extents of branching of 10mole%, 4mole% and 3mole%, respectively; indicating that although the crystallisation temperature increases with increasing branching, the effect is not directly proportional to the extent of incorporation. Sufficiently high molecular weights were not obtained for copolymers of 1mole% and 2mole% branching and consequently, the effect of incorporating one branch point on the crystallisation transition temperature of these systems could not be determined.

Remarkably, samples with 12.5mole% branching, i.e. an average of seven linear units to every branch point, could still crystallise, albeit to a significantly lesser extent than copolymers with a higher proportion of linear units. An increase to 15mole% branching resulted in non-crystallisable materials. Figure 4.14, a plot of enthalpy of fusion, measured by DSC, against number average molecular weight, determined by ^{1}H NMR spectroscopy, demonstrates the effect of increasing extents of branching on sample crystallinity.

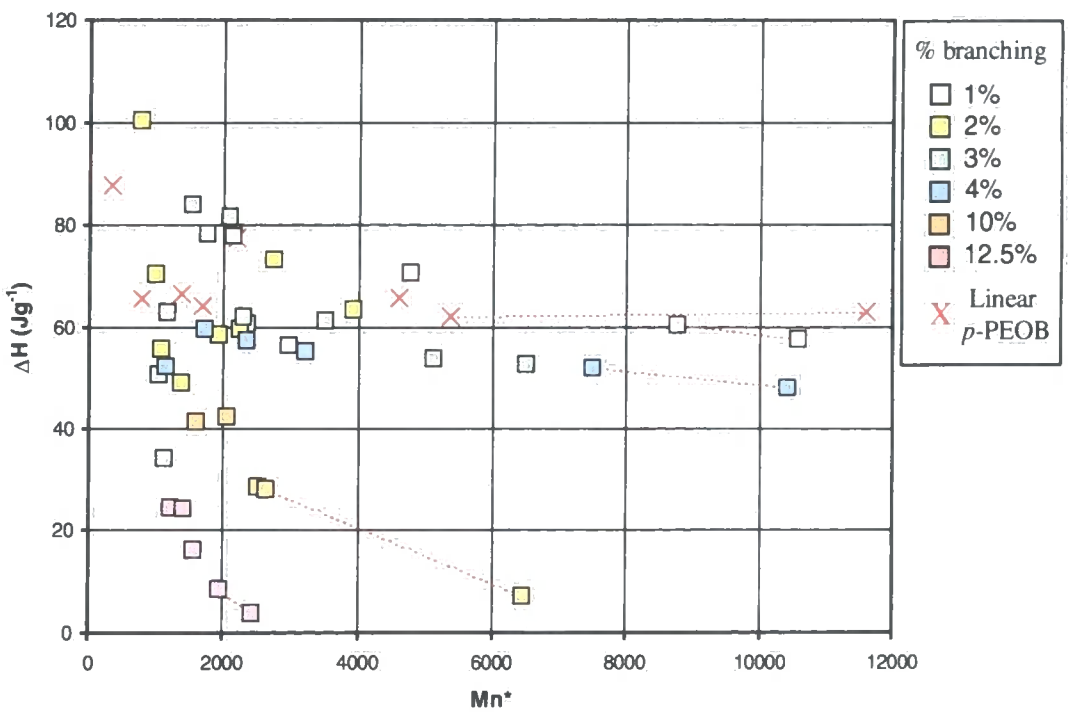

Fig. 4.14 Enthalpy of fusion plotted against Mn for *p*-PEOB homopolymers and copolymers with 1mole% to 12.5mole% branching.

* Mn measured by ^{1}H NMR spectroscopy

The data, although scattered, show a general decrease in the enthalpy of fusion with increasing branching content and molecular weight. This is emphasised by the lines drawn between data points for the samples of linear homopolymer and copolymers of 1mole%, 4mole%, 10mole% and 12.5mole% branching. In addition to the general trend, it would appear that there is more crystallinity in copolymers with 1mole% branching than in low molecular weight samples of linear *p*-PEOB; however, this observation is inconclusive.

4.2.5(iii) The premelting / secondary crystallisation phenomenon

Secondary crystallisation, or premelting, occurs when crystalline regions are reorganised, at the molecular level, into more perfectly ordered crystallites. This phenomenon is common to both PET and *p*-PEOB homopolymers and has been found to occur for *p*-PEOB copolymers with up to 4mole% branching composition, see Figure 4.15. In contrast to the trend observed for the initial crystallisation process, the reorganisation of crystallites is made progressively easier with the introduction of branch points, i.e. premelting transition temperatures are reduced. The recorded data form a consistent trend with increasing branching composition. However, no evidence has been found for the presence of secondary crystallisation in samples with branching compositions of 10mole% or more.

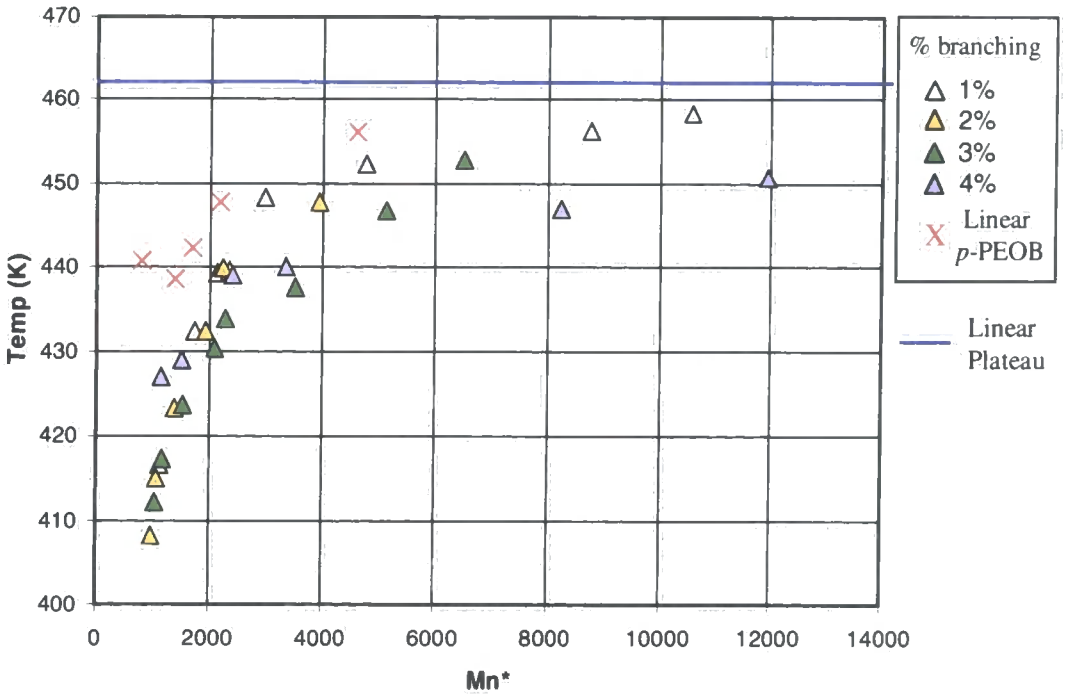

Fig. 4.15 Secondary crystallisation temperatures plotted against Mn for *p*-PEOB homopolymers and copolymers with 1mole% to 4mole% branching.

* Mn as measured by ^{1}H NMR spectroscopy

Crystallisation exotherms were analysed to assess the effects of branching on crystallite reorganisation. Figure 4.16 shows enthalpies of crystallisation (Tc_2) plotted against number average molecular weight, as determined by NMR spectroscopy, for homo and copolymers of *p*-PEOB. Compared to the initial crystallisation transition (Tc_1) (~30Jg^{-1}), secondary crystallisation is small (~6Jg^{-1}) and the standard deviation large ±4Jg^{-1}, consequently the resulting data are very scattered. In fact, they are so scattered that no correlation between the percentage branching, molecular weight and the enthalpy change associated with premelting, can be found.

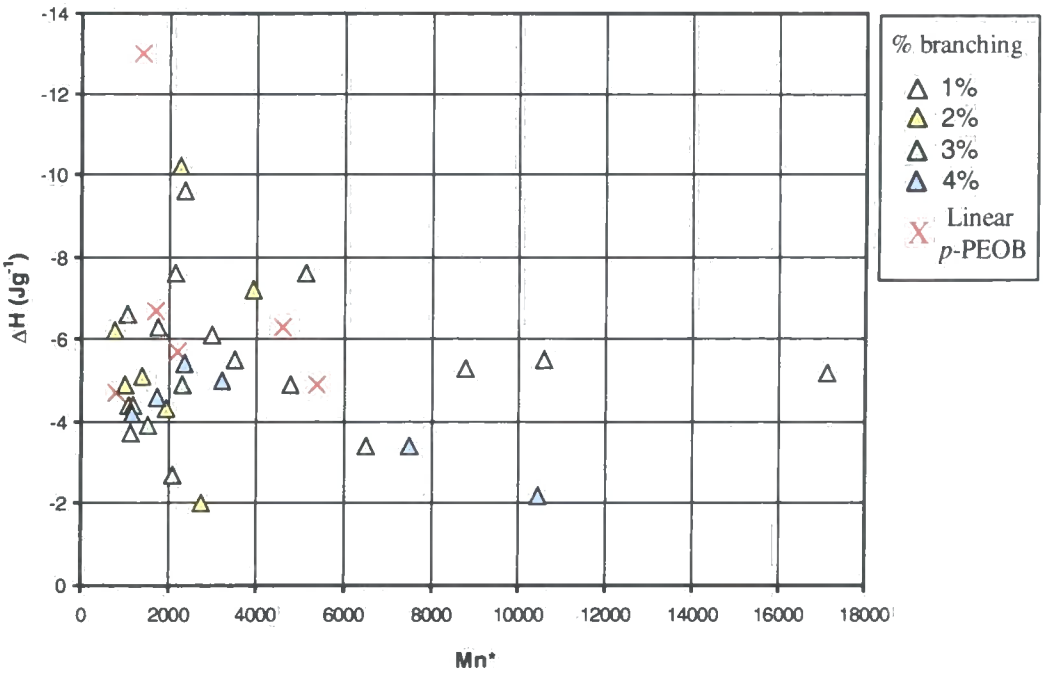

Fig. 4.16 Changes in enthalpy associated with secondary crystallisation, plotted against Mn for homopolymers of *p*-PEOB and copolymers with 1mole% to 4mole% branching.

* Mn as measured by ^{1}H NMR spectroscopy

4.2.5(iv) Melting

The effect of branching composition on the melting temperature, Tm, of *p*-PEOB is shown in Figure 4.17. A rapid 'fall-off' is observed for both linear and branched materials below a number average molecular weight of 1800. The plateau value is reached at Mn values of approximately 5000-7000 for linear *p*-PEOB and materials with up to 4mole% branching. However, it is apparent that the Tm plateau is reached at lower number average molecular weights, approximately 2000-3000, for copolymers with 10mole% branching or more.

Lower molecular weight copolymers with 10mole% branching revealed two distinct melting transitions, which coalesced above the plateau molecular weight value. A typical thermograph is shown in Figure 4.18. As the data for the 10mole% branched copolymer were reproduced after 18 months of sample storage, Figure 4.21 (see later), it is clear that this was not a transitory effect. Copolymers with 12.5mole% branching

did not exhibit any of the distinctive multi-melting behaviour, observed for the copolymer with 10mole% branching. However, they displayed little crystallinity and very broad melting transitions.

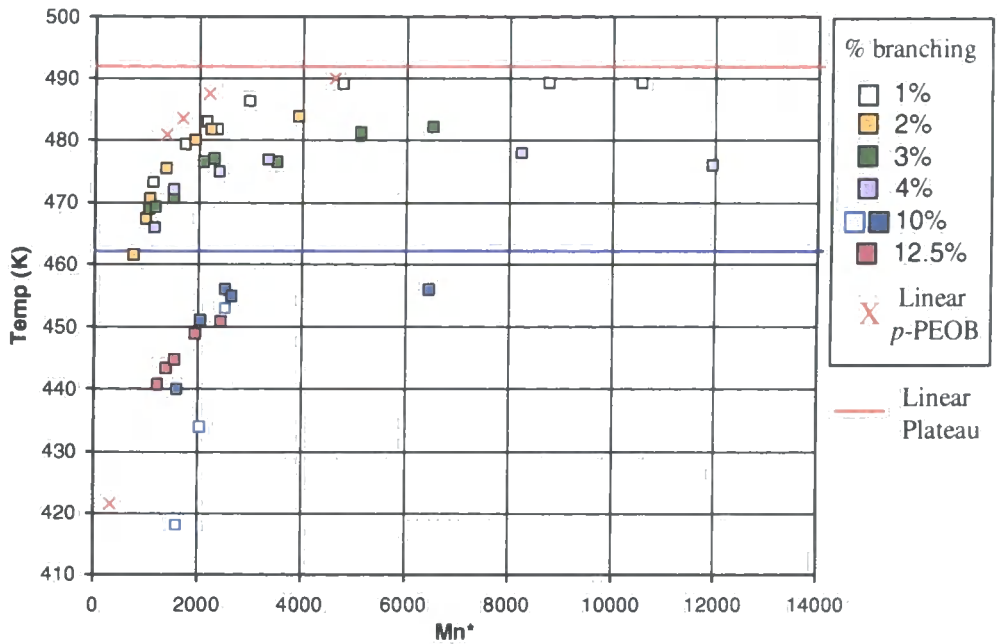

Fig. 4.17 Melting temperatures plotted against Mn for copolymers with 1mole% to 12.5mole% branching. (* Mn as measured by ^{1}H NMR spectroscopy)

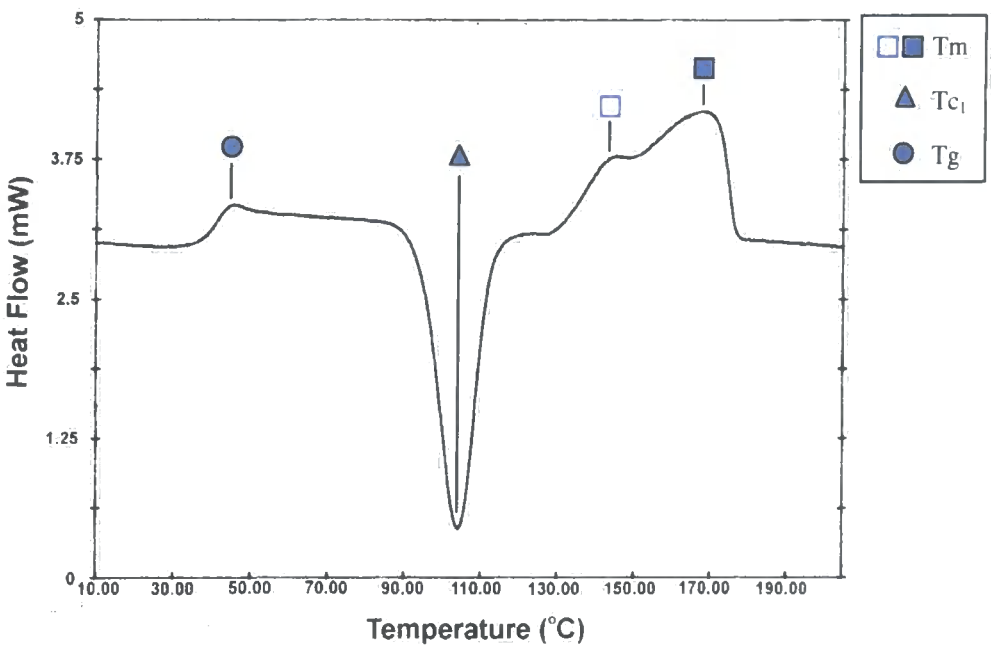

Fig 4.18 Typical DSC trace of a *p*-PEOB copolymer with *ca.* 10mole% branching.

reached when, on average, there are less than two branch points incorporated into the polymer.

4.2.5(v) Residual crystallinity

Samples of *p*-PEOB might be expected to be amorphous if quenched rapidly from the melt. In reality, due to high rates of crystallisation and the limit of instrument cooling rate, crystallites with enthalpies of fusion of $23.1 \pm 8.9 Jg^{-1}$ are formed during the rapid cooling stage of the DSC analysis. 'Residual crystallinity' was evaluated by taking the difference between enthalpies of fusion and crystallisation. Figure 4.20 shows the quantity of residual crystallinity, as determined for samples of linear and branched *p*-PEOB, expressed as a percentage of the total crystallinity observed at the melting point, plotted against number average molecular weight.

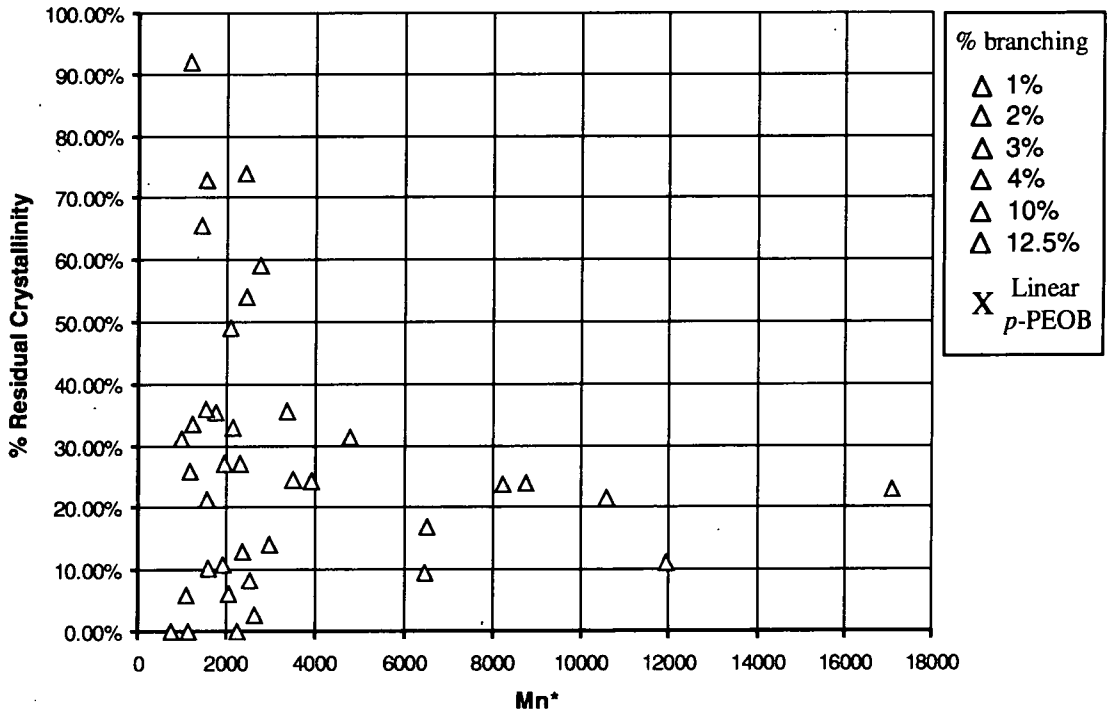

Fig. 4.20 Residual crystallinities (ΔHm+ΔHc) of linear and branched poly(ethylene oxybenzoate) expressed as a percentage of total crystallinity measured at the melt point, plotted against Mn.

(* Mn as measured by ^{1}H NMR spectroscopy)

For the samples with 4mole% branching there is an apparent trend in that the amount of residual crystallinity decreases with increasing molecular weight. However, for all the other samples there are no discernible correlations and consequently, no useful conclusions can be drawn from these data.

4.2.6 Hydrolysis

Expecting that the presence of water, and the age of the polymer would have serious implications for the thermal properties of poly(ethylene oxybenzoate) and its branched copolymers, it was decided to re-analyse aged samples with 4mole% and 10mole% branching. Results obtained by DSC for 18 month old samples, stored under normal laboratory conditions, without drying, are presented in Figure 4.21.

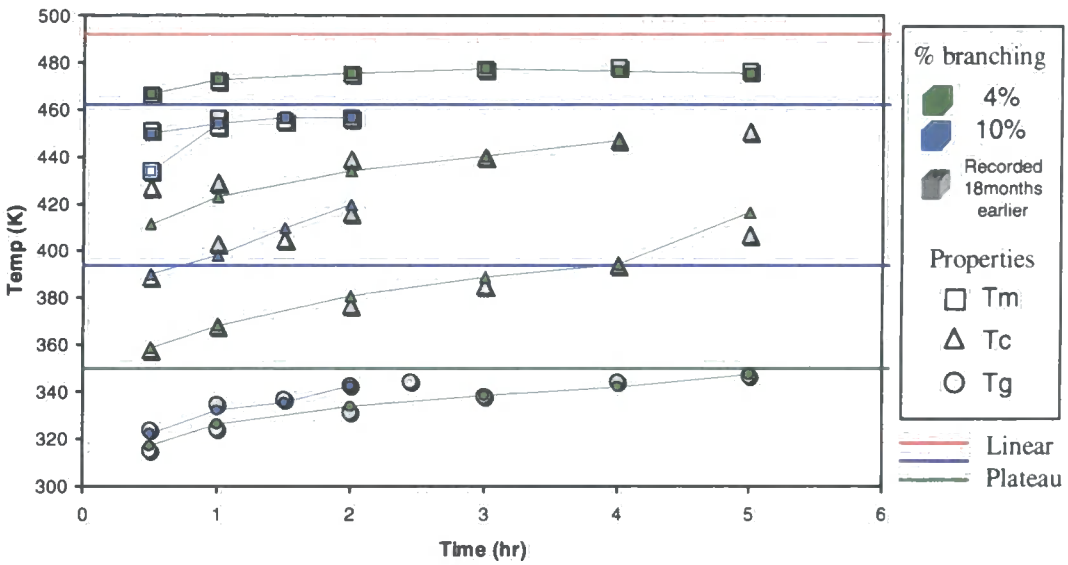

Fig. 4.21 Glass transition, crystallisation and melting point data for 4mole% and 10mole% branched copoly(ethylene oxybenzoate)s, as plotted against reaction time.

With the possible exception of crystallisation, the effects of moisture and ageing on the thermal properties of the polymer are insignificant as compared to instrument variation. Following this assessment, no significant efforts were made to dry samples prior to analysis.

4.3 References

1. Gaynor S.G., Edelman S., Matyjaszewski K., *Macromol.*, **29**, (1996), 1079
2. Oun A.M., *Polym. Inter.*, **29**, (1992), 307-312
3. Rosu R.F., Shanks R.A., Bhattacharya S.N., *Polym. Inter.*, **42**, (1997), 267
4. Manaresi P., Munari A., Pilati F., Alfonso G.C., Russo S., Sartirana M.L., *Polymer*, **27**, (1986), 955
5. Neff B.L., Overton J.R., *ACS Polym. Prep.*, **23**, (1982), 130
6. Munari A., Pilati F., Pezzin G., *Rheol. Acta.*, **23**, (1984), 14
7. Munari A., Pilati F., Pezzin G., *Rheol. Acta.*, **29**, (1990), 469
8. Munari A., Manaresi P., Pilati F, Milani G., Bonora V., *Eur. Polym.* J., **23**, (1987), 265
9. Flory P.J., *J. Am. Chem. Soc.*, **74**, (1952), 2718
10. Kricheldorf H.R., Zang Q., Schwarz G., *Polymer*, **23**, (1982), 1821
11. Schiff H., *Ber. Dtsch. Chem. Ges.*, **15**, (1882), 2588
12. Gilkey R., Caldwell J.R., *J. Appl. Polym. Sci.*, **2**, (1959), 198
13. Kim Y.H., Webster O.W., *J. Am. Chem. Soc.*, **112**, (1990), 4592
14. Kricheldorf H.R., Stöber O., Lübbers D., *Macromol. Chem. Phys.*, **169**, (1995), 3549

Chapter 5

Amorphous Copolymers of Branched
p-Poly(ethylene oxybenzoate)

5.1 Amorphous branched copolymers of *p*-PEOB

In this chapter copolymers with greater than 12.5mole% branching are discussed. Copolymers of *p*-PEOB, branched with 15mole% or more of monomer **(3)**, were found to be completely amorphous and displayed increased solubility with respect to their crystalline analogues. Consequently, solution phase analytical techniques such as gel permeation chromatography could be used in the characterisation of these materials.

5.1.1 Branching Content

The branching content of the amorphous copolymers was determined using the technique described in Chapter 4. However, the disruption of crystallinity and its subsequent effect on solubility, allowed NMR analyses to be performed in both $CDCl_3$ and TFA/$CDCl_3$. Data recorded in Tables 5.1 and 5.2 reveal the average branching content of several amorphous copolymer compositions, as evaluated from solutions of $CDCl_3$ and $CDCl_3$/TFA, respectively. The letters A to D used in the column head formulae, in Tables 5.1 and 5.2, represent the signal intensities of the peaks labelled in Figure 4.7 (page 101).

$CDCl_3$					
Weighed* [mole%]	C/(C+B) [mole%]	C/(C+D) [mole%]	2A/(2A+B) [mole%]	2A/(2A+D) [mole%]	Average** [mole%]
20%	21.0 ± 0.5	20.7 ± 0.5	20.0 ± 1.1	19.7 ± 1.3	20.5 ± 0.9
40%	40.6 ± 0.3	40.5 ± 0.7	38.8 ± 2.4	38.8 ± 1.9	39.7 ± 1.0
60%	57.4 ± 5.9	60.8 ± 2.6	55.2 ± 5.9	58.7 ± 1.1	58.2 ± 3.5
80%	80.2 ± 0.9	79.9 ± 0.5	80.4 ± 0.9	80.1 ± 0.6	80.1 ± 0.5

Table 5.1. Percentage branching of poly(ethylene oxybenzoate) samples, as determined by ^{1}H NMR spectroscopy in $CDCl_3$.

$CDCl_3$/TFA					
Weighed* [mole%]	C/(C+B) [mole%]	C/(C+D) [mole%]	2A/(2A+B) [mole%]	2A/(2A+D) [mole%]	Average** [mole%]
15%	14.7 ± 0.2	14.1 ± 0.2	12.5 ± 0.3	12.0 ± 0.2	13.3 ± 0.2
20%	23.0 ± 1.0	22.5 ± 1.0	25.0 ± 2.4	24.5 ± 2.4	23.7 ± 1.7
40%	40.4 ± 0.3	40.2 ± 0.1	39.3 ± 0.4	39.1 ± 0.5	39.7 ± 0.2
60%	59.7 ± 1.1	59.8 ± 1.2	57.4 ± 1.4	57.5 ± 1.2	58.5 ± 0.4
80%	80.6 ± 1.2	80.6 ± 1.7	80.2 ± 0.9	80.2 ± 1.2	80.4 ± 1.1

Table 5.2 Percentage branching of poly(ethylene oxybenzoate) samples, as determined by ^{1}H NMR spectroscopy in $CDCl_3$/TFA.

* Percentage branching, as calculated from monomer weights; ** Average percentage branching, as calculated from the NMR data; A, B, C and D correspond to signal intensities of peaks labelled in Figure 4.7.

Similarly, as reported for the crystalline copolymers, there is general agreement between the extents of branching determined by NMR spectroscopy and the predictions based on monomer weights. In addition, there is good agreement between values determined in the two solvent systems. Differences between the various columns of data in Tables 5.1 and 5.2 are apparent, but appear to be no more significant than reported previously for the crystalline copolymers of *p*-PEOB.

5.1.2 I.R. Measurements

IR spectra of the amorphous branched copolymers of *p*-PEOB with various extents of branching are recorded in Figure 5.1. It is clear from inspection that changes within the IR spectrum of *p*-PEOB occur with the introduction of branching units. However, these variations are relatively minor and not readily interpreted. The main absorptions: carbonyl stretches (1720cm^{-1}), aromatic ring stretches (1600cm^{-1}), aromatic C-H stretches (3080cm^{-1}) and saturated C-H stretching (2960cm^{-1}) appear to remain the same regardless of the extent of branching.

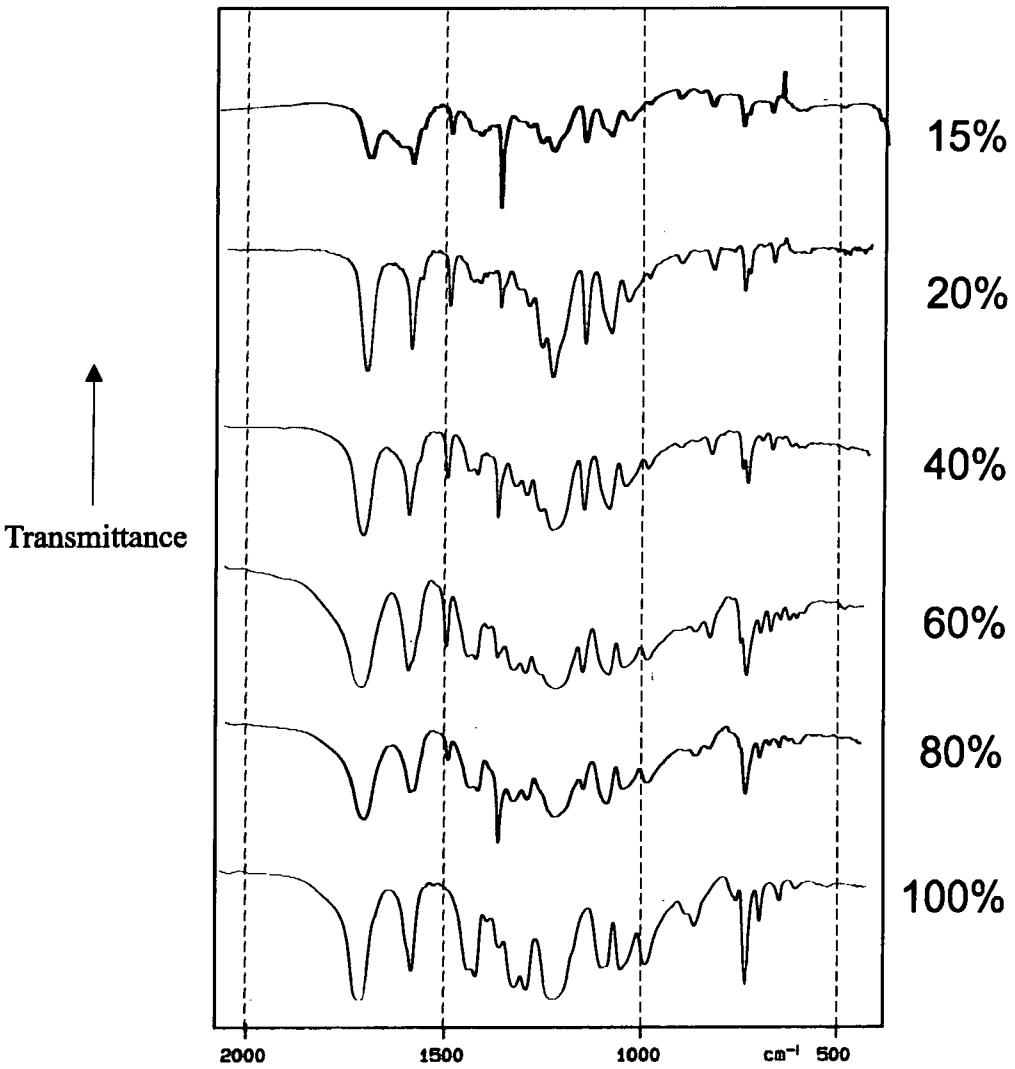

Fig. 5.1 Infrared spectra of the amorphous branched *p*-PEOB copolymers and its hyperbranched analogue.

5.1.3 Theoretical Considerations

The complete unambiguous characterisation of highly branched *p*-PEOB copolymers using ^{13}C NMR proved too difficult to achieve. The principal reason for this failure was the extent of structural diversity. To illustrate the point, the following paragraphs offer some insight into the extent of structural complexity within branched copolymers.

Flory[1] remarked that the expressions derived from his theoretical treatments of branched $AB_{(f-1)}/AB$ copolymers were, "too cumbersome to be of much practical use". Consequently, to simplify the problem, he enumerated structures in terms of numbers of branching units; taking into consideration the lengths and distributions of linear segments, separately; Section 1.5. However, to obtain a more detailed view of polymer structure, i.e. the distribution of sub-units, an alternative methodology was required. The analysis presented below relies on the fact that polymer structure can be considered as an assembly of the smaller units shown in Figure 5.2. Indeed, it is the statistical probability of finding these arrangements of units within a branched copolymer that is of interest in this analysis.

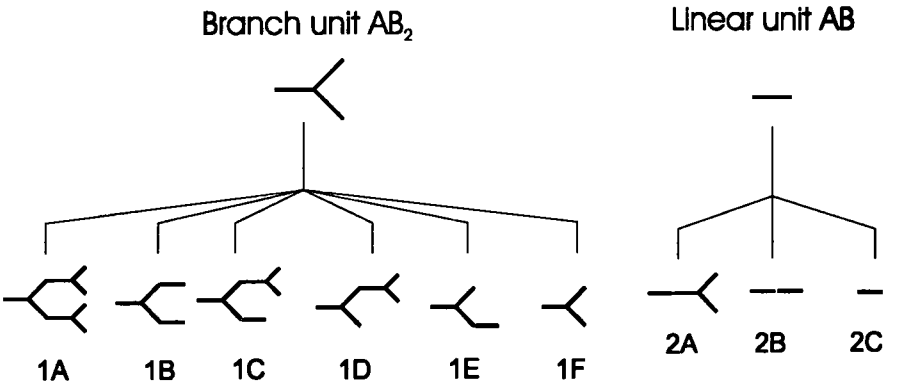

Fig. 5.2 Structural diversity in branched/linear copolymers.

Nine basic combinations of linear and branching units are shown. Of these, six permutations belong to the reaction of B groups in an AB_2 branching unit; the addition of two branching monomers (1A), the addition of two linear units (1B) and so on. In the case of an AB linear residue, there are only three possible outcomes; the addition of a branching unit (2A), addition of a second linear residue (2B), or no further reaction (2C). More complex arrangements of units are possible but these are all combinations of these nine basic permutations.

The advantage of this treatment becomes apparent when one considers the characterisation of branched materials using techniques such as ^{13}C NMR. The limit of resolution of the available NMR spectrometers is such that, beyond the nine basic combinations depicted above, the identification of more complex arrangements is

unlikely. A comparison between the relative number and frequency of structural units predicted by theory and those resolved and measured by NMR spectroscopy may provide evidence for the nature of the process, i.e. whether it is a statistical or selective polymerisation. Furthermore, this type of analysis may assist the assignment of peaks in the spectrum.

The probability of 'finding' any specific arrangement of structural units within the copolymer is dependent upon two factors; the ratio of reacted to unreacted B groups and the structural composition. For an AB/AB_2 copolymer at **100% conversion**, it can be shown that the fraction of unreacted B groups, R, is dependent solely upon the monomer feed composition used to make polymer, Equation 5.1. In the monomer feed, the number of A groups is equal to b+l, where b and l are the numbers of branching and linear units respectively. The number of B groups is equal to 2b+l. Consequently, at one hundred percent conversion, the fraction of reacted 'B' groups is given by (b+l)/(2b+l). Likewise, the fraction of unreacted B groups must be:

$$R \sim 1-[(b+l)/(2b+l)] \qquad \text{Eq. 5.1}$$

Where R = fraction of unreacted 'B' groups as compared to the total number of B groups present in the feed; b = fraction of AB_2 branching units; l = fraction of linear AB units

This relationship is illustrated in Figure 5.3 using a plot of the mole fraction of branching units in the polymer *vs.* the fraction of unreacted B groups.

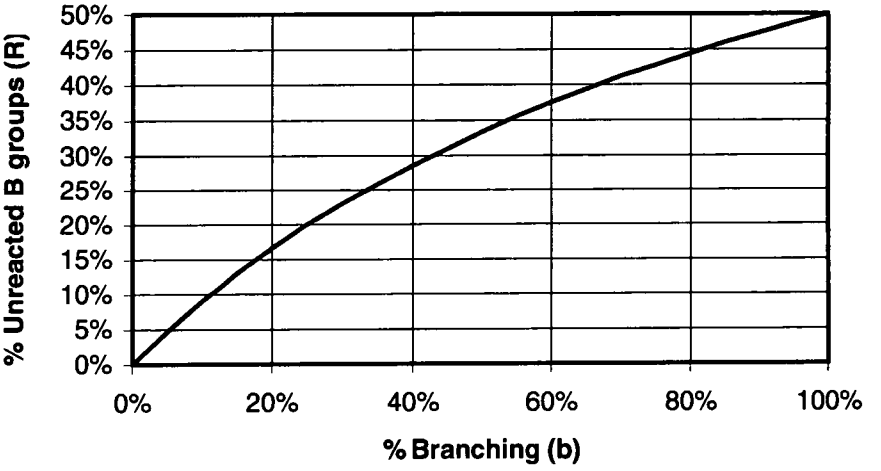

Fig. 5.3 Plot showing how the fraction of unreacted B groups (R), at 100% conversion, varies with branching composition (b).

Formulae, recorded in Table 5.1, describe the copolymer composition in terms of the relative numbers of structural units depicted in Figure 5.2. These are calculated for a statistically distributed copolymer at 100% conversion. The methodology used in the formulation of these equations with reference to the example shown in Figure 5.4, namely unit 1C.

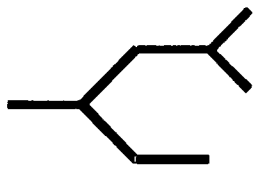

Fig. 5.4 Structural unit: 1C.

The probability, R, that a given B functionality remains unreacted at 100% conversion, is given by Equation 5.1. Clearly, the function (1-R) must equate to the fraction of incorporated B groups. When formulating statistical probabilities, such as those listed in Table 5.1, the number of R terms is determined by the number of possible reactions. In the case of branching units, there are two B groups and hence two possible reactions, whereas for linear residues there is only one. For the example shown a $(1\text{-}R)^2$ term is required as both B groups have reacted. Structural composition is also an important consideration. Every sub-unit must be represented in the formula by the mole fraction of its species. The presence of two branching units and one linear residue, in the example considered, requires an additional b^2l term. Finally, the multiplicity of ways of forming units 1C, 1D and 1E adds an additional factor of two. Thus, by collecting all relevant terms, an expression relating the relative numbers of structural units to the structural composition of the copolymer, at 100% conversion, is obtained.

$$^{(\%)}1C = 2.(1\text{-}R)^2.b^2.l_{\,(x100\%)} \qquad \text{Eq. 5.2}$$

A table of probabilities, based on statistical considerations for all nine structural units shown in Figure 5.2, has been generated; see Table 5.1.

1A	1B	1C	1D	1E	1F
$(1-R)^2.b^3$	$(1-R)^2.b.l^2$	$2.(1-R)^2.b^2.l$	$2.R.(1-R).b^2$	$2.R.(1-R).b.l$	$R^2.b$

2A	2B	2C
$(1-R).l.b$	$(1-R).l^2$	$R.l$

Table 5.1 Expressions relating numbers of structural units in AB/AB_2 copolymers to copolymer composition at 100% conversion, see Figure 5.2.

Using these general expressions, data has been generated for copolymers with various branching compositions and collected in Table 5.2.

b	l	R	1A	1B	1C	1D	1E	1F	2A	2B	2C
0%	100%	0%	0.00%	0.00%	0.00%	0.00%	0.00%	0.00%	0.00%	100.00%	0.00%
10%	90%	9.1%	0.08%	6.69%	1.49%	0.17%	1.49%	0.08%	8.18%	73.64%	8.18%
20%	80%	16.7%	0.56%	8.89%	4.44%	1.11%	4.44%	0.56%	13.33%	53.33%	13.33%
30%	70%	23.1%	1.60%	8.70%	7.46%	3.20%	7.46%	1.60%	16.15%	37.69%	16.15%
40%	60%	28.6%	3.27%	7.35%	9.80%	6.53%	9.80%	3.27%	17.14%	25.71%	17.14%
50%	50%	33.3%	5.56%	5.56%	11.11%	11.11%	11.11%	5.56%	16.67%	16.67%	16.67%
60%	40%	37.5%	8.44%	3.75%	11.25%	16.88%	11.25%	8.44%	15.00%	10.00%	15.00%
70%	30%	41.2%	11.87%	2.18%	10.17%	23.74%	10.17%	11.87%	12.35%	5.29%	12.35%
80%	20%	44.4%	15.80%	0.99%	7.90%	31.60%	7.90%	15.80%	8.89%	2.22%	8.89%
90%	10%	47.4%	20.19%	0.25%	4.49%	40.39%	4.49%	20.19%	4.74%	0.53%	4.74%
100%	0%	50.0%	25.00%	0.00%	0.00%	50.00%	0.00%	25.00%	0.00%	0.00%	0.00%

Table 5.2 Statistical data generated from probability formulae recorded in Table 5.1 for AB/AB_2 copolymers at 100% conversion.

Where R = fraction of unreacted 'B' groups as compared to the total number of B groups present in the feed; b = branching units (%); l = linear units (%)

Table 5.2 reveals several sub-unit structures that occur with equal probability. These include units (1A/1F), (1C/1E) and (2A/2C). Although at first glance the expressions used to generate these data appear to be unrelated, a substitution for R using Equation 5.3 reveals that they are in fact identical.

$$R = (1\text{-}R).b \qquad \text{Eq. 5.3}$$

For clarity, data from Table 5.2 has been plotted in Figure 5.5. Since the probabilities for (1A/1F), (1C/1E) and (2A/2C) are identical only one curve is presented for each, even though the structural units are different.

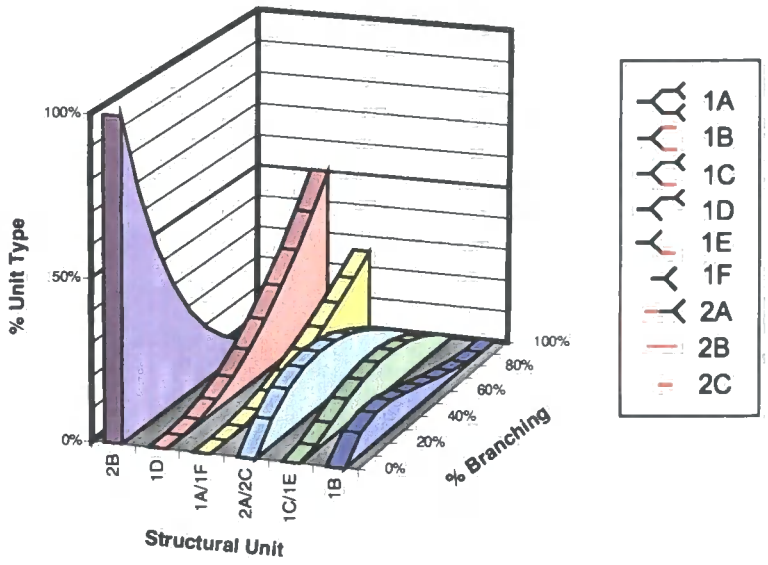

Fig. 5.5 Percentage distribution of structural units, as listed in Table 5.2.

By adding together the relative numbers of structural units, 1F and 2C, we obtain the fraction of units that are end groups. This fraction can be divided into probabilities of attachment to more complex structural arrangements, depicted in Figure 5.2. As an example, consider the structural unit 1E (Figure 5.6) as an 'end group'.

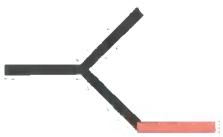

Fig. 5.6 Structural unit: 1E.

The mole fraction of structural units of the type 1E has been evaluated to be 2.R.(1-R).b.l. However, this formula takes into account both end groups and residues incorporated into the body of the polymer. To ascertain the relative number of end

groups, an additional factor R, the probability that the linear residue has not reacted, must be included.

$$^{(\%)}1E^{[\text{end groups}]} = 2.(1\text{-}R).R^2.b.l\ _{(x100\%)} \qquad \text{Eq. 5.4}$$

Where R = fraction of unreacted 'B' groups as compared to the total number of B groups present in the feed; b = fraction of branching units; l = fraction of linear units

Indeed, any combination of linear and branching units may be considered in this way. Expressions for the four units of interest are shown in Table 5.3.

1B	1E	1F	2C
$R^2(1\text{-}R)^2.b.l^2$	$2.R^2.(1\text{-}R).b.l$	$R^2.b$	R.l

Table 5.3 Equations relating the numbers of end groups in an AB/AB$_2$ copolymer to copolymer composition at 100% conversion.

b	1F	1E	1B	2C – 1E – (2x1B)	Total
0%	0.0000	0.0000	0.0000	0.0000	0.000
10%	0.0009	0.0015	0.0006	0.0873	0.090
20%	0.0067	0.0089	0.0030	0.1452	0.164
30%	0.0208	0.0224	0.0060	0.1756	0.225
40%	0.0457	0.0392	0.0084	0.1840	0.277
50%	0.0833	0.0556	0.0093	0.1759	0.324
60%	0.1350	0.0675	0.0084	0.1556	0.367
70%	0.2018	0.0712	0.0063	0.1262	0.405
80%	0.2844	0.0632	0.0035	0.0898	0.441
90%	0.3837	0.0404	0.0011	0.0475	0.473
100%	0.5000	0.0000	0.0000	0.0000	0.500

Table 5.4 End group data: generated for AB/AB$_2$ copolymers at 100% conversion from the expressions in Table 5.3.

Using the general expressions shown in Table 5.3, theoretical data has been generated for copolymers with various branching compositions and collected in Table 5.4. Although, end groups 1B and 1E belong to the set of 2C, they are considered separately. This is achieved by subtracting the mole fraction of sub-units from the parent group. These data are represented graphically in Figures 5.7 and 5.8 in two formats. The first plot shows the relative number of end groups compared to all other units in the copolymer; Figure 5.7. The second representation shows the data as a fraction of end groups in the polymer; Figure 5.8.

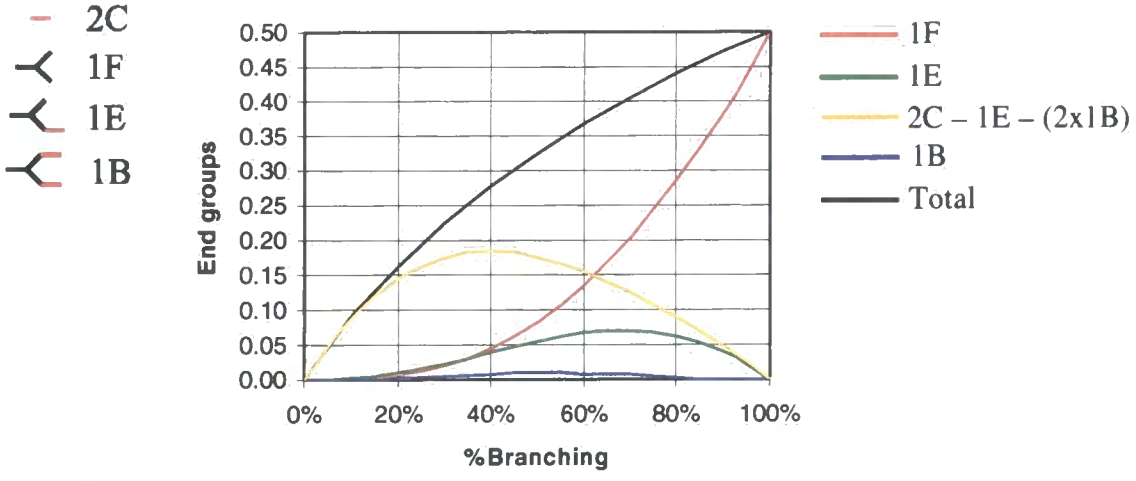

Fig. 5.7 Graph showing relative numbers of end groups *vs.* branching composition for copolymers at 100% conversion.

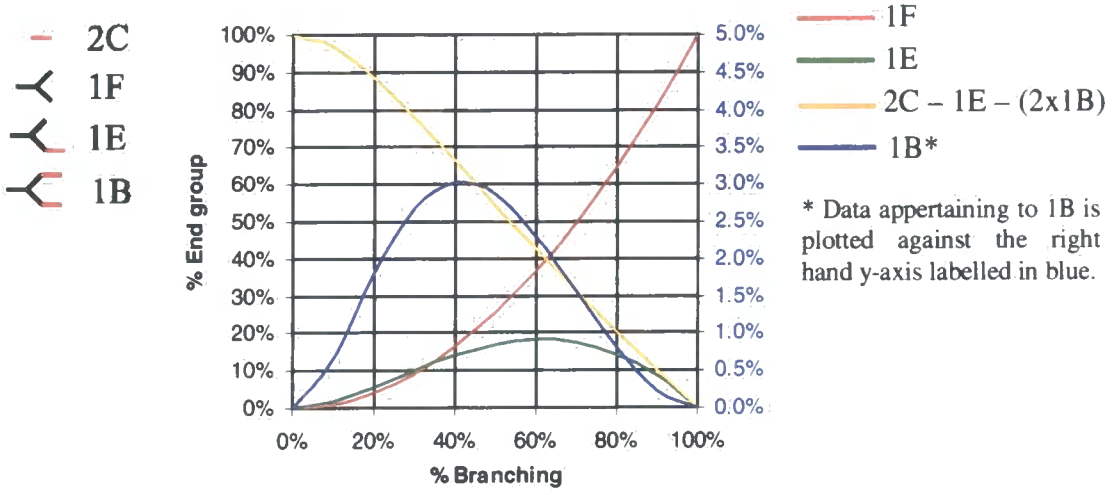

Fig. 5.8 Graph showing percentage of end groups *vs.* branching composition for copolymers at 100% conversion.

5.2 ^{13}C NMR spectroscopy

Figures 5.9 and 5.10 show ^{13}C NMR spectra obtained for amorphous *p*-PEOB copolymers branched with various quantities of monomer **3**, and recorded in $CDCl_3$/TFA and $CDCl_3$ solutions, respectively.

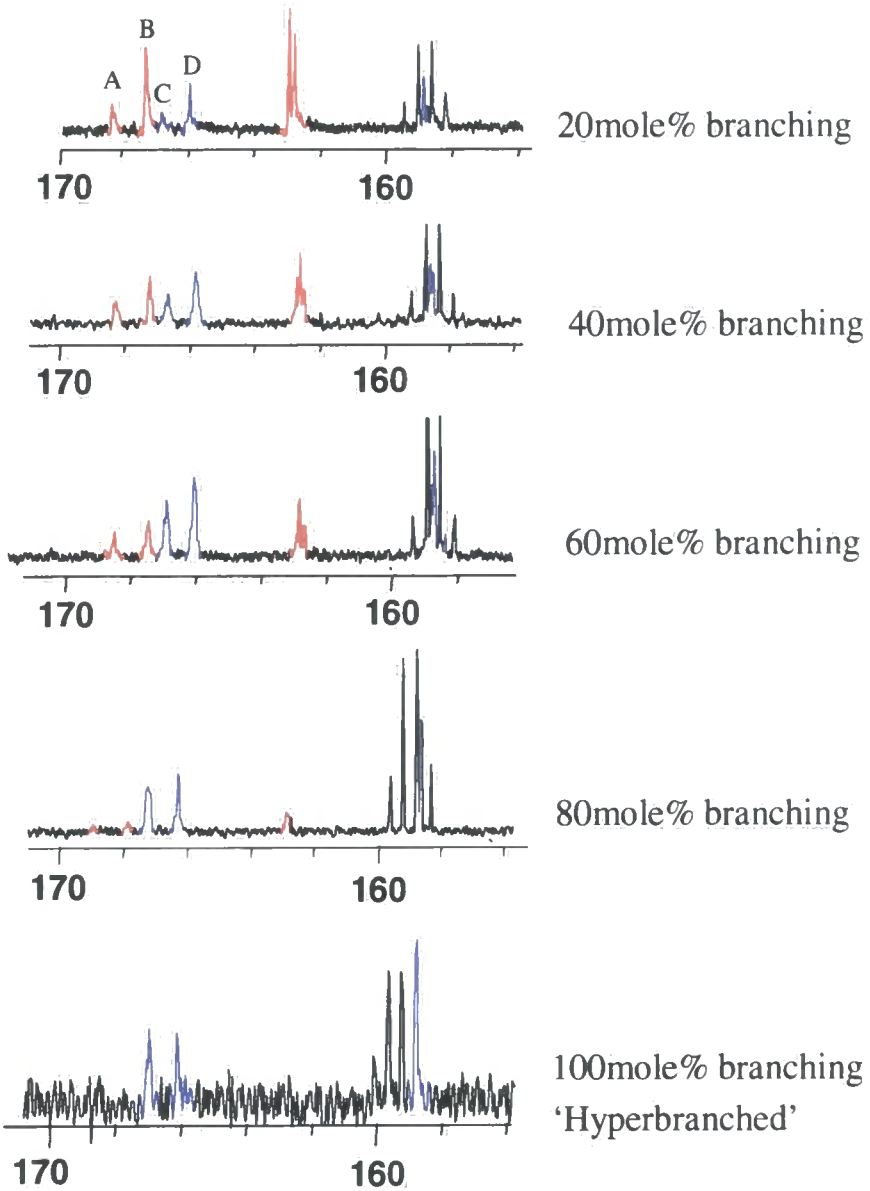

Fig. 5.9 ^{13}C NMR spectra (156-170ppm) of branched *p*-PEOB samples as recorded in $CDCl_3$/TFA.

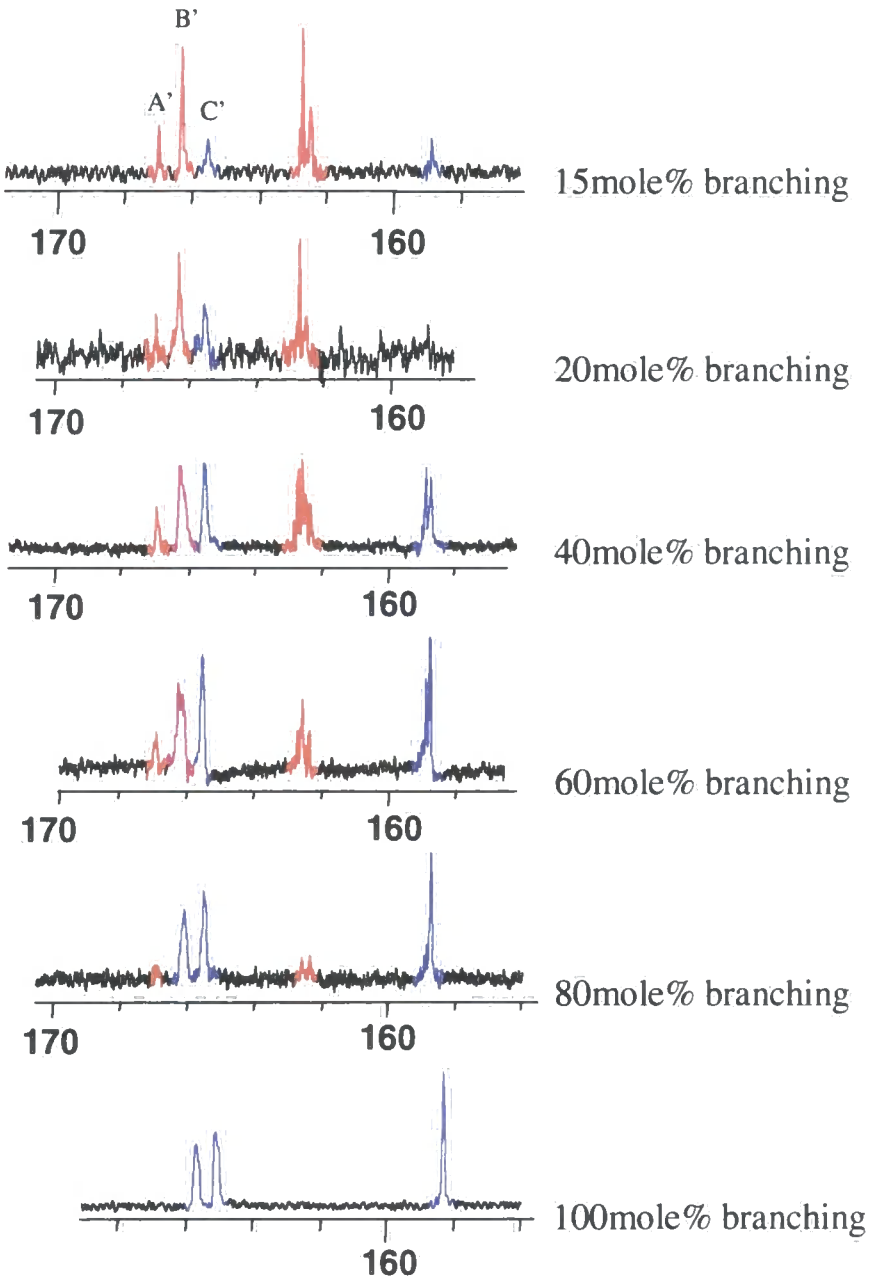

Fig. 5.10 ^{13}C NMR spectra (156-170ppm) of branched *p*-PEOB samples as recorded in $CDCl_3$.

In conjunction with the results of the theoretical analysis, discussed in Section 5.1.3, ^{13}C NMR has proved to be a useful tool in the structural characterisation of branched *p*-PEOBs. Although the measurement of signal intensities was not quantitative, it seems reasonable to assume a negligible difference between the relaxation times of the various carbonyl units since they occur in similar environments.

The carbonyl region, 164-170ppm, reveals several distinct signals, labelled A to D in Figure 5.9. The relative heights of these peaks were measured, normalised and plotted against branching composition in Figure 5.11. Peaks labelled A' to C' in Figure 5.10 were analysed in an identical manner and plotted in Figure 5.12. To a first approximation, the relative numbers of structural units can be determined by measuring the resolved carbonyl signals. The challenge is to assign these signals to a particular structural unit.

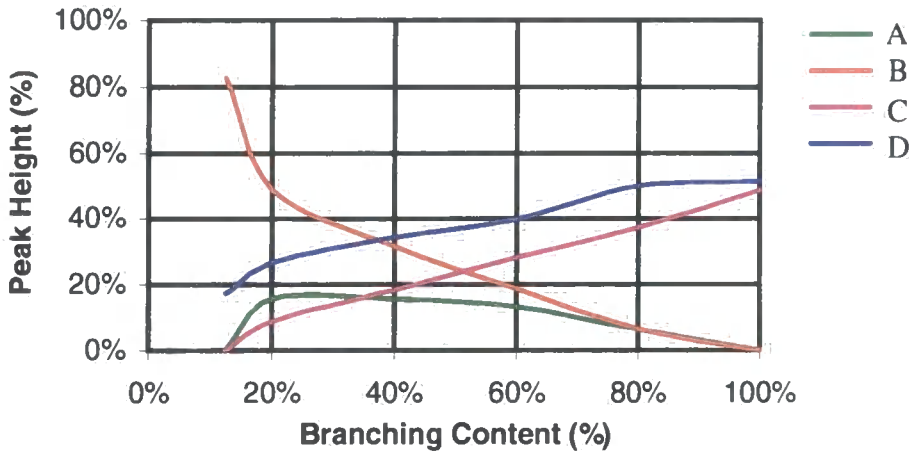

Fig. 5.11 Normalised ^{13}C NMR carbonyl peak heights of branched *p*-PEOB samples, as measured in $CDCl_3$/TFA.

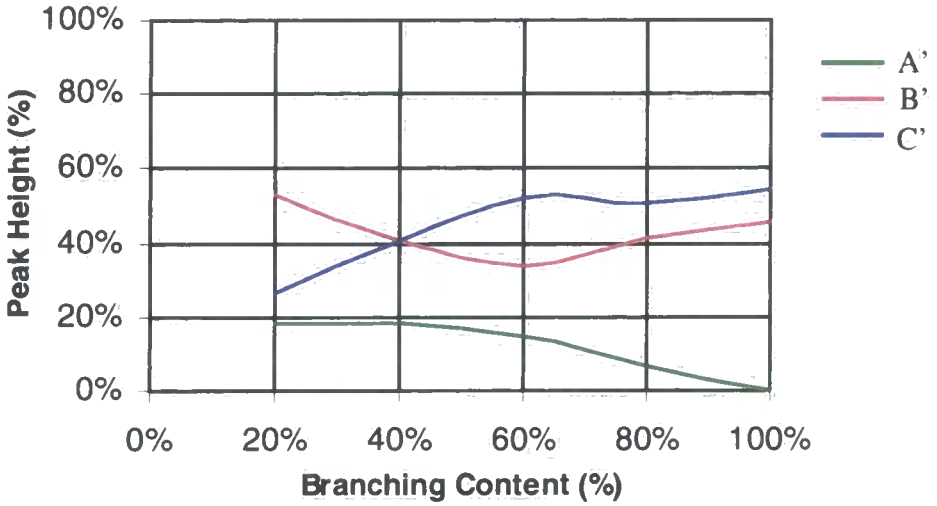

Fig. 5.12 Normalised ^{13}C NMR carbonyl peak heights of branched *p*-PEOB samples, as measured in $CDCl_3$.

The characterisation of these ^{13}C NMR carbonyl signals was achieved for samples in $CDCl_3$/TFA solution by comparing the distribution of signal intensities with branching composition, predicted theoretically *vide supra.* A summary of our findings is given below.

The distribution of signal intensities measured for peak A as a function of extent of branching is plotted alongside the theoretically predicted distribution of linear end groups (type 2C) in green in Figure 5.13. Similarly, the distribution of signal intensities observed for peak B is also shown in Figure 5.13 plotted against the theoretically predicted distribution of linear residues incorporated in the body of the copolymer (red). The statistical data are recorded in Table 5.5. In both cases, the observed intensities and theoretical predictions correlate well. Similarly, we were able to show, based on the distribution of the intensities for peaks C and D, which carbonyl signals were associated with reacted ester functionalities and which were associated with unreacted methyl ester groups; see Figure 5.14 and Table 5.6. A more detailed evaluation of the analysis is described in the paragraphs that follow. The results obtained for samples in pure $CDCl_3$ NMR spectra were not analysed in detail as the contributions from both linear and branching units overlapped (signal B', Figure 5.10). This peak was only resolved into its constituents (B and C, Figure 5.9) with the addition of trifluoroacetic acid.

Before a comparison between theory and experiment could be undertaken, it was necessary to convert the branching content of the copolymer into fractions of carbonyl groups associated with linear and branching residues. This was due to the fact that the theoretical analysis generated data in terms of relative numbers of linear and branching units and not, as measured by ^{13}C NMR spectroscopy, as the fraction of carbonyl groups in the copolymer. The difference arises because branching monomers carry twice as many carbonyl functionalities as linear residues. Consequently, a conversion factor of $\mathbf{2b/(2b+l)}$ is required; where b and l correspond to the mole fractions of branching and linear units respectively.

Figure 5.2 shows the nine basic arrangements of branched and linear units in the copolymer. Branched species may be subdivided into three groups; namely, fully branched species, 1A, 1B and 1C, partially branched species, 1D and 1E, and end

groups, 1F. By adding appropriate columns of theoretical data from Table 5.2 and applying the conversion factor, the numbers of reacted and unreacted ester groups, associated with branching units, may be determined. Results of this analysis are collected in Table 5.6 and plotted in Figure 5.14 against experimental data. It is clear from the figure that the fit is not perfect. However, the results are remarkable when one considers that signal intensities were measured as a function of peak height, spectra were not recorded quantitatively, the signal to noise ratio was quite poor and the theoretical data were generated for copolymers at 100% conversion.

The correlation between theoretical predictions and ^{13}C NMR measurements would suggest that peak C, Figure 5.9, is almost certainly generated by carbonyl moieties associated with unreacted methyl ester groups in branching units. Furthermore, peak D is likely to have been generated by carbonyl functionalities associated with reacted ester groups in branching units. However, carbonyl groups in more complex structural arrangements were not resolved.

b	2b/(2b+l) x100%	Linear End Groups* 2C	Internal Linear* 2A + 2B
0%	0.0%	0.0%	100.0%
10%	18.2%	7.4%	74.4%
20%	33.3%	11.1%	55.6%
30%	46.2%	12.4%	41.4%
40%	57.1%	12.2%	30.6%
50%	66.6%	11.1%	22.2%
60%	75.0%	9.4%	15.6%
70%	82.4%	7.3%	10.4%
80%	88.8%	4.9%	6.2%
90%	94.7%	2.5%	2.8%
100%	100.0%	0.0%	0.0%

Table 5.5 Percentage of linear ester groups.

b = branching content of copolymer (mole%); l = linear content of copolymer (mole%) * data obtained from statistical analysis (Table 5.2, converted to percentage of ester functionalities)

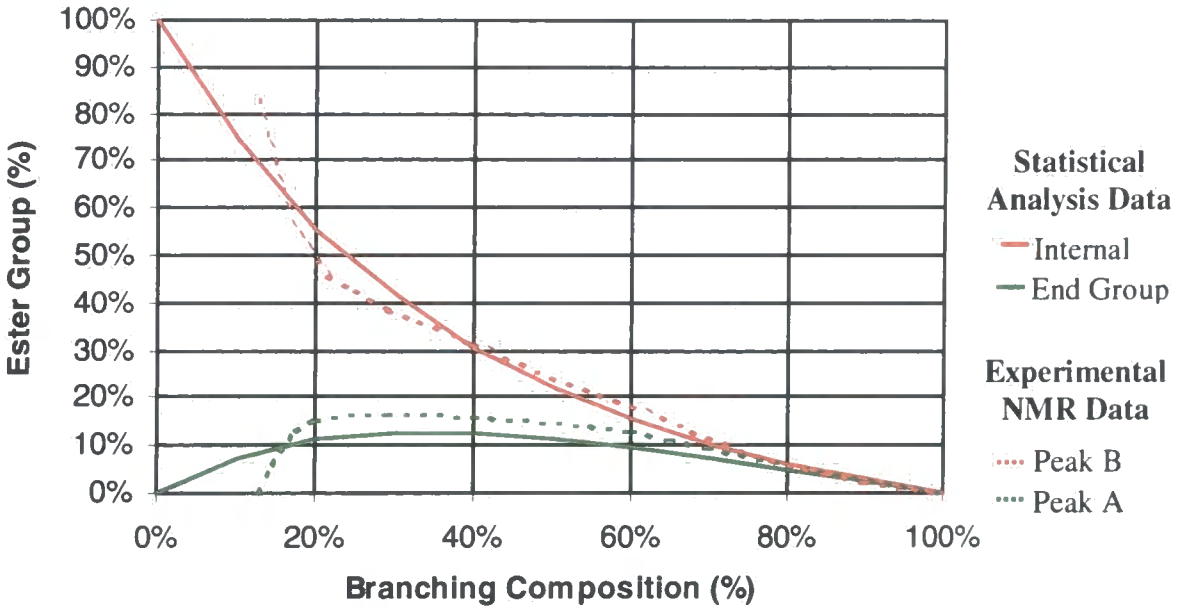

Fig. 5.13 Percentage of linear ester groups (type 2C), experimental *vs.* statistical analysis.

b	2b/(2b+l) x100%	Reacted* 1A + 1B + 1C + ½1D + ½1E	Unreacted* 1F + ½1D + ½1E
0%	0.0%	0.0%	0.0%
10%	18.2%	16.5%	1.7%
20%	33.3%	27.8%	5.6%
30%	46.2%	35.5%	10.7%
40%	57.1%	40.8%	16.3%
50%	66.6%	44.4%	22.2%
60%	75.0%	46.9%	28.1%
70%	82.4%	48.4%	33.9%
80%	88.8%	49.4%	39.5%
90%	94.7%	49.9%	44.9%
100%	100.0%	50.0%	50.0%

Table 5.6 Reacted and unreacted ester groups of branching units, presented as a percentage of the total numbers.

b = branching content of copolymer (mole%); l = linear content of copolymer (mole%) * data obtained from statistical analysis (Table 5.2, converted to percentage of ester functionalities

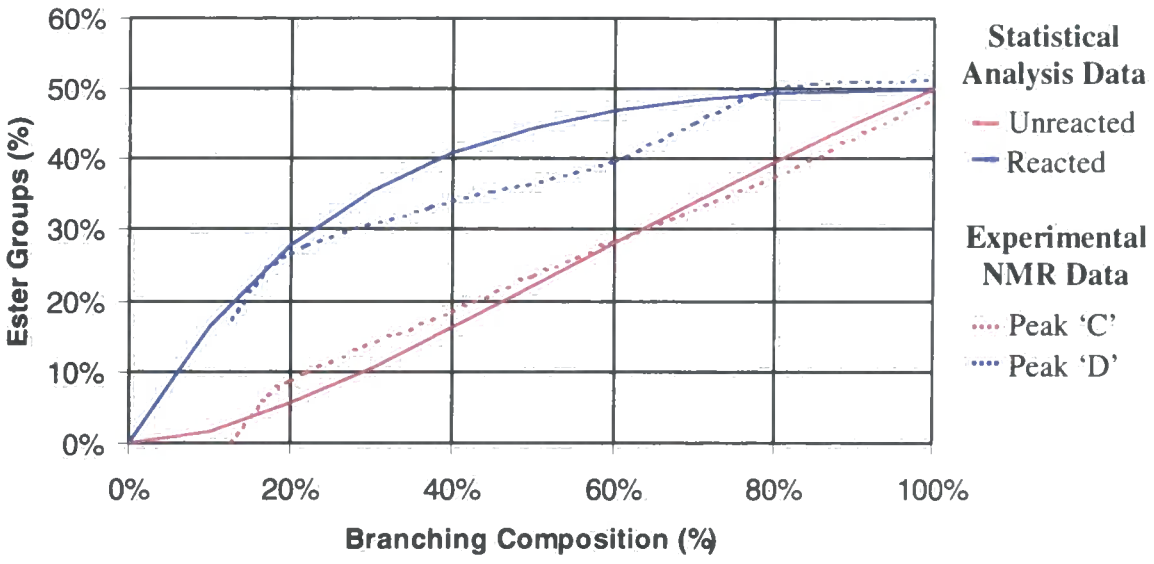

Fig. 5.14 Percentage of reacted and unreacted ester functionalities associated with branching units (type 1F), experimental *vs.* statistical analysis.

The overall conclusion of this analysis, resulting from the good agreement between predictions based on an assumed statistical copolymerisation and ^{13}C NMR experimental observations, is that these copolymerisations appear to be statistical and not selective.

5.3 Matrix Assisted LASER Desorption Ionisation Time of Flight (MALDI-TOF) Mass Spectrometry

MALDI-TOF mass spectroscopic analysis, like other spectroscopic analyses, was not without its limitations. The technique was used successfully to obtain spectra of samples of low molecular branched amorphous *p*-PEOB. Furthermore, a detailed analysis of the spectrum of 40mole% branched *p*-PEOB, using MALDI TOF mass spectrometry, revealed evidence for the incorporation of branching units. However, the quality and ease with which spectra were acquired, appeared to deteriorate with increasing molecular weight and decreasing extents of branching.

For the analysis of *p*-PEOB copolymers, dihydroxybenzoic acid (DHB) was found to be the matrix of choice. Prepared in aqueous solution (10mg ml^{-1}), the matrix was doped with sodium chloride and delivered to the sample slide with a 10µl syringe.

After drying, 10µl of polymer solution 1mg ml^{-1} (95:5 TFA:chloroform) were cautiously transferred to the matrix coated slide in a fume cupboard.

Figure 5.15 shows the mass spectrum of a sample of 40mole% branched *p*-PEOB in the region 1500 to 5000 m/e, with the mass scale calibrated using PEG standards. It was evident from the analysis that the oligomers flew preferentially as sodium ions (MNa^+). Thus, by doping with sodium chloride, we were able to suppress other ionic species to reduce the overall complexity of the spectrum. Despite the relatively poor signal to noise ratio and poor resolution, we were able to assign peaks in the spectrum using the formula presented in Equation 5.5. The ionic masses of hypothetical polymer molecules, consisting of (**x**) linear units and (**y**) branching residues, were calculated and then assigned to peaks in the spectrum.

$$\textbf{Mass} = \textbf{focus} + \textbf{linear units} + \textbf{branching units} + \textbf{end groups} + \textbf{Na}^+$$
$$= 17 + 164.x + 207.y + 15.(y+1) + 23 \qquad \text{Eq. 5.5}$$

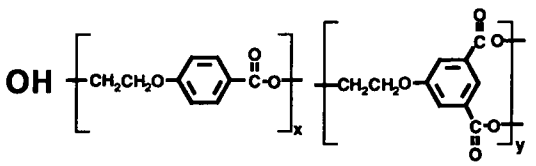

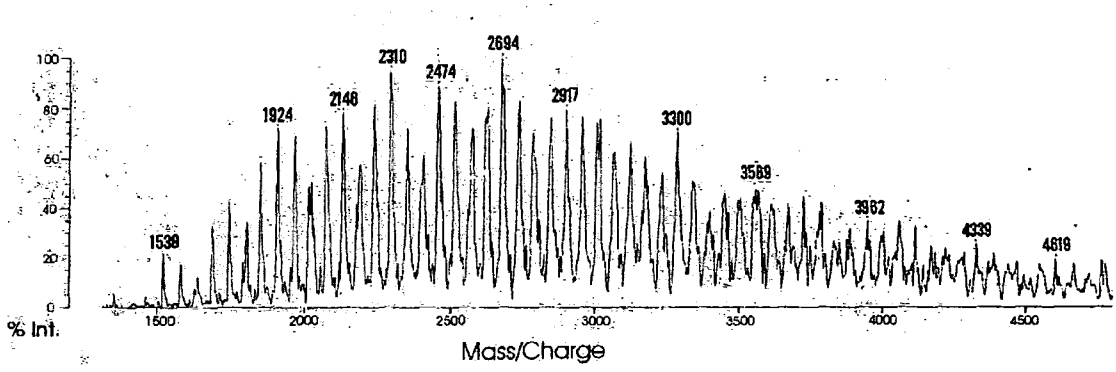

Fig. 5.15 MALDI-TOF spectrum of 40mole% branched *p*-PEOB calibrated with PEG standards (matrix: $DHB_{(aq)}$, $NaCl_{(aq)}$).

Figure 5.16 shows an expanded region of the spectrum (1400-1924 m/e), complete with peak assignments; the numbers in the brackets indicating the number of linear and branching units respectively. Owing to poor resolution and a low signal to noise ratio, in the most extreme cases, peaks would be assigned with uncertainties of ±4

mass units. However, on average, they were found to be within 2.4 units of their calculated masses.

A summary of peak assignments obtained for the MALDI-TOF mass spectrum of 40mole% branched *p*-PEOB is shown in Figure 5.17. The molecular compositions of the ions are indicated by solid red circles, marked at the x, y intercept; where x is the number of linear units and y is the number of branching units.

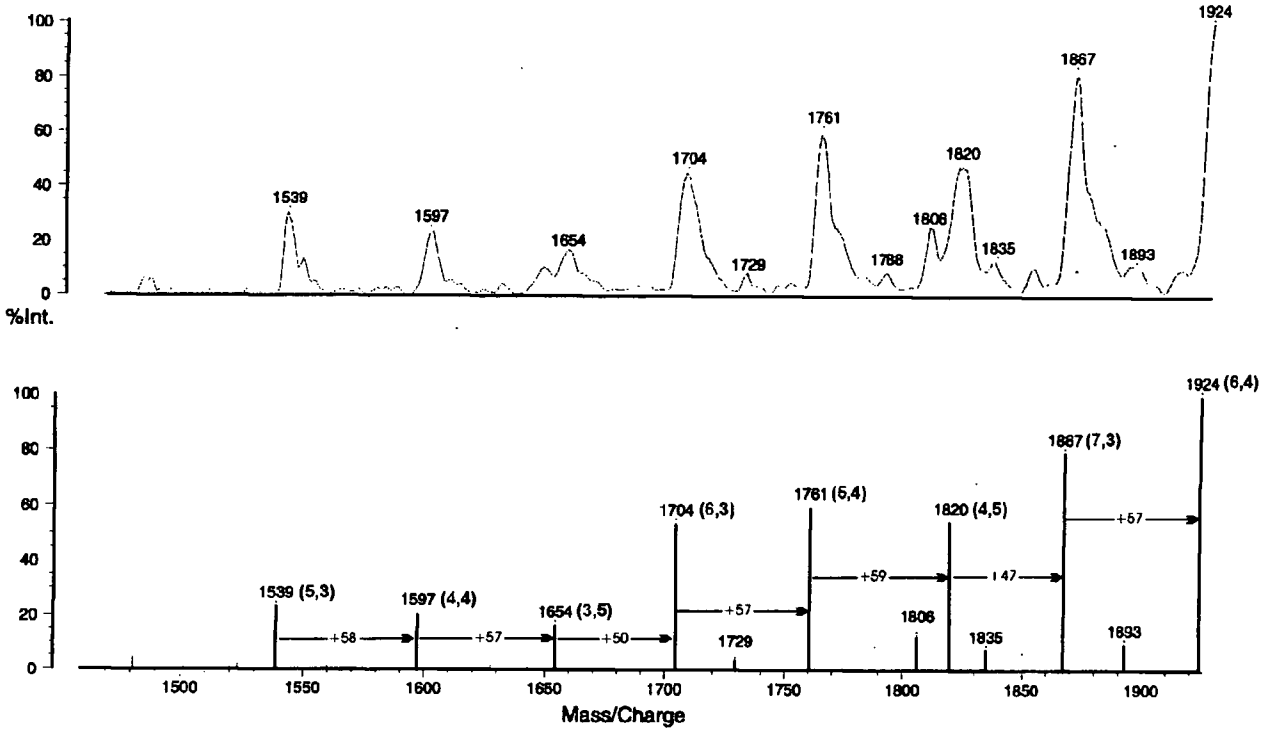

Fig. 5.16 Expanded Region (1500-2000m/e)

Peaks are identified using an (**x,y**) cartesian reference which corresponds to the numbers of **linear** and **branching** units; see Figure (5.17).

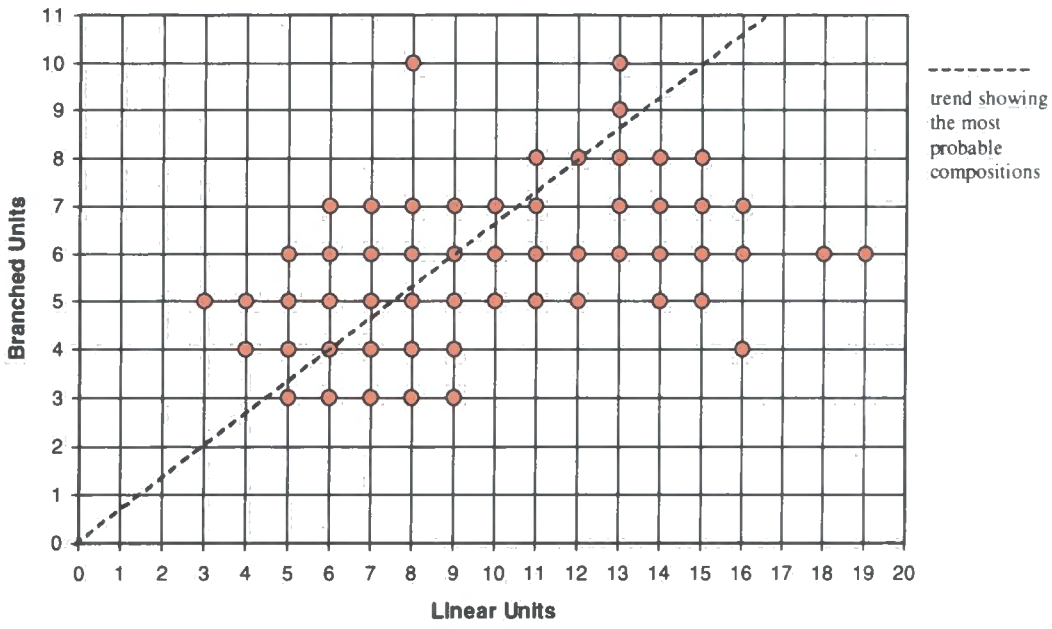

Fig. 5.17 Summary of the MALDI-TOF characterisation data.

Molecular ions with fewer than eight residues were not detected by the instrument. This resulted in a notable absence of ions from the low molecular weight end of the characterisation table. Furthermore, due to a loss of instrument resolution, peak assignments at higher molecular masses were made with increasing ambiguity.

MALDI-TOF mass spectroscopy, as used in this study, did not reveal evidence in support of intramolecular cyclisation. If intramolecular reactions of hydroxyl foci had occurred, the expulsion of methanol from the polymer, with the subsequent loss of 32 mass units, would have provided evidence of cyclisation. No such peaks were identified in the MALDI-TOF spectrum of 40% branched *p*-PEOB, however, this does not exclude the possibility of cyclisation unambiguously since it is unlikely that the recorded spectra represent total sampling of the polymer.

Cyclisation had been observed by Keeney and Parker et al,[2] for a series of hyperbranched analogues synthesised from dimethyl 5-(hydroxyalkoxy)isophthalates with various spacer lengths, using MALDI-TOF mass spectroscopy. It was expected that similar behaviour would be observed for the branched copolymers of *p*-PEOB. However, no evidence for cyclisation was found.

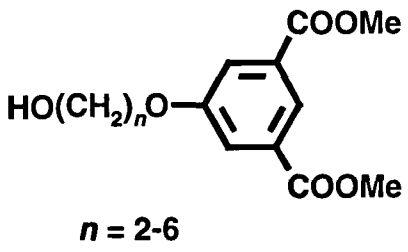

Fig. 5.18 Dimethyl 5-(hydroxyalkoxy)isophthalates, as polymerised and studied by Keeney and Parker et al.[2]

MALDI mass spectrometry is useful for identifying polymer composition, i.e. numbers and types of repeat units, and determining whether cyclisation occurs. However, it is not effective as a technique for determining the molecular weight distribution. This is due primarily to non-uniform sampling. Furthermore, many factors influence the observed distribution; including, sample preparation, laser power, concentration of polymer in the matrix and the nature of the matrix and dopant. The data in Figure 5.16, although probably incomplete due to the limitations of the analysis, indicate copolymer formation. Furthermore, these data are consistent with a statistical copolymerisation but are not of high enough quality to merit further analysis.

5.4 Molecular Weight Determination

As discussed previously, the copolymerisation of meta and para methyl 4-(2-hydroxyethoxy)benzoate produced material with properties which differed significantly from either of the two linear homopolymers, see Chapter 3. Similar effects on material crystallinity and solubility of *p*-PEOB were observed with the insertion of ethylene oxyisophthalate branch points. A detailed investigation revealed a total breakdown of crystallinity in materials with 15mole% branching or more. The resultant increase in solubility presented an opportunity to perform analyses that had not previously been possible, specifically gel permeation chromatography (GPC).

5.4.1 ^{1}H NMR Spectroscopy: End group counting

The use of end group counting, as described in detail in Chapter 6, as a method for determining number average molecular weight was developed for use with *p*-PEOB copolymers and has been used extensively throughout this study.

Figure 5.19 shows number average molecular weights, determined in $CDCl_3$/TFA for copolymers with various extents of branching, plotted against polymerisation time. Although, within one class, there is generally increasing molecular weight with increasing reaction time, it is evident that these data do not reveal well-defined systematic trends. A comparison with the crystalline materials reported in Chapter 4 reveals that the data scatter is more pronounced for the amorphous materials. This effect is not unexpected, see Chapter 6 for detailed discussion.

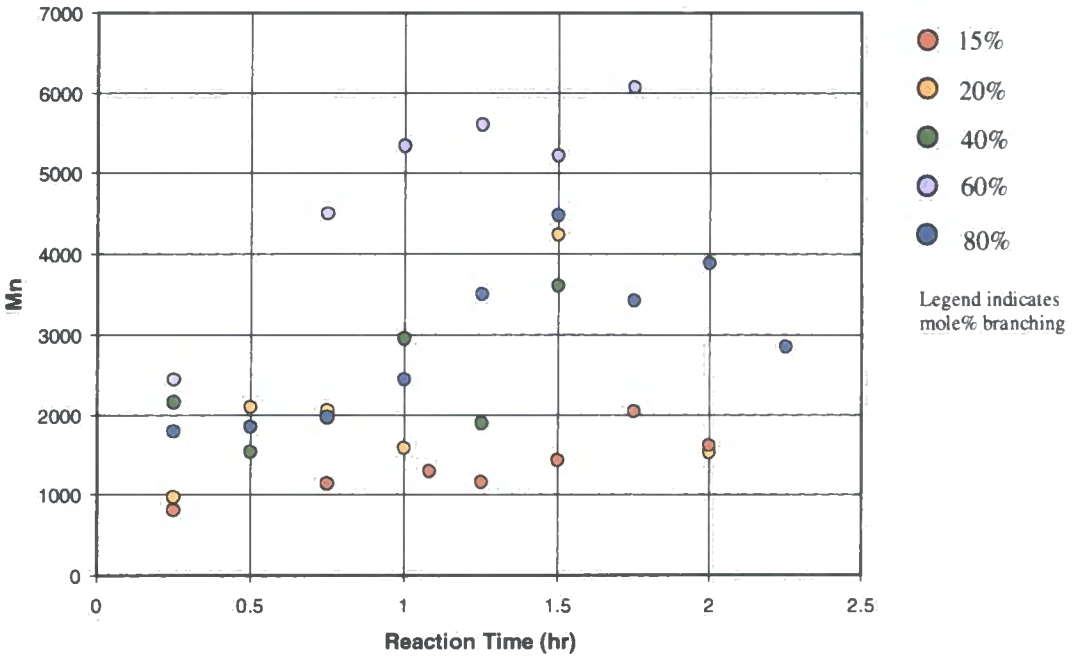

Fig. 5.19 Plot of reaction time *vs.* Mn as measured in $CDCl_3$/TFA using ^{1}H NMR spectroscopy.

A comparison between the Mn values of branched *p*-PEOB, determined by ^{1}H NMR end group counting in pure chloroform-d and in $CDCl_3$/TFA is presented in Figure 5.20. Although these data are significantly scattered, a relationship between

branching composition, molecular weight and NMR solvent is apparent. The three coloured lines in Figure 5.20 are drawn based on linear regression analyses and have correlation coefficients (R^2) of 0.35 (red, 15mole% branching), 0.72 (green, 40mole% branching), and 0.45 (purple, 60mole% branching). If this technique had worked well, identical values for Mn should be obtained in both NMR solvents and the data points would fall on the line y=x, indicated in black. The fact that this does not occur illustrates the limitations of this analytical technique. Indeed, it only really allows broad trends to be detected in these highly branched copolymers.

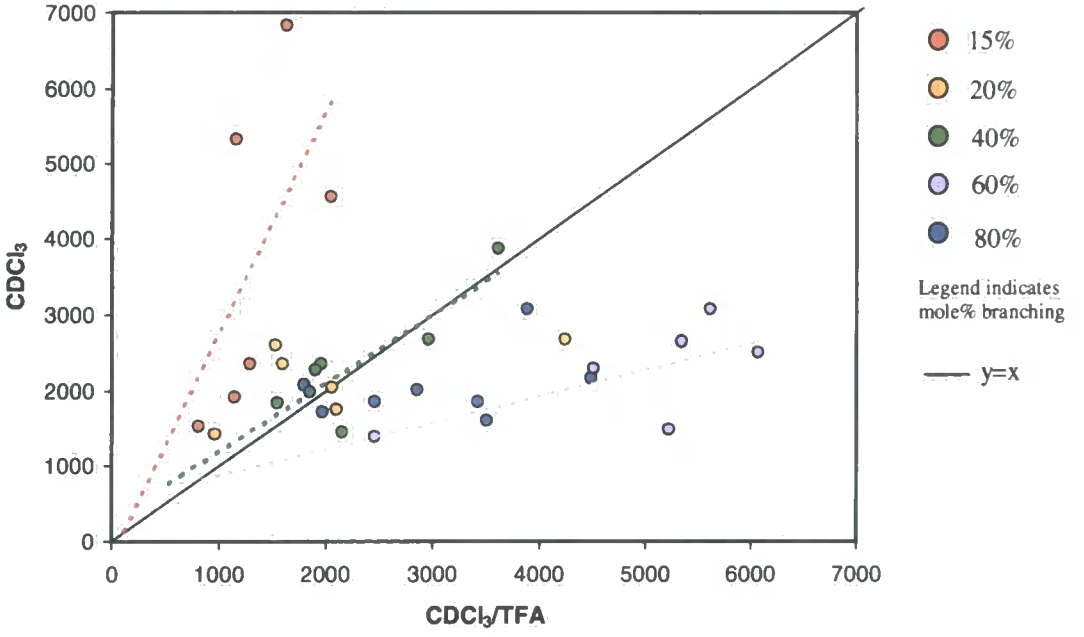

Fig. 5.20 Plot of $CDCl_3$/TFA *vs.* $CDCl_3$ Mn values, as measured using ^1H NMR end group counting.

5.4.2 Chloroform Gel Permeation Chromatography (GPC)

Chloroform GPC, calibrated with polystyrene standards, has been used to determine the number and weight average molecular weights of a range of amorphous branched *p*-PEOB copolymer samples. Figure 5.21 shows a typical set of results obtained for a series of 20mole% branched *p*-PEOB copolymers.

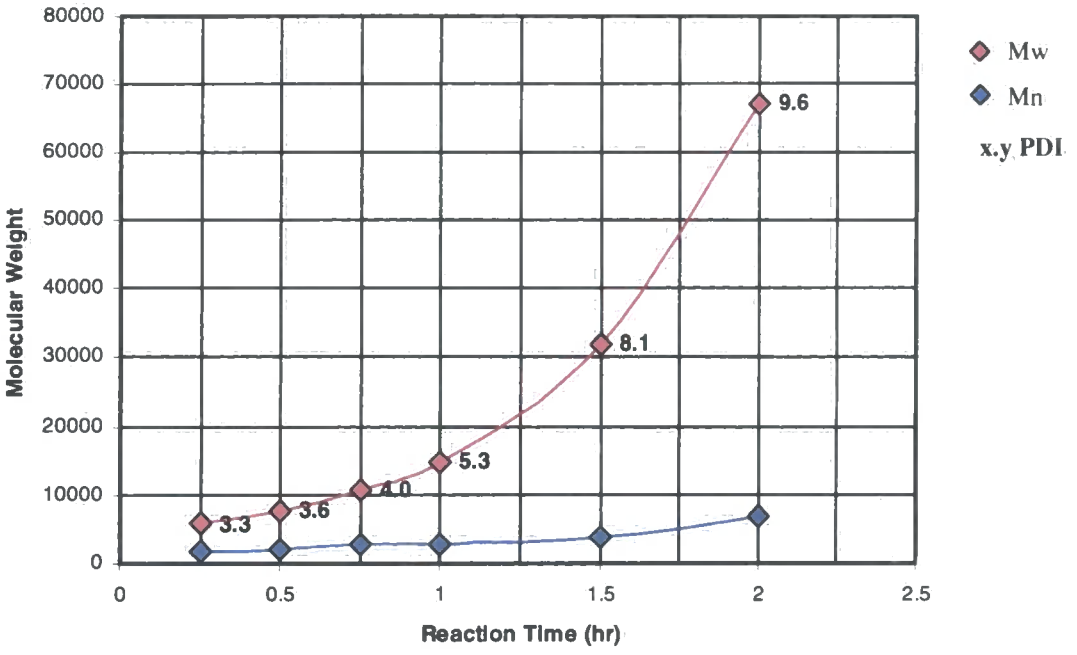

Fig. 5.21 Plot of Mn and Mw, as measured by conventional GPC ($CHCl_3$, 5μm gel columns of 100Å, 10^3Å, 10^5Å pore size, PS standards), against reaction time for 20mole% branched *p*-PEOB.

It was anticipated, based on Flory's theoretical treatment of AB_x polymers,[1] that Mw would increase at a faster rate than Mn and furthermore, unlike linear step growth polymers, the polydispersity would tend to infinity rather than to a value of two. The relationship between the rate of increase of polydispersity and molecular weight was expected to depend upon the composition of the monomer feed, i.e. the greater the mole fraction of branching monomer the faster the increase in dispersity. However, under scrutiny, this prediction was not fulfilled.

Molecular weight data, as recorded using conventional GPC, for *p*-PEOB copolymers with various extents of branching are shown in Figures 5.22, 5.23 and 5.24. Figures 5.22 and 5.23 reveal a systematic increase in molecular weight with reaction time, as expected. The plot of Mn against Mw in Figure 5.24 shows that the change in sample polydispersity with molecular weight appears to be independent of the extent of branching. However, because of the uncertainty in the absolute molecular weights of these materials, the apparent relationship must be treated with caution.

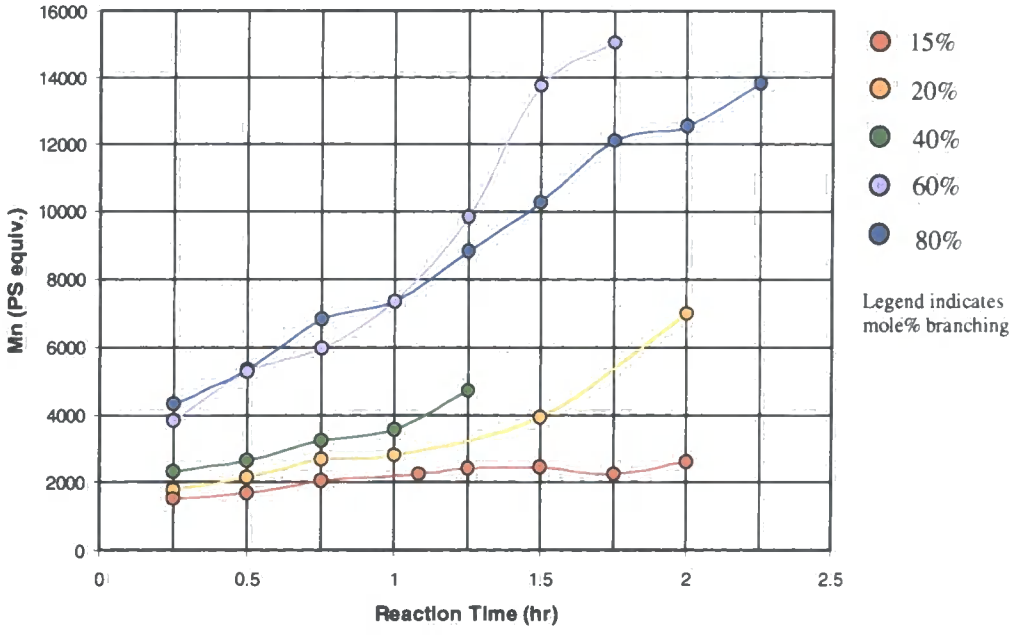

Fig. 5.22 Plot of Mn *vs.* reaction time for *p*-PEOB copolymers with varying extents of branching as measured by conventional GPC ($CHCl_3$, 5μm gel columns of 100Å, 10^3Å, 10^5Å pore size, PS standards).

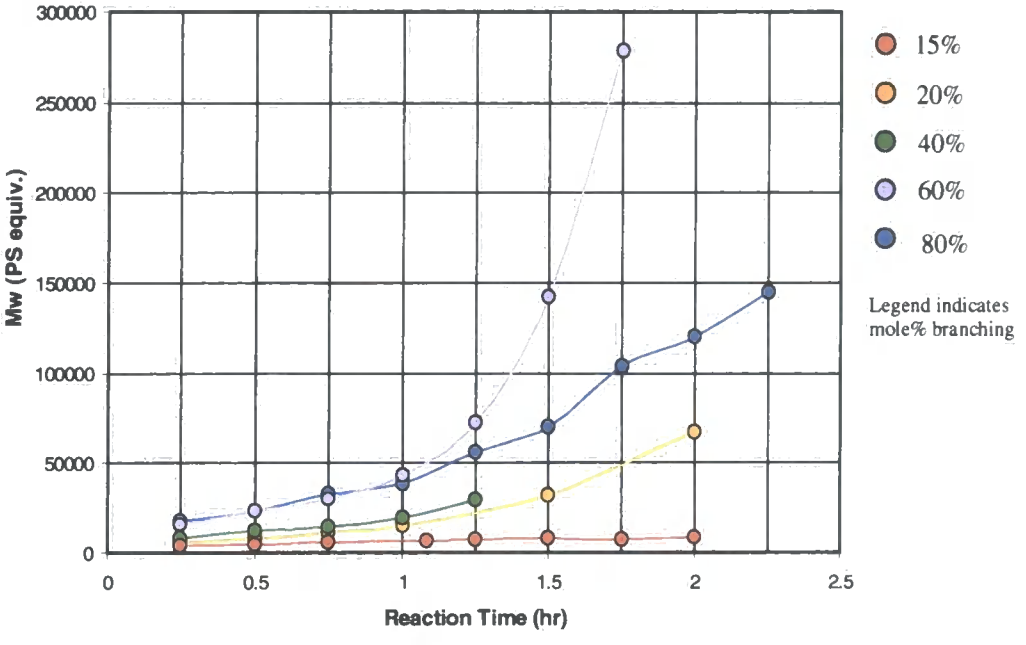

Fig. 5.23 Plot of Mw *vs.* reaction time for branching *p*-PEOB copolymers of varying composition as measured by conventional GPC ($CHCl_3$, 5μm gel columns of 100Å, 10^3Å, 10^5Å pore size, PS standards).

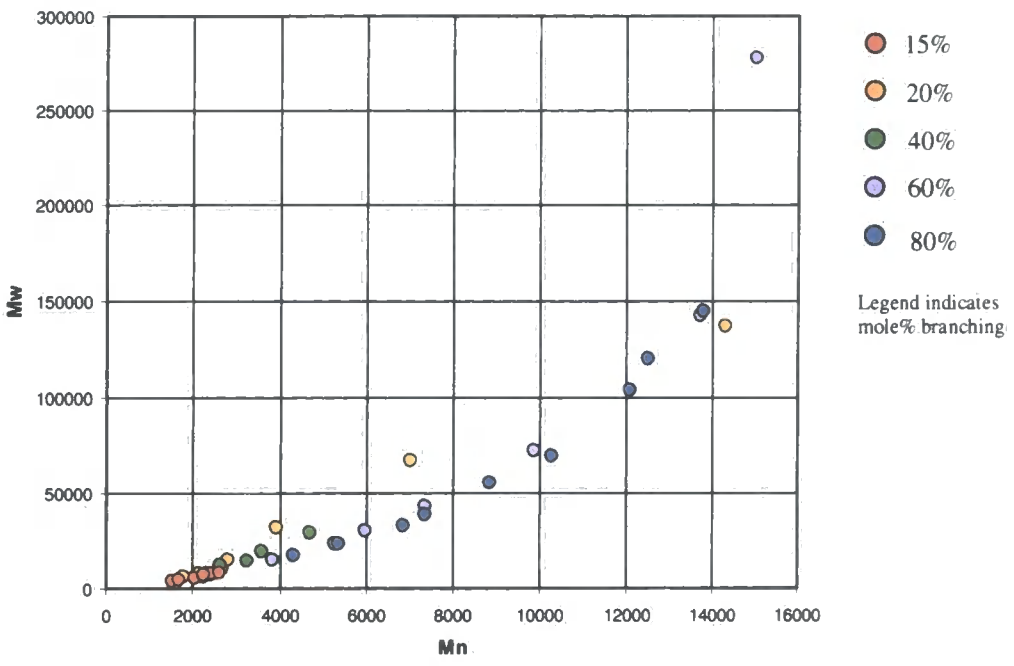

Fig. 5.24 Plot of Mw *vs.* Mn for branching *p*-PEOB copolymers of varying composition as measured by conventional GPC ($CHCl_3$, 5μm gel columns of 100Å, 10^3Å, 10^5Å pore size, PS standards).

Figure 5.25 shows number average molecular weights determined from NMR measurements in $CDCl_3$/TFA, plotted against GPC polystyrene equivalents. There is some correlation, but only for the data points of copolymers with less than 40% branching and then, only for samples with number average molecular weights of less than 2000. At higher molecular weights and increasing extents of branching the data becomes increasingly scattered. For almost every sample, GPC returned a higher number average molecular weight than ^{1}H NMR spectroscopy. For comparison purposes, number average molecular weights, as determined by ^{1}H NMR spectroscopy in pure $CDCl_3$ are plotted against GPC polystyrene equivalents, in Figure 5.26. Copolymer Mn values appear to correlate fairly well for samples with less than 50mole% branching and less than 3000 Mn. However, as observed previously, in Figure 5.25, the data becomes increasingly scattered at higher molecular weights and higher extents of branching.

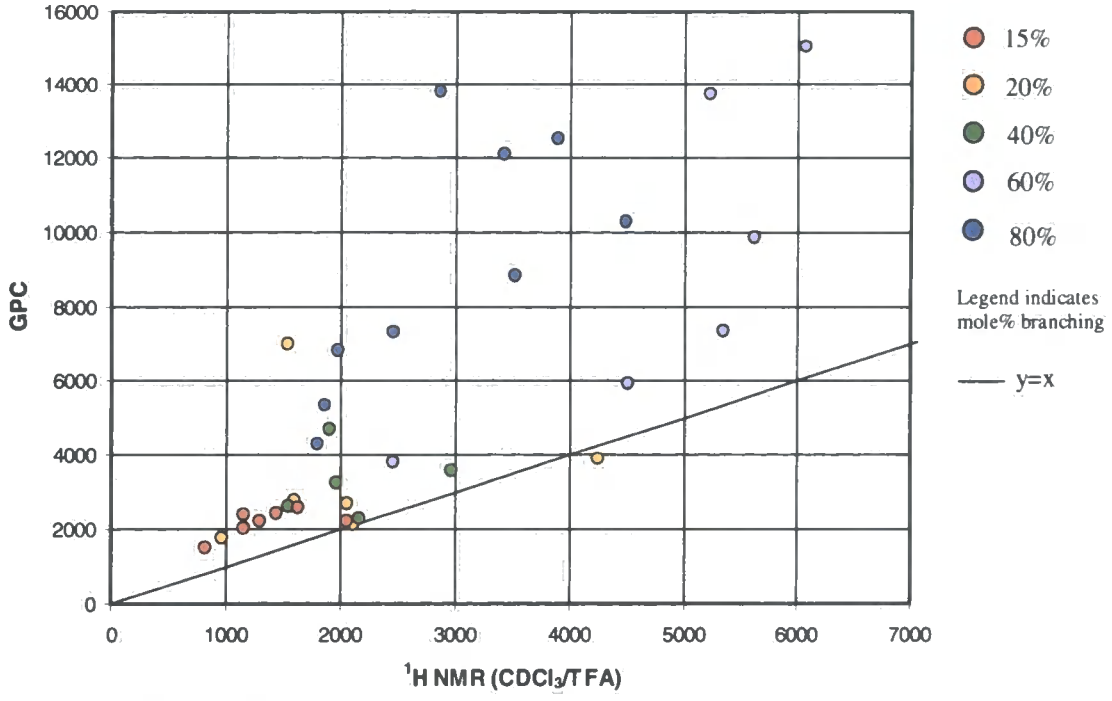

Fig. 5.25 Plot of Mn results, as measured by GPC and ^{1}H NMR ($CDCl_3$/TFA).

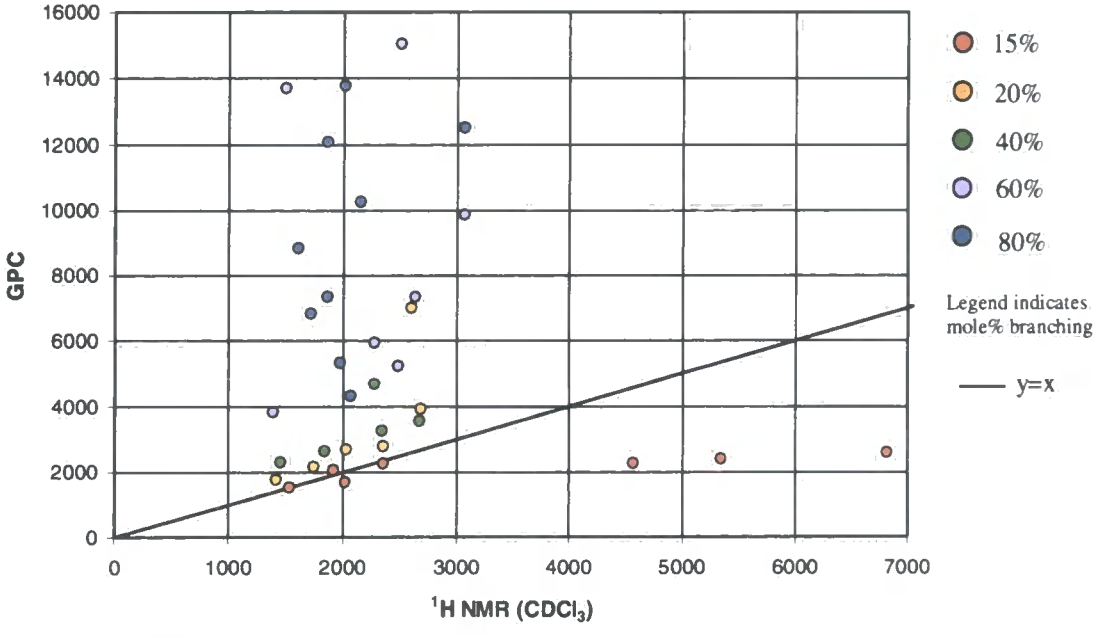

Fig. 5.26 Plot of Mn results, as measured by GPC and ^{1}H NMR ($CDCl_3$).

From the data presented in Figures 5.19, 5.20, 5.25 and 5.26, the limitations of NMR end group counting are clear. The difference between Mn values of copolymers measured in various NMR solvents and the apparent increase in uncertainty, which occurs with increasing molecular weight and extent of branching, have all been cause for concern. Indeed, the results obtained for the crystalline copolymers of *p*-PEOB, in Chapter 4, were more consistent than those recorded here for the highly branched amorphous materials. It is for this reason that amorphous branched *p*-PEOB will be analysed with respect to polystyrene equivalent molecular weights, measured using conventional chloroform GPC.

5.4.3 RI Detector Traces

Throughout this chapter we have reported average molecular weights, as determined from conventional GPC analysis. However, in systems where multimodal weight distributions are observed, detector-response curves are more revealing than simple listings of molecular weights. Figure 5.27 shows the RI detector response for a series of 80% branched *p*-PEOB copolymers (1-8), plotted against elution time. It is evident that, even in the early stages of the polymerisation (30min-45min), 1 and 2, the weight distribution is clearly bimodal; see Figure 5.27. Furthermore, in every analysed sample the retention time of the low molecular weight shoulder A, appears to be independent of the extent of polymerisation. In the later stages of reaction (1hr 15min), a higher molecular weight component C becomes visible, 4. This emerging shoulder develops rapidly, growing in concentration, until it can be clearly distinguished from the main distribution B, 6. In the final stages of the polymerisation (1hrs 45min) a shoulder close to the GPC exclusion limit, is evidence that a fourth molecular weight component D may be present, as indicated in 7 and 8.

Similar multimodal distributions were observed in other chloroform soluble branched copolymers, including the hyperbranched analogue. By contrast, the 50:50 para/meta linear analogue revealed only one weight distribution; refer to Section 3.6. However, the processes through which branched polymers develop multimodal weight distributions are not presently understood but merit further investigation. It may be that the polymer is not being analysed as single isolated coils but as aggregates. A

detailed investigation of this phenomenon was not possible within the time scale of this study.

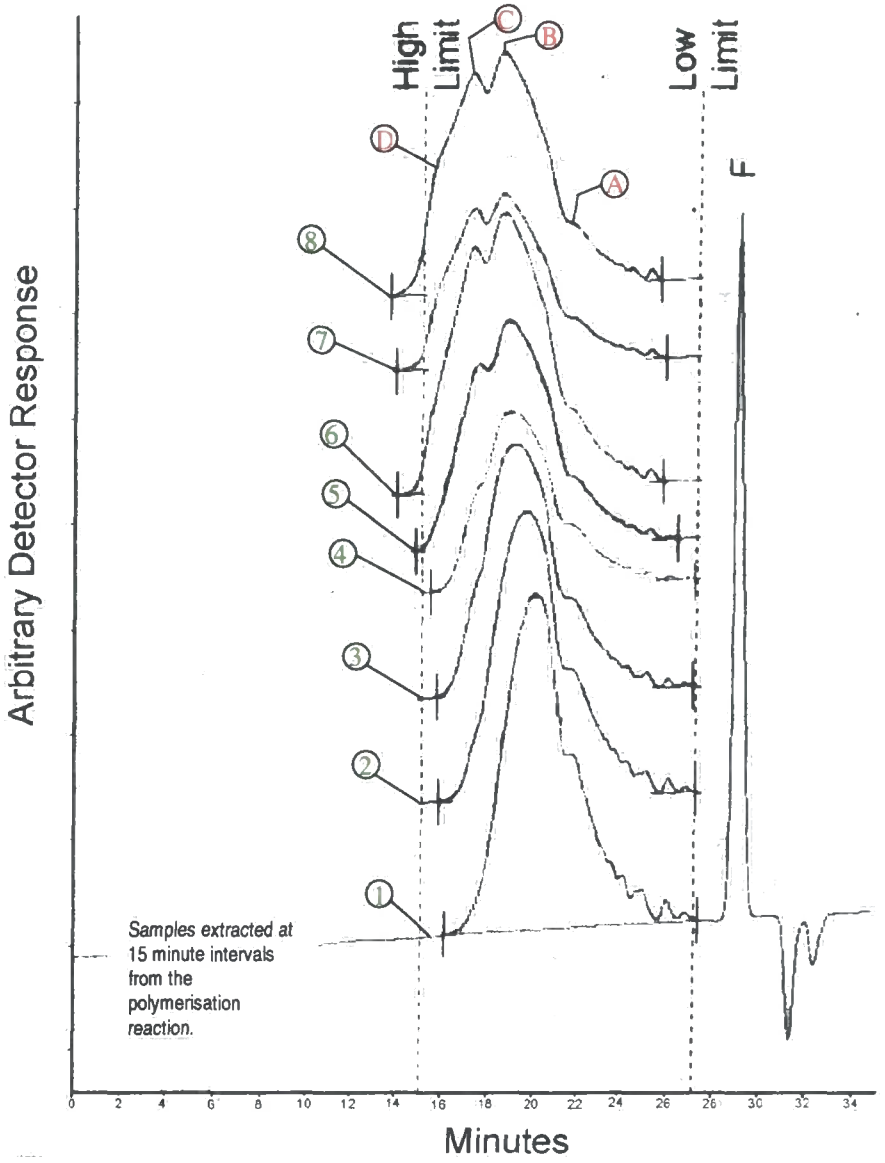

Fig. 5.27 $CHCl_3$ GPC, RI detector traces of 80% branched *p*-PEOB.

5.4.4 THF Gel Permeation Chromatography

There are many advantages to using a TRISEC instrument, foremost, is the ability to determine absolute molecular weights using light scattering methods. Conventional GPC requires calibration with standards of known molecular mass. However, suitable branched calibrants are difficult to obtain, commercially. As a consequence, linear polymer standards such as polystyrene and butadiene are often used. A TRISEC service became available in the closing stages of this project. However, conventional polystyrene equivalent molecular weights have provided the majority of results included in this thesis. Special consideration is given here to copolymers of 80mole% branching, analysed using a THF TRISEC instrument fitted with a refractive index, viscosity and RALLS detectors. Triple detector traces of samples extracted at 15minutes and 2 hours, are shown in Figures 5.28 and 5.29.

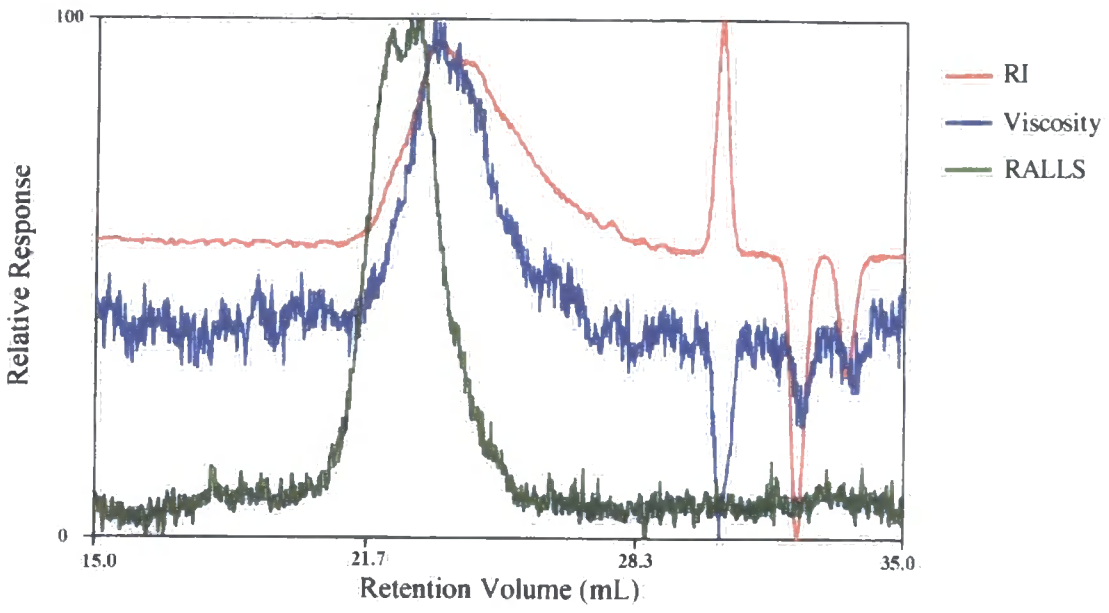

Fig. 5.28 Plot showing the detector response curves of RI, viscosity and RALLS detectors, measured against retention volume for low molecular weight 80% branched *p*-PEOB (GPC, THF, 3x mixed bed 10μm columns).

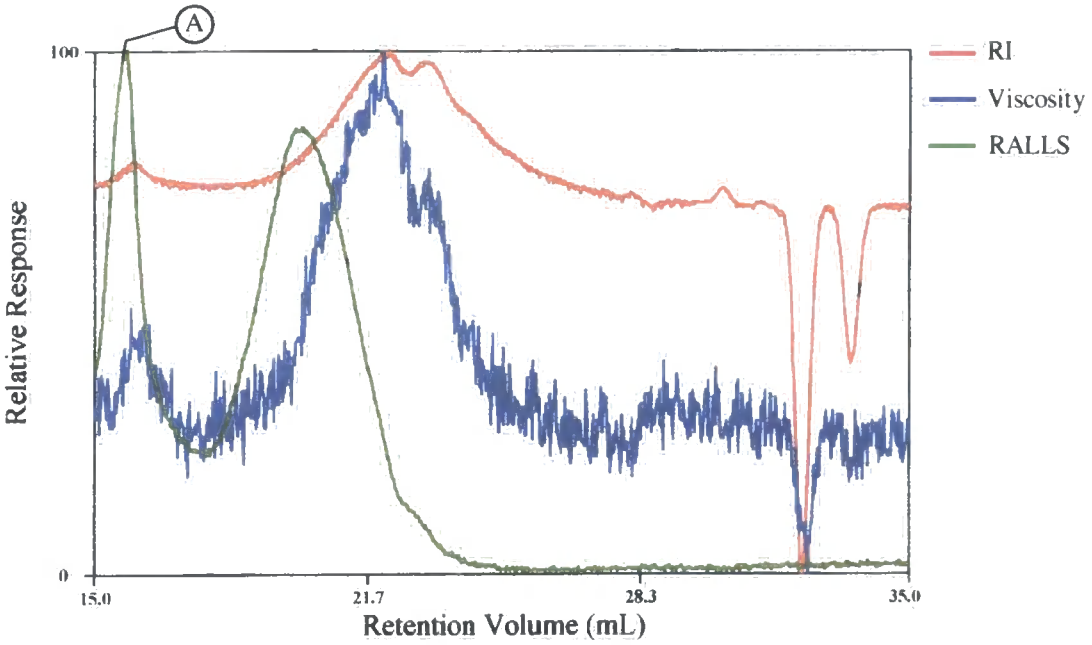

Fig. 5.29 Plot showing the detector response curves of RI, viscosity and RALLS detectors, measured against retention volume for high molecular weight 80% branched *p*-PEOB (GPC, THF, 3x mixed bed 10μm columns).

RI traces of 80% branched *p*-PEOB in THF reveal similar multimodal distributions as observed in chloroform, but with one important difference. As a consequence of THF being a thermodynamically less favourable solvent, hydrodynamic volumes are reduced, which lead to larger retention volumes, increased elution times and apparently lower average molecular weights. During the analysis of 80% branched *p*-PEOB, the RALLS detector recorded several distributions of disproportionately large macromolecules, labelled as **A** and **B** in Figure 5.30. Although these species are present in small numbers, the sensitivity of the RALLS detector, increasing as the fourth power of the molecular radius, makes their detection possible.

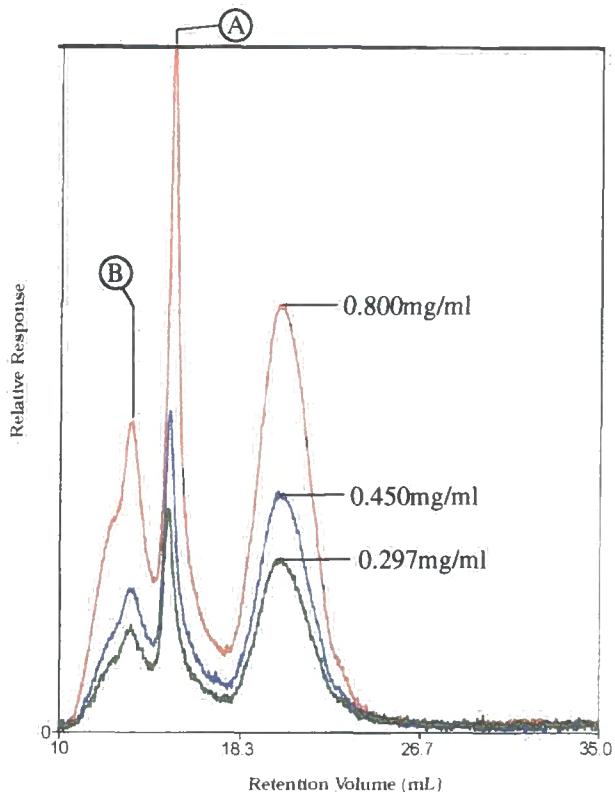

Fig. 5.30 RALLS traces of 80mole% branched *p*-PEOB recorded for three concentrations of high molecular weight polymer.

Peak **A** was first observed in samples extracted after one hour. The light scattering response grew steadily for samples extracted and analysed at intervals of 15 minutes, however, the retention volumes of these species remained unchanged. The fact that the RI detector barely registered a response indicates that the concentration of these larger macromolecules was extremely low. Aggregates were initially postulated as an explanation for this phenomenon. However, as no changes were observed in the GPC traces of solutions exposed to ultrasound, prior to analysis, this explanation seems less likely. Furthermore, changes in concentration did not appear to effect the resultant GPC trace; Figure 5.30. Consequently, the origins of these high molecular weight species remain a mystery but merit further investigation.

A summary of molecular weight analyses of 80% branched *p*-PEOB are collected in Tables 5.7 and 5.8

Reaction Time	TRISEC THF	Conventional THF	Conventional $CHCl_3$	^1H NMR $CHCl_3$	^1H NMR $CHCl_3$/TFA
15 min	3850	3440		2070	1790
30 min	5490	15700	5350	1980	1850
45 min	7950	19400	6830	1720	1970
1 hr	3950	4530	7340	1860	2450
1 hr 15 min	4290	6370	8830	1610	3510
1 hr 30 min	4390	6180	10270	2160	4480
1hr 45 min	1010	9000	12080	1860	3420
2 hr	630	11000	12510	3070	3880
2hr 15 min	760	730	13790	2010	2850

Table 5.7 Mn: 80% branched *p*-PEOB.

Conventional GPC measurements, recorded in chloroform, produced the only data set to form a consistent and systematic trend between molecular weight and reaction time. The signals from the TRISEC detectors were noisy and broad leading to considerable uncertainties in defining base lines and limits for the analysis.

Reaction Time	TRISEC THF	Conventional THF	Conventional $CHCl_3$
15 min	21500	12200	
30 min	30100	29200	23900
45 min	38500	36500	32800
1 hr	83700	24300	38500
1 hr 15 min	94900	28400	55800
1 hr 30 min	128100	35400	69600
1hr 45 min	513500	41400	103700
2 hr	144900	43600	120200
2hr 15 min	128600	47800	144800

Table 5.8 Mw: 80% branched *p*-PEOB.

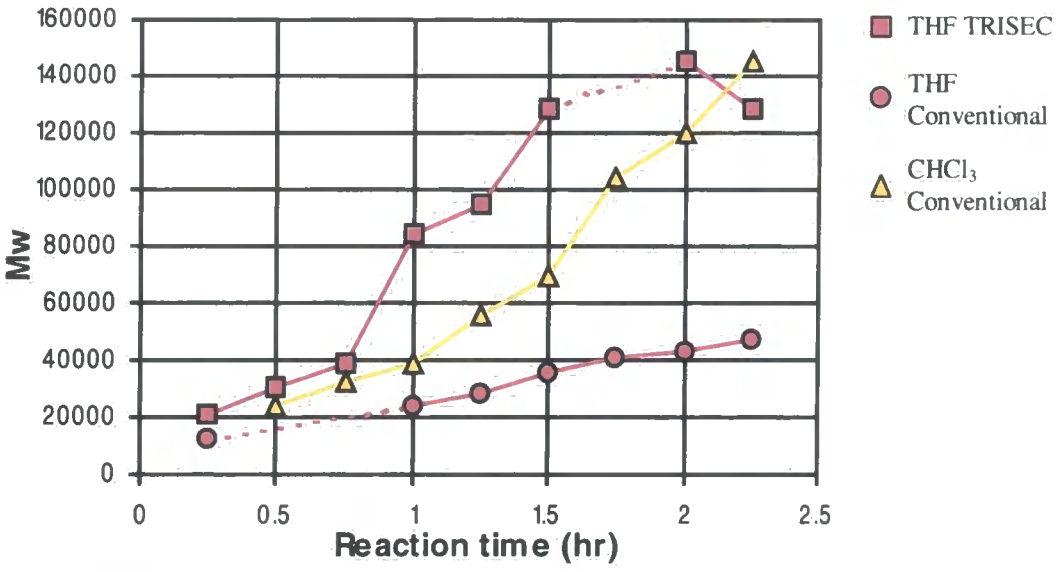

Fig. 5.31 Plot of Mw, measured using conventional and TRISEC GPC, against reaction time for a series of 80mole% branched *p*-PEOB samples.

Some of the data included in Table 5.8 are summarised in Figure 5.31.

5.5 The Glass Transition

As discussed in Section 5.4.1, the ^{1}H NMR number average molecular weights, as obtained for the amorphous branched copolymers of *p*-PEOB, were subject to considerable errors. It is for this reason that the relationship between Tg, extent of branching and molecular weight is considered here with respect to conventional GPC molecular weights, only. Figures 5.32 and 5.33 show Tg as recorded by DSC, plotted against number and weight average molecular weights.

As for the linear polymers, a rapid increase in the glass transition temperature with molecular weight is observed for low molecular weight branched materials. This is followed by a steady decrease in rate of change of Tg with molecular weight as the plateau value is approached.

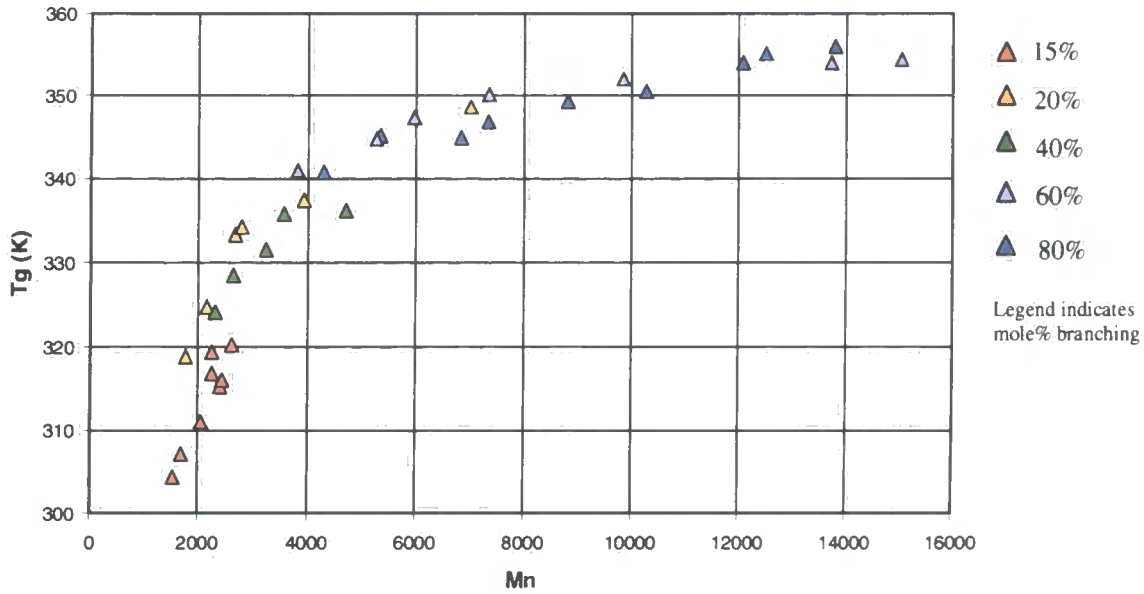

Fig. 5.32 Plot of Tg *vs.* Mn, as measured for branched amorphous *p*-PEOB copolymers (GPC, $CHCl_3$, 5μm gel columns of 100Å, 10^3Å, 10^5Å pore size, PS standards).

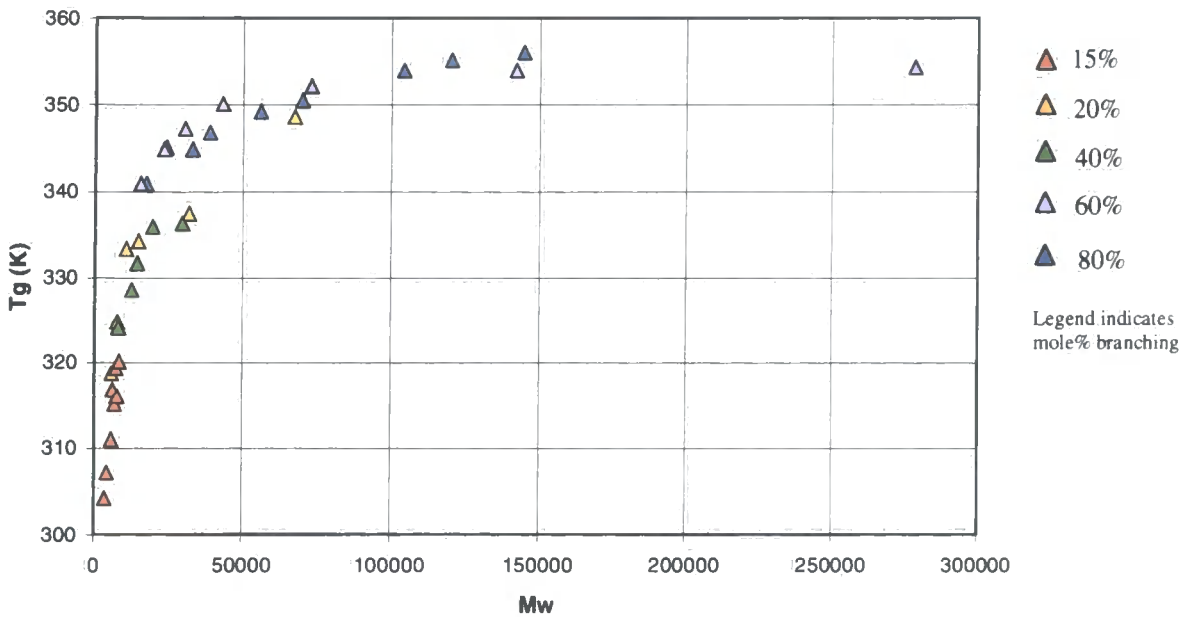

Fig. 5.33 Plot of Tg *vs.* Mw, as measured for branched amorphous *p*-PEOB copolymers (GPC, $CHCl_3$, 5μm gel columns of 100Å, 10^3Å, 10^5Å pore size, PS standards).

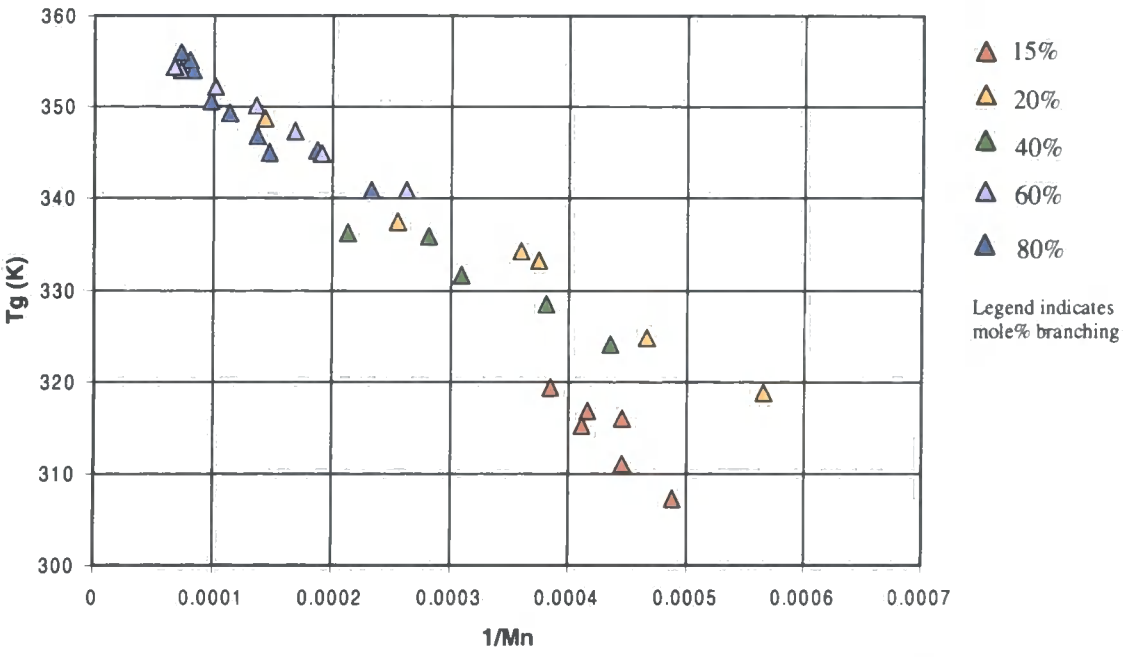

Fig. 5.34 Plot of glass transition temperatures *vs.* 1/Mn, as measured for branched amorphous *p*-PEOB copolymers (GPC, $CHCl_3$, 5μm gel columns of 100Å, 10^3Å, 10^5Å pore size, PS standards).

Mole% Branching	a	b	R^2
15%	-55273	340.3	0.874
20%	-66323	357.5	0.978
40%	-69264	354.3	0.961
60%	-71279	359.2	0.992
80%	-91395	360.8	0.898

Table 5.9 Linear regression analyses: 1/Mn *vs.* Tg for branched *p*-PEOB copolymers (y = ax + b, correlation coefficient R^2).

The results correlate well with the proposed relationship. Furthermore, with the exception of the 15mole% branched copolymer, the relationship between molecular weight and Tg does not appear to alter drastically with the branching composition. Whether the discrepancy in the data is an artefact or a real effect, due to the proximity of the amorphous-crystalline transition, is not known. However, the overall fit is improved with the exclusion of 15mole% data; the linear regression coefficient, R^2,

increasing from 0.93 to 0.96. So, in as far as the Bueche relationship is concerned there is similarity between linear and branched materials.

For comparison purposes, other molecular weight relationships have been analysed with respect to Tg. The correlation coefficients, determined from linear regression analysis, are collected in Table 5.10.

Branching	Mn	1/Mn	Log (Mn)	Mw	1/Mw	Log(Mw)
15mole%	0.86	0.87	0.87	0.88	0.89	0.90
20mole%	0.85	0.98	0.73	0.79	0.92	0.82
40mole%	0.81	0.96	0.88	0.79	0.95	0.91
60mole%	0.85	0.99	0.94	0.57	0.99	0.87
80mole%	0.96	0.90	0.98	0.93	0.89	0.96

Table 5.10 R^2 linear correlation coefficients of various Tg *vs.* molecular weight relationships, as determined for the branched *p*-PEOB copolymers.

Highlighted values indicate the molecular weight relationships which correlated most accurately with the observed changes in Tg. In the majority of cases, this was the relationship with 1/Mn. Linear regression analysis, as performed on the combined data, shows that the relationships 1/Mn and 1/Mw both correlate equally well with Tg; see Table 5.11. However, the plateau value, predicted from the 1/Mn copolymer data, agrees more accurately with the value determined by experiment for the hyperbranched analogue.

Branching	Mn	1/Mn	Log (Mn)	Mw	1/Mw	Log(Mw)
Combined	0.72	0.93	0.88	0.44	0.93	0.84

Relationship	a	b	R^2
1/Mn	-89670	360.4	0.93
1/Mw	-236700	353.0	0.93

Table 5.11 Linear regression analyses: 1/Mn, 1/Mw *vs.* Tg for all amorphous branched *p*-PEOB copolymers (y = ax + b, correlation coefficient R^2).

The hyperbranched analogue, 5-PEOI, has been researched extensively by D. Parker at Durham University's Interdisciplinary Research Centre (IRC). With his permission, Tg data recorded for the hyperbranched analogue are shown in Figure 5.35 plotted alongside the *p*-PEOB copolymer. Results of linear regression, as performed on this data, are disclosed in Table 5.12.

Mole% Branching	a	b	R^2
100%	-37827	363.3	0.771

Table 5.12 Linear regression analysis: Hyperbranched 5-PEOI (y = ax + b).

The results show that far from conforming to the proposed relationship, the hyperbranched polymer displays behaviour that is very different from that observed for branched *p*-PEOB copolymers.

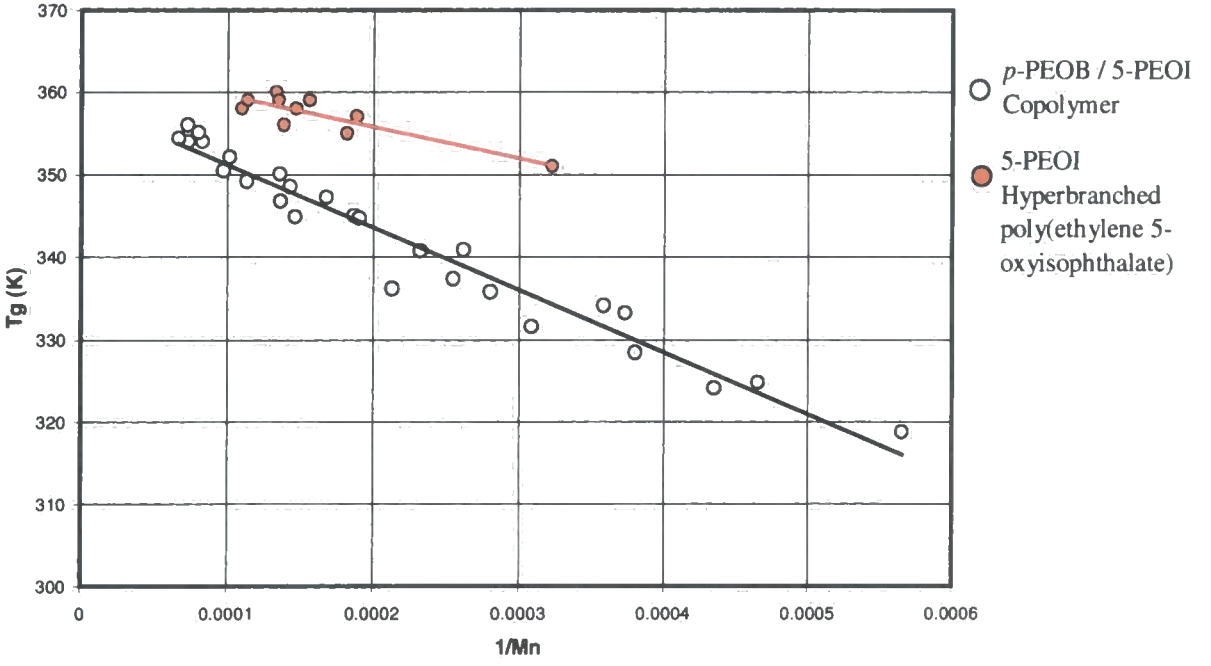

Fig. 5.35 Comparison between copolymer and hyperbranched glass transition data (GPC, $CHCl_3$, 5μm gel columns of 100Å, 10^3Å, 10^5Å pore size, PS standards).

The thermal behaviour of these systems has been analysed in detail but clearly, more work is required if the intricacies of these branched systems are to be understood.

5.6 Viscometry

Solution viscosities were measured by comparing the flow time, t, of a specific volume of polymer solution through a capillary, against an equal volume of solvent, efflux time t_0. During the analysis, flow times of several concentrations of polymer were measured. Reduced and inherent viscosities were then plotted against concentration and extrapolated to zero concentration to evaluate the intrinsic viscosity. Optimal results were obtained using efflux times of 100s or more and maintaining solution temperatures of 25°C to within ±0.02°C.

In the majority of polymer-solvent systems, solution behaviour may be described using the relationships shown below. However, it is stipulated in textbooks that these empirical relationships are only valid for linear polymer systems. This generalisation will be given further consideration.

Relative viscosity	$\eta_r = \eta/\eta_0 \sim t/t_0$
Specific viscosity	$\eta_{sp} = \eta_r - 1$
Reduced viscosity	$\eta_{red} = \eta_{sp}/c$
Inherent viscosity	$\eta_{inh} = (\ln \eta_r)/c$
Intrinsic viscosity	$[\eta] = (\eta_{sp}/c)_{c=0}$

where η is solution viscosity, η_0 is solvent viscosity and c is solution concentration

Huggins equation (1942)	$\eta_{sp}/c = [\eta] + k'[\eta]^2c$	Eq. 5.6
Kraemer equation (1938)	$(\ln \eta_r)/c = [\eta] + k''[\eta]^2c$	Eq. 5.7
	$k' - k'' = ½$	Eq. 5.8

The relationship between molecular size and the number of incorporated branch points was proposed by Zimm et al in 1949.[3] He used **g**, the ratio of the radii of gyration of branched and linear structures, to describe polymers of the same DP. Over

the years, many theories have been proposed, relating g to the intrinsic viscosities of linear and branched materials. These theories are complex and specific to a particular structural arrangement, i.e. star, comb or random branched polymers. Furthermore, to be effective the radius of gyration of the purely linear polymer is required. It is for these reasons that the parameter g will not be considered further.

$$g = \langle S^2 \rangle_{(branched)} / \langle S^2 \rangle_{(linear)} \qquad \text{Eq. 5.9}$$

Increased solubility of *p*-PEOB copolymers, arising from the introduction of branch points, has allowed viscosity measurements to be made on samples in pure chloroform. Figure 5.36 shows the intrinsic viscosities of copolymers with 20mole% to 80mole% in the form of Mark-Houwink plots. The empirical relationship between molecular weight and intrinsic viscosity, given by the Mark-Houwink equation (Equation 5.10) is believed to only be valid for linear polymers. However, the results obtained from the analyses of branched *p*-PEOB indicate that this is not so.

$$[\eta] = KM_v^a \qquad \text{Eq. 5.10}$$

Although viscosity average molecular weights are stipulated for use in the Mark-Houwink equation, substitution by weight average molecular weight is adequate for calculating **K** and **a** over a limited molecular weight range. Remarkably, linear relationships extending between 5,000 and 300,000 Mw were observed for the branched copolymer compositions analysed. However, it must be stressed that Mw could only be determined in terms of polystyrene equivalent molecular weights. Even more remarkable were the identical α values (α~0.41) determined by linear regression analysis for these materials and the resultant linear relationship between log K and the extent of branching; Figure 5.37. Results, established independently by D. Parker at the University of Durham for the hyperbranched analogue, are consistent with the findings for branched *p*-PEOB copolymers. Although apparently compelling, in the absence of absolute molecular weights these data must be treated with caution.

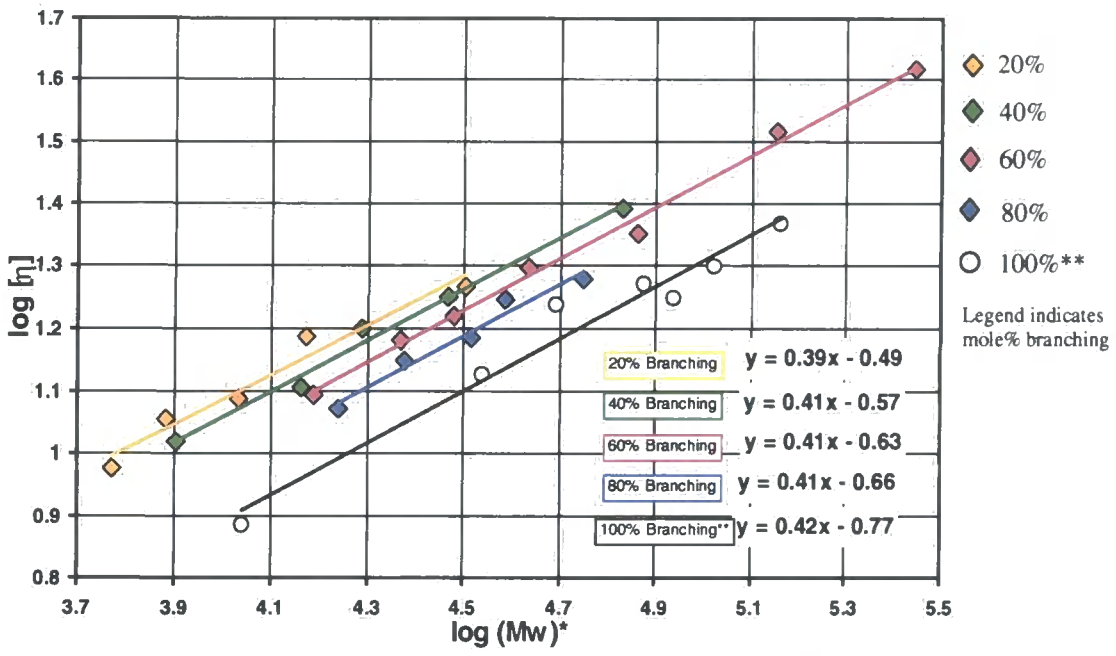

Fig. 5.36 Mark Houwink plot showing log Mw *vs.* log [η] for amorphous branched copolymers of various extents of branching.

*GPC, $CHCl_3$, 5μm gel columns of 100Å, 10^3Å, 10^5Å pore size, PS standards

** Results provided by D. Parker.

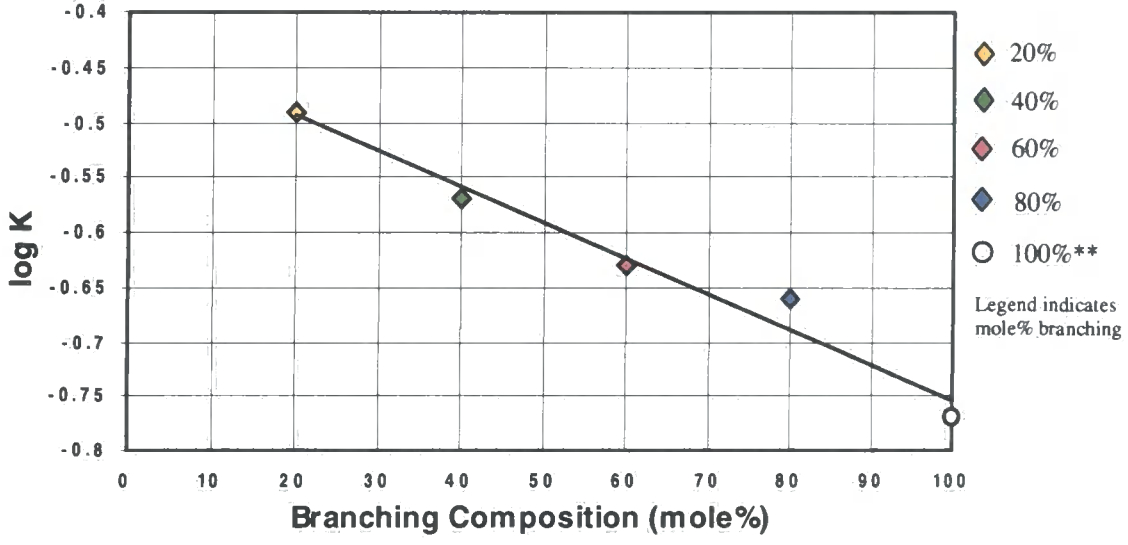

Fig. 5.37 Plot showing log K *vs.* branching composition of amorphous branched p-PEOB copolymers measured in $CHCl_3$.

There is no theoretical basis on which to explain these results but empirically, given any two of the following parameters, molecular weight, intrinsic viscosity or percentage branching we can calculate the third. Equation 5.11 describes the linear relationship between log K and the mole fraction of branching units in the *p*-PEOB copolymer, as determined by linear regression analysis for the data in Figure 5.37. The R^2 correlation coefficient for these data has been determined to be 0.97.

$$\log K = -0.0033x - 0.429 \qquad \text{Eq. 5.11}$$

Where x = mole fraction of branching units in the copolymer

Assuming that the Mark-Houwink **a** value is constant for all amorphous branched *p*-PEOB copolymers (a=0.41), which has been substantiated in $CHCl_3$, the relationship between intrinsic viscosity, Mw and extent of branching may be written as Equation 5.12.

$$\log[\eta] = 0.41\log(Mw) - 0.0033x - 0.429 \qquad \text{Eq. 5.12}$$

$$x = (0.41\log(Mw) - \log[\eta] - 0.429) / 0.0033$$

$$\log(Mw) = (\log[\eta] + 0.0033x + 0.429) / 0.41$$

Where intrinsic viscosity [η] is measured in $CHCl_3$ (ml g^{-1}), Mw measured using GPC, $CHCl_3$, 5μm gel columns of 100Å, 10^3Å, 10^5Å pore size, PS standards, x is the mole fraction of 5-PEOI branching units in the *p*-PEOB copolymer.

Thus, there appears to be a systematic relationship between [η], Mw and branching content for *p*-PEOB copolymers with between 20mole% and 100mole% of 5-PEOI branch points.

5.7 References

1. Flory P.J., *J. Am. Chem. Soc.*, **74**, (1952), 2718
2. Feast W. J., Keeney A. J., Kenwright A. M. and Parker D., *Chem. Comm.*, (1997), 1749
3. Zimm B.M., Stockmayer W.M., *J. Chem. Phys.*, **17**, (1949), 1301

Chapter 6

Molecular Weight Determination for Branched Copolymers using ^{1}H NMR spectroscopy

6.1 Molecular Weight Determination for Branched Copolymers

In this chapter, ^{1}H NMR end group counting, as applied to branched *p*-PEOB copolymers, is discussed. By gaining an appreciation for the limitations of the process, we might better understand the factors that may influence the outcome of the analysis. The possibility for intramolecular cyclisation is one such consideration. Indeed, to avoid complicating the analyses of linear and branched systems, the effects of cyclisation are usually ignored, following Flory's examples.[1,2] However this inevitably leads to inaccuracies, for example in the determination of Mn by end group counting.

The cyclisation of linear polyesters is an equilibrium process, which results in the formation of cyclic oligomers with typically three to nine repeat units. Larger macrocycles are subject to an increase in entropy of formation which result in a rapid decrease in their relative number. However, by varying the concentration of monomer in the feed, the mole fraction of cyclic material can be effectively controlled; an increase in the concentration of monomer resulting in a reduction in the mole fraction of cyclised material. The behaviour of hyperbranched polymers, on the other hand, differs markedly from that of their linear analogues.

Matrix assisted laser desorption ionisation spectroscopy (MALDI) has been used to show that the cyclic content of melt polymerised hyperbranched polymers, specifically poly(ethylene 5-oxyisophthalate), 5-PEOI, and analogues with spacers with 3-6 methylene units shown below, increases with the extent of polymerisation.[3,4]

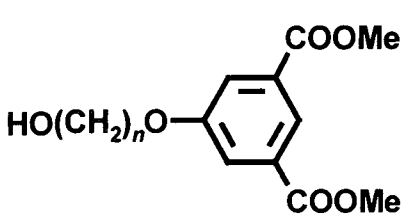

n = 2-6

The cyclic content of these polymers increased with molecular weight until, within the detection limit of the technique, all of the analysable material had been cyclised, i.e. there were no focal groups remaining. Interestingly, on reaching this point in the reaction, the hyperbranched polymer with the $n = 2$ spacer continued to grow in weight average molecular weight (measured by GPC with a polystyrene

calibration) while the number average molecular weight remained constant.[5] In contrast, hyperbranched materials with longer spacers (3-6 methylene units) did not undergo further change; their number and weight average molecular weights remaining fixed at a characteristic plateau value, which was dependent upon the spacer length. Clearly, if as suggested, every focus is intramolecularly cyclised, a mechanism must exist to account for the continuing growth in molecular weight of 5-PEOI. Polyesters undergo transesterification; a process which may be used to explain these observations.[5] Transesterification can result in the dynamic randomisation of structure which may occur *via* cleavage and reformation of the ester bond *via* a variety of mechanisms; including end group initiated processes, direct ester-ester interchange and processes mediated by catalysts. Although there is no direct evidence to link ester exchange to the continued growth of Mw in cyclised 5-PEOI, the suggestion can be shown to be a reasonable one.[5]

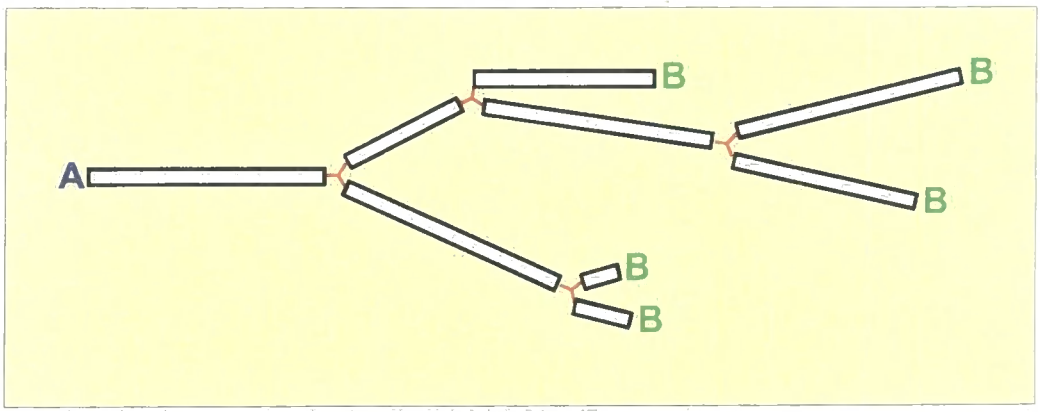

Fig. 6.1 Schematic diagram of a randomly branched copolymer.

A representation of an AB/AB_2 copolymer is shown in Figure 6.1; the solid white rectangles representing linear sections, joined *via* branching residues (red). The focal group A is shown in blue and the end groups B, in green.

Cyclisation occurs when the focus and an end group of the same molecule react intramolecularly. As illustrated in Figure 6.2, the number of these reactions is limited to one per molecule. It appears that a greater quantity of cyclic material is present in hyperbranched polyesters than in their linear analogues. However, very little is known about the cyclic content of branched/linear copolymers. Although not conclusive, a

detailed analysis of 40mole% branched *p*-PEOB, using MALDI-TOF spectroscopy, revealed no evidence for cyclisation; see Section 5.3. However, on the evidence for the hyperbranched polymer, 5-PEOI, it seems reasonable to suppose that the cyclic content of *p*-PEOB must increase as a function of branching content and molecular weight.

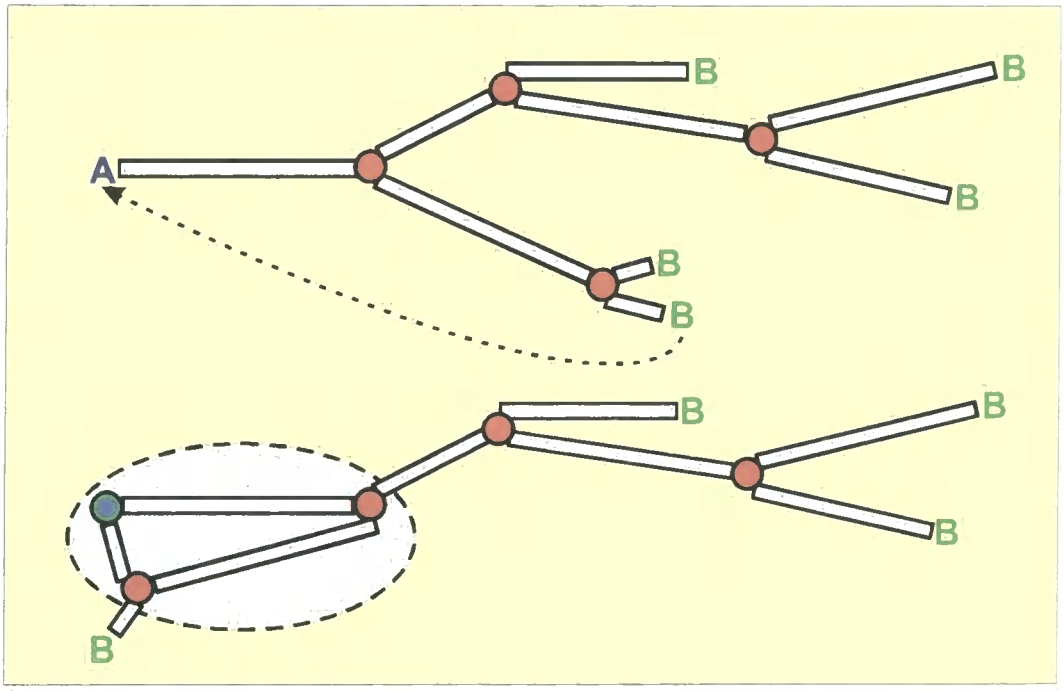

Fig. 6.2 Schematic diagram showing the intramolecular cyclisation of an AB/AB$_2$ copolymer.

For a fixed mole fraction of cyclised polymer the error in determining the number average molecular weight, using B group counting, is predicted to decrease as a function of increasing branching composition and molecular weight. This is due to a reduction in the fraction of cyclisable end groups, as illustrated for 30% cyclised samples of linear, singly and doubly branched systems in Figure 6.3. However, any reduction in the error, resulting from an increase in the branching content, is likely to be offset by the increasing amount of cyclic material. In any event, the errors resulting from cyclisation in linear and branched *p*-PEOBs are not anticipated to differ significantly. An identical relationship between Tg and Mn was revealed for linear *p*-PEOB and its crystalline copolymers with up to 12.5mole% branching, see Figure 4.12,

which is consistent with the hypothesis that the error in measuring Mn by B group counting is not significantly different for linear and branched polyesters of this type.

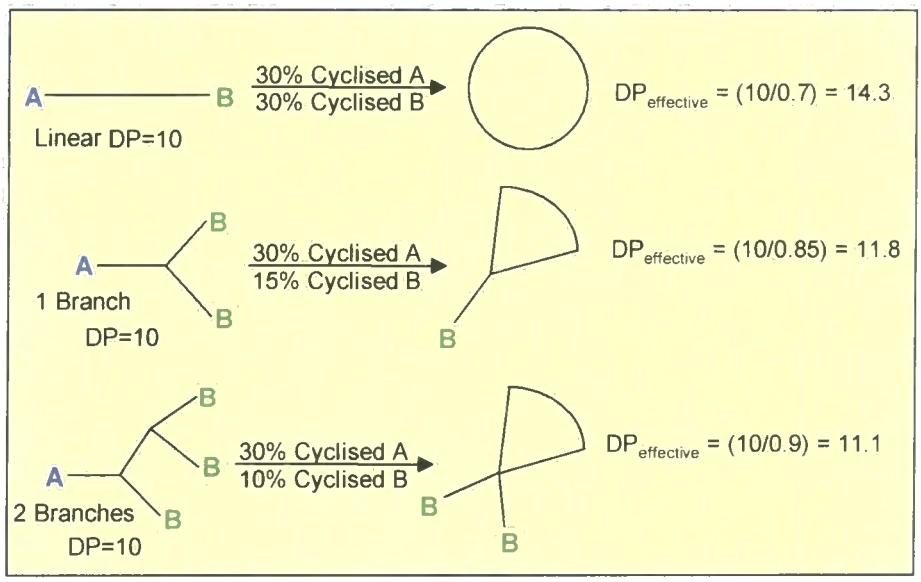

Fig. 6.3 The effect of increasing the branching composition of an AB/AB$_2$ copolymer on the measured DP, as determined by B group counting.

6.1.1 Monomer reactivity and the distribution of branching units

To obtain a statistically distributed copolymer there must be no significant difference between the rates of monomer addition to different sites in the growing polymer. By determining the rate constants k_1 and k_2, for the model reaction shown in Figure 6.4, we were able to measure the relative reactivities of monomers **1**, **2** and **3**; Figure 6.5.

The esterification of PET end groups with trifluoroacetic acid has been studied by Richards, Kenwright and Peace et al,[6] as part of a larger study on polyester blends. A pseudo first order rate constant $(7.8\pm1.8)\times10^{-6}s^{-1}$ was determined at ambient temperatures for this reaction, using ^{1}H NMR spectroscopy with an excess of TFA.

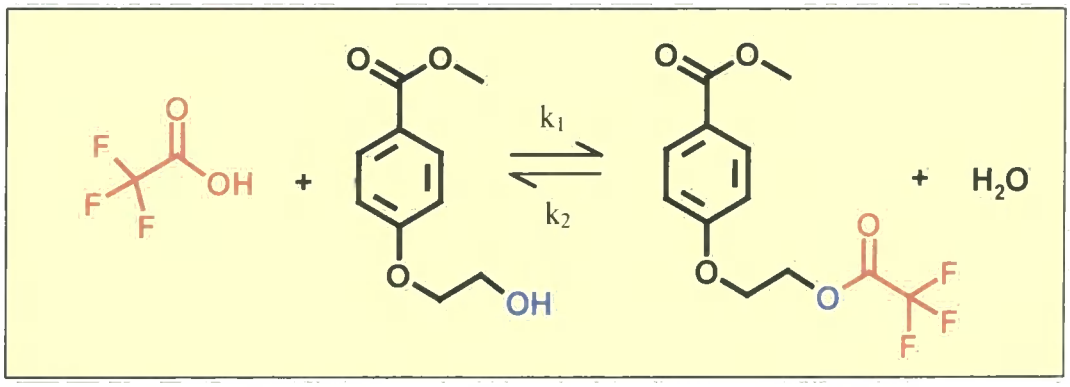

Fig. 6.4 'Model reaction': The esterification reaction of TFA and monomer 1.

A similar method to that described by Peace et al was used to determine the rates of esterification between TFA and monomers **1**, **2** and **3**. All reactants were weighed accurately to four decimal places; refer to Table 6.1. Small amounts of monomer (0.02-0.06g) were dissolved in known quantities of NMR grade deuterated chloroform. Once dissolved, a drop of reactant-grade trifluoroacetic acid was added to the chloroform solution. Solutions were then mixed thoroughly, weighed and transferred to dry NMR tubes which were sealed in preparation for analysis. Samples were analysed using a 200 MHz ^{1}H NMR spectrometer at intervals of twenty-four hours, over a period of nine days; Figures 6.7 and 6.8. The results are shown in Figures 6.9, 6.10 and 6.11.

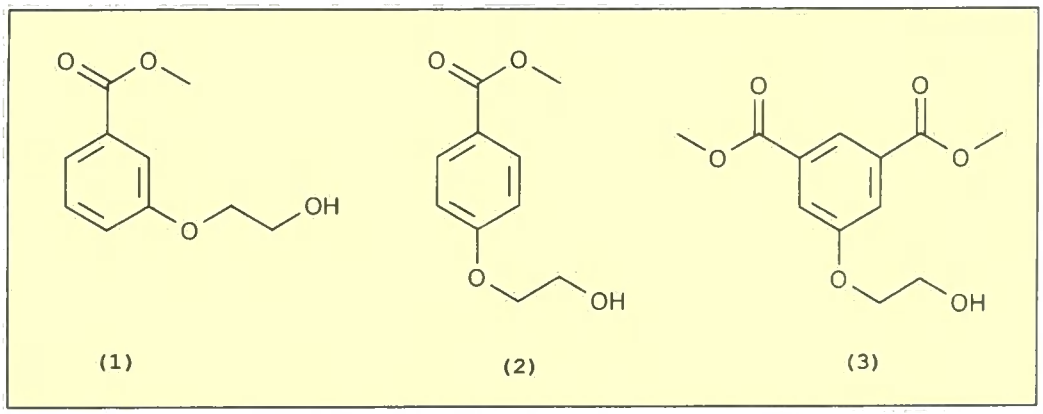

Fig. 6.5 Monomers.

Monomer	Concentration w/w (Monomer:Solvent)	TFA w/w (TFA:$CDCl_3$)	$CDCl_3$
(1)	$0.0564gg^{-1}$	1.3%	0.9805g
(2)	$0.0221gg^{-1}$	1.9%	1.0568g
(3)	$0.0308gg^{-1}$	1.5%	1.2350g

Table 6.1 Reactant concentrations.

The most notable differences between the spectra of monomers containing TFA and those obtained in pure deuterated chloroform are the chemical shifts of alkoxy CH_2 groups, see Figure 6.6 and Table 6.2. Consider monomer **2**; in pure chloroform-d (A03-1), CH_2 peaks are observed at 4.00ppm and 4.14ppm. The addition of TFA results in a shift to 4.10 and 4.17ppm (C, D) with a marked reduction in resolution, shown schematically in Figure 6.6; the actual spectrum is shown in Figure 6.7. However, as the CH_2 peaks of the resultant ester (A, B) are shifted significantly further downfield to 4.33 and 4.70ppm, indicated in red in Figure 6.7 and 6.8, the reaction could be monitored unambiguously.

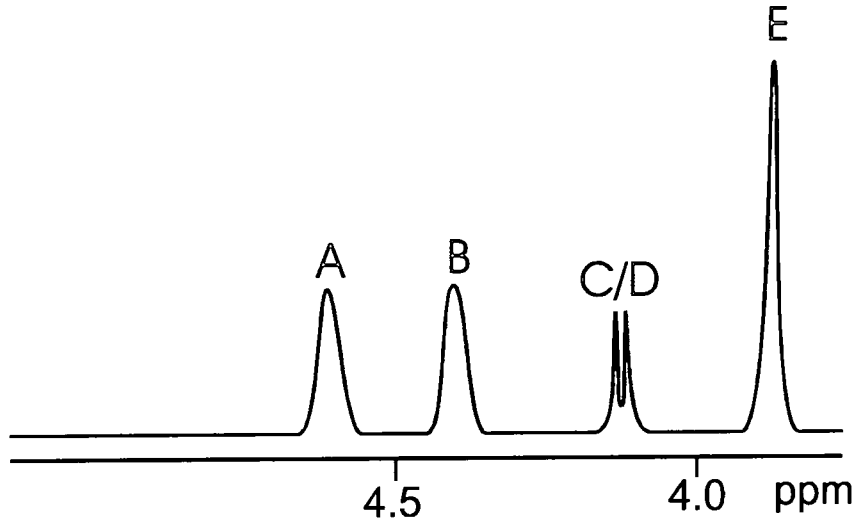

Fig. 6.6 Schematic ^1H NMR spectrum of $CDCl_3$/TFA monomer solutions, showing approximate positions of CH_2 and CH_3 groups.

Monomer	'A' (ppm)	'B' (ppm)	'C' (ppm)	'D' (ppm)	'E' (ppm)
(1) Meta	4.70	4.30	4.10	4.00	3.90
(2) Para	4.70	4.30	4.17	4.10	3.92
(3) Isophthalate	4.70	4.35	4.20	4.10	3.93

Table 6.2 ^{1}H NMR chemical shifts (3.90-4.70ppm) of monomers 1, 2 and 3 in $CDCl_3$/TFA.

The 200 MHz ^{1}H NMR spectra of 2, as recorded in TFA/$CDCl_3$ solution immediately after TFA addition and eight days into the reaction are shown in Figures 6.7 and 6.8.

The progress of the esterification reaction was monitored over a period of eight days by comparing the integrated intensities of signals A to D against the methyl ester signal (E). The intensities of peaks A, C and E were substituted into Equations 6.1 and 6.2 to calculate the percentage of reacted and unreacted **1** and **2** in solution.

$$\textbf{\% Reacted monomer} = (i^A/2) \times (3/i^E) \times 100\% \qquad \textbf{Eq. 6.1}$$

$$\textbf{\% Unreacted monomer} = (i^C/2) \times (3/i^E) \times 100\% \qquad \textbf{Eq. 6.2}$$

i^A = signal intensity of peak A, i^C = signal intensity of peak C, i^E = signal intensity of peak E

The integrated intensity of the methyl ester group in the meta and para monomers, (peak 'E') was assigned as the equivalent of three protons. The relative intensities of the remaining signals, 'A' and 'C', were compared against E to determine the fraction of reacted and unreacted molecules in solution. The signal generated by the two methyl ester groups of the isophthalate isomer was assigned as six protons. When normalised with respect to 'E' the summed intensities of A-D were marginally greater than allowed by molecular stoichiometry. In the extreme case, anticipated values were exceeded by 15%. Consequently, the data in Figures 6.9, 6.10 and 6.11, which show mole fractions of reacted and unreacted 1, 2 and 3 plotted against time, are somewhat overestimated.

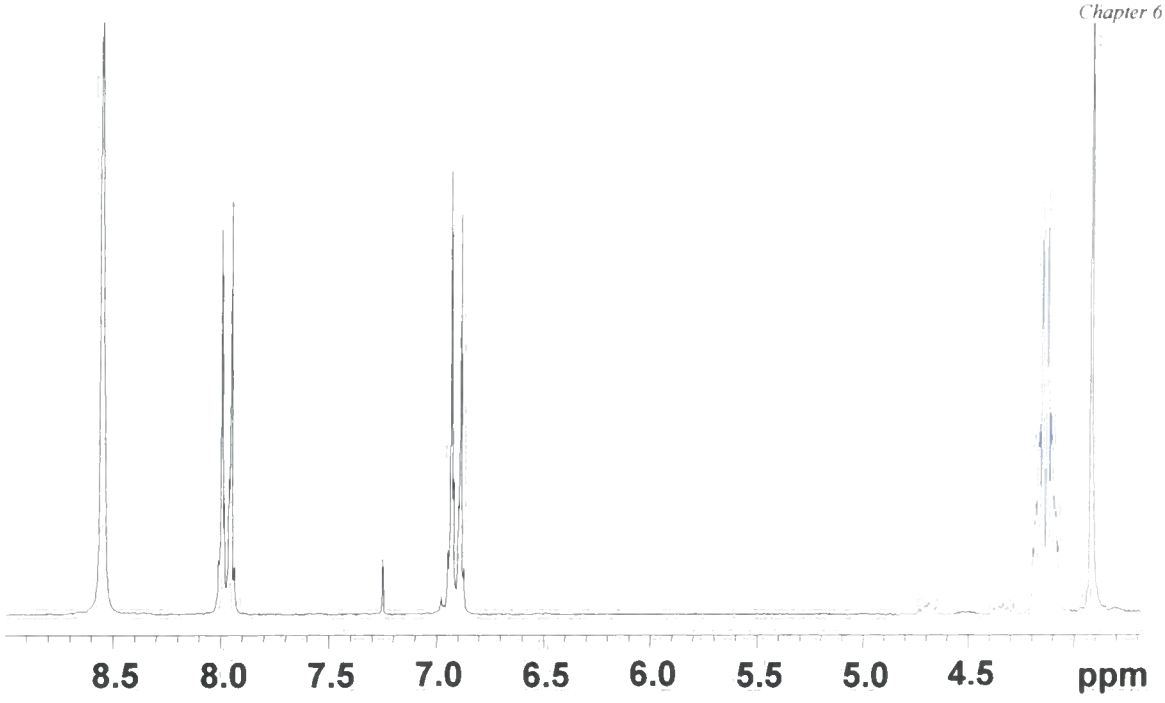

Fig. 6.7 200MHz ^{1}H NMR spectrum of monomer (2) immediately after the addition of TFA.

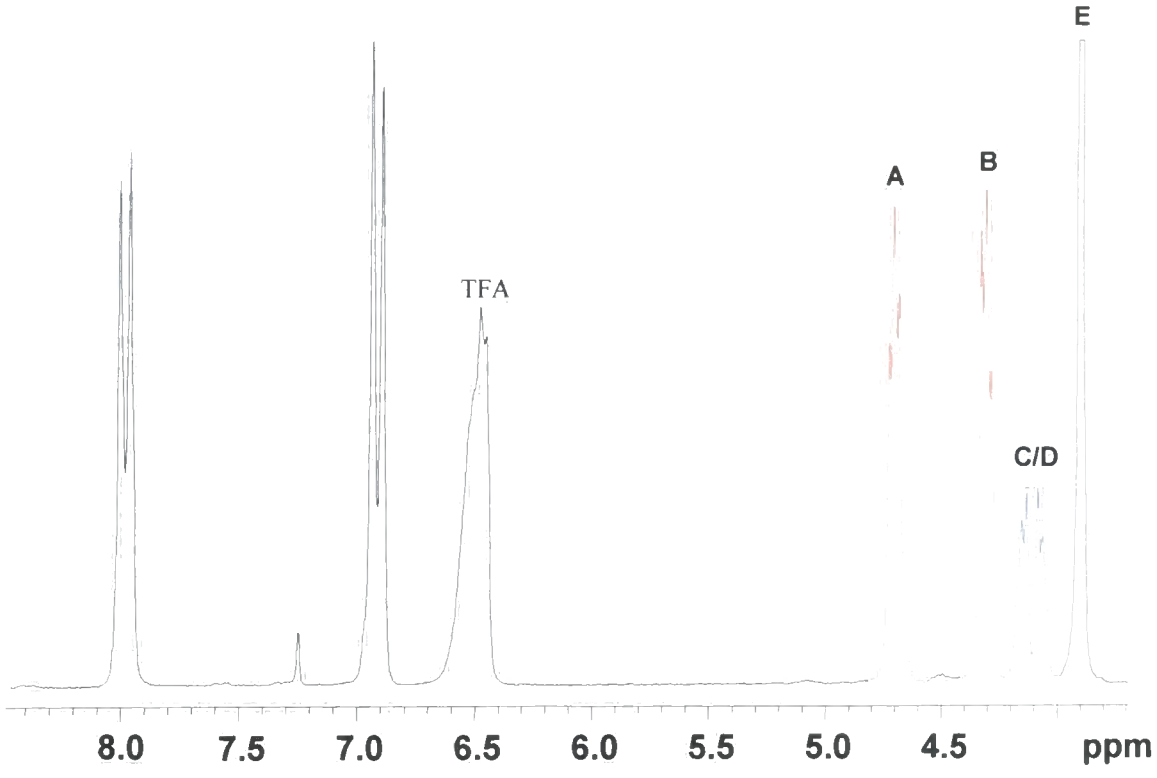

Fig. 6.8 200MHz ^{1}H NMR spectrum of monomer (2) eight days after the addition of TFA.

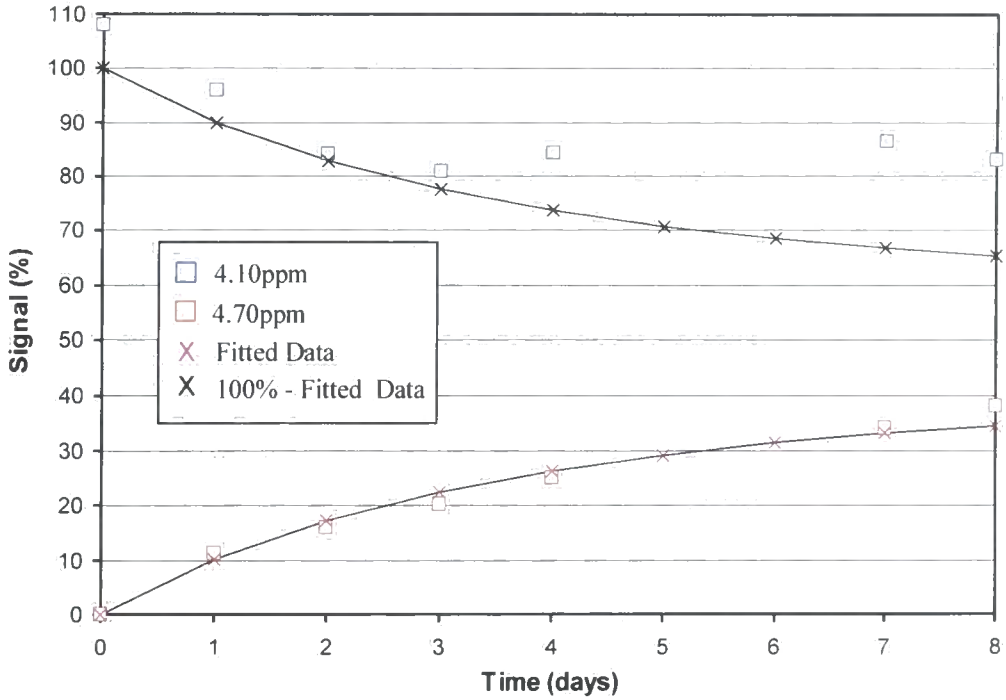

Fig. 6.9 Percentage of reacted □ and unreacted □ 1, as monitored over eight days by ^{1}H NMR spectroscopy.

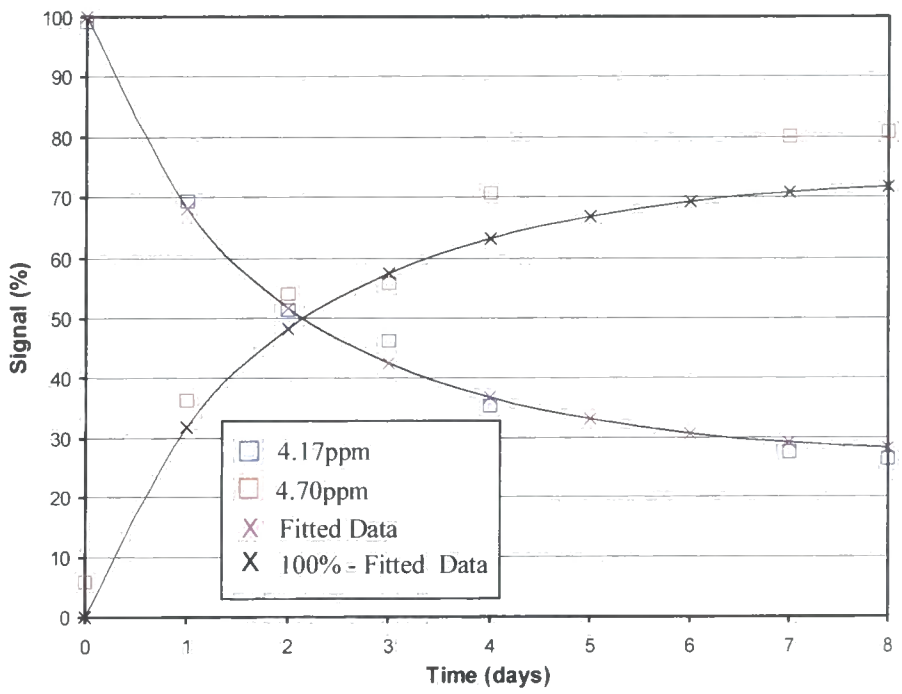

Fig. 6.10 Percentage of reacted □ and unreacted □ 2, as monitored over eight days by ^{1}H NMR spectroscopy.

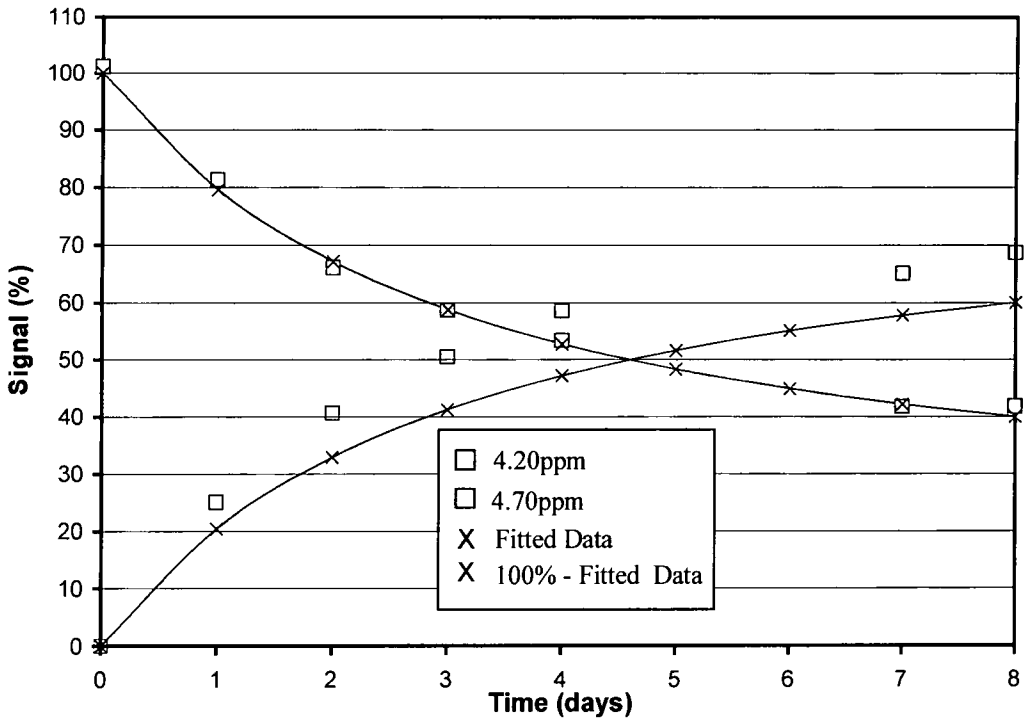

Fig. 6.11 Percentage of reacted □ and unreacted □ 3, as monitored over eight days by ^{1}H NMR spectroscopy.

A computer algorithm was used to simulate the equilibrium reaction shown below.

$$[A] + [B] \underset{k_2}{\overset{k_1}{\rightleftharpoons}} [C] + [D]$$

Given the concentrations of 'A' and 'B' and the rates of reaction k_1 and k_2 the algorithm would predict the progress of a reaction with time. Alternately, knowing the precise concentrations of A and B, the rate constants k_1 and k_2 could be adjusted to fit the generated data to experimental results. The results of these analyses are collected in Table 6.3. Fitted data are represented in Figures 6.9, 6.10 and 6.11 as magenta crosses.

Monomer	k_1 (kg mol^{-1} hr^{-1})	k_2 (kg mol^{-1} hr^{-1})	Relative rate
Meta (**1**)	0.039	0.006	1.0
Para (**2**)	0.142	0.028	3.6
Isophthalate (**3**)	0.093	0.0005	2.4

Table 6.3 Rate constants

These results indicate that the meta isomer is the least reactive and the para substituted reactant is esterified 1.5 times faster than the isophthalate branching agent. Whether these rates of esterification, with TFA, bear any relation to the rates of monomer addition in the polymerisation remains to be substantiated. Any tendency toward compositional drift is likely to be offset by the effects of transesterification. Evidence for this is provided by the ^{13}C NMR analysis of amorphous branched *p*-PEOB copolymers, in Section 5.2, which shows the distribution of branching units to resemble a statistical copolymer at 100% conversion.

The two main assumptions, required for end group counting to be effective in AB/AB_2 copolymers, appear to have been upheld for branched *p*-PEOB systems; these are, that the effects of intermolecular cyclisation are negligible, and branch points are statistically distributed.

6.2 Calculating Mn in Statistical Branched Copolymers

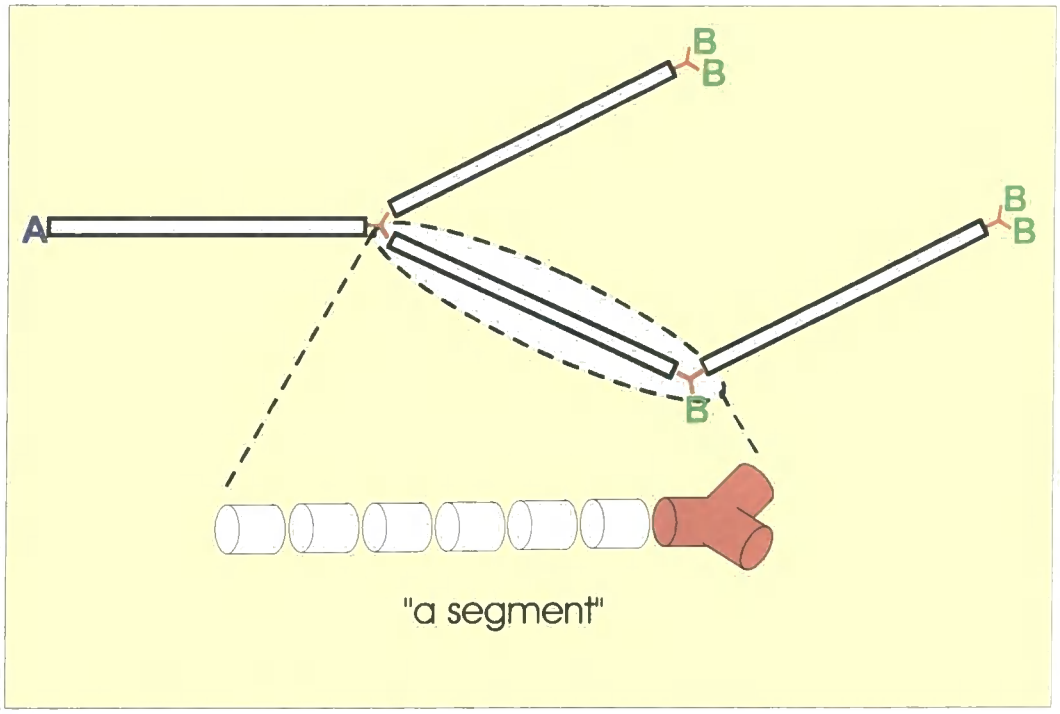

Fig. 6.12 A chain 'segment'.

A statistically branched copolymer may be represented as an 'average' structure, as shown in Figure 6.12 for a copolymer with 14.3mole% branching units, using what will be defined as chain segments. A 'chain segment' is the statistical repeat unit of the copolymer at one hundred percent conversion, which contains the average number of linear residues between branch points and one branching residue. The segment length may be determined from the branching content of the copolymer using Equation 6.3.

$$N_l = (100\text{-}b)/b \qquad \text{Eq. 6.3}$$

where N_l = no. of linear units per segment, b = branching composition (%)

The branching content of poly(ethylene oxybenzoate) copolymers based on the weight of monomers in the feed was compared with the values determined using ^1H NMR spectroscopy. Values were in good agreement, differing by approximately 0.4%

on average. The ^{1}H NMR analysis used to determine the number average molecular weight of branched p-PEOB copolymers is explained below.

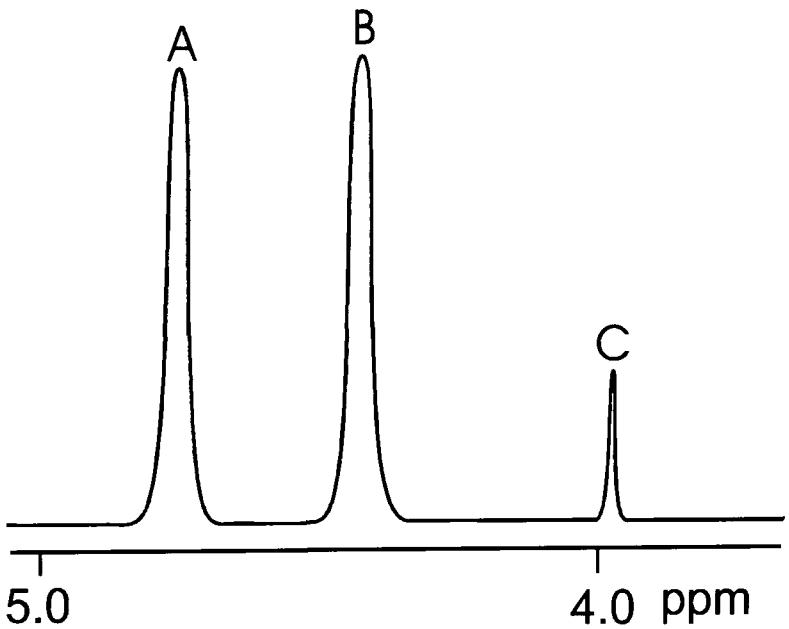

Fig. 6.13 Schematic ^{1}H NMR spectrum of a branched *p*-PEOB copolymer in $CDCl_3$/TFA solution, showing approximate positions of CH_2 and CH_3 groups.

The peak area C/3 is proportional to the number of methyl ester groups in the polymer and equates to the number of branching units plus one (x+1). Peak areas A/2 and B/2 are representative of the total numbers of linear and branched residues in the polymer, given as $(N_l+1).x$; where N_l is the average segment length and x is the average number of segments per molecule; see Figure 6.14. Thus the ratios of signal intensities B:C, and A:C designated, r, may be defined as shown in Equation 6.4.

$$r = 2.(N_l+1).\,x\,/\,3.(x+1) \qquad \text{Eq. 6.4}$$

where N_l = number of linear units per segment, x = average number of segments per molecule

In order to evaluate the number average molecular weight of the polymer we require x, the average number of segments per molecule. An expression for x is derived from Equation 6.4 and shown in Equation 6.5.

i. $r = 2(N_I+1)x / 3(x+1)$ [multiply by $(x+1)$]

ii. $r(x+1) = 2(N_I+1)x / 3$ [divide by (x . r)]

iii. $(x+1) / x = 1+(1/x) = 2(N_I+1) / 3r$ [subtract 1]

iv. $(1/x) = [2(N_I+1) / 3r] - 1 = (2(N_I+1)-3r) / 3r$ [Cross multiply]

$$x = 3r / (2(N_I+1)-3r) \qquad \text{Eq. 6.5}$$

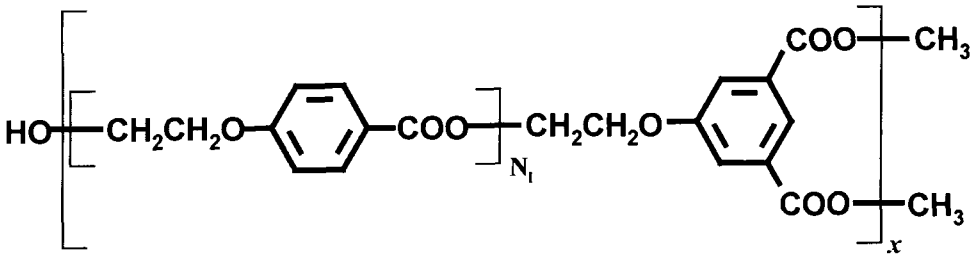

Fig. 6.14 Structural representation of a *p*-PEOB branched copolymer.

The value, r, is taken directly from measurements of ^{1}H NMR spectroscopy and N_I from the branching content of the copolymer. These values are then substituted into Equation 6.5 to obtain x, which in turn, is used to determine Mn from Equation 6.6. The formula assumes that there are (N_I. x) linear residues, (x) branching units, (x+1) CH_3 end groups and one hydroxyl focal unit. Although Equation 6.6 is specific to *p*-PEOB, as branched with **3**, the process of end group counting is general and should work for other branched systems. However, this is only true when the assumptions that govern the technique are valid and end groups may be distinguished from other features in the polymer.

$$\mathbf{Mn_{(Copolymer)} = (N_I.\ x.\ 164) + (x.\ 207) + [(x+1).\ 15] + 17} \qquad \text{Eq. 6.6}$$

6.2.1 Limitations of end group counting

Limitations of end group counting were predicted, based on the following considerations. The ratio *r*, (numbers of CH_2 protons):(numbers of CH_3 protons), could not be measured accurately, using ^1H NMR spectroscopy, to a value greater than 80. Consequently, in linear poly(ethylene oxybenzoate)s this limits the accuracy of end group counting to Mns of approximately 20,000 (DP~120). However, the addition of a small quantity of branching agent would cause the relationship between Mn and *r* to veer away from linearity, as illustrated in Figure 6.15.

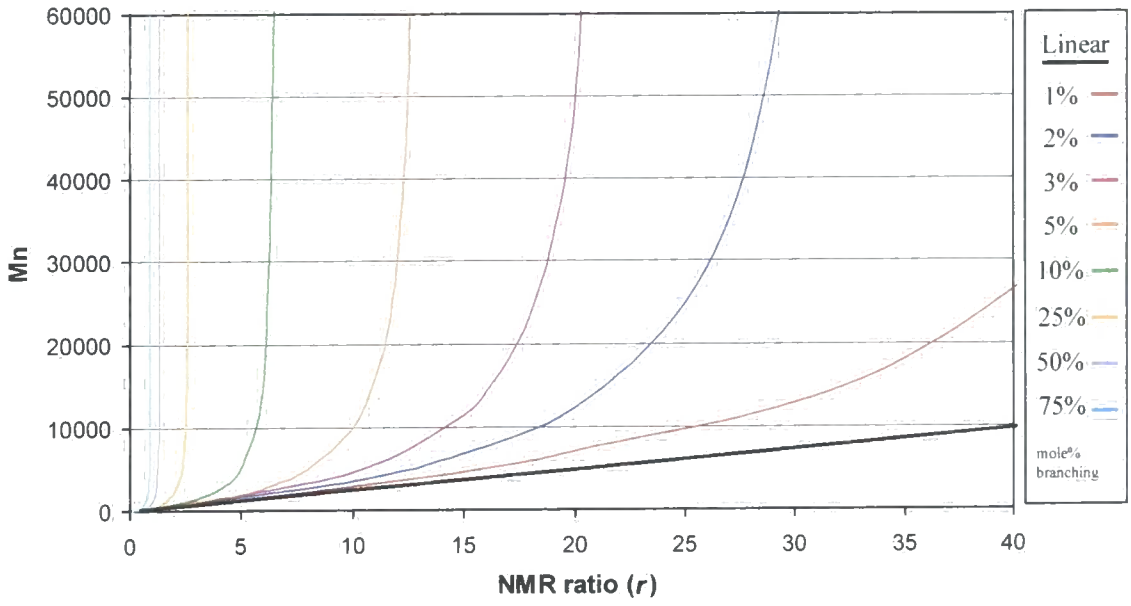

Fig. 6.15 Plot showing Mn, as determined by end group counting for various extents of branching, plotted against the NMR ratio *r* ($2.CH_2$:$3.CH_3$).

Analysis reveals that the addition of one or two percent branching will, in theory, raise the accuracy of Mn measurements to values of 100,000+ (DP~600). However, the limiting factor in the determination of molecular weight is then the accuracy with which the extent of branching can be ascertained.

The rate of increase of molecular weight with *r* (dMn/d*r*), as predicted by this theoretical treatment, is dependent on several factors which include the extent of branching and molecular weight. As the branching composition increases, the range of measurable Mns decreases, i.e. with 25% branching the detection limit is

approximately 10,000 Mn; 50% branching, approximately 4,000 Mn; 75% branching approximately 2,000 Mn, as shown in Figure 6.16. Measurements of branched *p*-PEOB copolymers have revealed that these estimates are somewhat optimistic. In reality, sensible number average molecular weights were never obtained for samples containing a branching composition of greater than 15mole%.

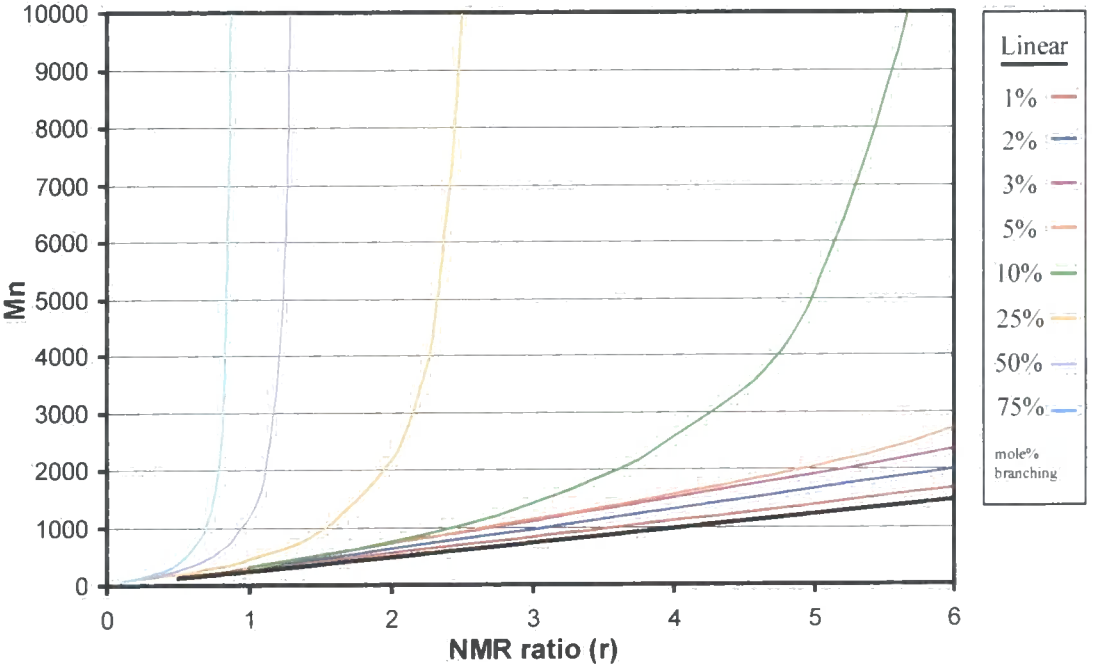

Fig. 6.16 Plot showing Mn, as determined by end group counting for various extents of branching, plotted against the NMR ratio *r* (CH_2:CH_3).

This analysis suggests that end group counting can provide a reasonable estimate of number average molecular weight in branched copolyesters providing the extent of branching is not excessive. Another limit, in the present case, arises from the reliability of NMR signal integration.

Chapter 6.3 References

1. Flory P.J., *J. Am. Chem. Soc.*, **58**, (1936), 1877
2. Flory P.J., *J. Am. Chem. Soc.*, **74**, (1952), 2718
3. Feast W. J., Keeney A. J., Kenwright A. M. and Parker D., *Chem. Comm.*, (1997), 1749

4. Keeney A.J., Ph D Thesis, University of Durham (1998)
5. Parker D., Feast W.J., unpublished personal communication
6. Kenwright A.M., Peace S.K., Richards R.W., Bunn A., MacDonald W.A., *Polymer*, **40**, (1999), 2035-2040

Chapter 7

Conclusions and Suggestions for
Further Work

7.1 Conclusions

Large-scale syntheses of monomers **1**, **2** and **3**, up to 200g, have been optimised and the resultant materials characterised using ^{1}H, ^{13}C NMR and IR spectroscopies, mass spectrometry and elemental analysis. In addition, homopolymers of **1** and **2** of various molecular weights have been generated using bulk polymerisation techniques described in Chapter 2. Their thermal properties have been analysed using differential scanning calorimetry (DSC) with the following plateau values observed for quenched samples, recorded at a heating rate of 10°C min^{-1}: polymers of **1**, Tg=51°C, Tc=133°C, Tm=178°C; polymers of **2**; Tg=77°C, Tc_1=121°C, Tc_2=190°C and Tm=219°C. Analysis of the glass transition temperatures of low DP oligomers of **2**, showed that they conformed to the empirical relationship defined by Beuche for amorphous linear polymers i.e., the variation in Tg was linear with respect to 1/Mn on the approach to the thermal plateau. The effect of copolymerising equimolar quantities of **1** and **2** was also investigated. Samples of the linear copolymer were amorphous and chloroform soluble, in contrast to homopolymers of **1** and **2**, which were semi-crystalline and insoluble in chloroform.

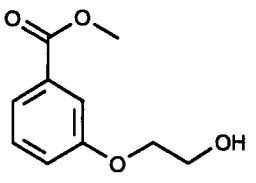

1

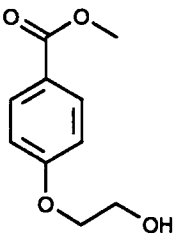

2

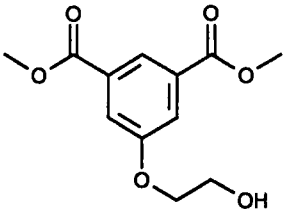

3

The main interest of this thesis has been the investigation into the effects of branching *p*-PEOB (homopolymers of **2**) with monomer **3**. To this end, a range of cross link free, highly functionalised copolymers with various extents of branching have been synthesised and characterised in detail using the following techniques: ^{1}H, ^{13}C NMR, and IR spectroscopies, TGA, DSC and viscometry. From the analyses of carbonyl signals in the ^{13}C NMR spectra, we were able to ascertain that the distribution of branch points in the polymer was statistical and not selective. Furthermore, the

analyses of copolymers with up to 12.5mole% branching revealed that they were crystalline and chloroform insoluble, in comparison to materials with higher extents of branching which were amorphous and soluble in chloroform. This leads us to conclude that solubility of *p*-PEOB is inextricably linked to structural regularity in the polymer.

The determination of number average molecular weight of *p*-PEOB copolymers with less than 15mole% branching was achieved using ^{1}H NMR end group counting, as described in detail in Chapter 6. However, the data obtained for materials with higher extents of branching was too scattered to be of use. Instead, molecular weight determinations of amorphous copolymer compositions, i.e. those materials with more than 12.5mole% branching, were made using conventional GPC measurements calibrated with linear polystyrene standards.

Analysis of the glass transition temperatures of these materials revealed no significant dependence on the copolymer branching composition. However, it was apparent that the melting temperature of *p*-PEOB decreased linearly with increasing branching composition up to 12.5mole%, given by the formula Tm=-339.6x+491.8K; where x is the mole fraction of branching units. Crystallisation was made increasingly difficult with the insertion of branch points, reflected in the increase in Tc_1 and the reduction in the enthalpy of fusion. This effect was more pronounced at higher molecular weights. Secondary crystallisation was, however, made progressively easier with an increase in the branching content of the copolymer, as indicated by a decrease in Tc_2. This maybe due to increased disorder in the crystal lattice, resulting from poorly formed crystallites, making the process of reorganisation easier. The disruption of crystallisation is consistent with branching units being excluded from the crystal matrix. Decomposition temperatures, recorded at 2% weight loss, appeared to be independent of architecture and composition; temperatures of 320°C being observed for all linear and branched materials. Furthermore, hydrolysis and ageing did not appear to have any significant effect on the results obtained from TGA or DSC. In comparison to PET, PEOB polymers appear to be much more resistant to hydrolysis.

Analysis of the results of chloroform solution viscometry revealed an unexpected relationship between log(intrinsic viscosity), log Mw and the branching composition for the amorphous copolymers with between 20mole% and 100mole%

branching. Indeed, Mark-Houwink plots revealed linear trend lines for the data of various branching compositions over a broad range of weight average molecular weights (3000 to 300,000). Furthermore, these data could be described by a single equation, $\log[\eta]=0.41\log[Mw]-0.0033x-0.429$; where $[\eta]$ is intrinsic viscosity (ml mg^{-1}), [Mw] is conventional polystyrene equivalent molecular weights as measured in chloroform and x is the mole fraction of branching units in the copolymer. This leads us to conclude that the solution structures of the amorphous branched copolymers must be similar. However, as molecular weights were measured against linear polystyrene equivalents, some uncertainty exists as to the interpretation of this data.

7.2 Furtherwork

The effects of branching are exploited in many commercial applications. For example, branching in polyethylene is used to increase clarity, impact strength and improve other properties in the polymer. Indeed, a reduction in the melt viscosity of PE can be achieved with a controlled increase in long chain branching. However, these effects are not always advantageous. For instance, LDPE is not used for structural applications because its highly branched architecture is subject to slow deformation, called creep, under low load stresses over prolonged periods of time. Furthermore, the bulk properties of polyesters, like polyethylene, are dependent on the extent of crystallinity in the material. Many polyester products, including bottles, films and fibres rely on the properties imparted by crystallinity in the polymer. Any disruption to the regularity of polymer structure will result in a decrease in the extent of crystallinity and subsequently, the suitability of these materials to their intended applications. Consequently, high extents of branching do not offer any advantages over conventional linear architectures. However, as exploited in polyethylene, long chain branching may provide a means of lowering the melt viscosity of the material without causing a significant disruption to crystallinity, which would give processing advantages. This consideration requires further investigation.

In order to consolidate our findings and improve our understanding of branched poly(ethylene oxybenzoate) systems, a comparison between the absolute molecular weights and measurements obtained against linear polystyrene equivalents would be

advantageous. This could be achieved *via* a detailed light scattering study. In addition, the fractionation and analysis of high molecular weight material would be beneficial to understanding the disproportionately large weight distributions observed during the THF TRISEC examination of 80mole% branched *p*-PEOB.

The effects of statistical branching in *p*-PEOB have been analysed in detail, however, a comparison with linear copolymers of various compositions of meta and para poly(ethylene oxybenzoate) units would be advantageous. In this way, the effects of branching could be differentiated from the effects of statistical copolymerisation.

APPENDIX (A)

Monomers and Precursors

A01: Dimethyl 5-hydroxyisophthalate

A02: Dimethyl 5-(2-hydroxyethoxy)isophthalate

A03: Methyl 4-(2-hydroxyethoxy)benzoate

A04: Methyl 4-(2-acetoxyethoxy)benzoate

A05: Methyl 3-(2-hydroxyethoxy)benzoate

^{1}H NMR Spectra: A00-**1**

^{13}C NMR Spectra: A00-**2**

IR Spectra: A00-**3**

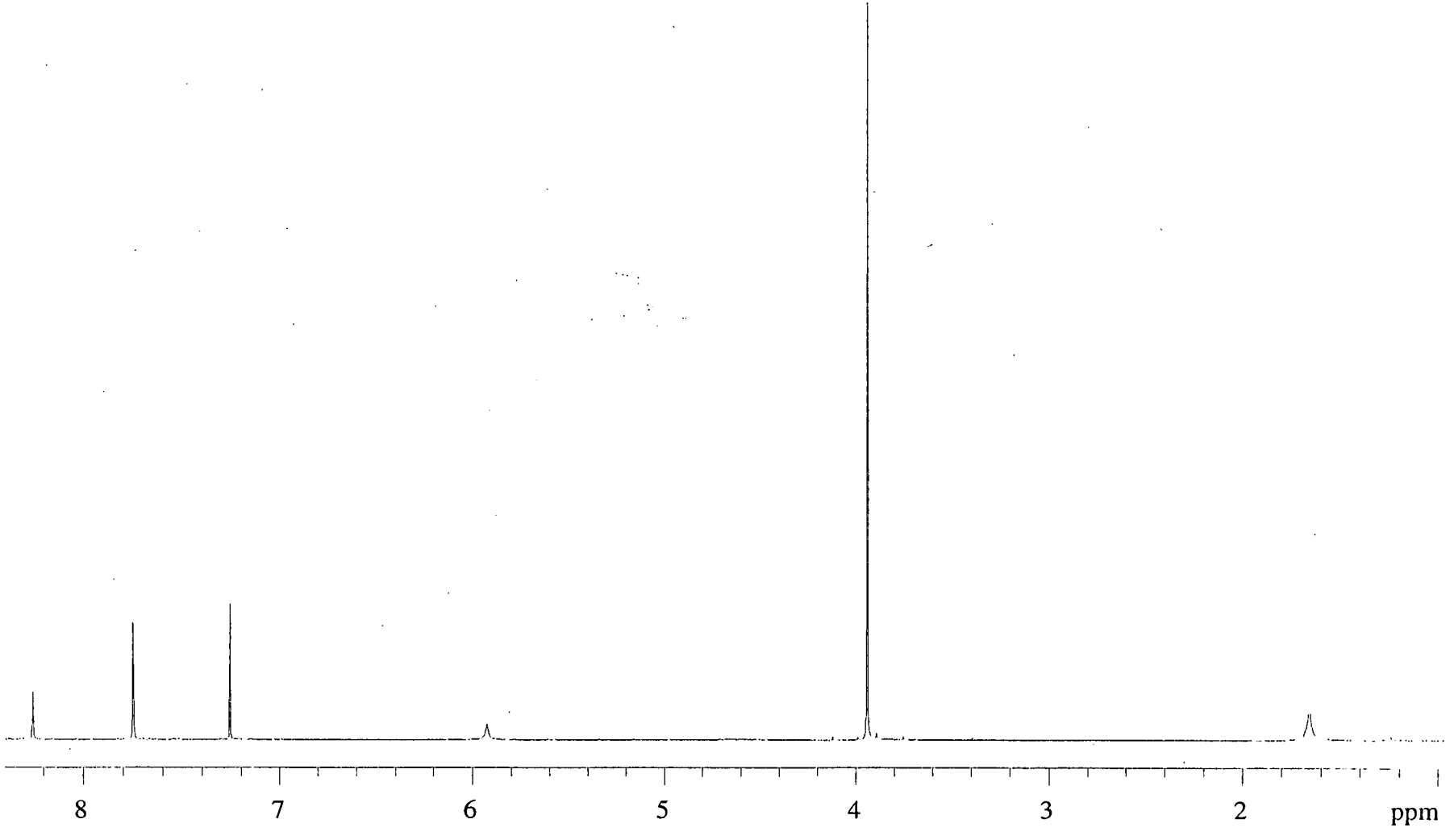

A01-1

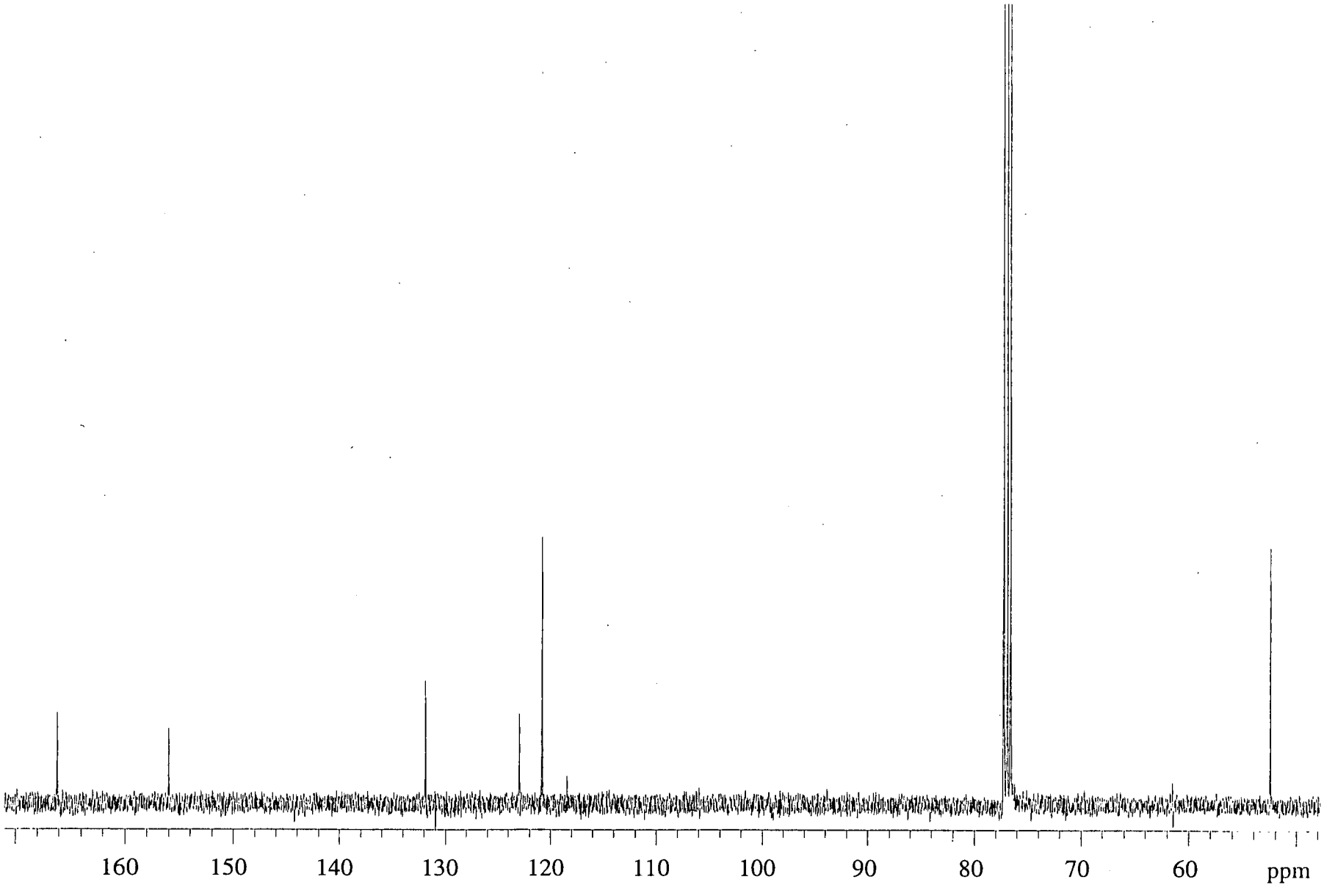

A01-2

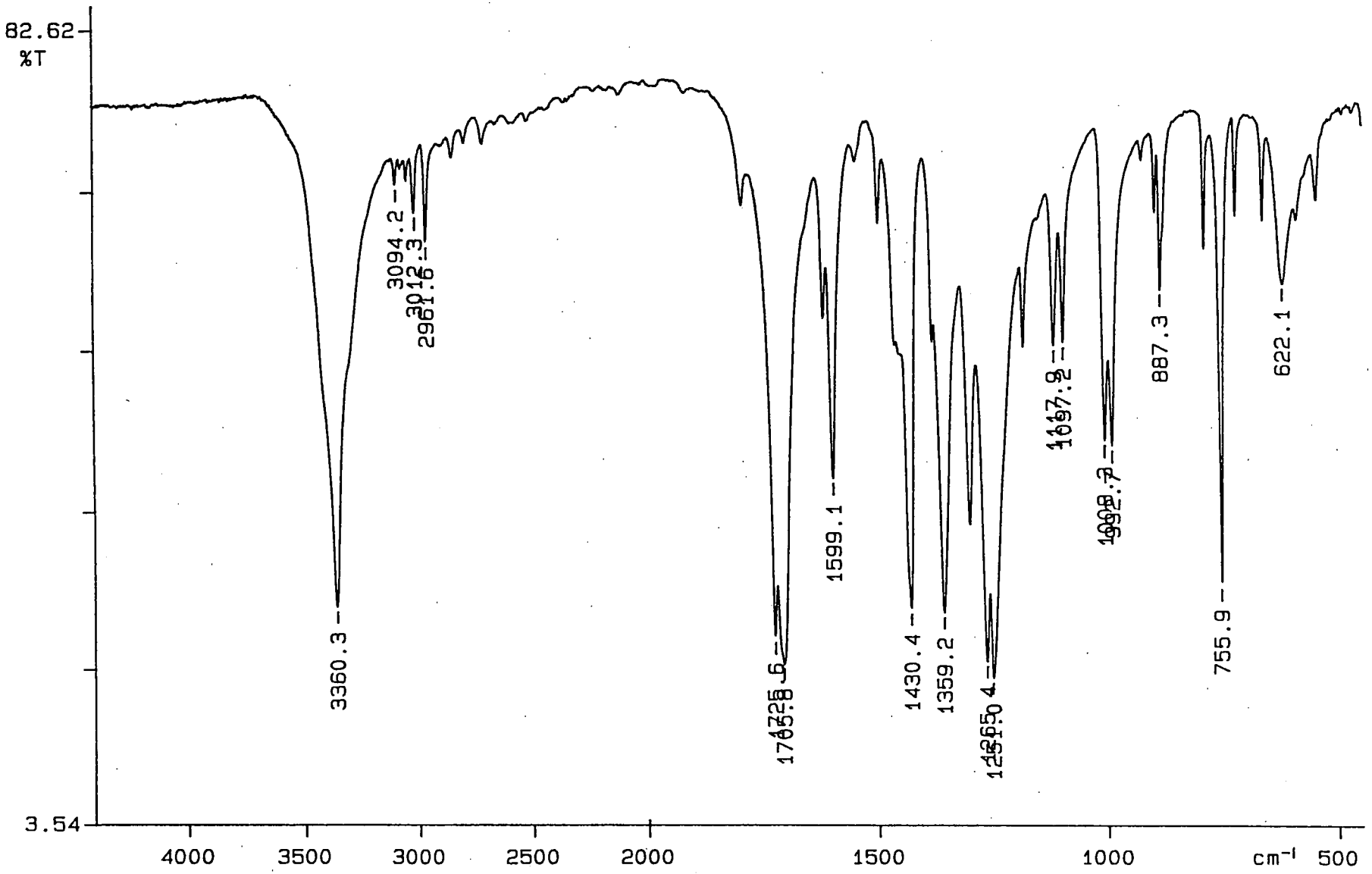
82.62
%T
3.54
3360.3
3094.2
3012.3
2961.6
1599.1
1430.4
1359.2
887.3
755.9
622.1
4000
3500
3000
2500
2000
1500
1000
cm-1
500

A01-3

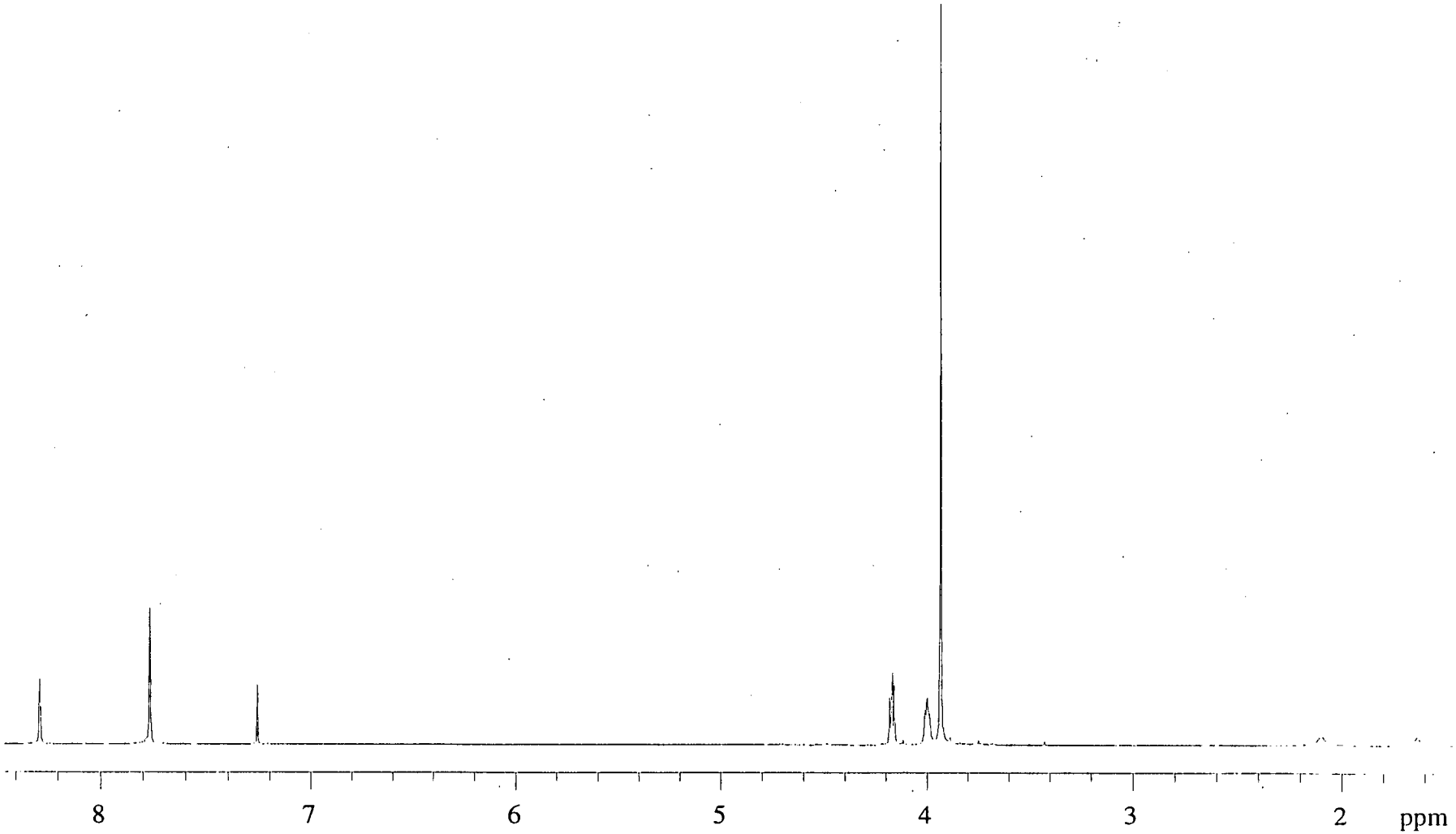

A02-1

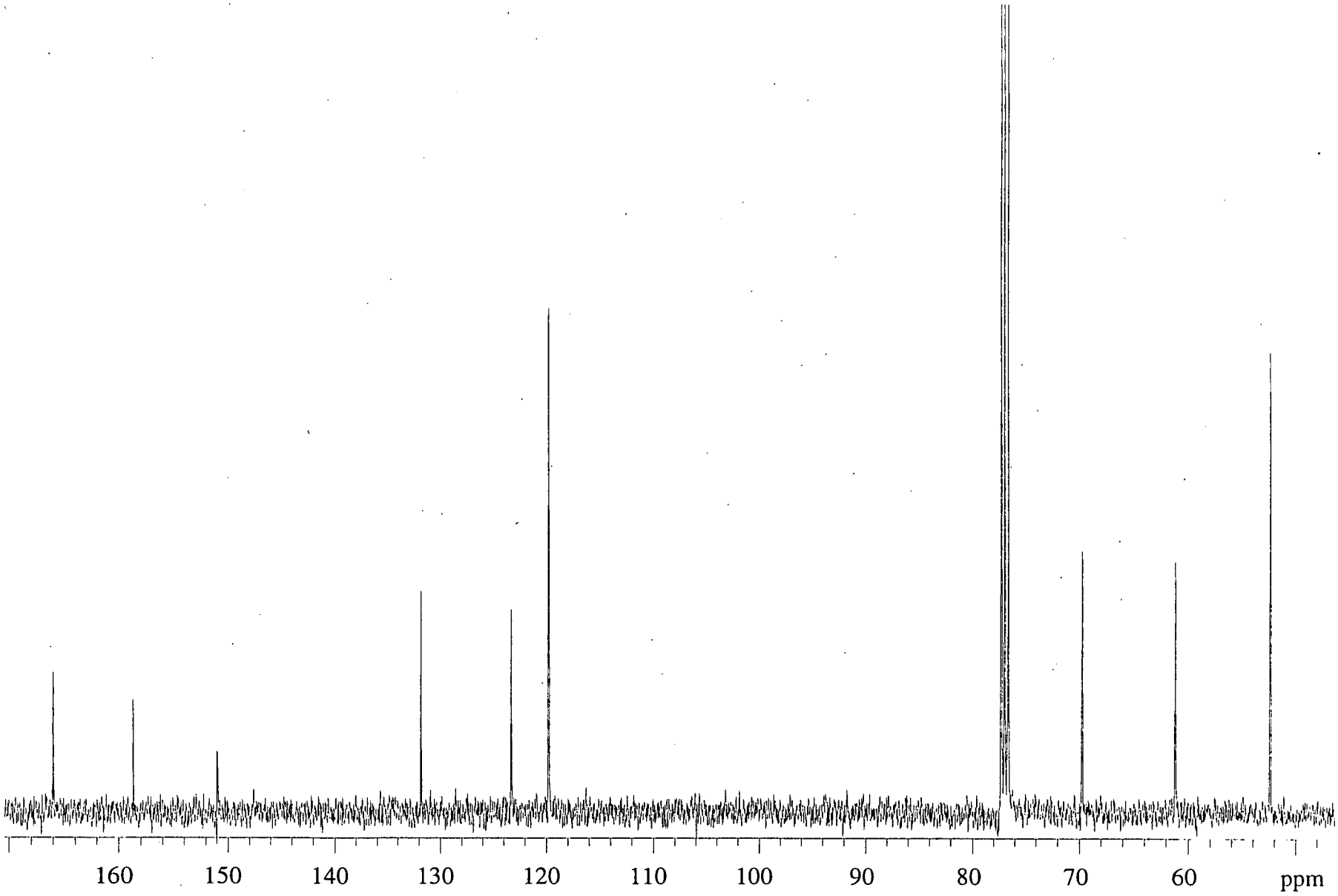

A02-2

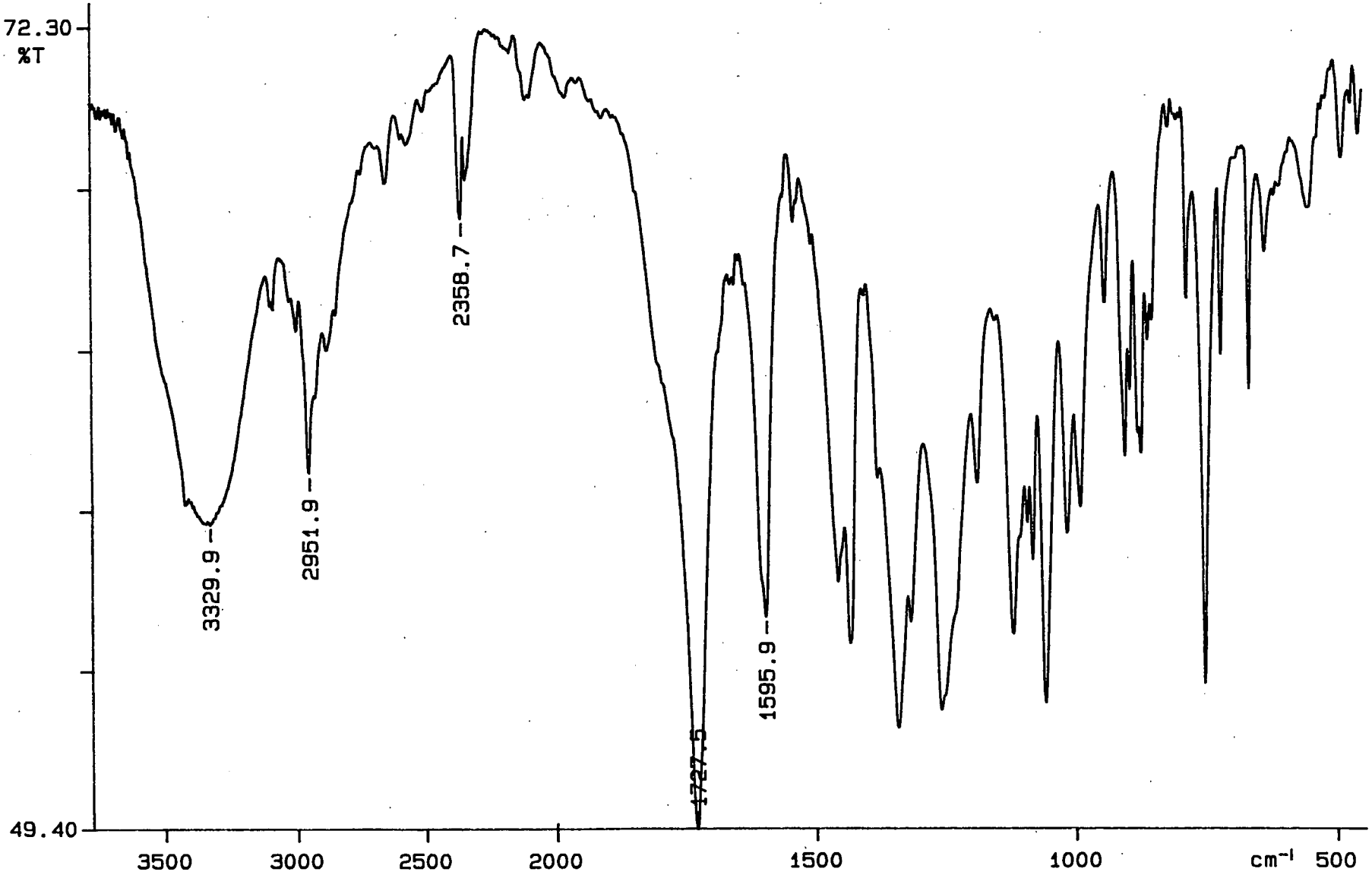

97/04/22 13: 17 s-373
Y: 16 scans, 4.0cm-1, flat

A02-3

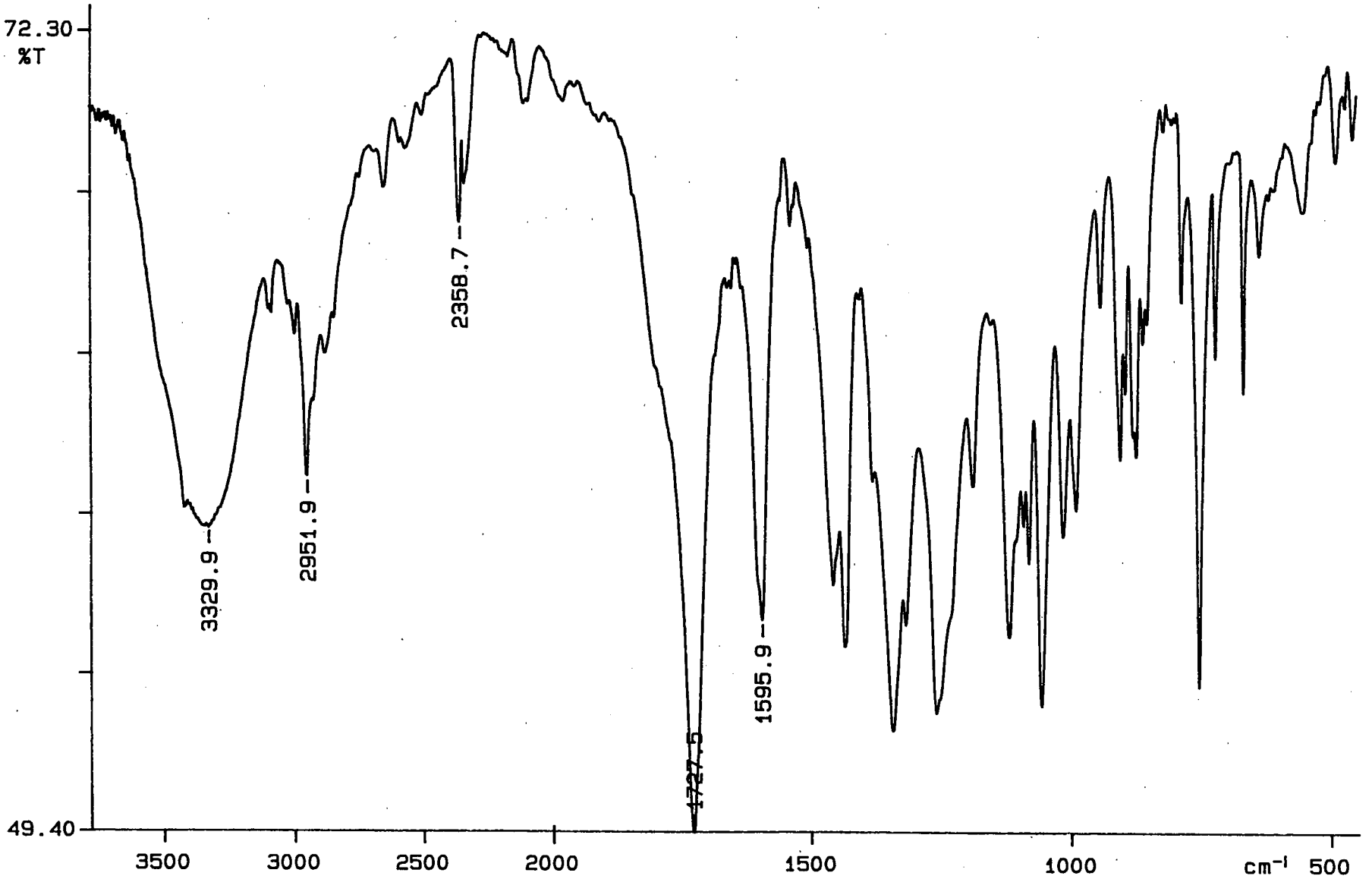

97/04/22 13: 17 s-373
Y: 16 scans, 4.0cm-1, flat

A02-3

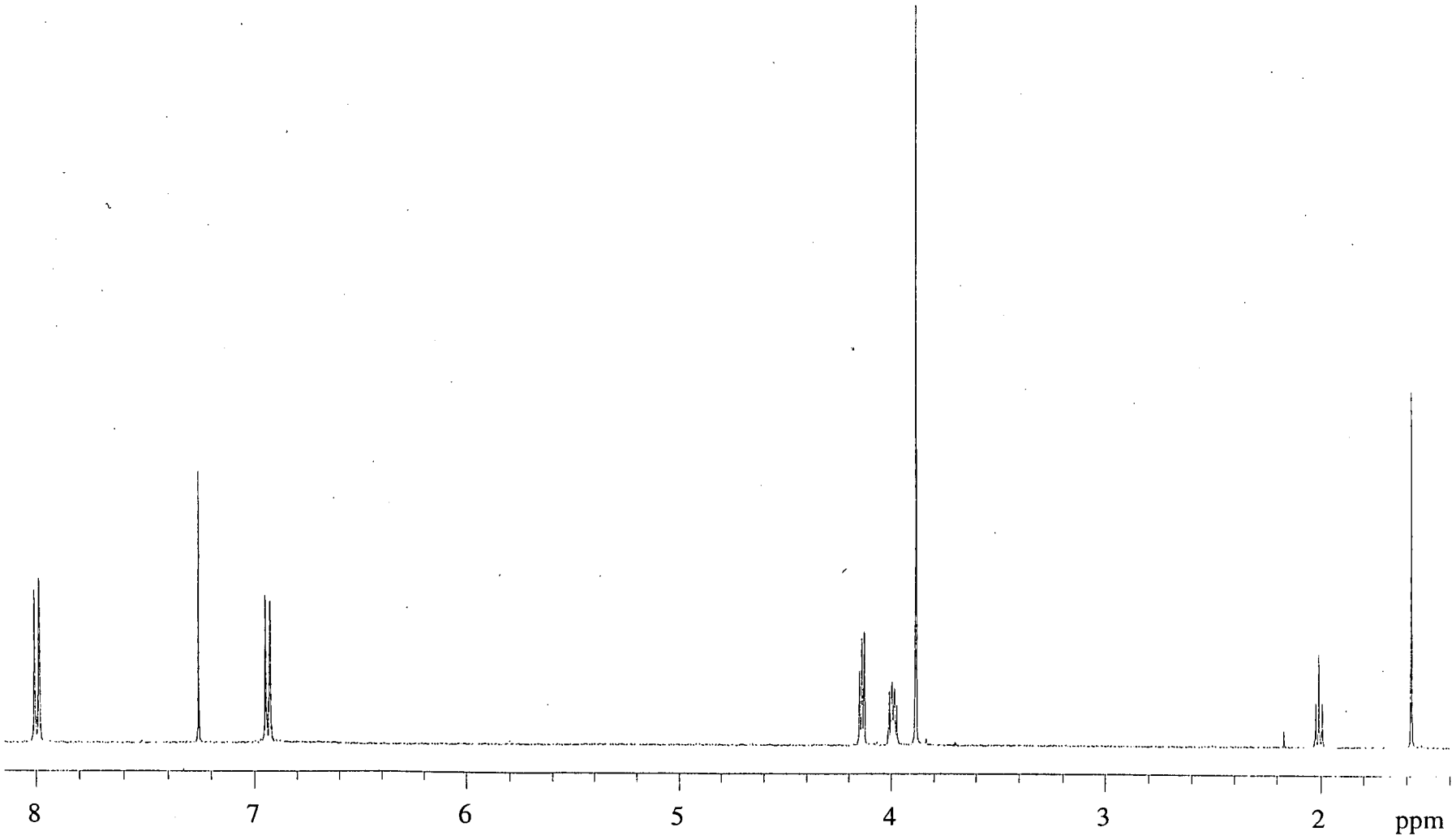

A03-1

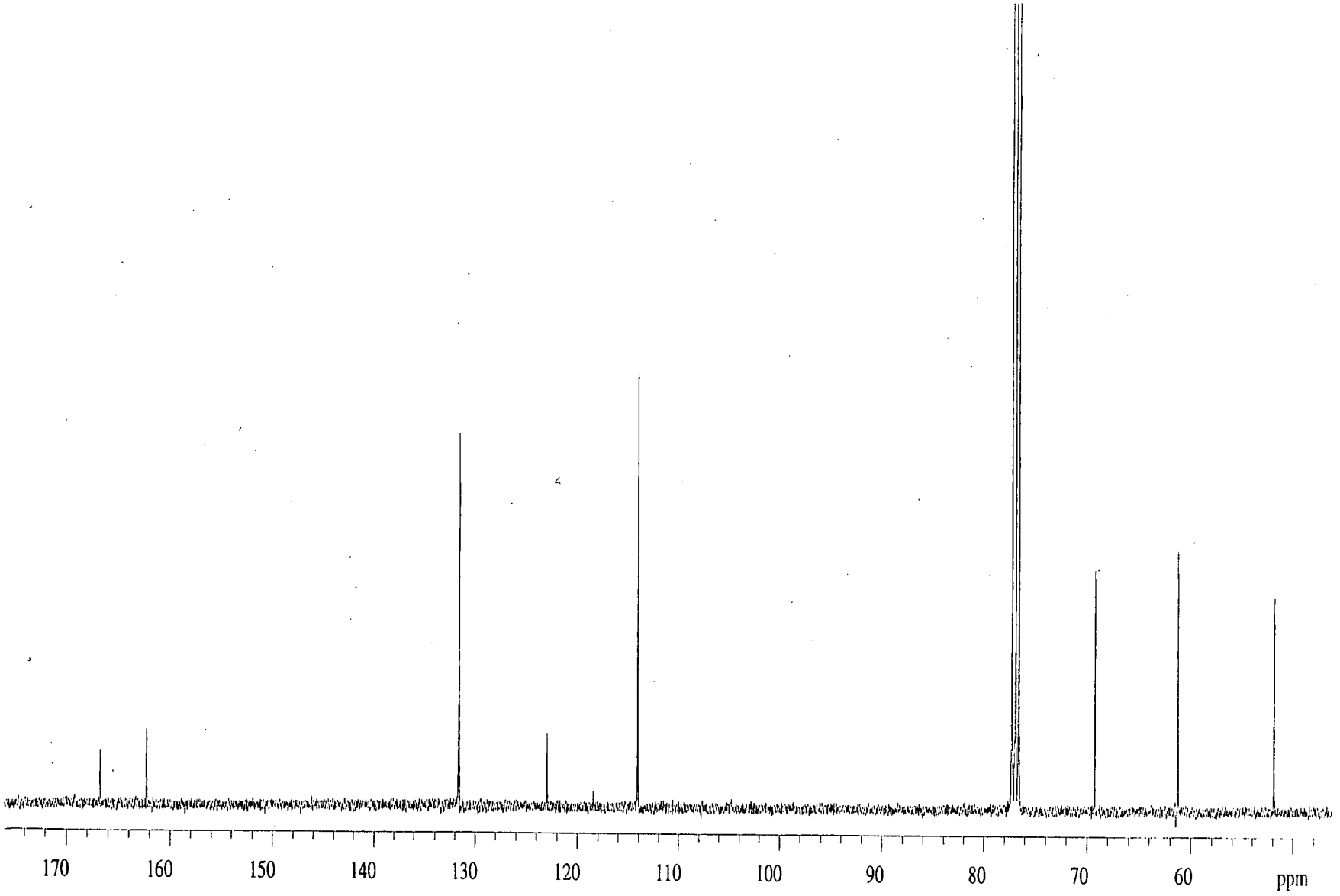

A03-2

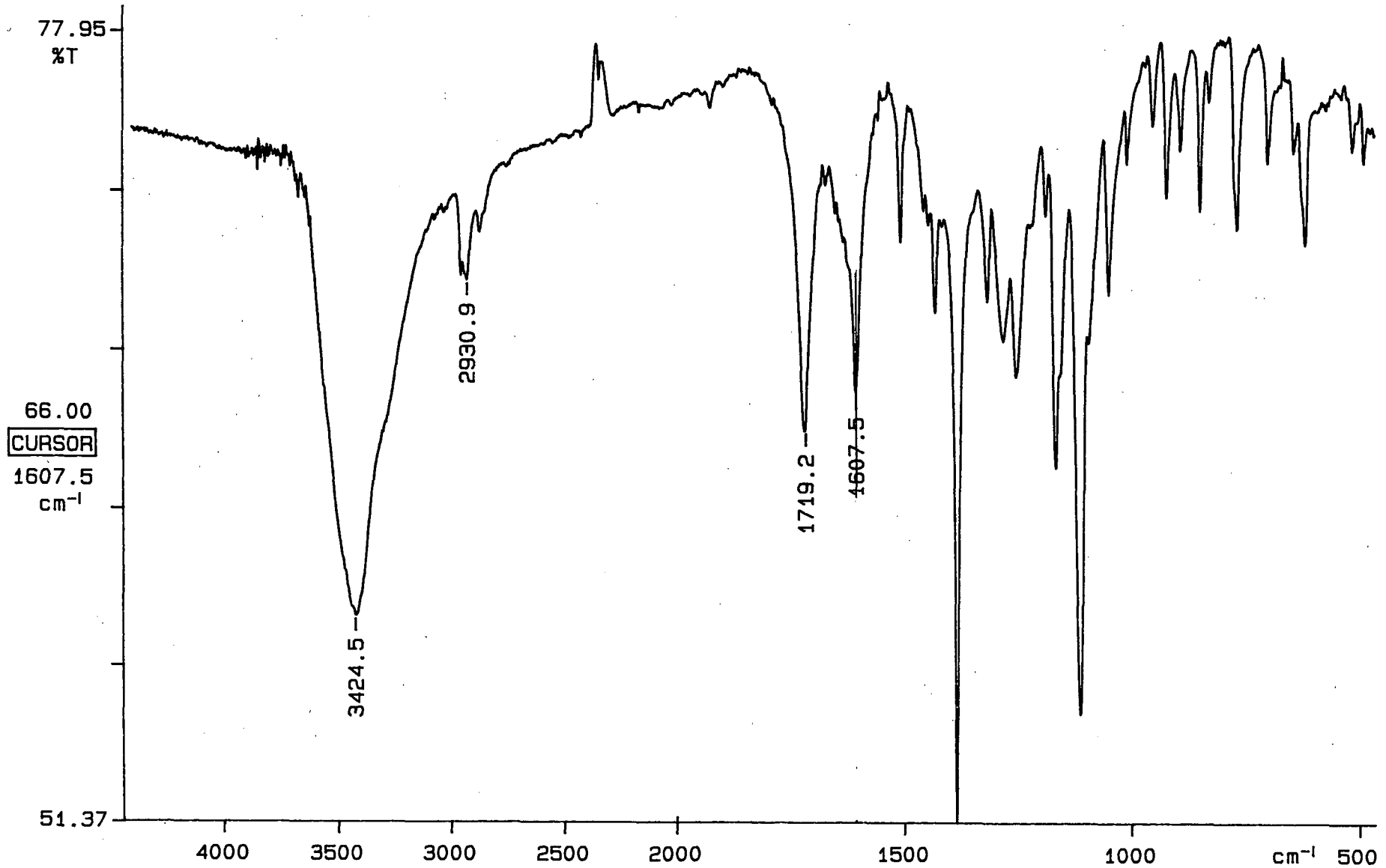

97/03/25 17:57
X: 16 scans, 4.0cm-1, flat

A03-3

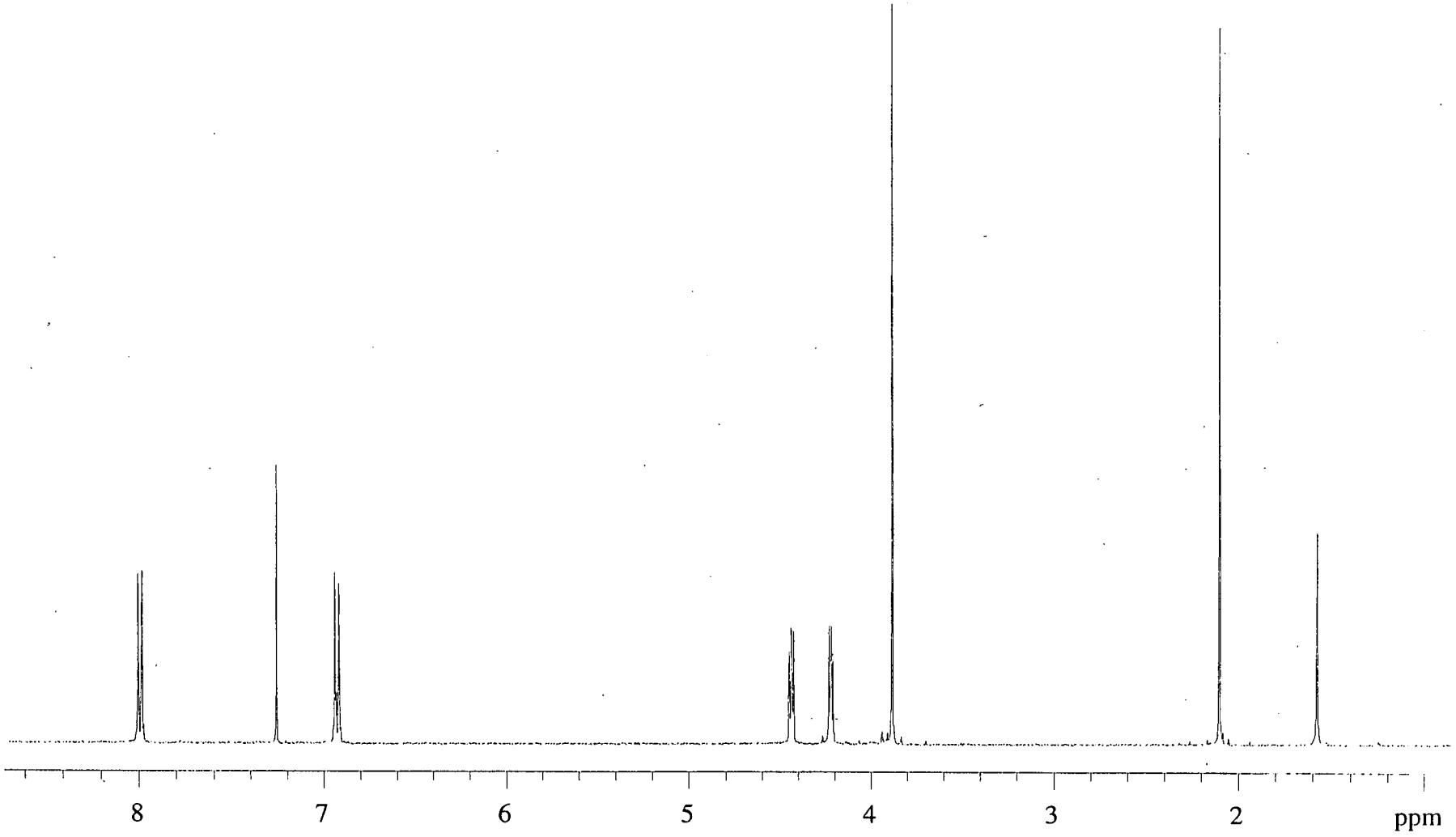

A04-1

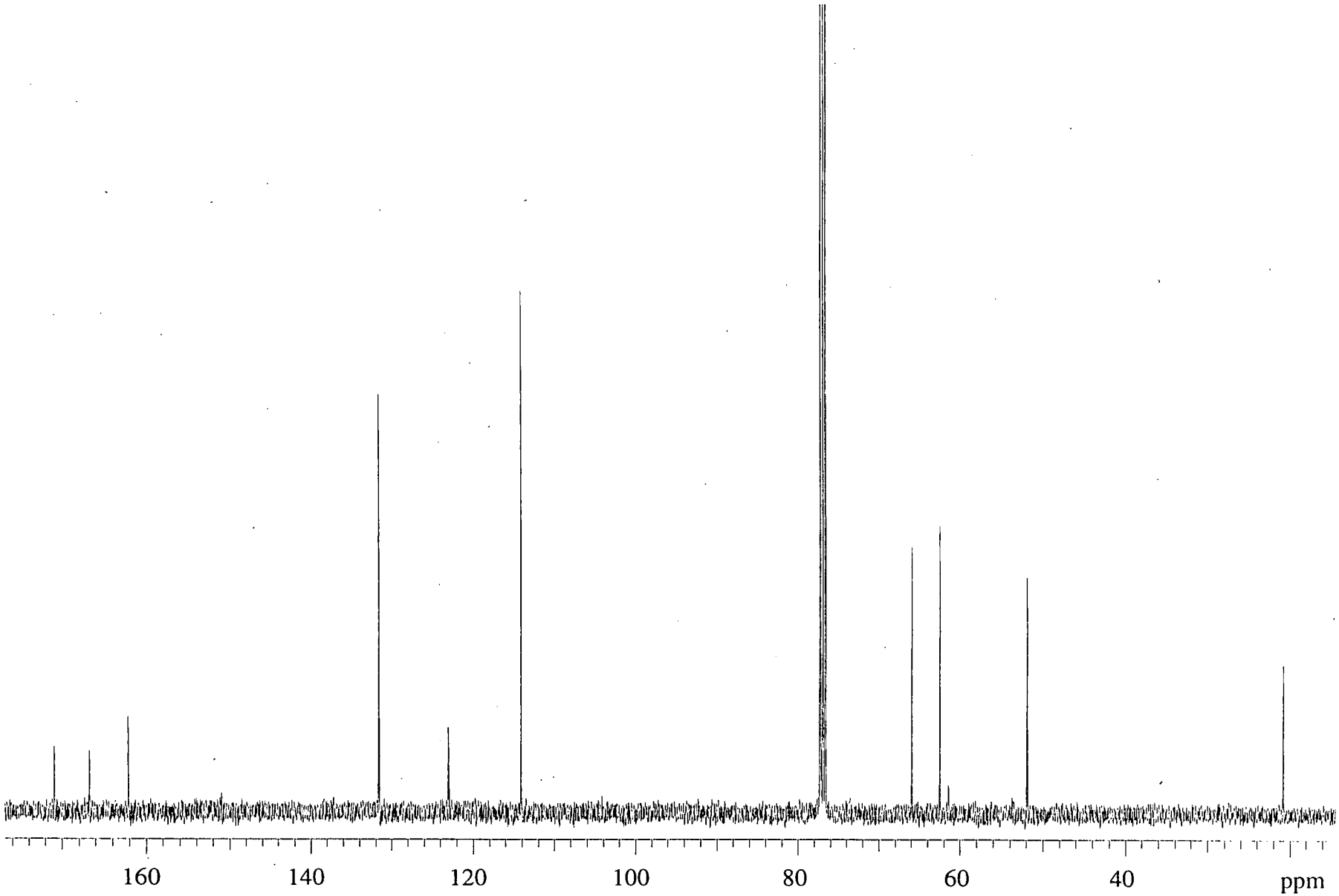

A04-2

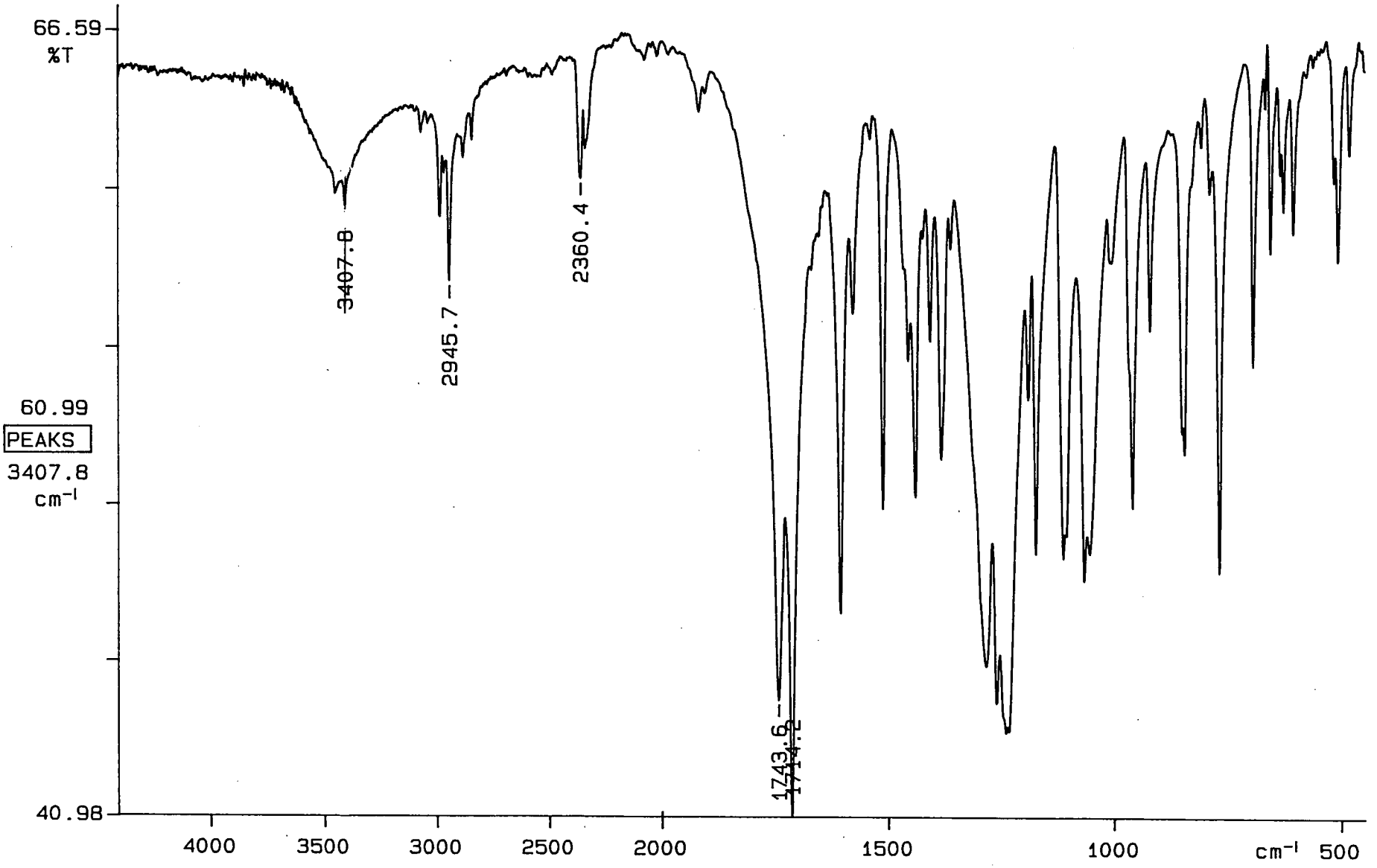

97/03/17 16:53
X: 16 scans, 4.0cm-1, flat

A04-3

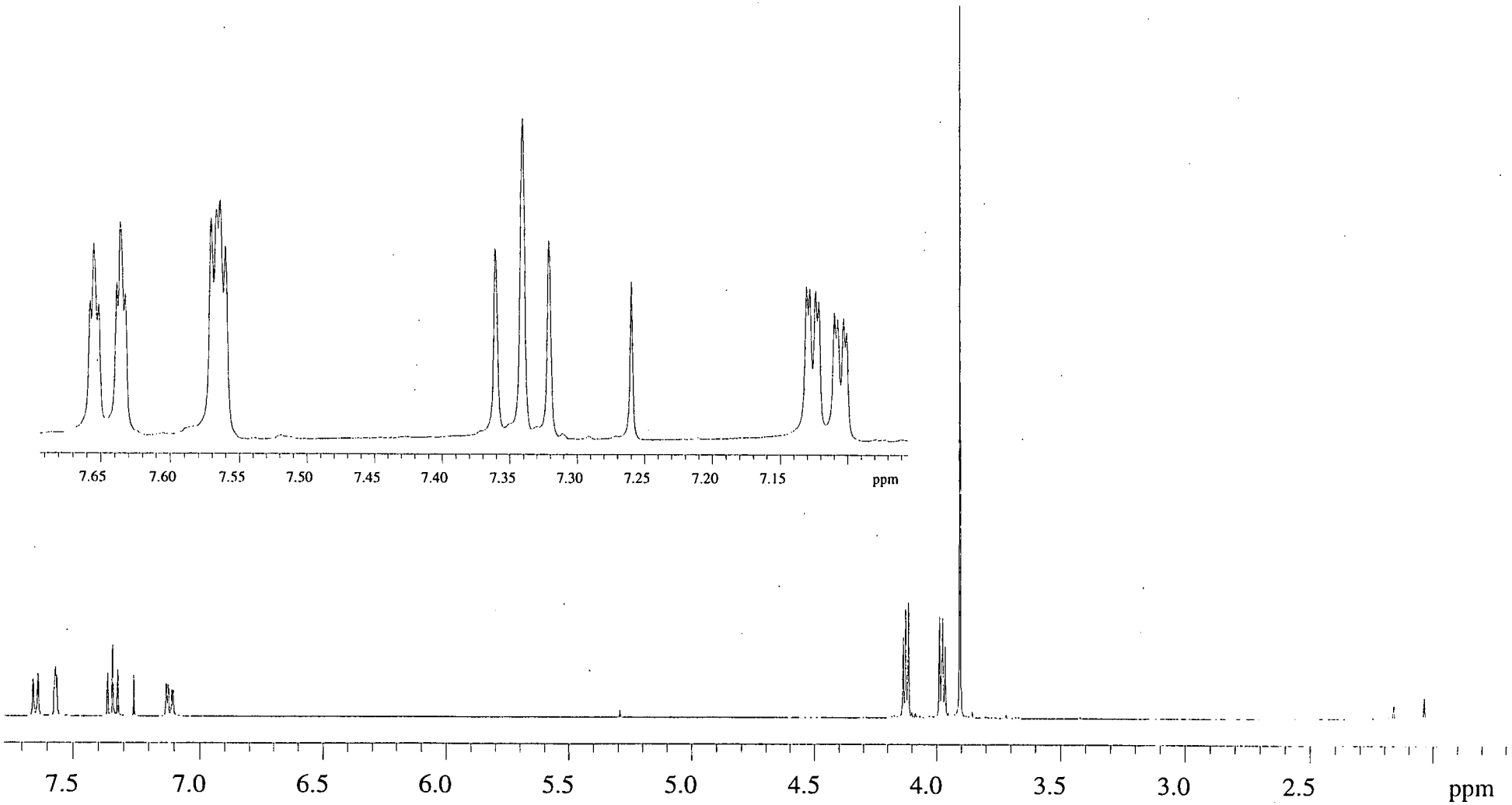
7.65
7.60
7.55
7.50
7.45
7.40
7.35
7.30
7.25
7.20
7.15
ppm
7.5
7.0
6.5
6.0
5.5
5.0
4.5
4.0
3.5
3.0
2.5
ppm

A05-1

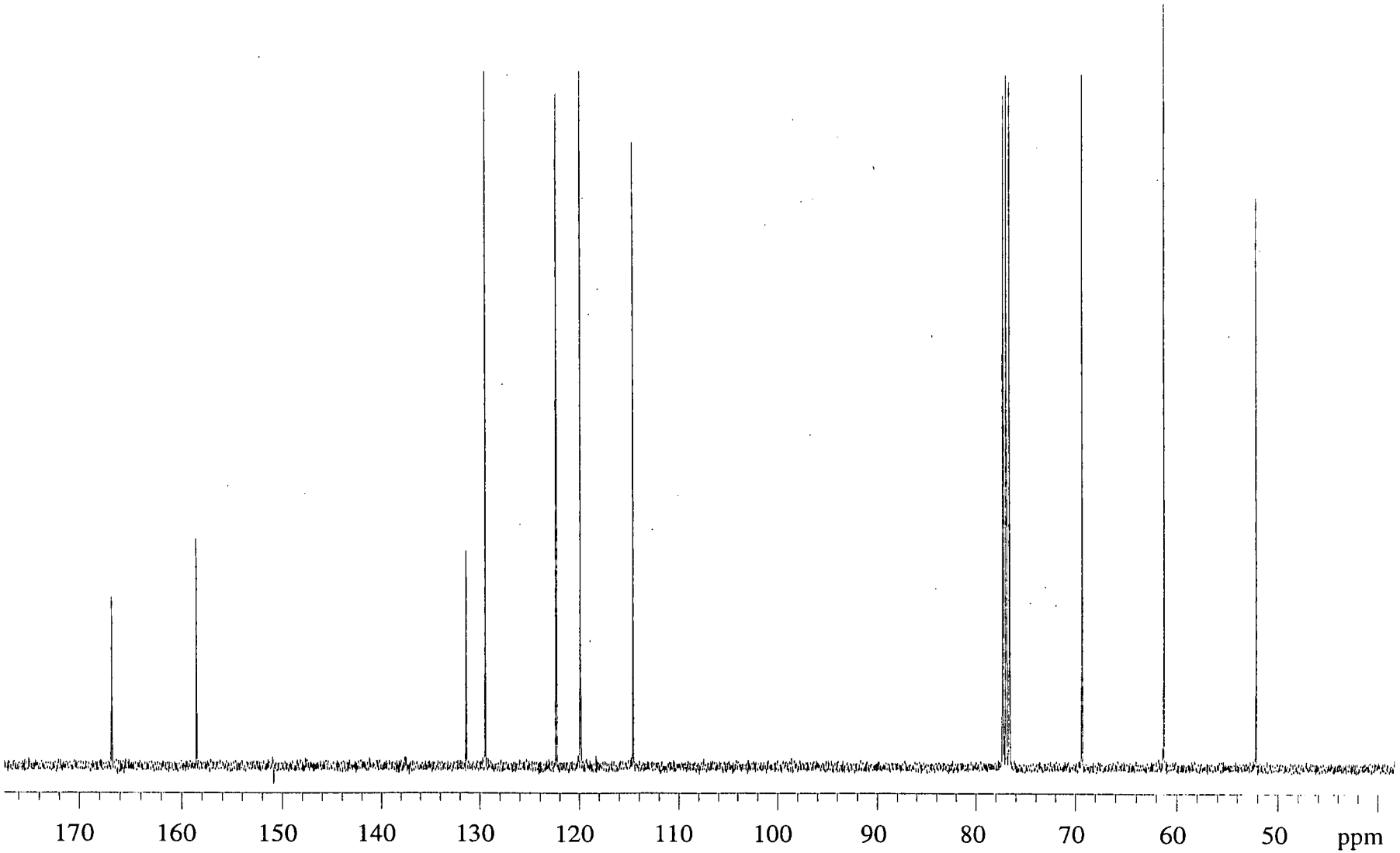

A05-2

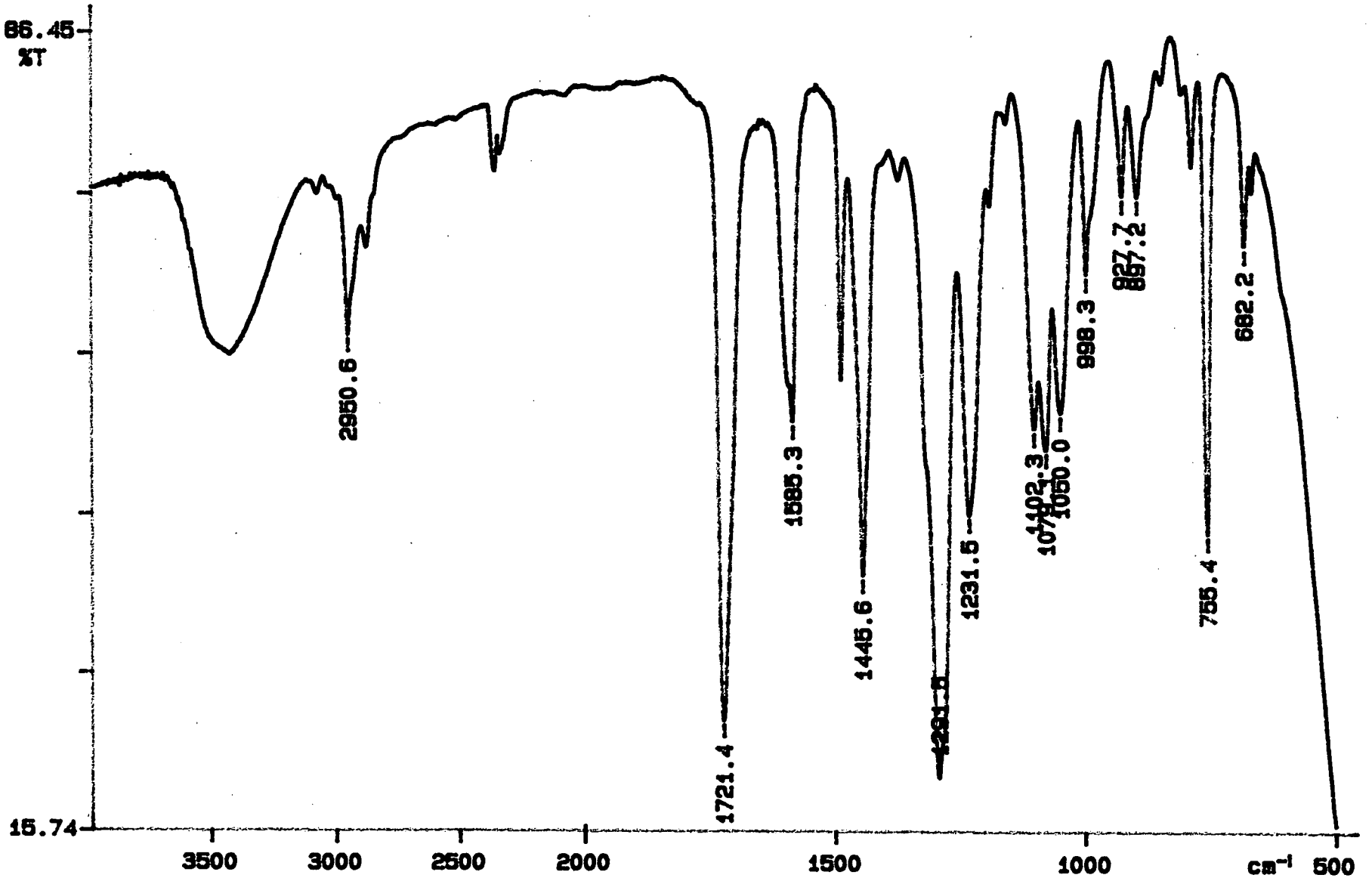

99/05/31 15:05 s-373
X: 16 scans, 4.0cm-1

APPENDIX (B)

Polymers

B01: *p*-Poly(ethylene oxybenzoate) (*p*-PEOB)

B02: *m*-Poly(ethylene oxybenzoate) (*m*-PEOB)

B03: 50:50 copolymer *m*:*p* Poly(ethylene oxybenzoate)

B04: Poly(ethylene oxyisophthalate) (5-PEOI)

B05: 80% 5-PEOI, 20% *p*-PEOB

B06: 60% 5-PEOI, 40% *p*-PEOB

B07: 40% 5-PEOI, 60% *p*-PEOB

B08: 20% 5-PEOI, 80% *p*-PEOB

B09: 15% 5-PEOI, 85% *p*-PEOB

B09-b: 12.5% 5-PEOI, 87.5% *p*-PEOB

B10: 10% 5-PEOI, 90% *p*-PEOB

B11: 4% 5-PEOI, 96% *p*-PEOB

B12: 3% 5-PEOI, 97% *p*-PEOB

B13: 2% 5-PEOI, 98% *p*-PEOB

B14: 1% 5-PEOI, 99% *p*-PEOB

IR Spectra:	**B00-1**
^{1}H NMR Spectra ($CDCl_3$/TFA):	**B00-2**
^{1}H NMR Spectra ($CDCl_3$):	**B00-3**
^{13}C NMR Spectra ($CDCl_3$/TFA):	**B00-4**
^{13}C NMR Spectra ($CDCl_3$):	**B00-5**
^{1}H NMR Spectra (DMSO):	**B00-6**
^{13}C NMR Spectra (DMSO):	**B00-7**

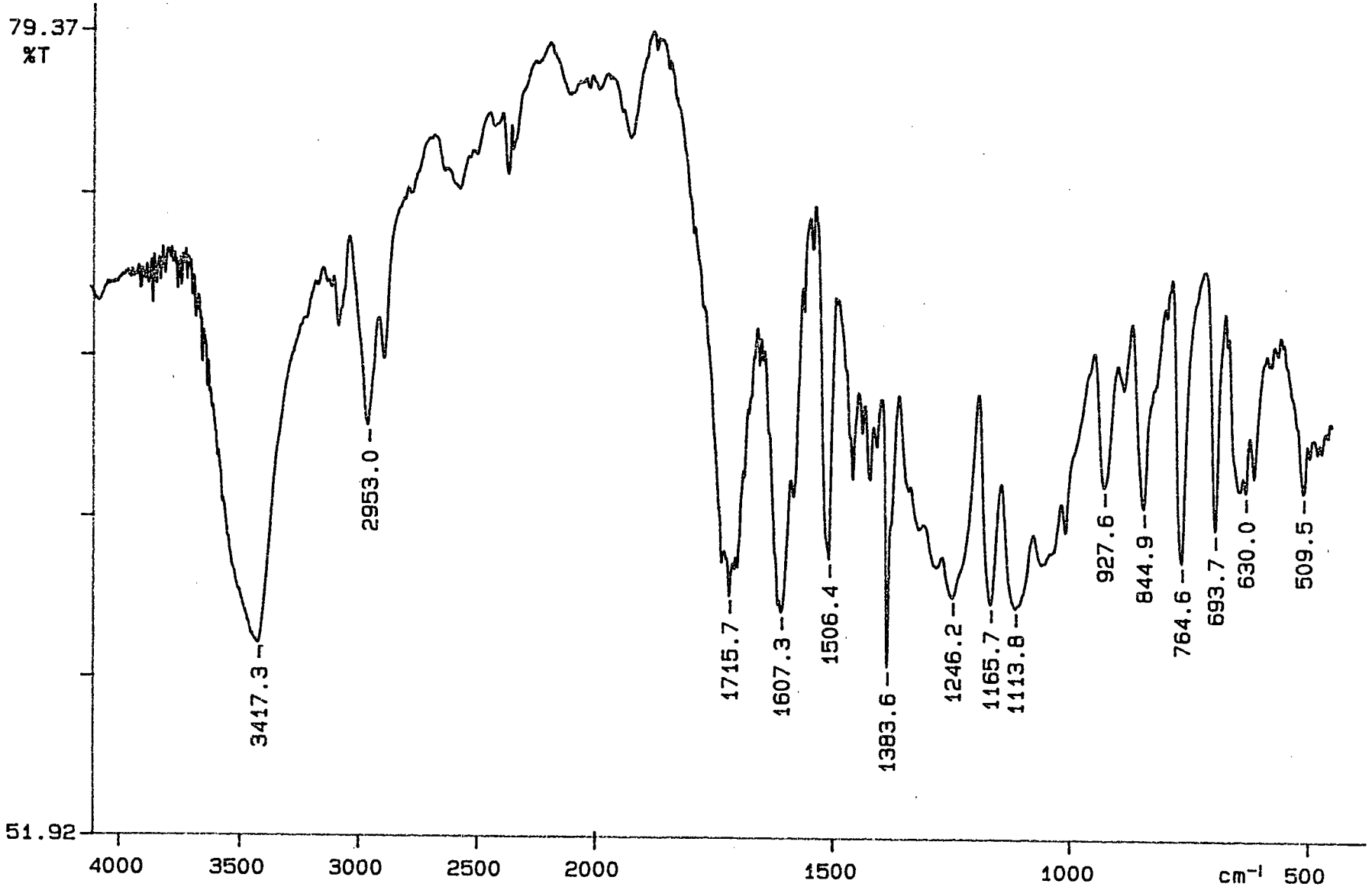

97/08/18 13:09 s-373
X: 16 scans, 4.0cm-1

B01-1

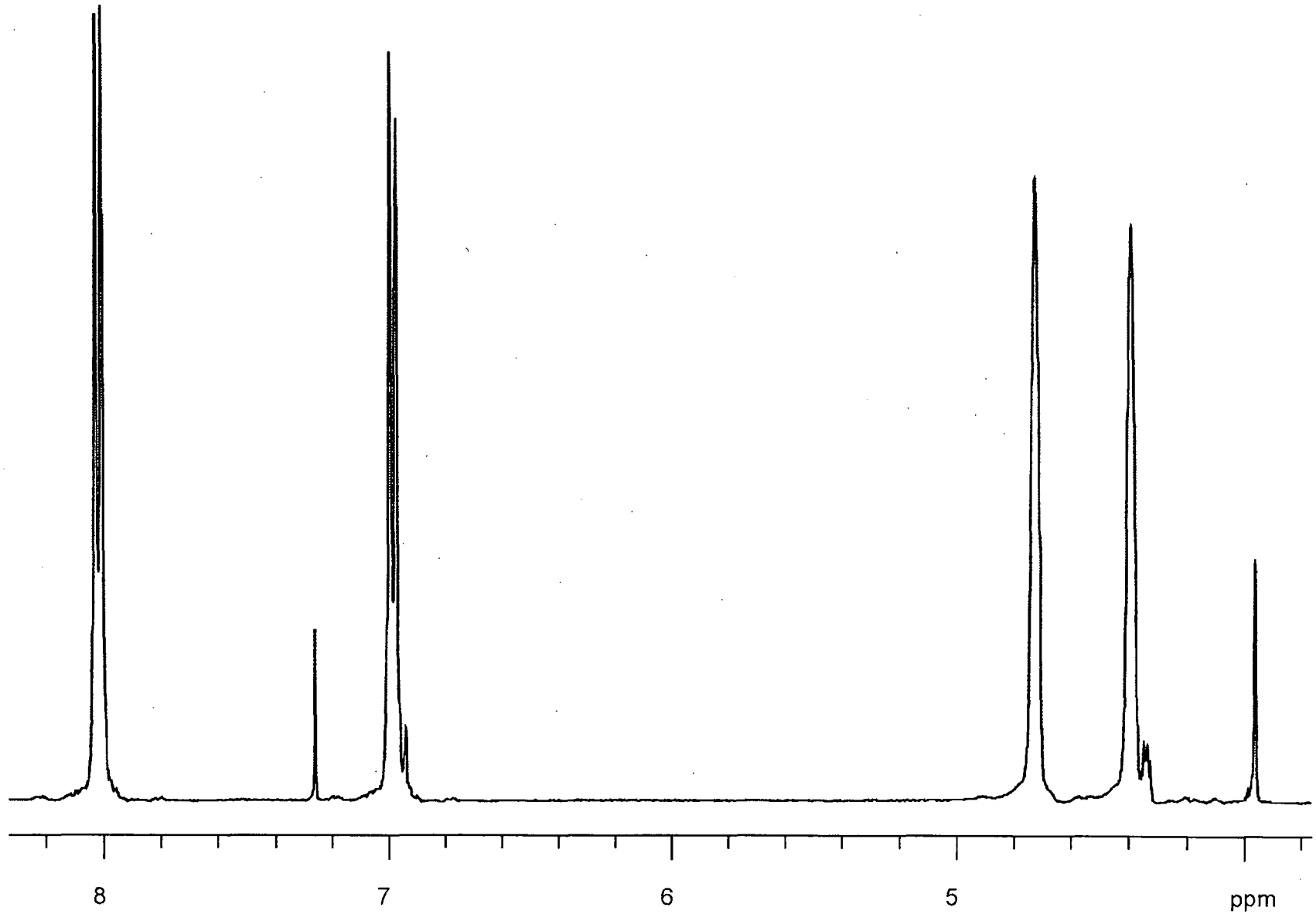

B01-2

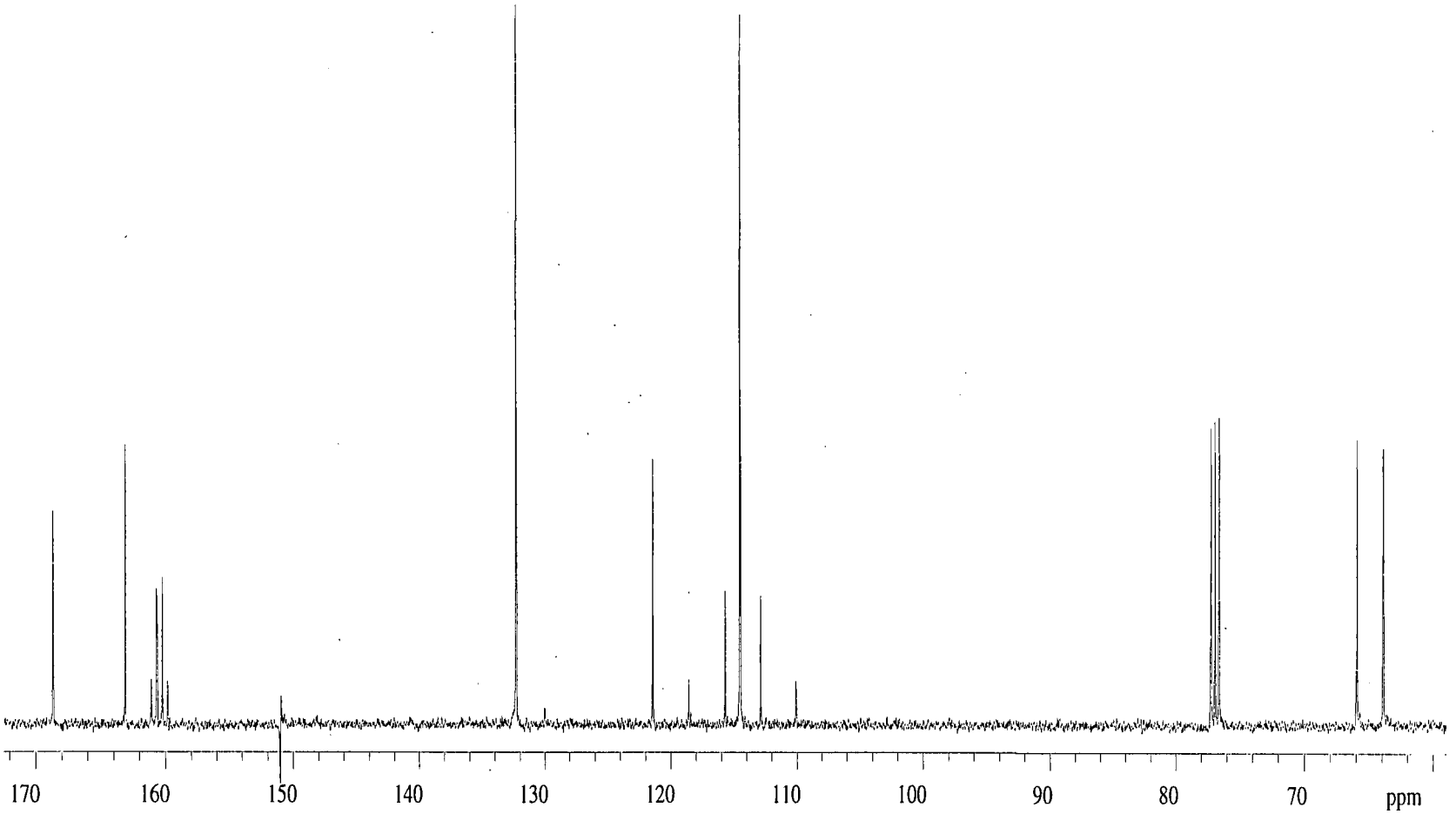

B01-4

B01-4

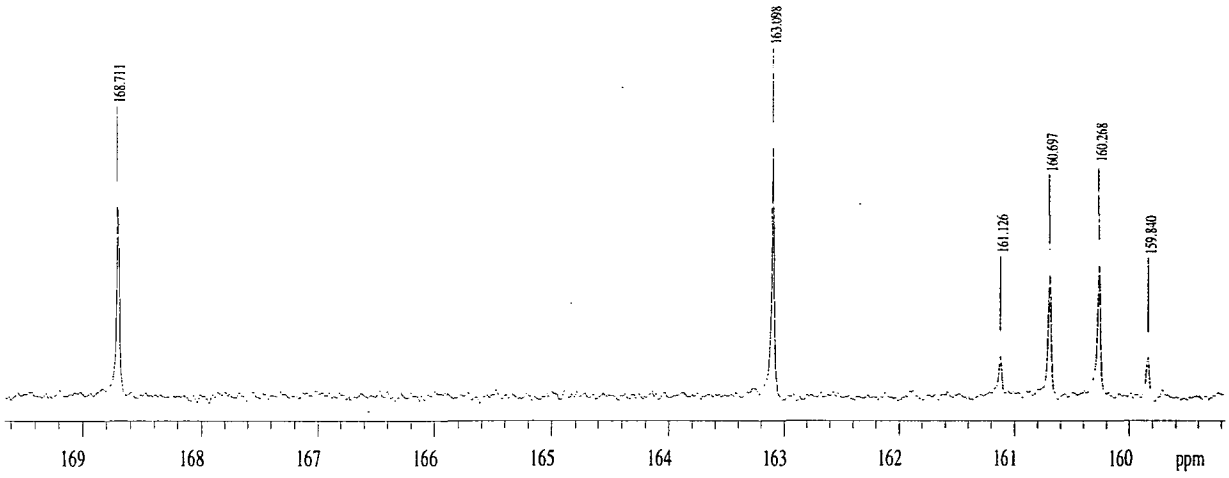
168.711
163.098
161.126
160.697
160.268
159.840
169
168
167
166
165
164
163
162
161
160
ppm

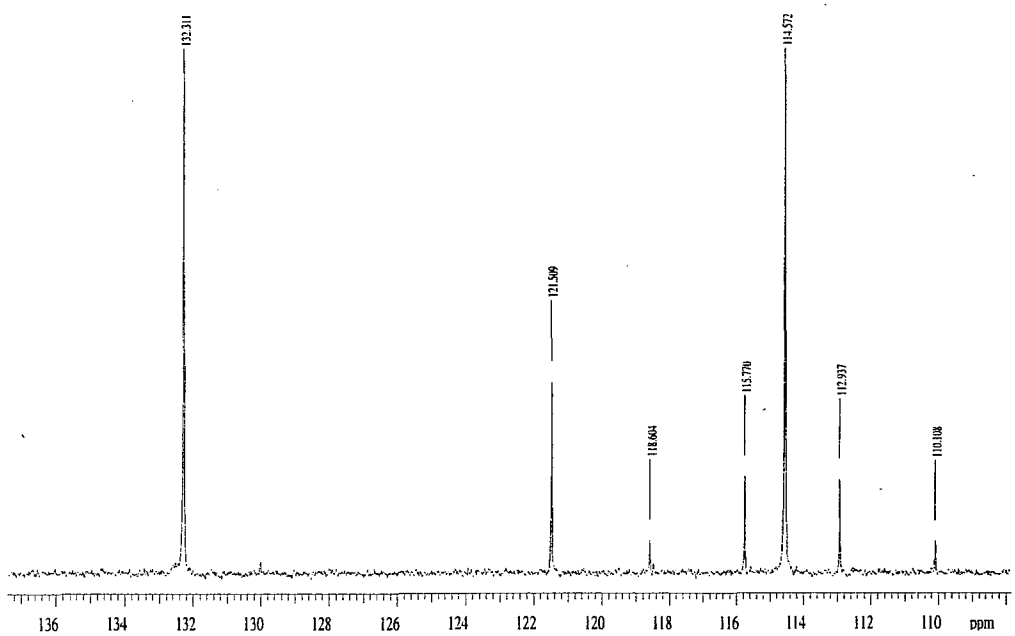
132.311
121.509
118.604
115.770
114.572
112.937
110.108
136
134
132
130
128
126
124
122
120
118
116
114
112
110
ppm

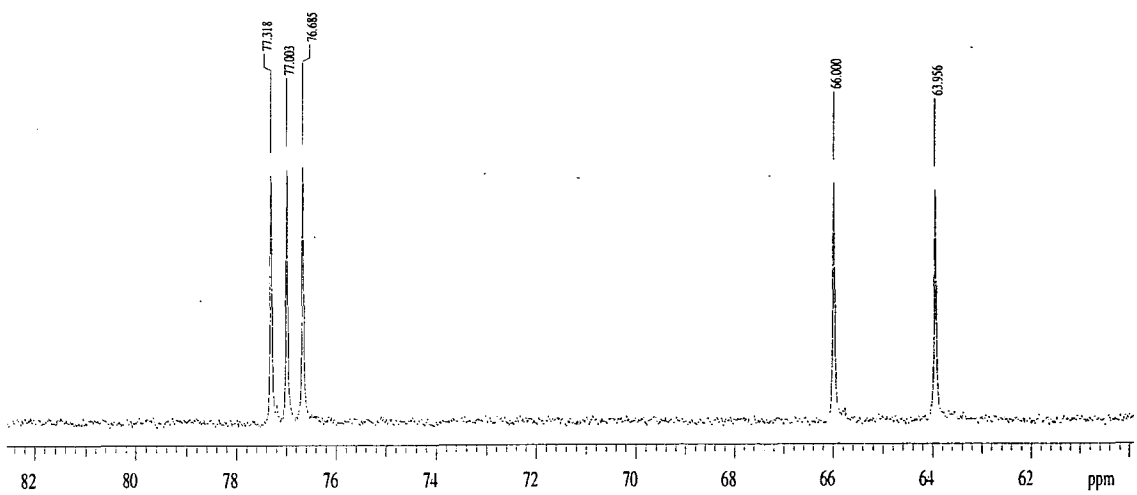
77.318
77.003
76.685
66.000
63.956
82
80
78
76
74
72
70
68
66
64
62
ppm

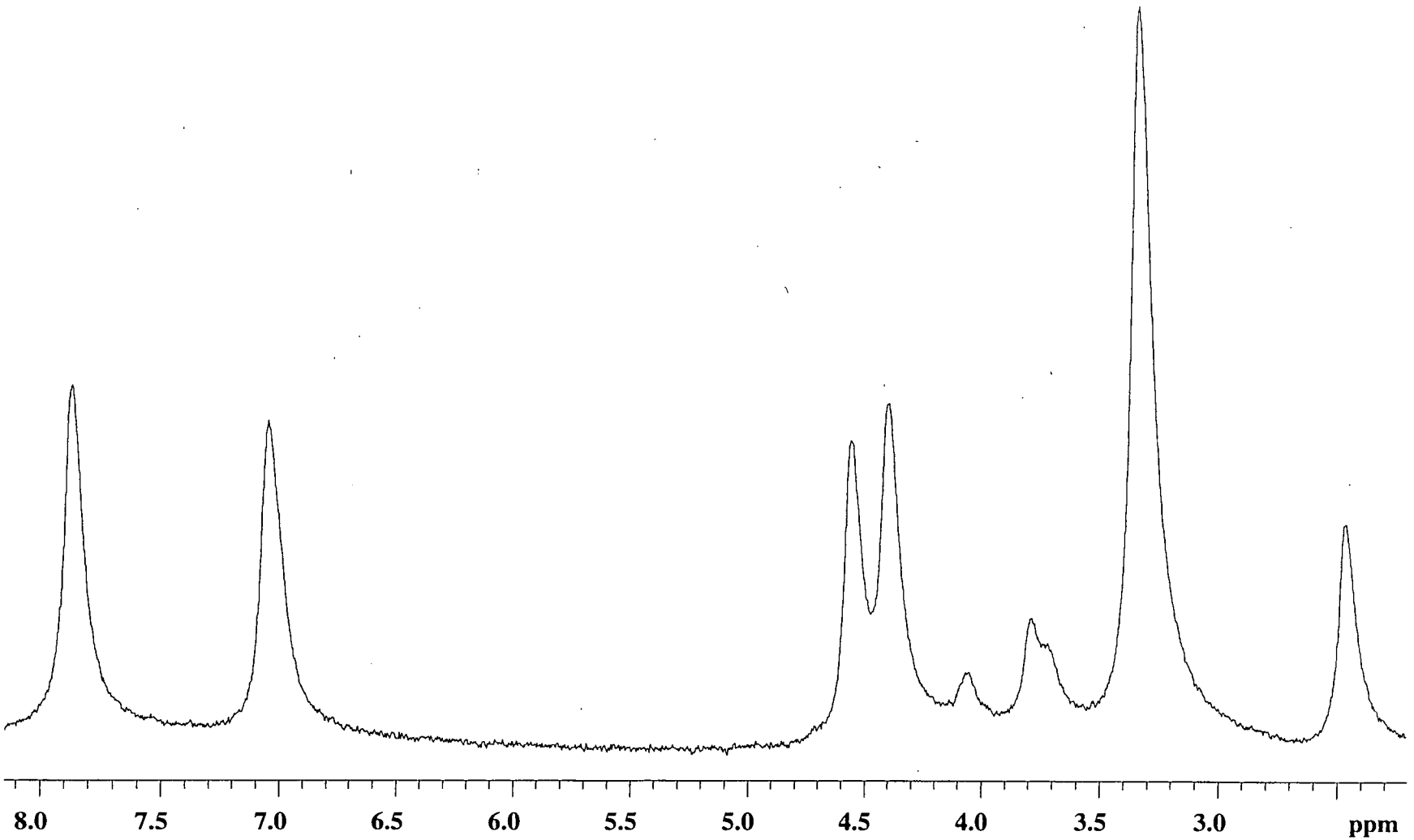

B01-6

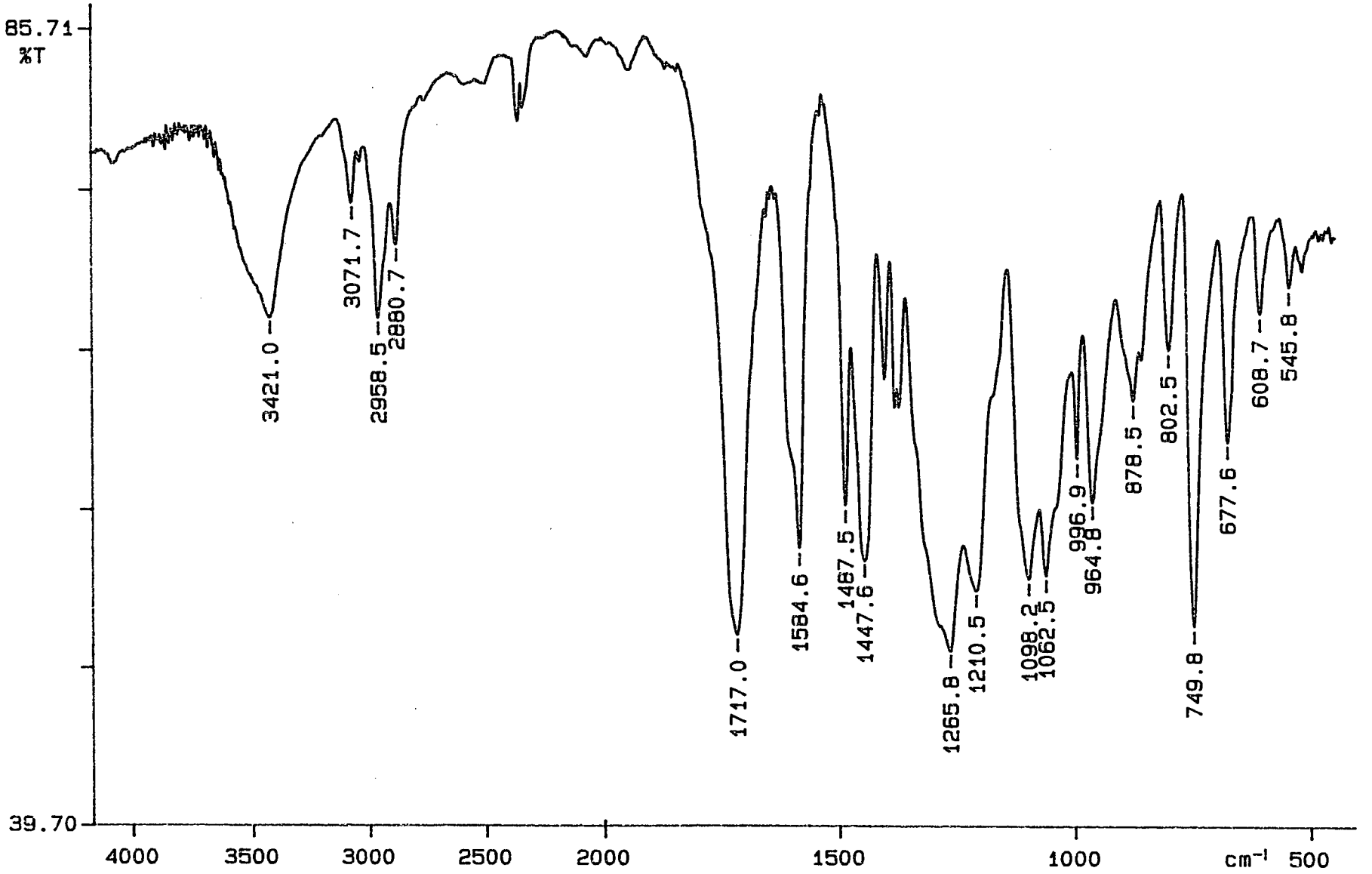

97/08/20 15:50 s-373
X: 16 scans, 4.0cm-1

B02-1

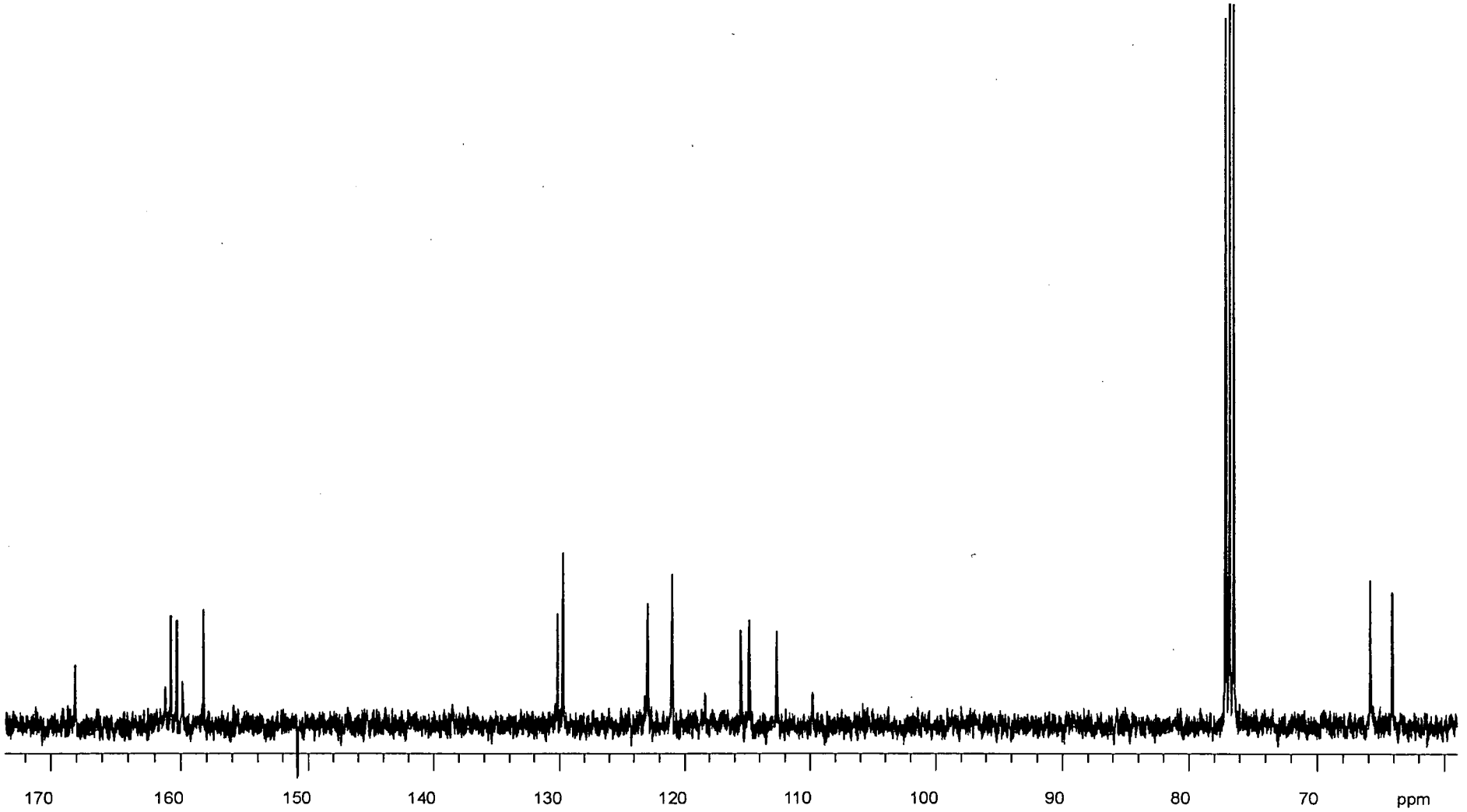

B02-4

B02-4

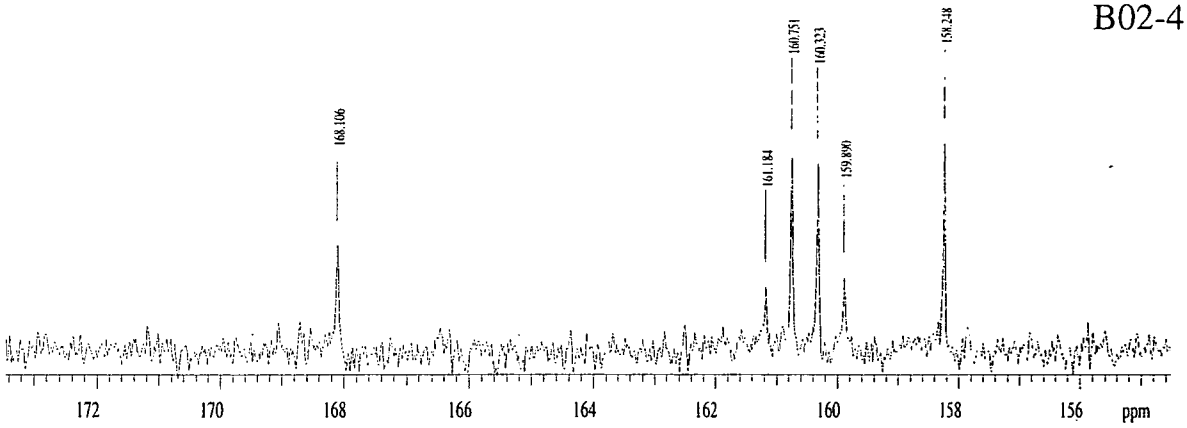
168.106
161.184
160.751
160.323
159.899
158.248
172
170
168
166
164
162
160
158
156
ppm

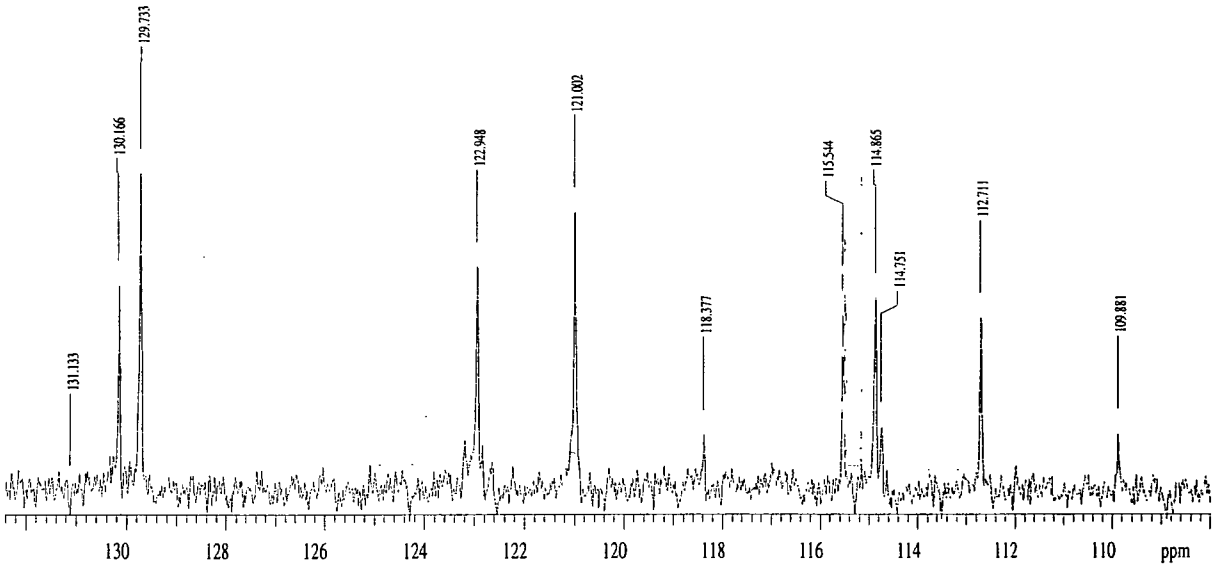
131.133
130.166
129.733
122.948
121.002
118.377
115.544
114.865
114.751
112.711
109.881
130
128
126
124
122
120
118
116
114
112
110
ppm

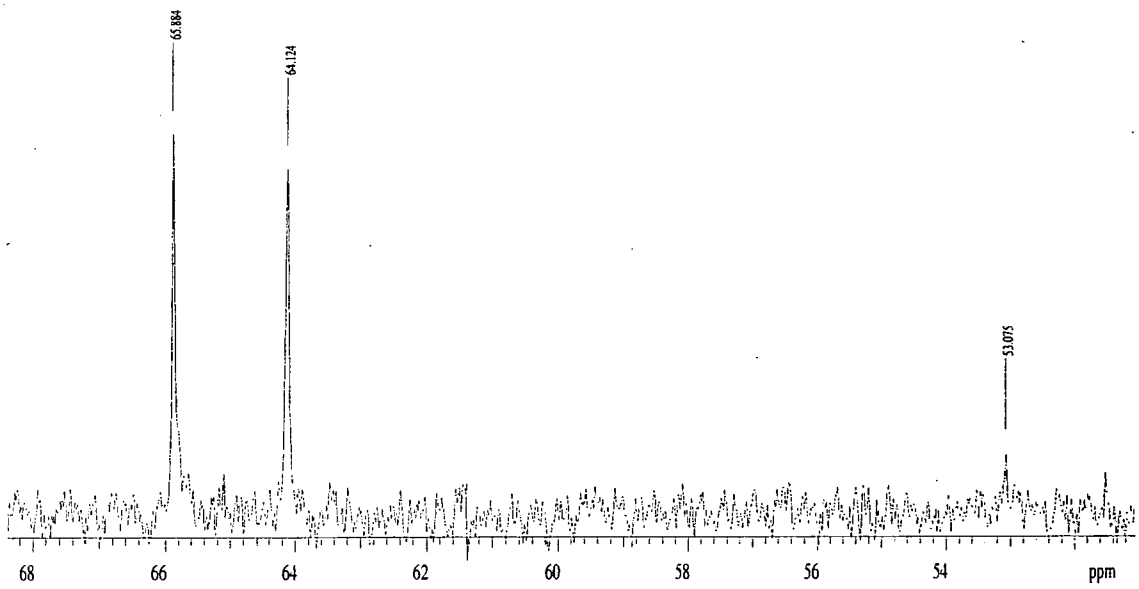
65.884
64.124
53.075
68
66
64
62
60
58
56
54
ppm

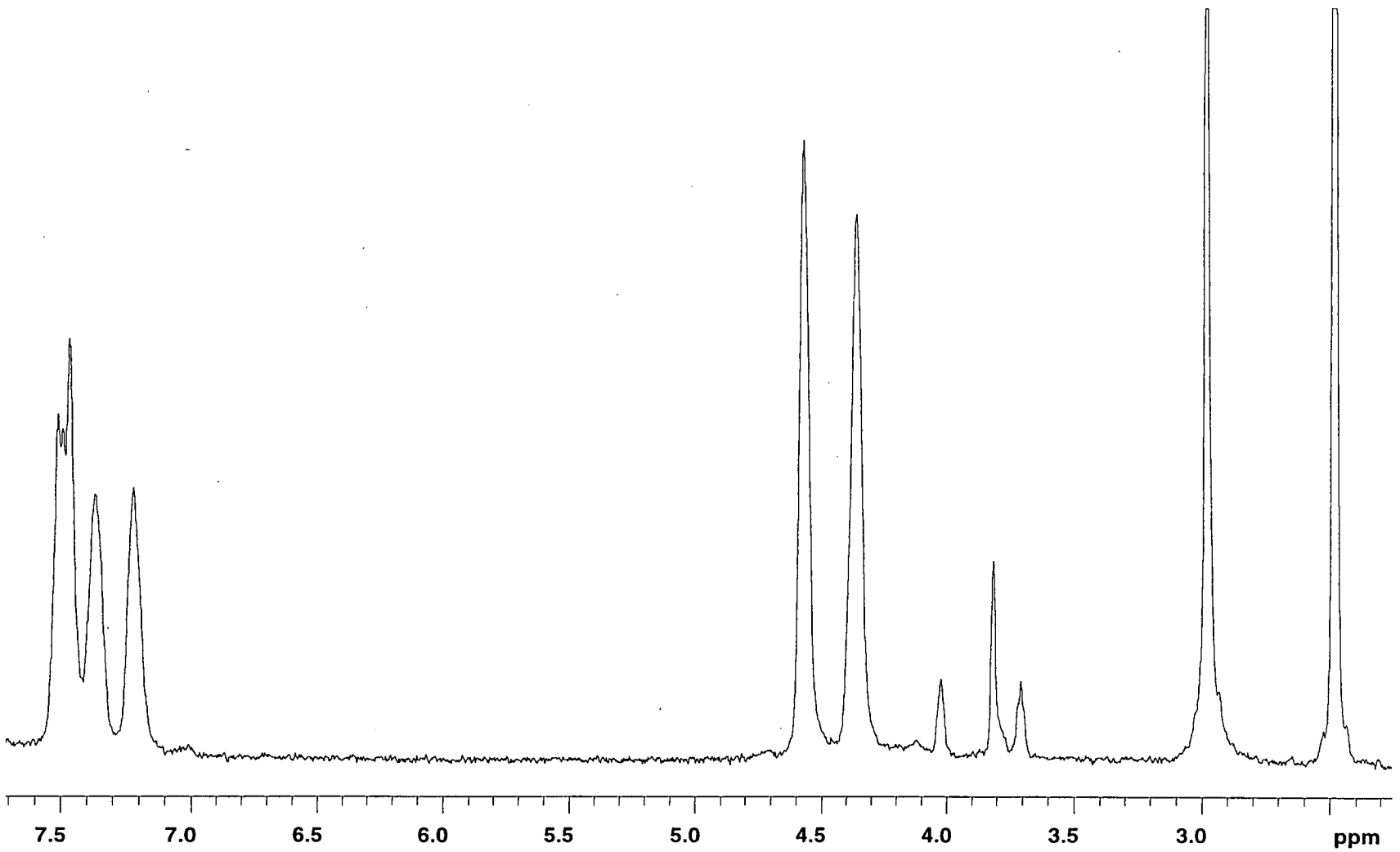

B02-6

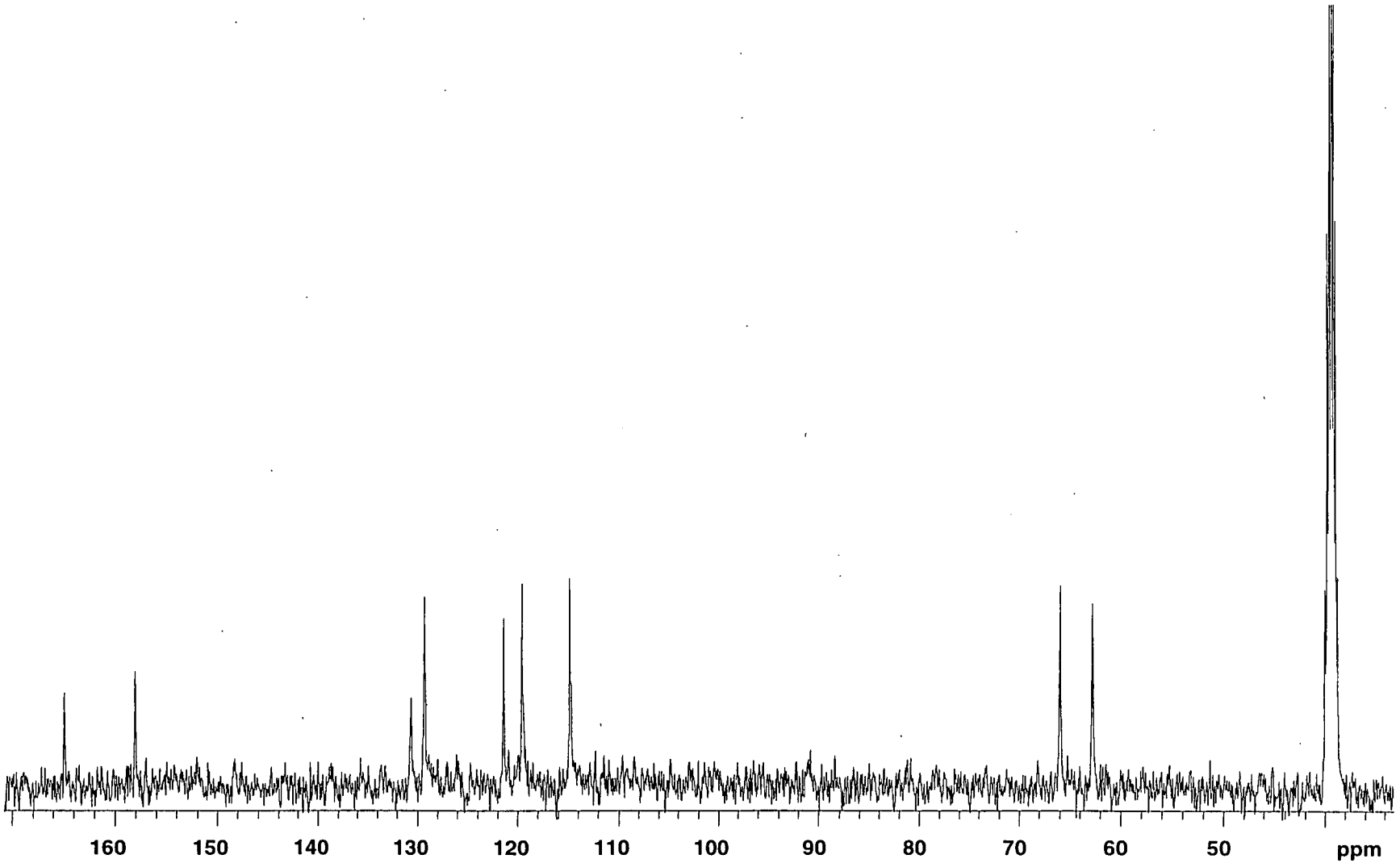

B02-7

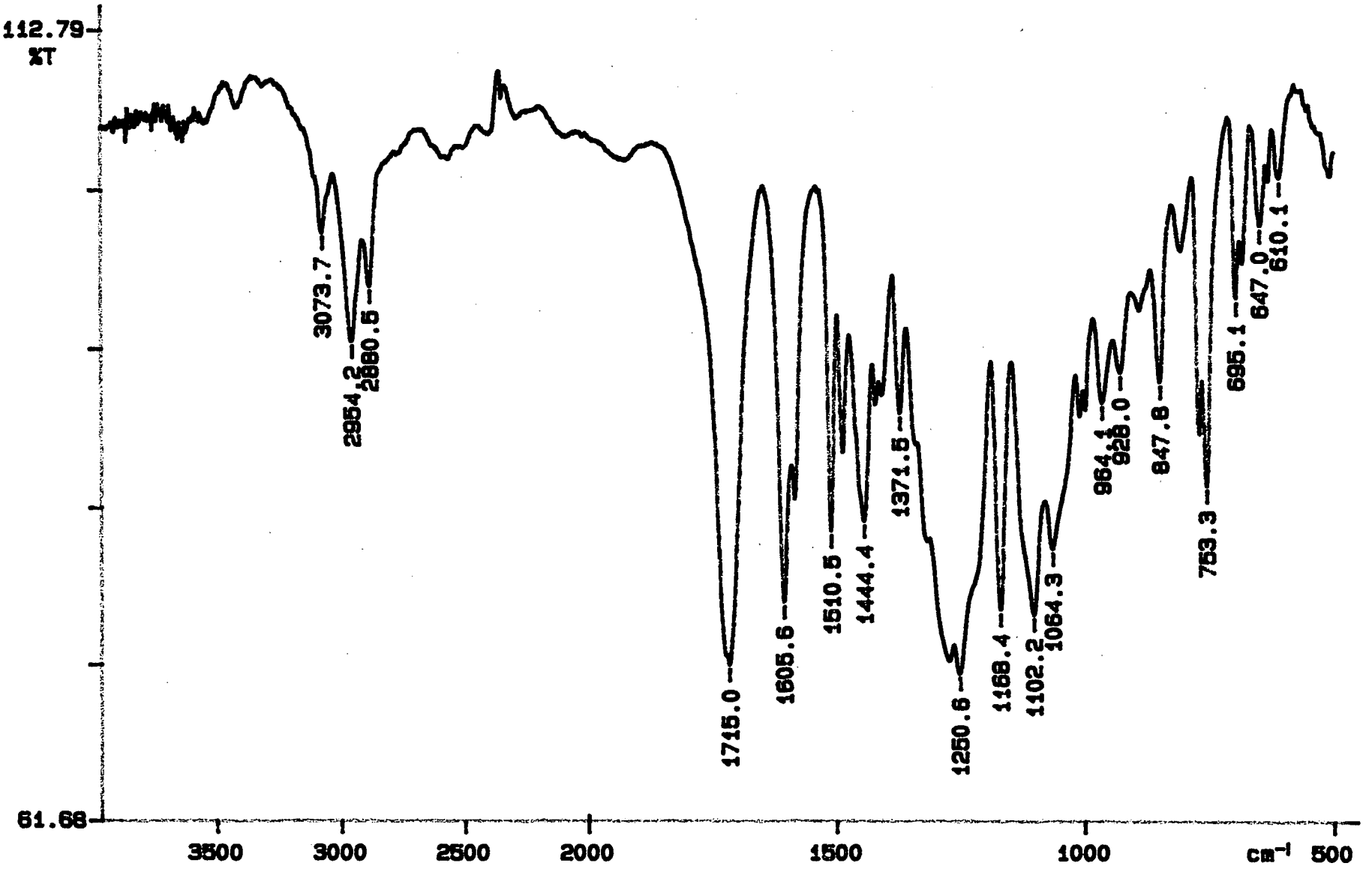

99/05/31 17:45 s-373
Z: 16 scans, 4.0cm-1, diff, flat

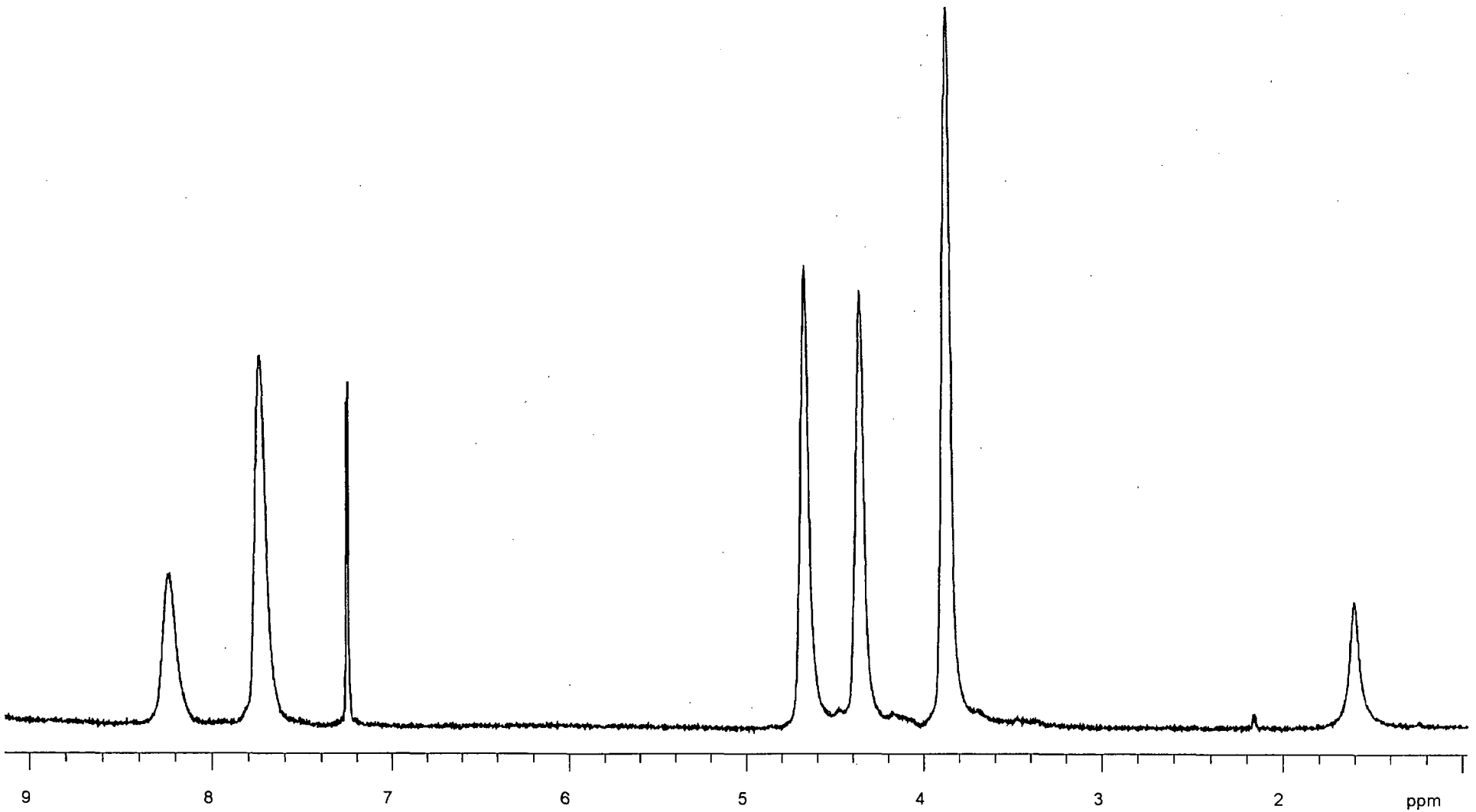

B03-2

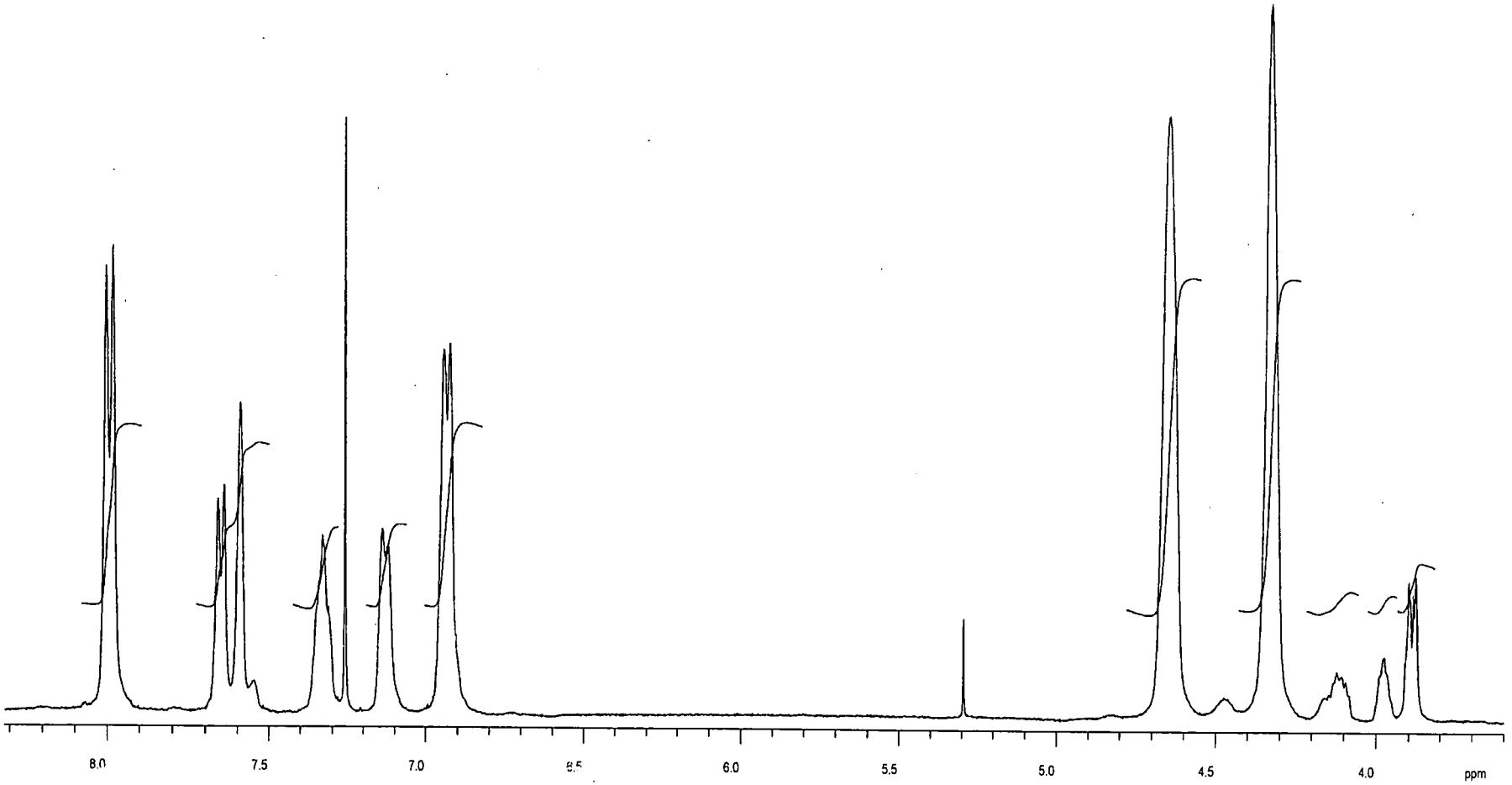

B03-3

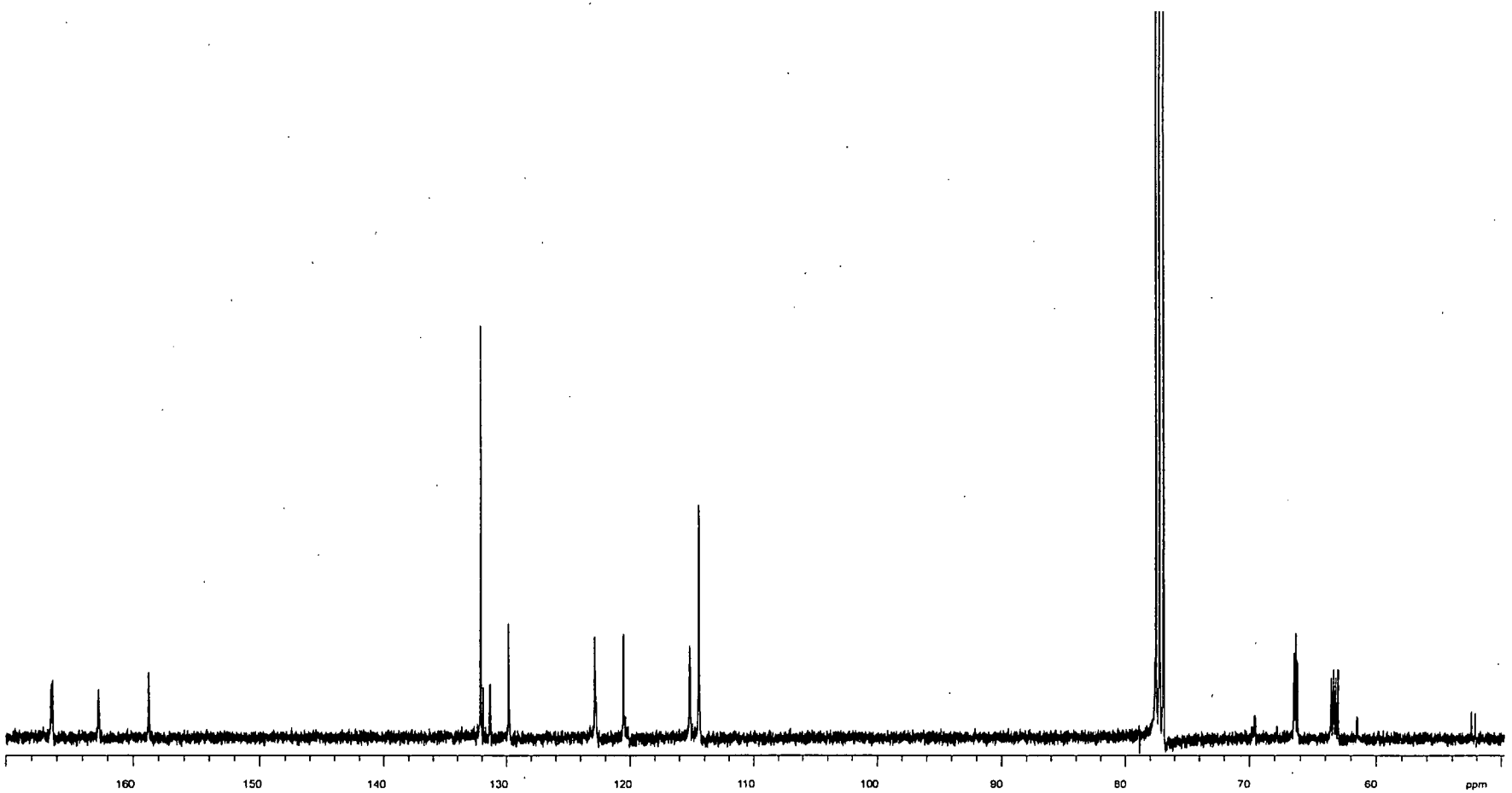

B03-5

B03-5

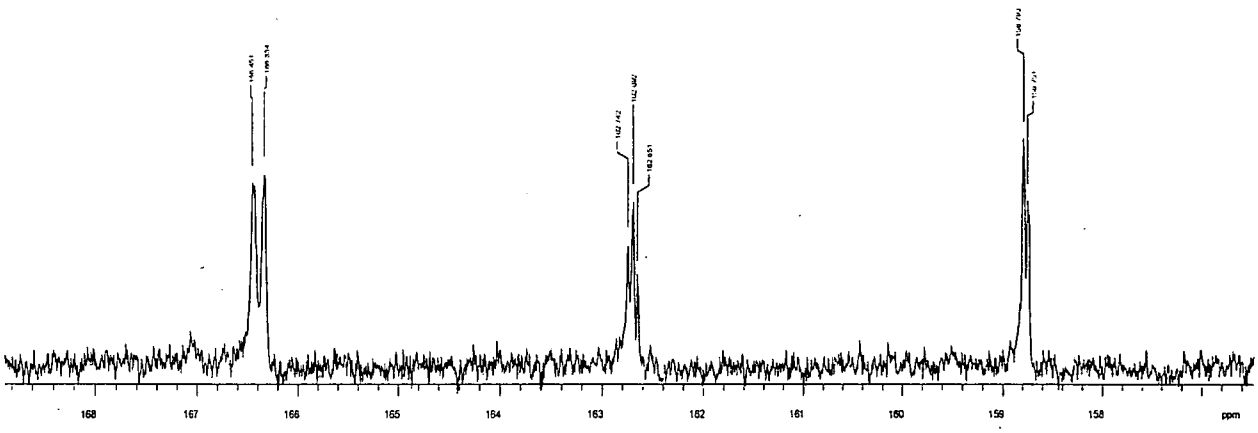
168
167
166
165
164
163
162
161
160
159
158
ppm

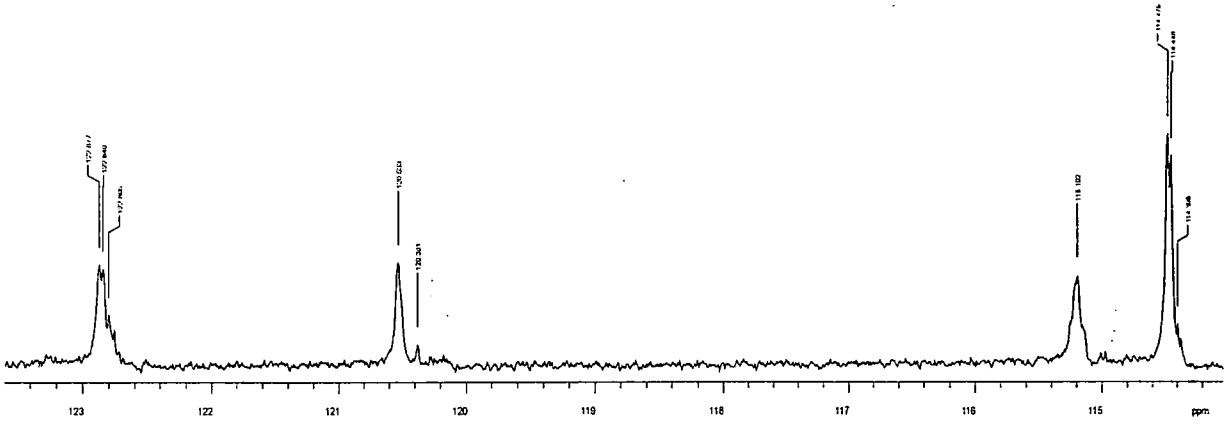
123
122
121
120
119
118
117
116
115
ppm

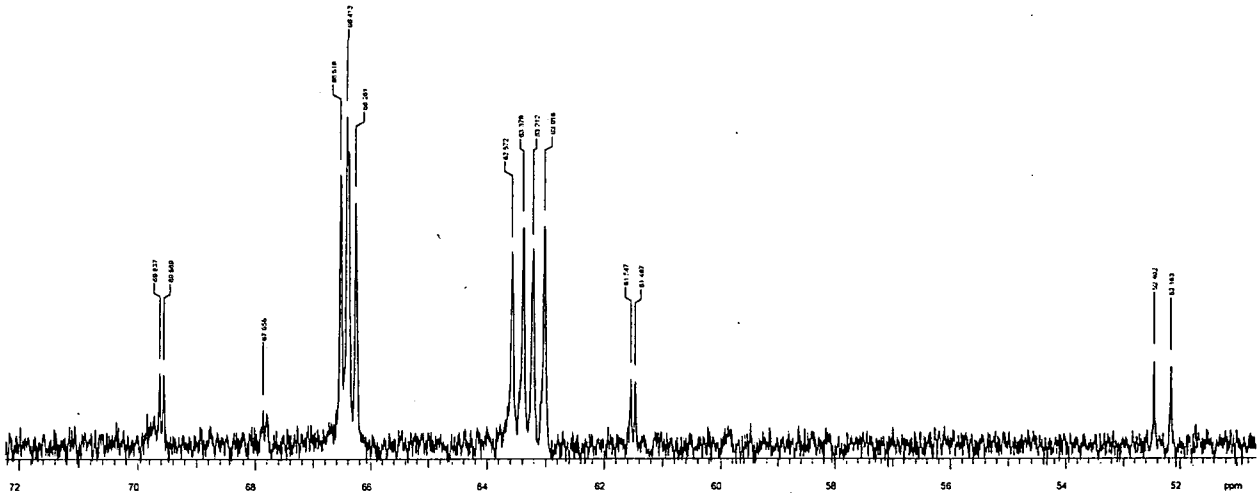
72
70
68
66
64
62
60
58
56
54
52
ppm

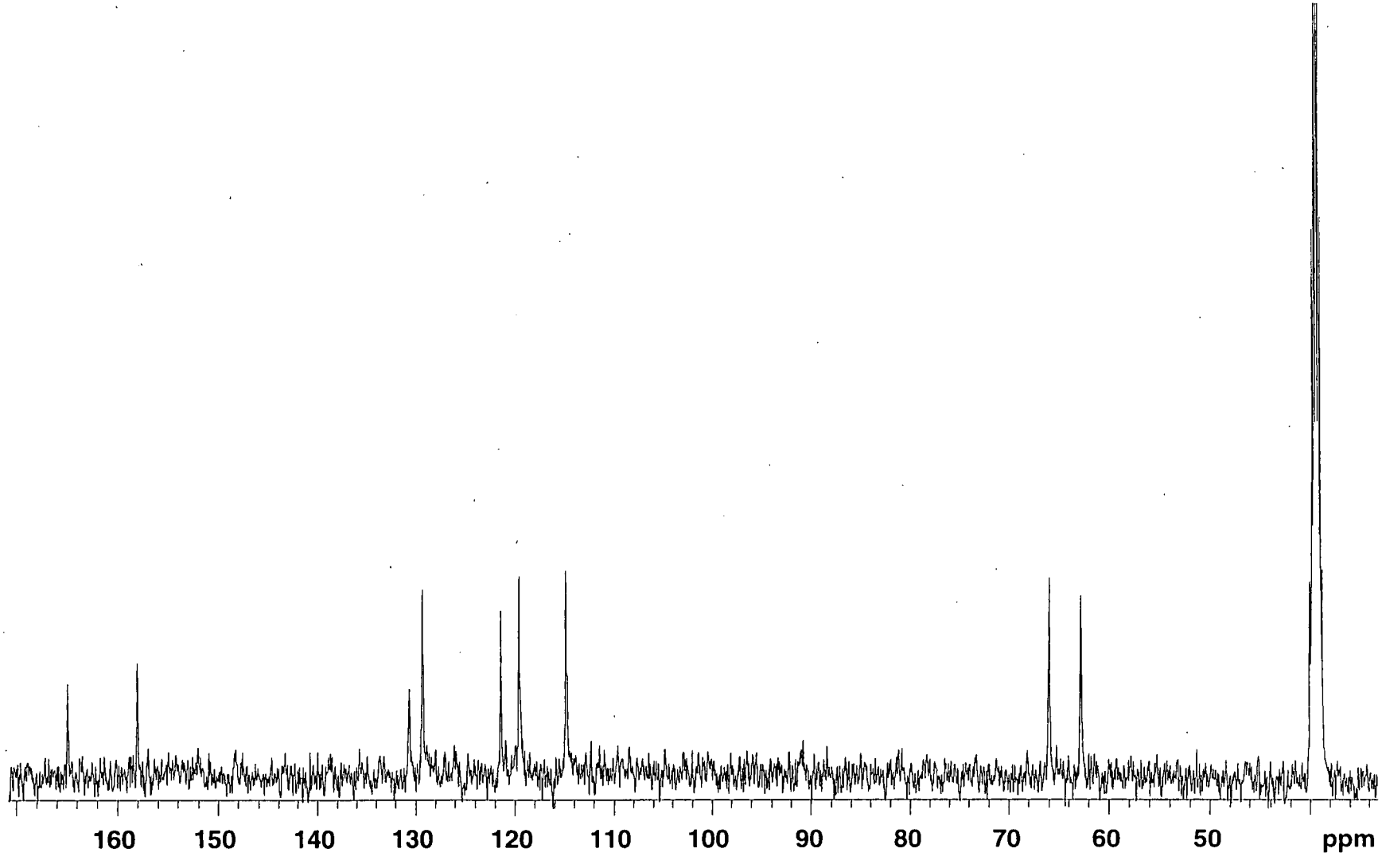
160
150
140
130
120
110
100
90
80
70
60
50
ppm

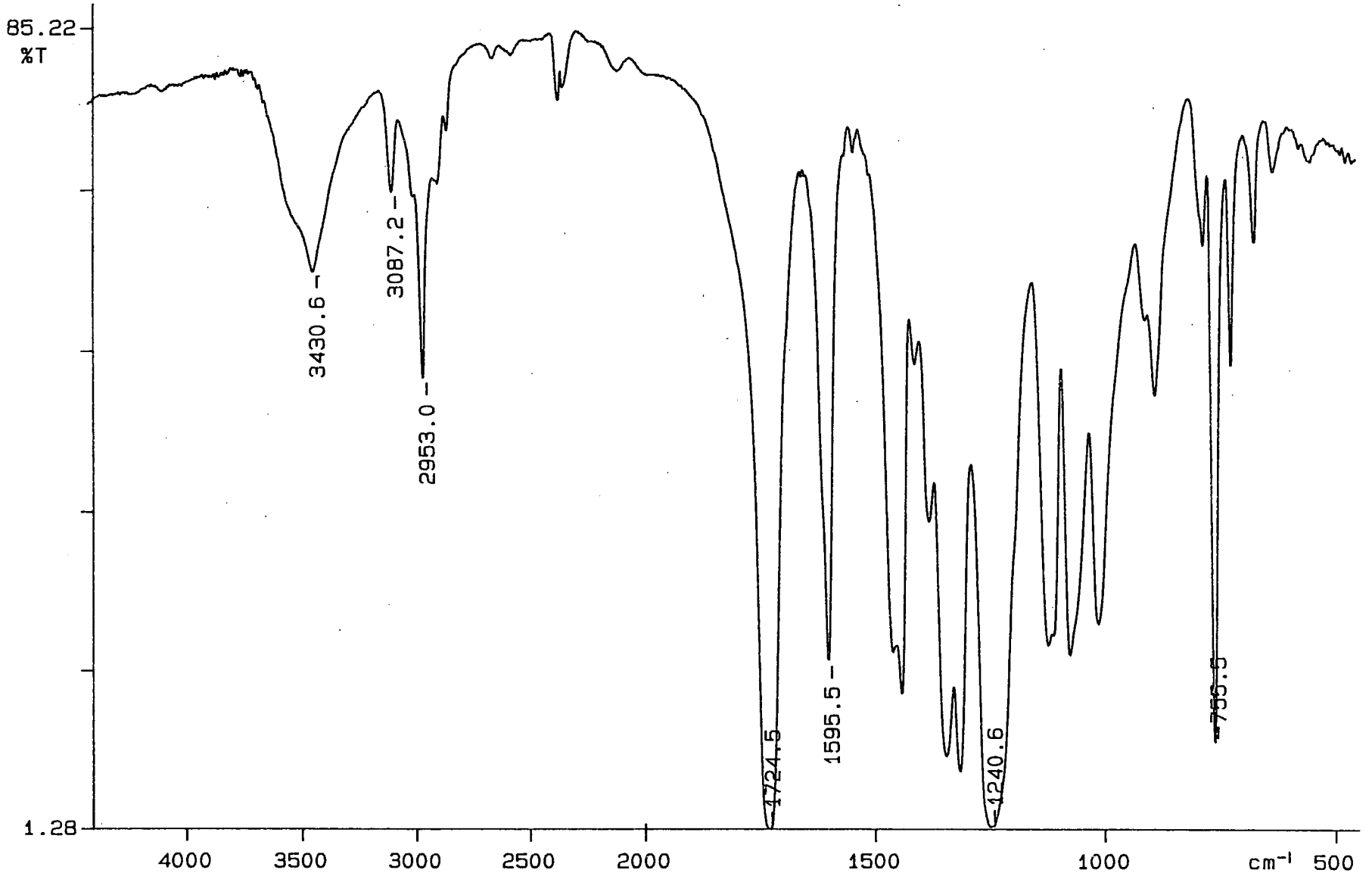
85.22
%T
3430.6
3087.2
2953.0
1724.5
1595.5
1240.6
755.5
1.28
4000
3500
3000
2500
2000
1500
1000
cm-1
500

B04-1

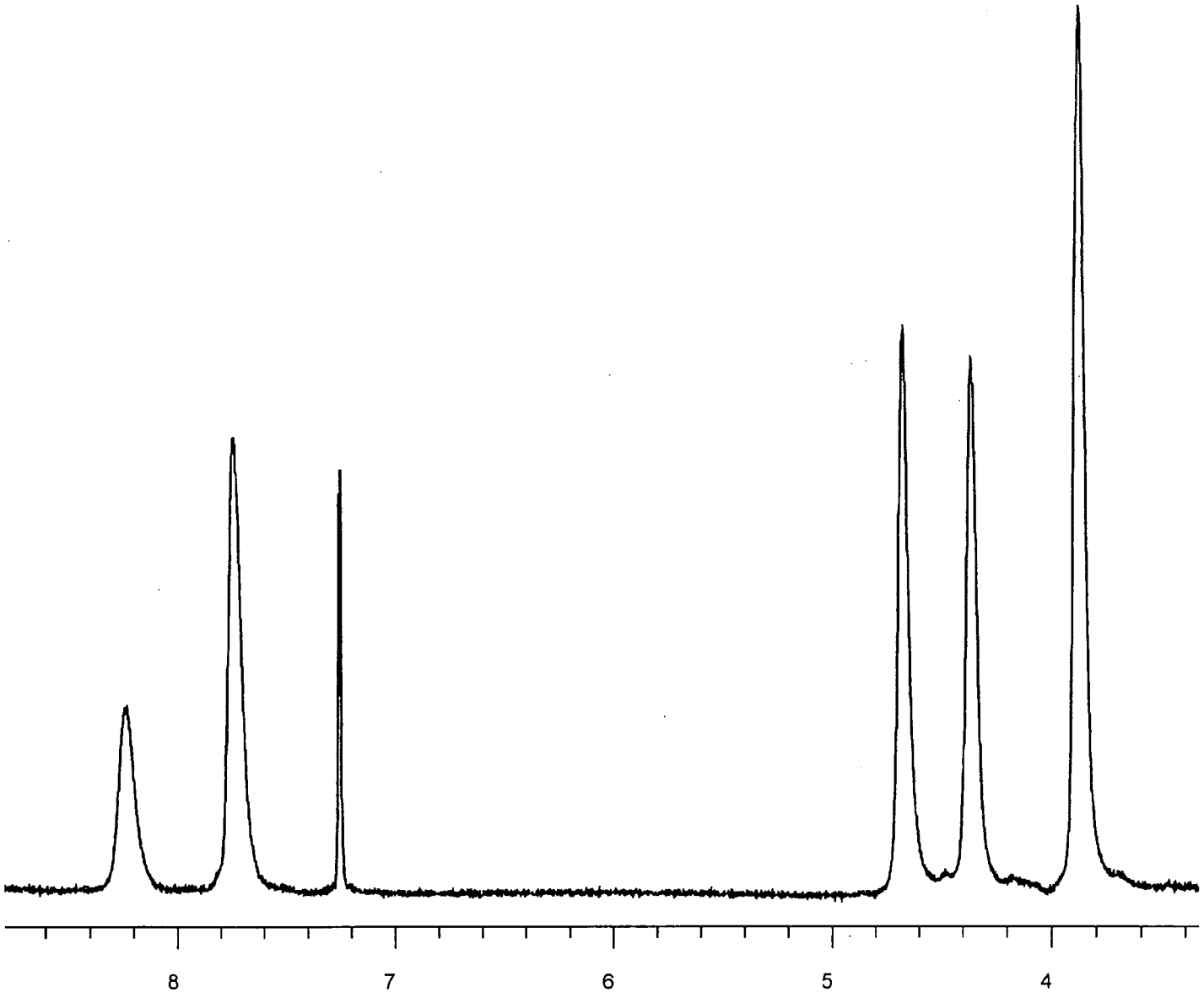

B04-2

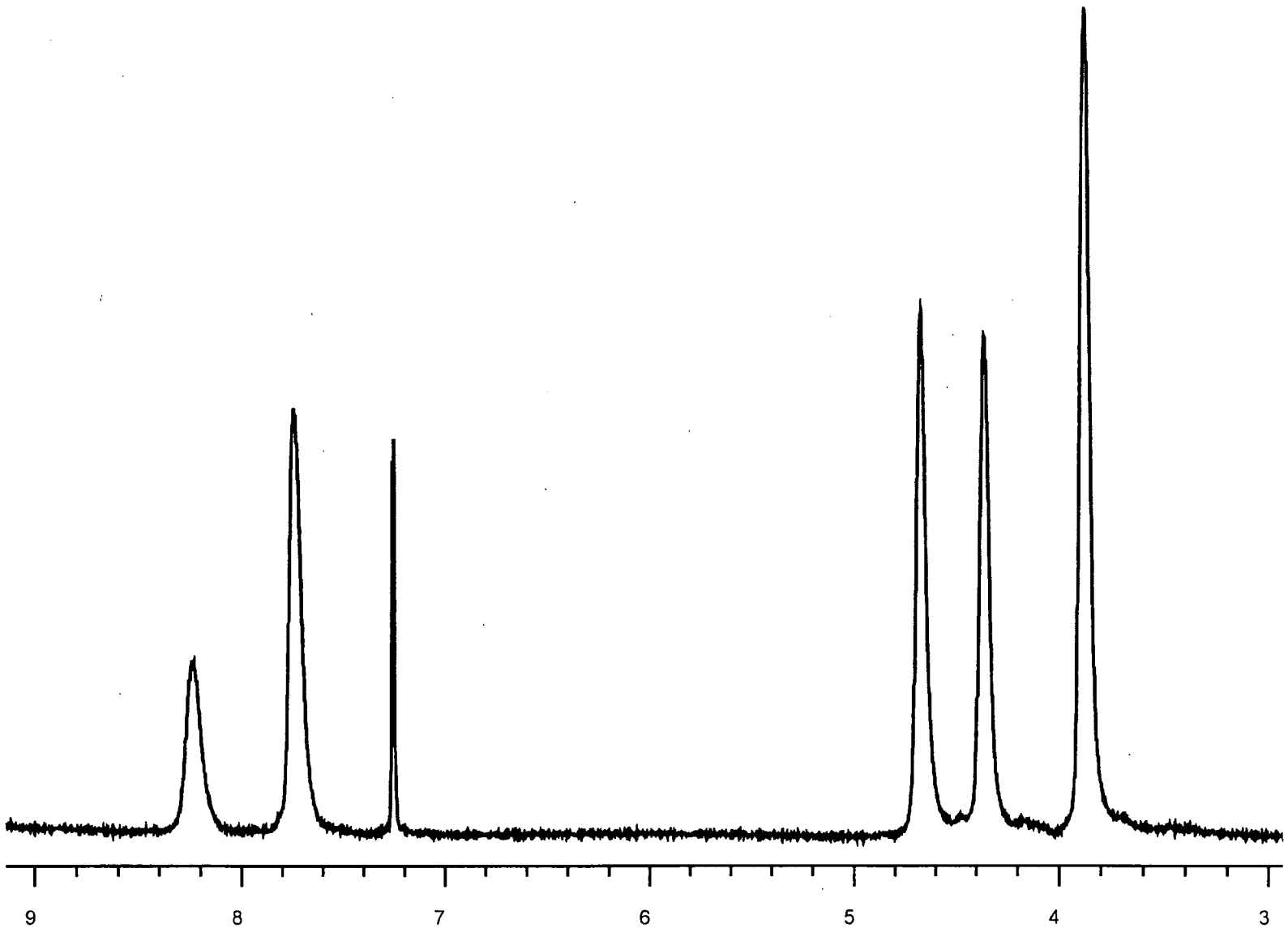

B04-3

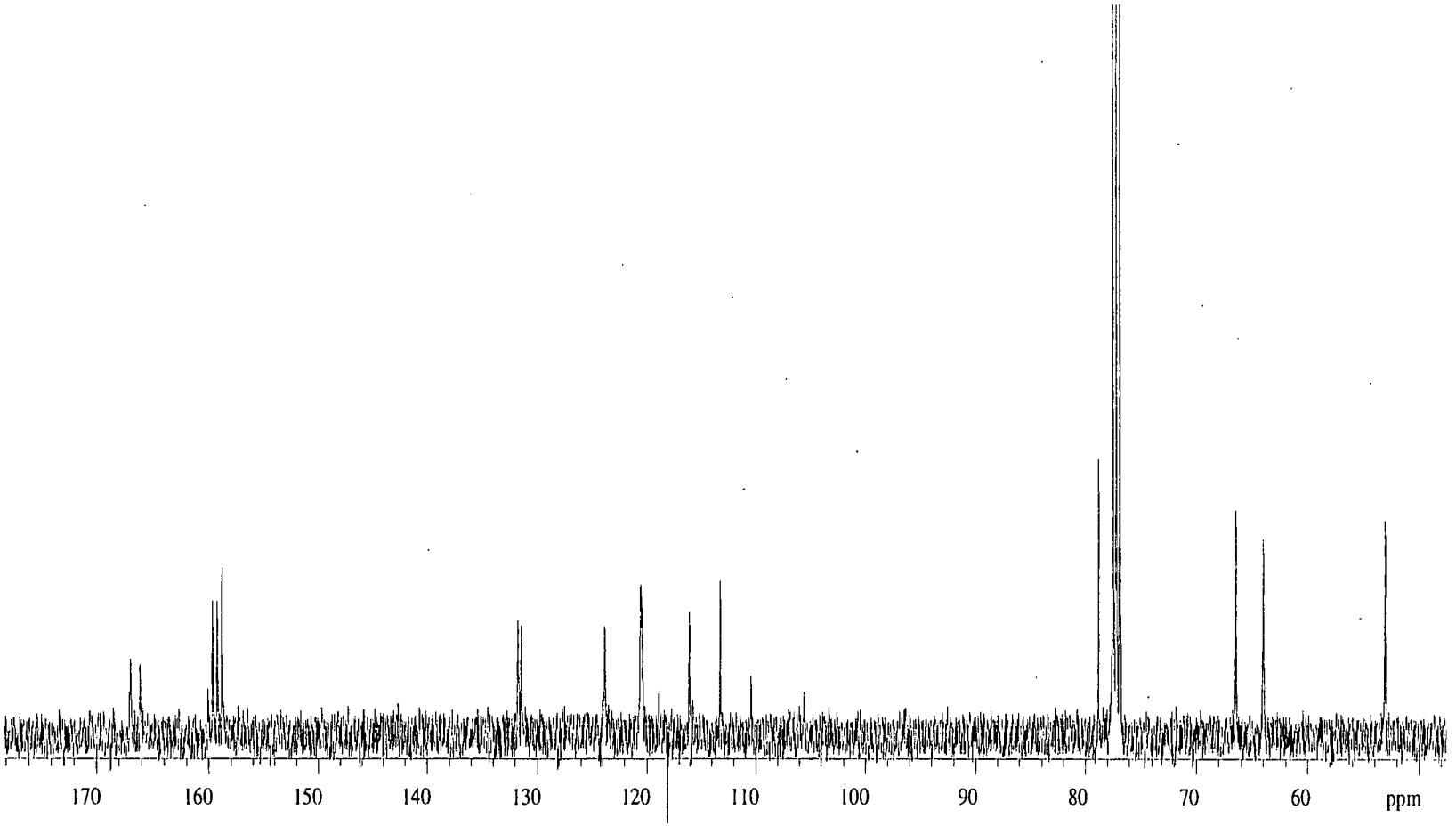

B04-4

B04-4

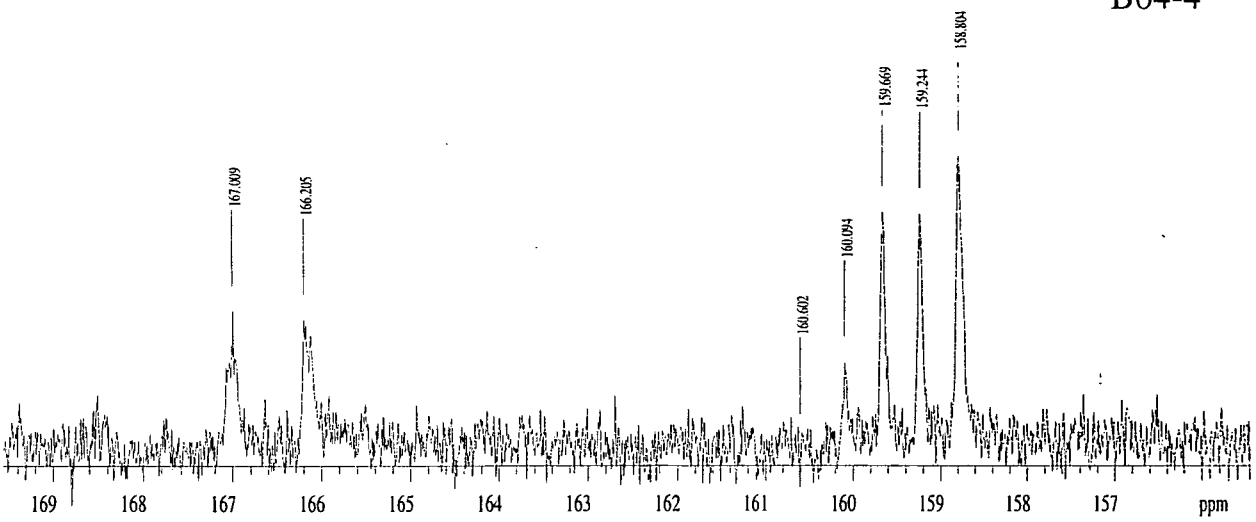
167.009
166.205
160.602
160.094
159.669
159.244
158.804
169
168
167
166
165
164
163
162
161
160
159
158
157
ppm

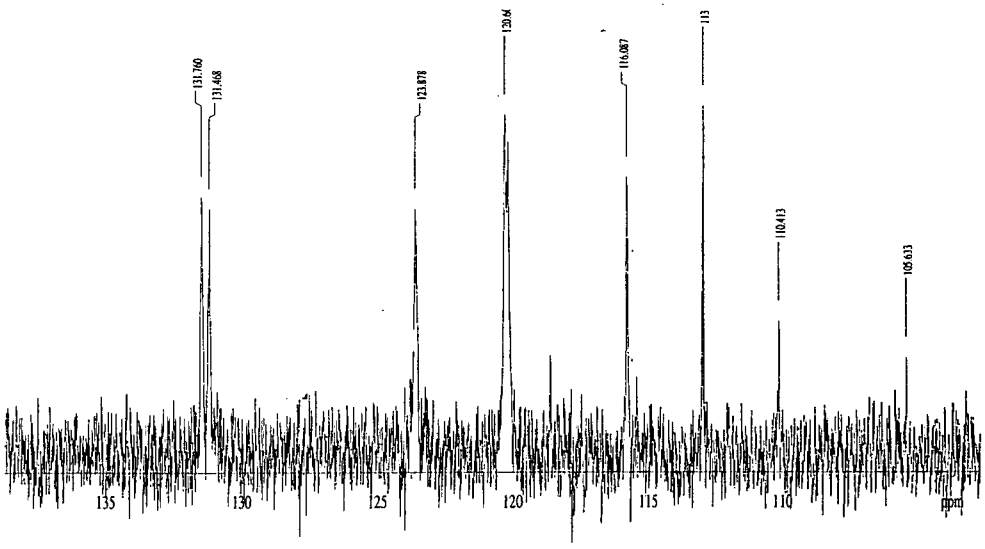
131.760
131.468
123.878
120.164
116.087
113
110.413
105.633
135
130
125
120
115
110
ppm

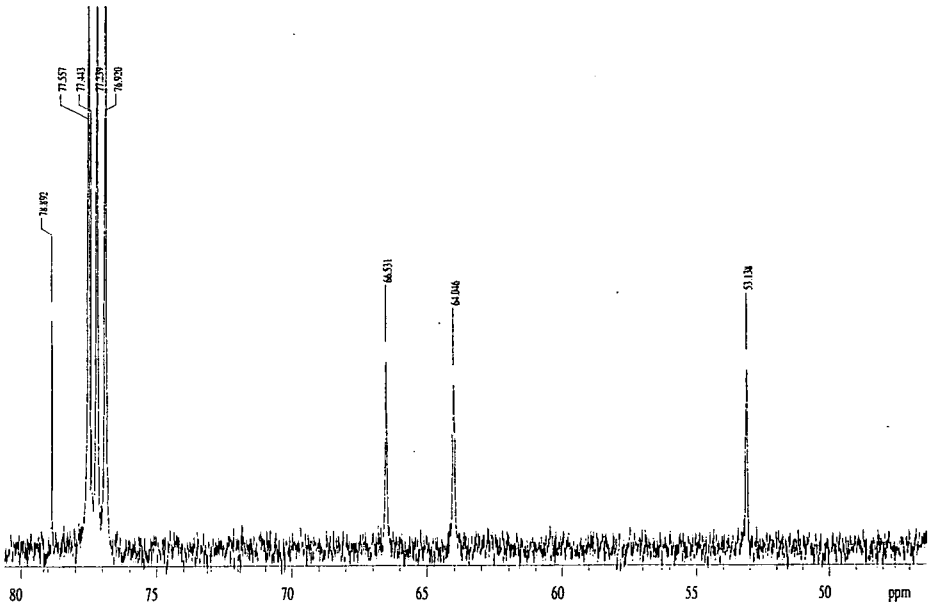
77.557
77.443
77.239
76.920
74.892
66.531
64.046
53.134
80
75
70
65
60
55
50
ppm

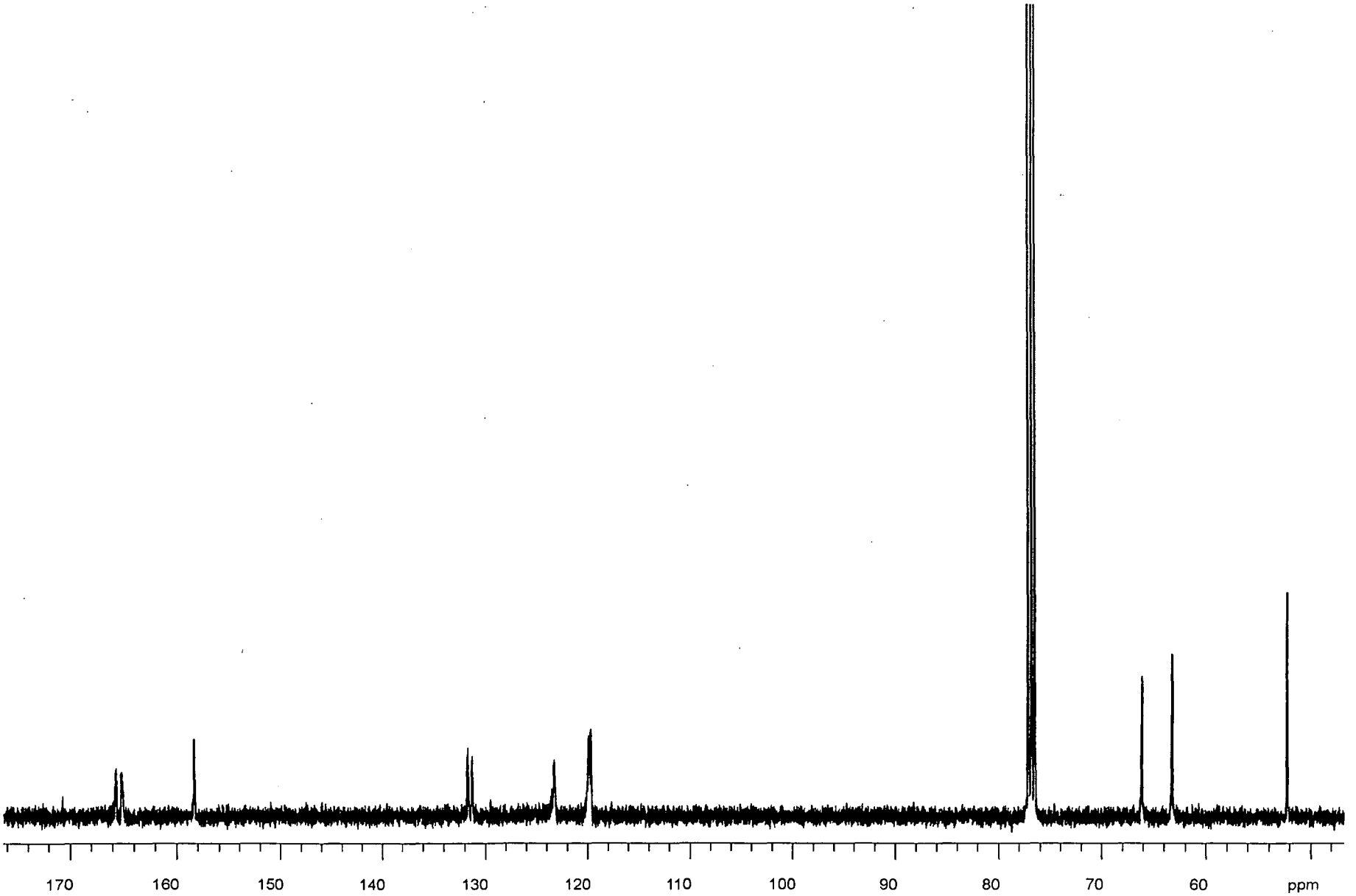

B04-5

B04-5

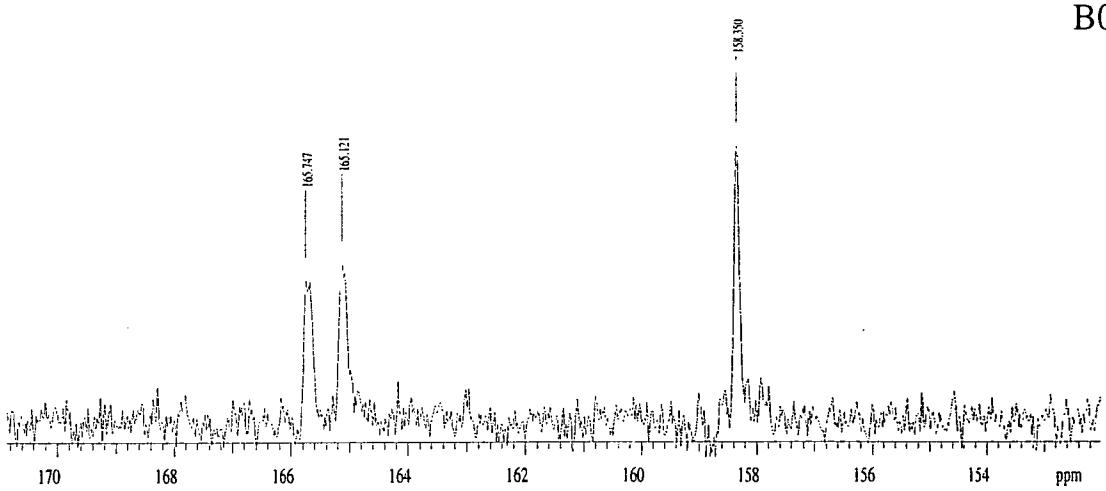
165.747
165.121
158.350
170
168
166
164
162
160
158
156
154
ppm

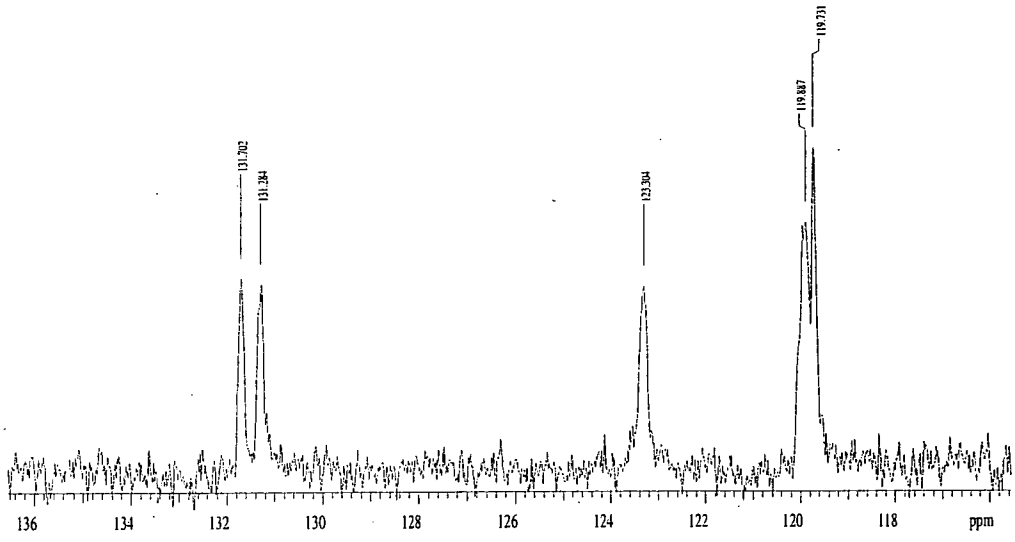
131.702
131.284
123.304
119.887
119.731
136
134
132
130
128
126
124
122
120
118
ppm

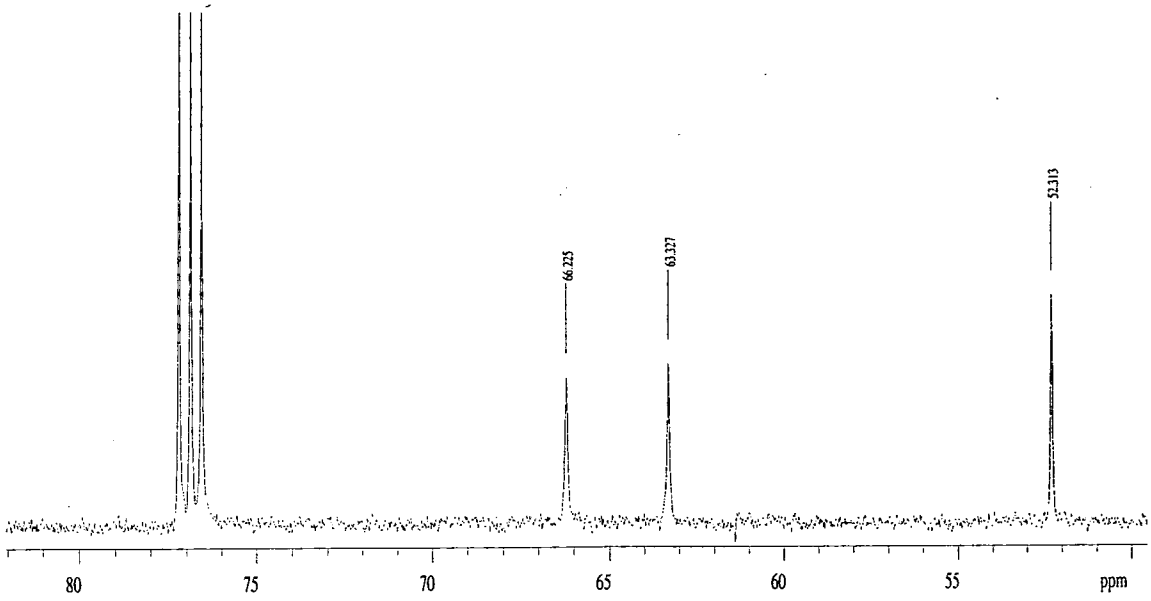
66.225
63.327
52.313
80
75
70
65
60
55
ppm

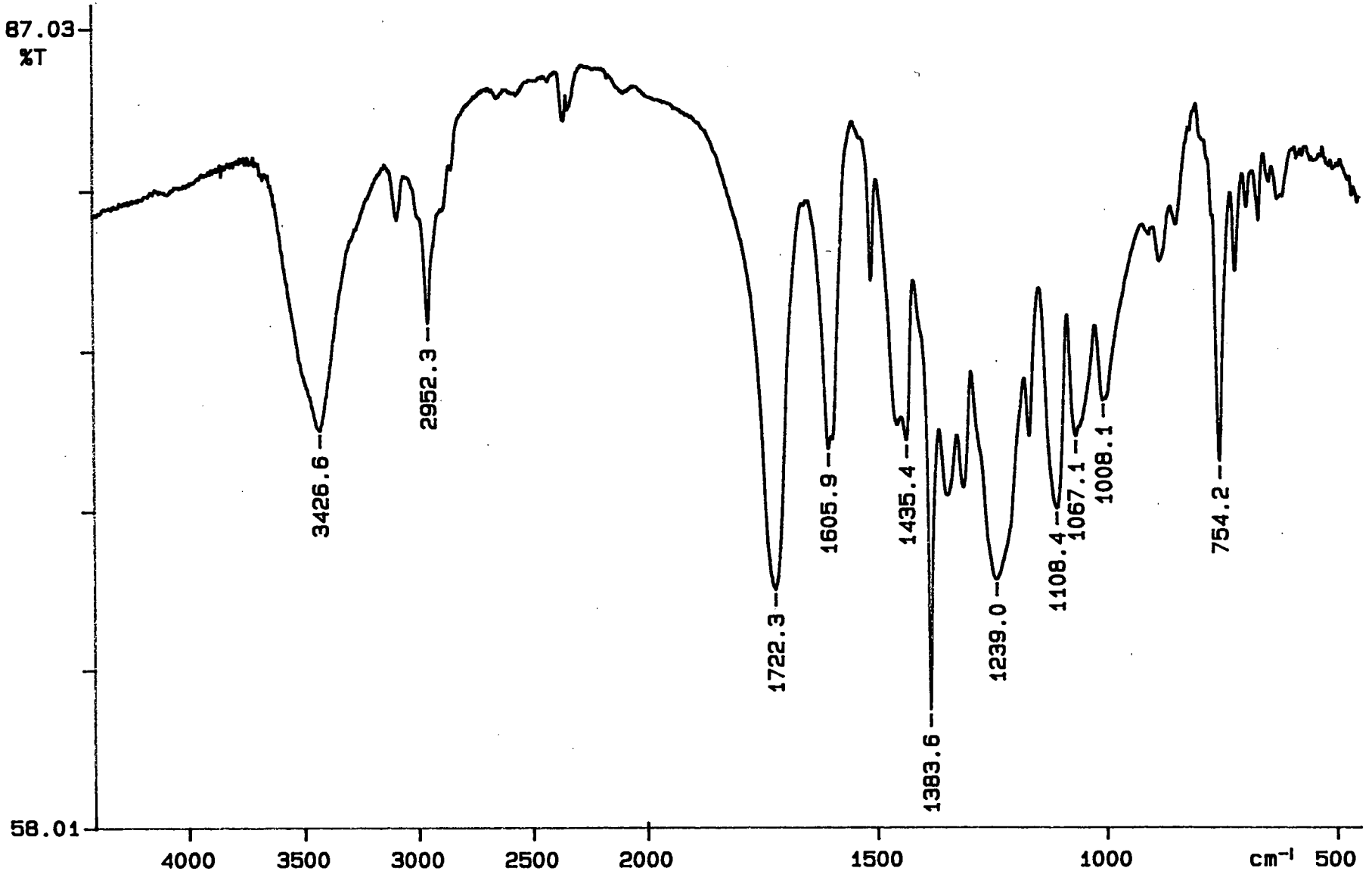

98/03/13 12:03 s-373
X: 16 scans, 4.0cm-1

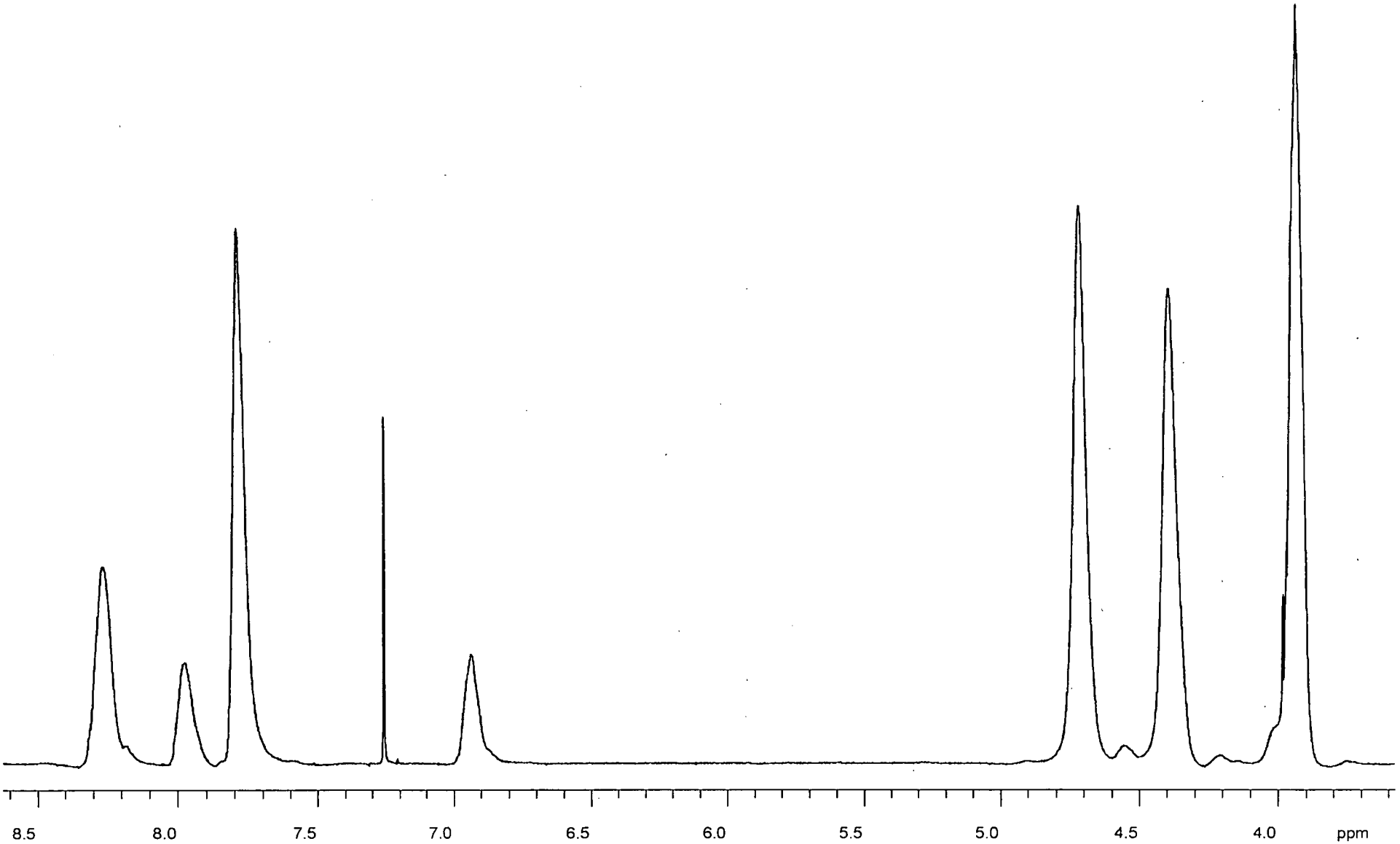

B05-2

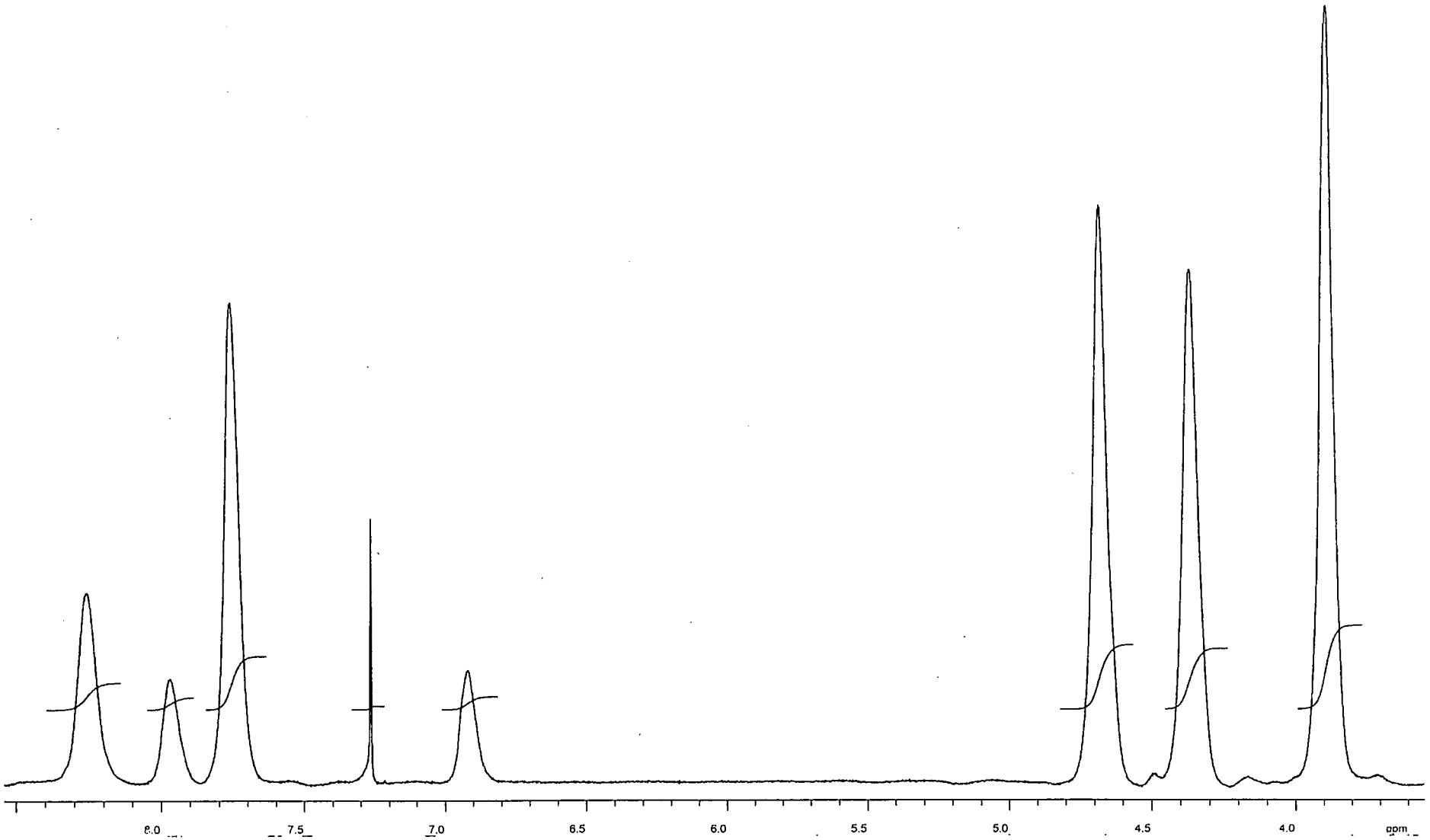

B05-3

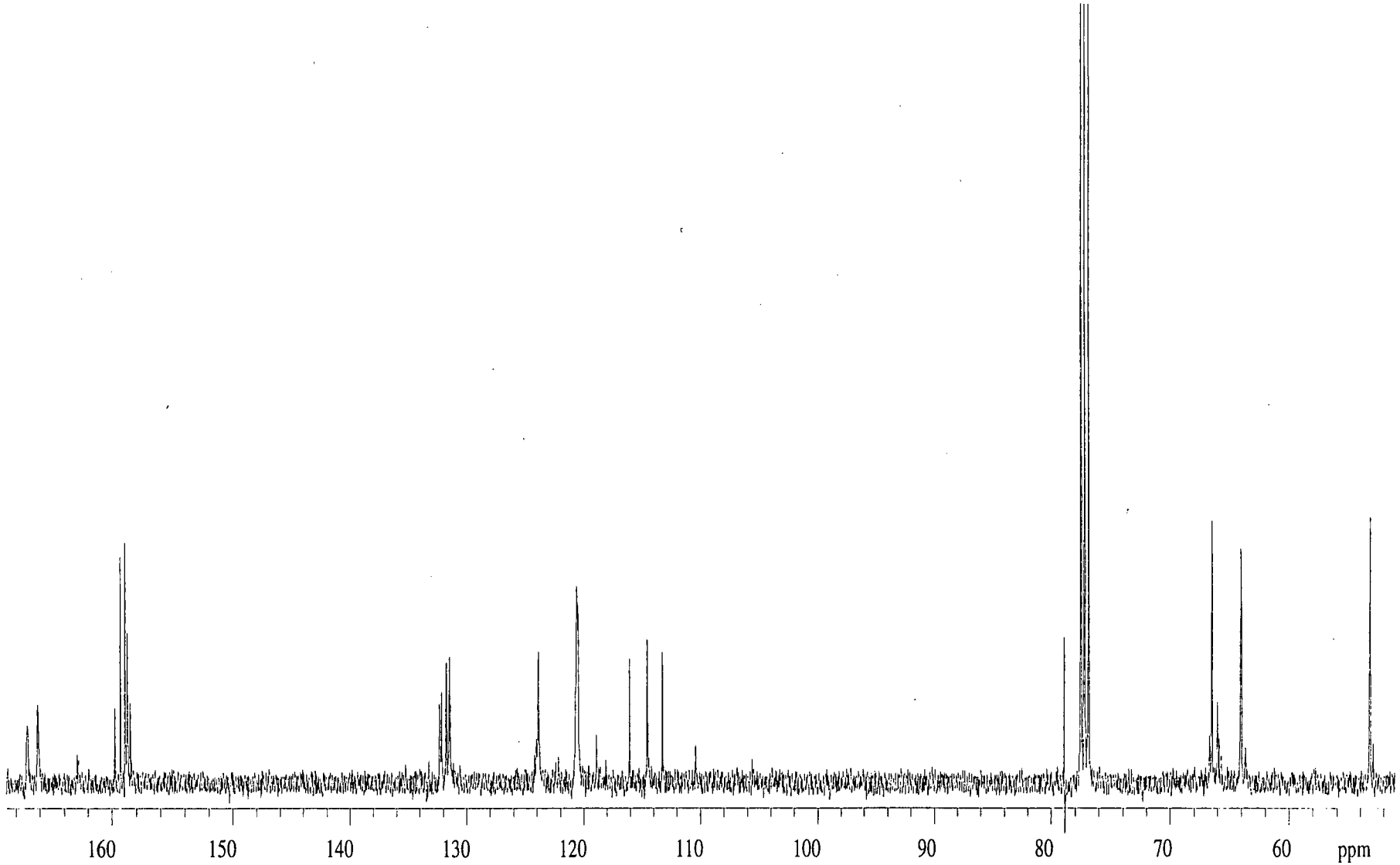

B05-4

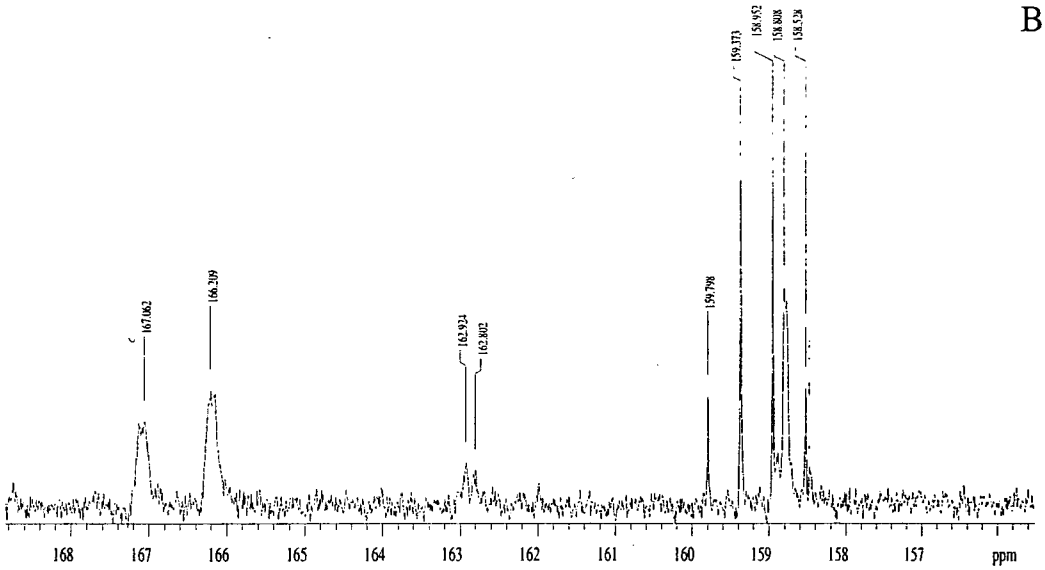
167.062
166.399
162.934
162.802
159.798
159.373
158.952
158.808
158.526
168
167
166
165
164
163
162
161
160
159
158
157
ppm

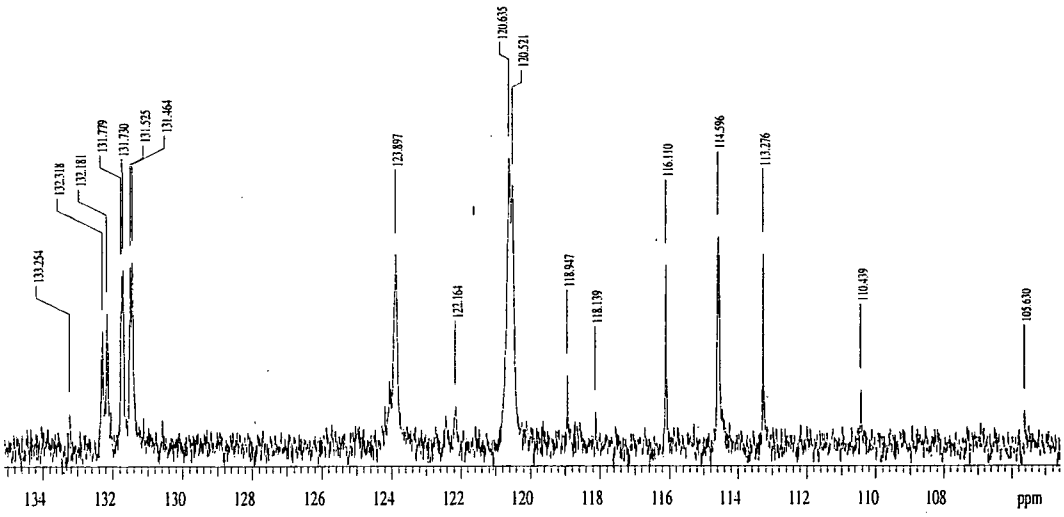
133.254
132.318
132.181
131.779
131.730
131.525
131.464
123.897
122.164
120.635
120.521
118.947
118.139
116.110
114.596
113.276
110.439
105.630
134
132
130
128
126
124
122
120
118
116
114
112
110
108
ppm

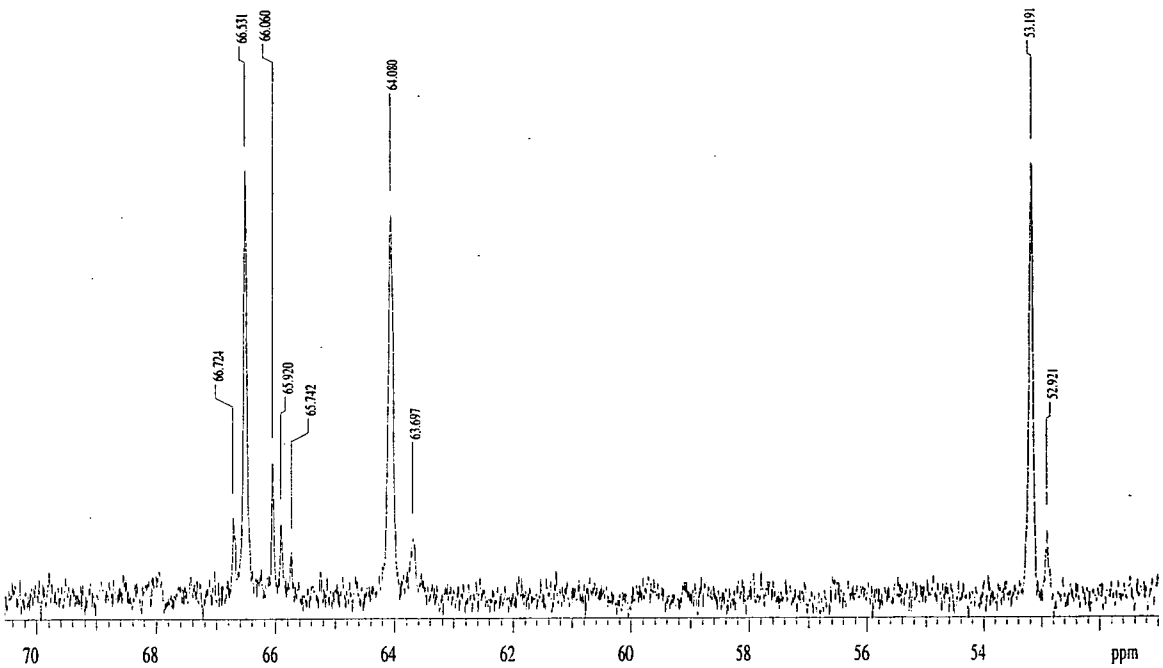
66.724
66.531
66.060
65.920
65.742
64.080
63.697
53.191
52.921
70
68
66
64
62
60
58
56
54
ppm

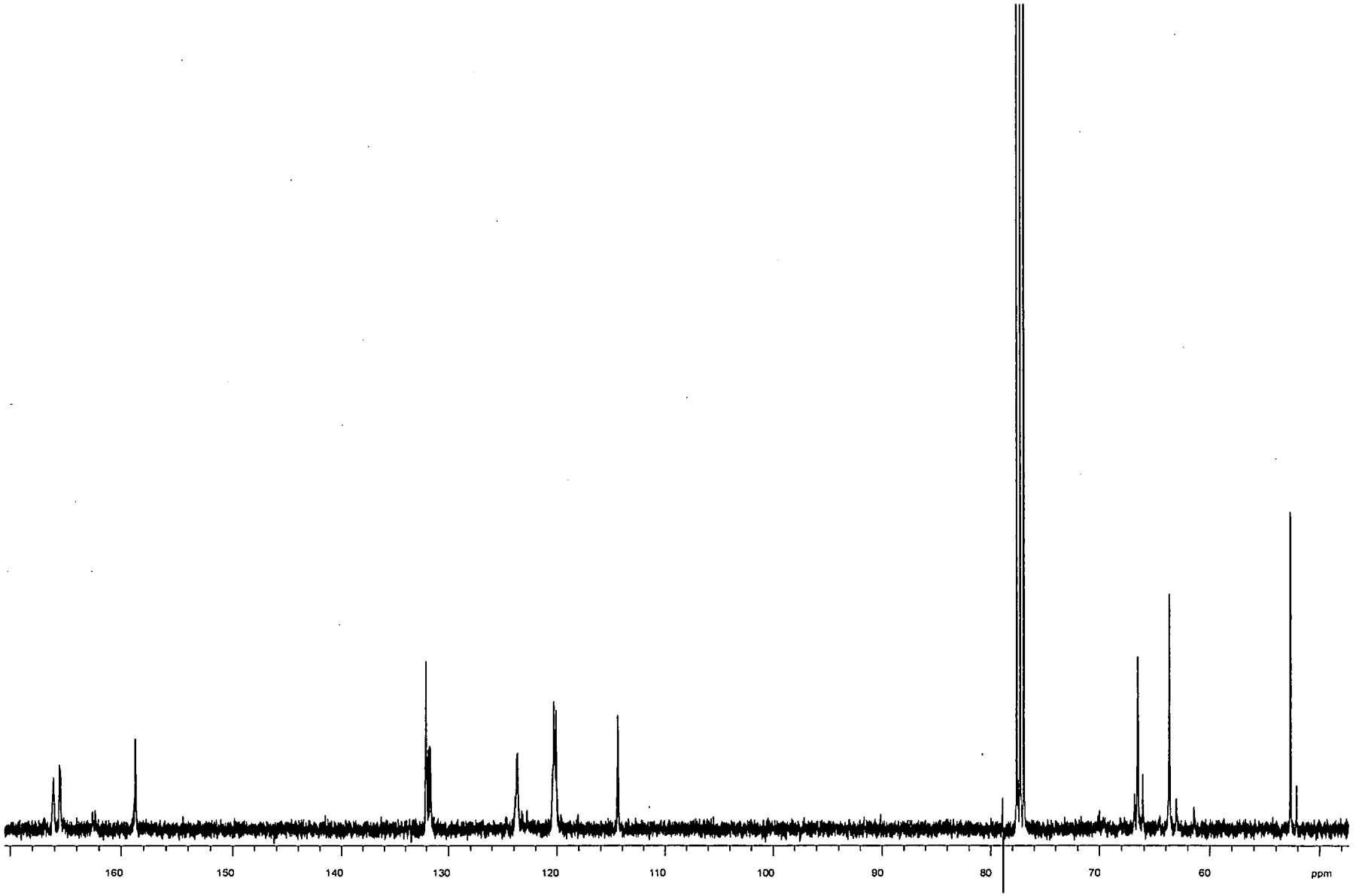

B05-5

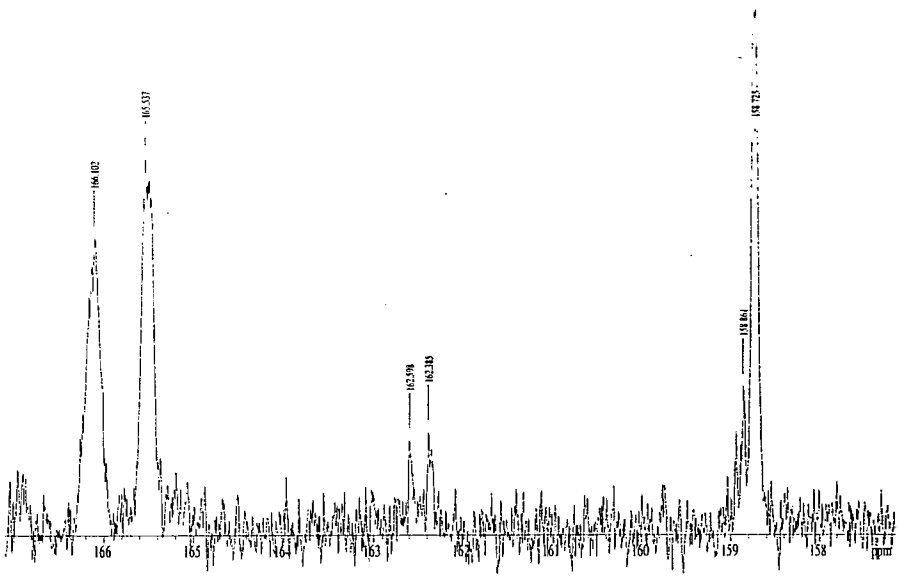
166.102
165.537
162.598
162.285
159.861
159.725
166
165
164
163
162
161
160
159
158
ppm

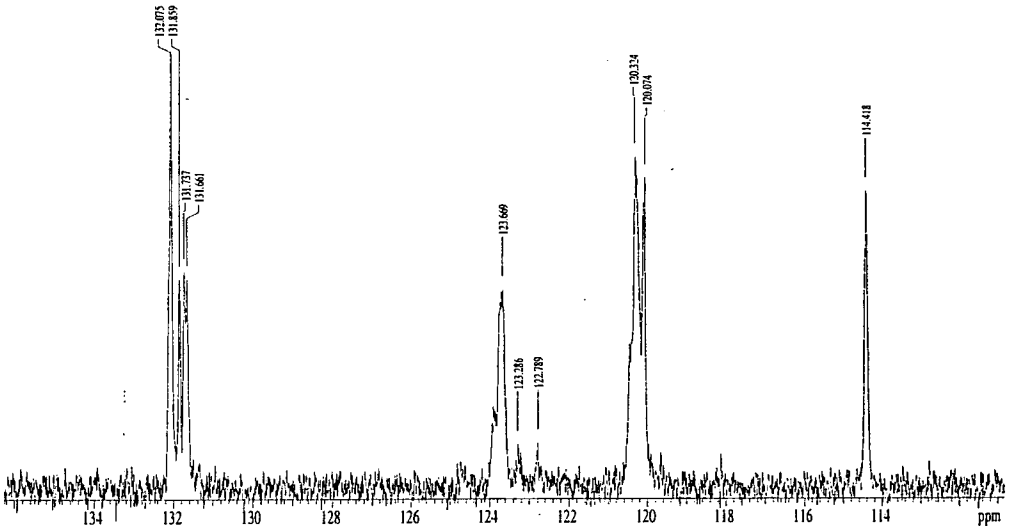
132.075
131.859
131.737
131.661
123.669
123.286
122.789
120.324
120.074
114.418
134
132
130
128
126
124
122
120
118
116
114
ppm

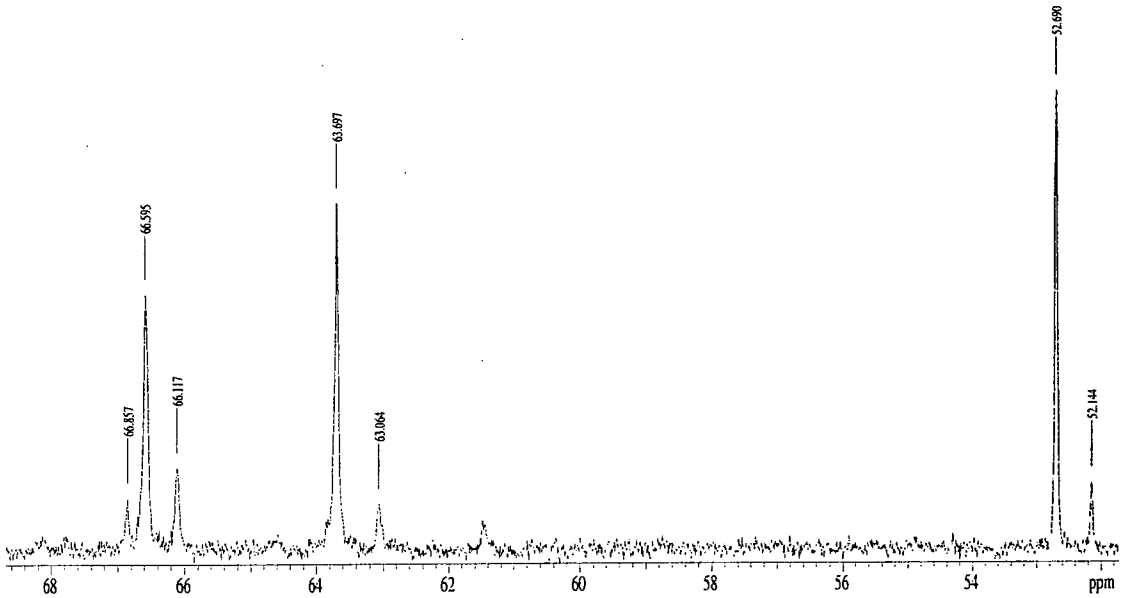
66.857
66.595
66.117
63.697
63.064
52.690
52.144
68
66
64
62
60
58
56
54
ppm

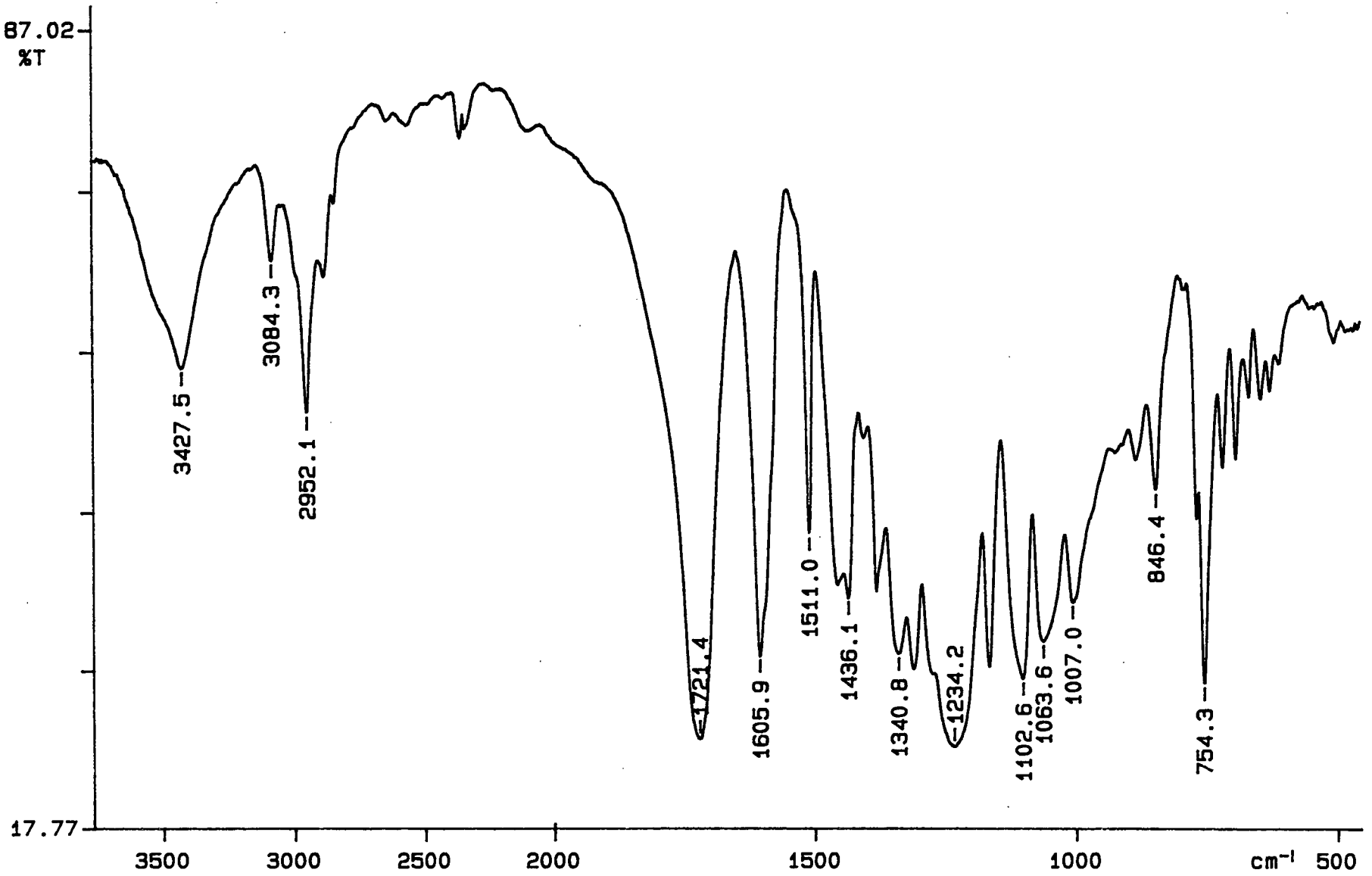

98/02/17 15: 12 s-373
X: 16 scans, 4.0cm-1

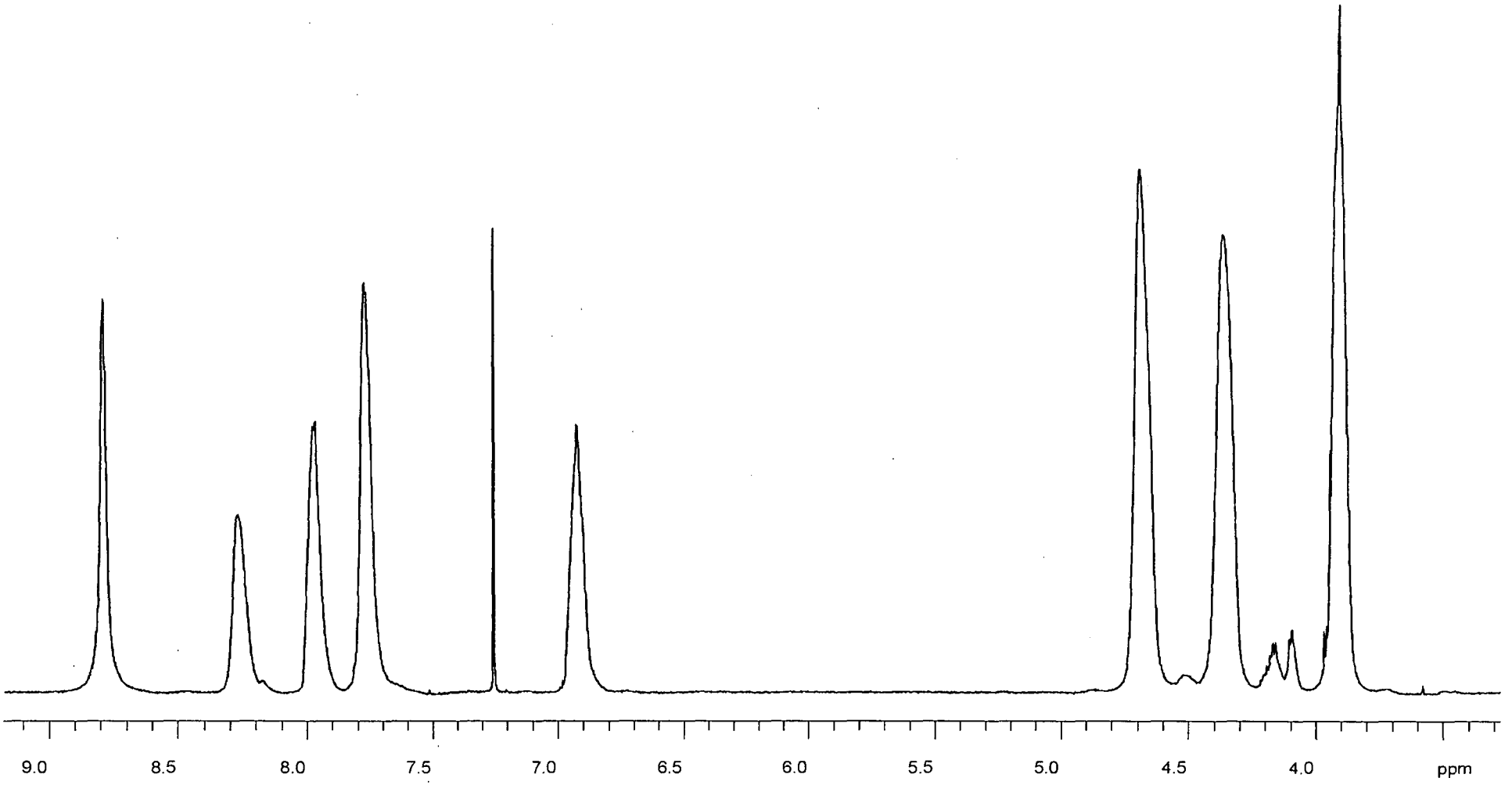

B06-2

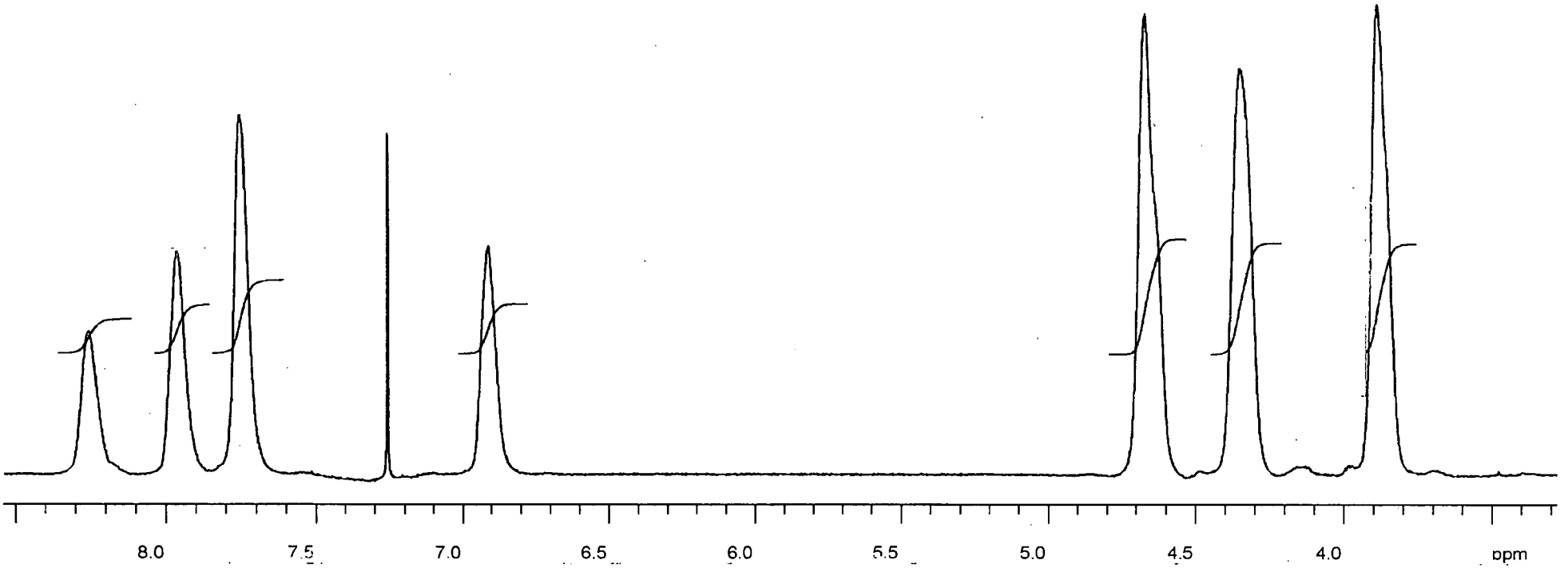
8.0
7.5
7.0
6.5
6.0
5.5
5.0
4.5
4.0
ppm

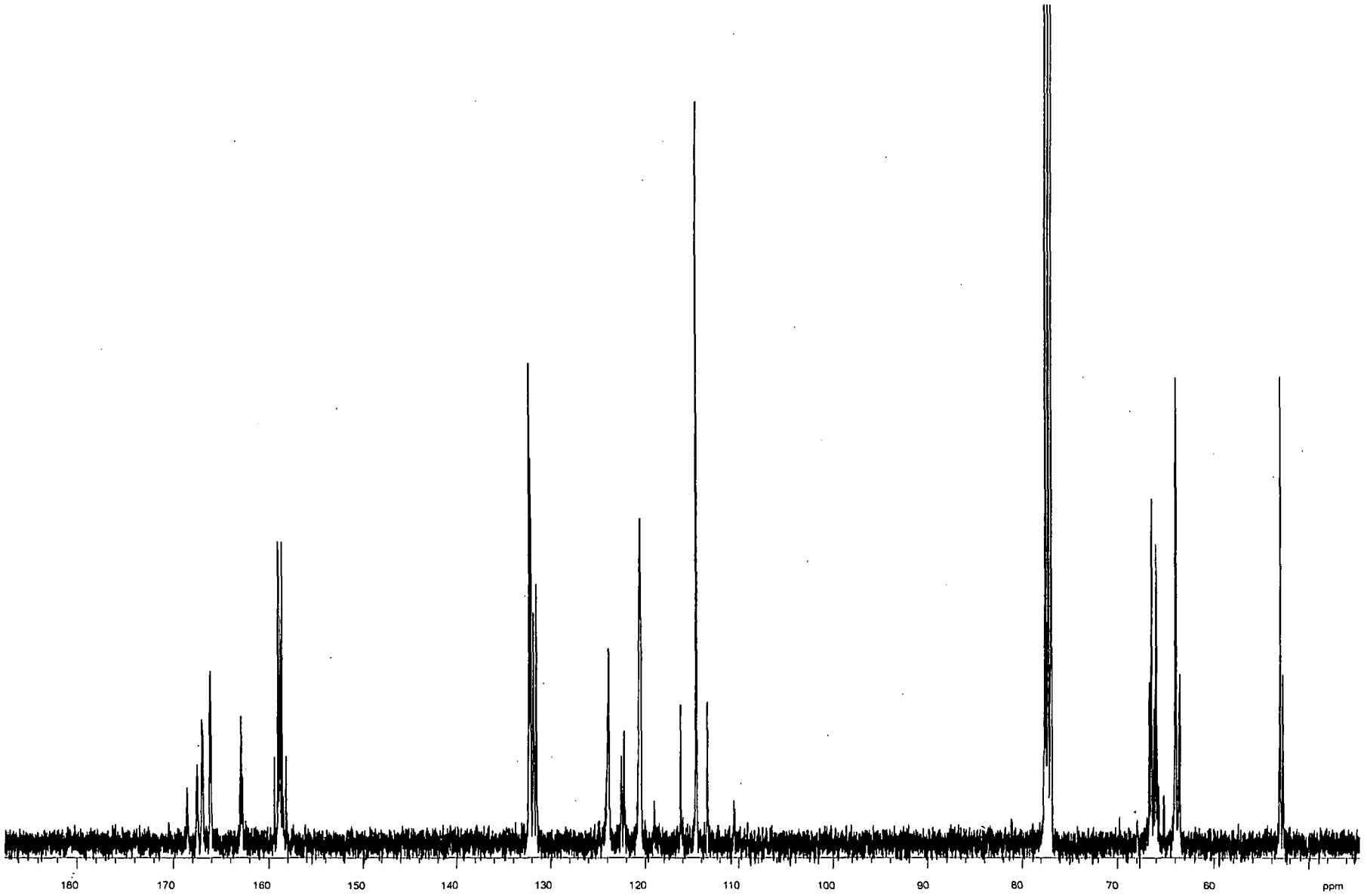

B06-4

B06-4

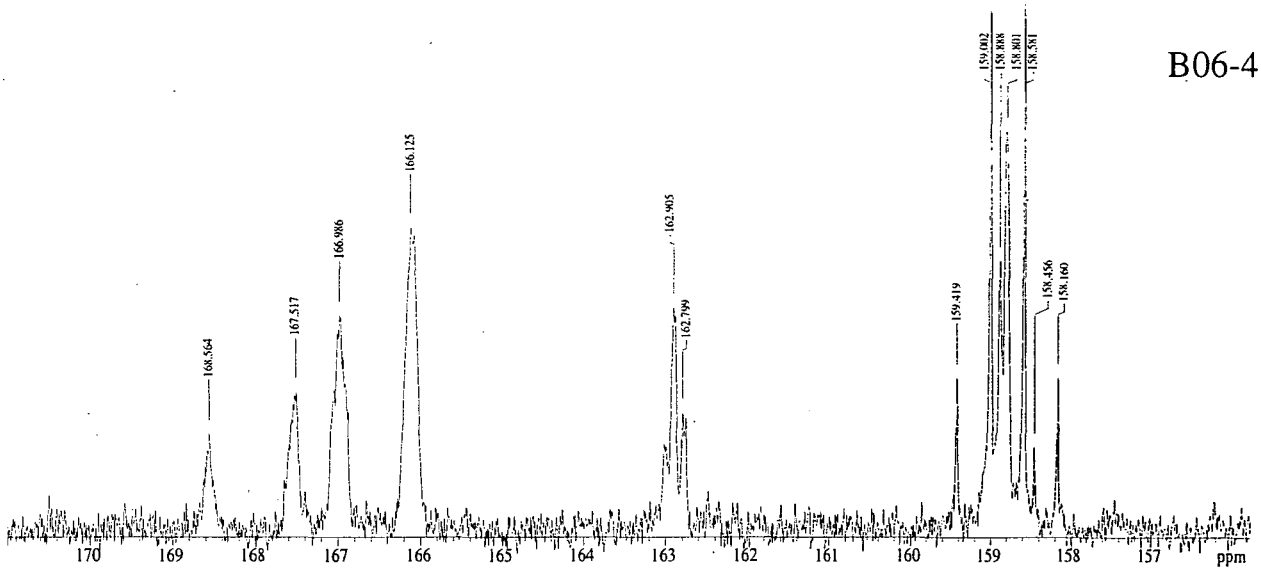
159.002
158.888
158.801
158.591
168.564
167.517
166.986
166.125
162.905
162.799
159.419
158.456
158.160
170
169
168
167
166
165
164
163
162
161
160
159
158
157
ppm

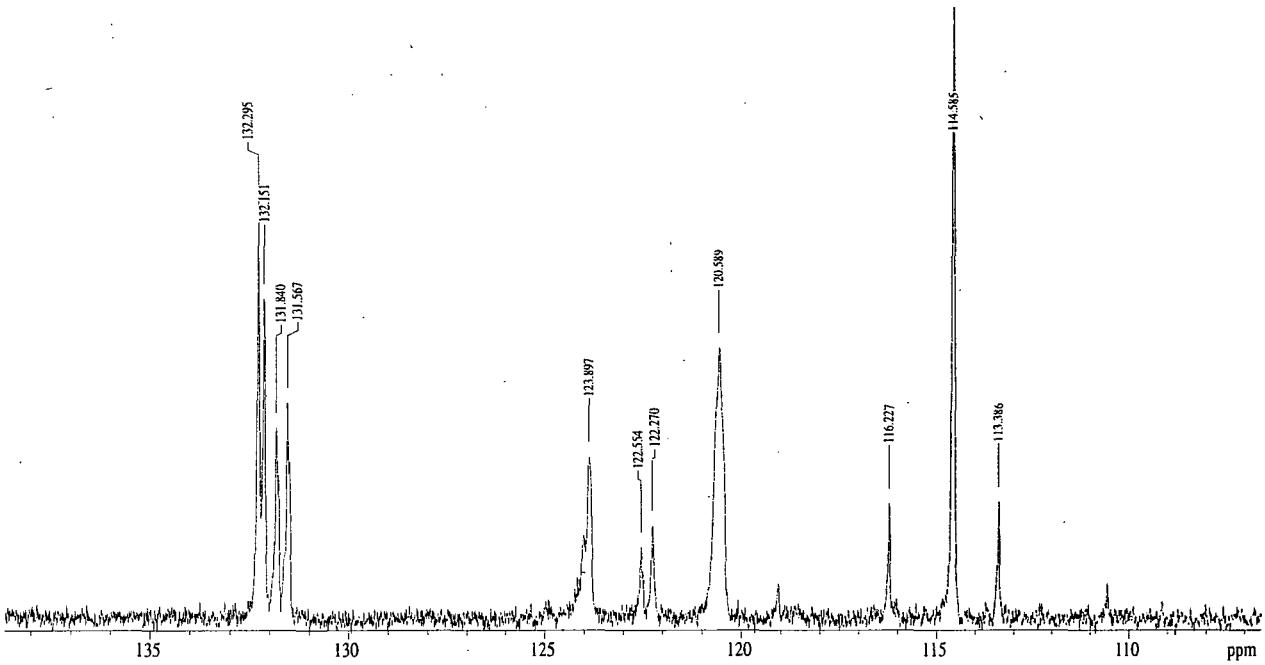
132.295
132.151
131.840
131.567
123.897
122.554
122.270
120.589
116.227
114.585
113.386
135
130
125
120
115
110
ppm

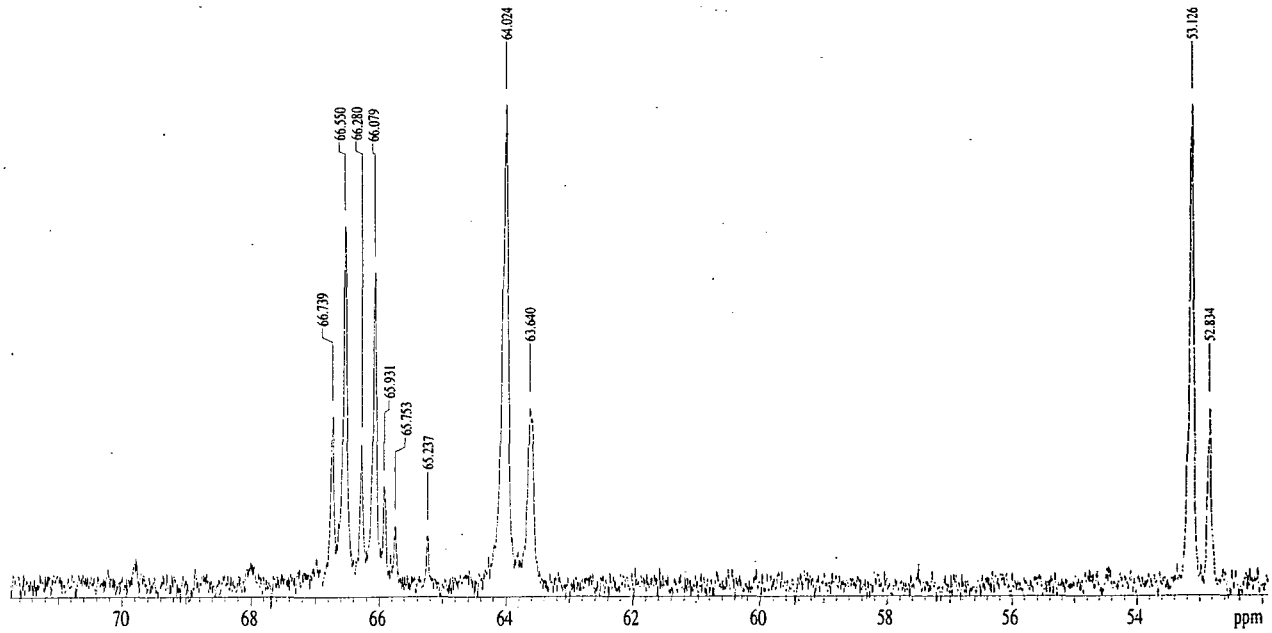
64.024
66.550
66.280
66.079
66.739
65.931
65.753
65.237
63.640
53.126
52.834
70
68
66
64
62
60
58
56
54
ppm

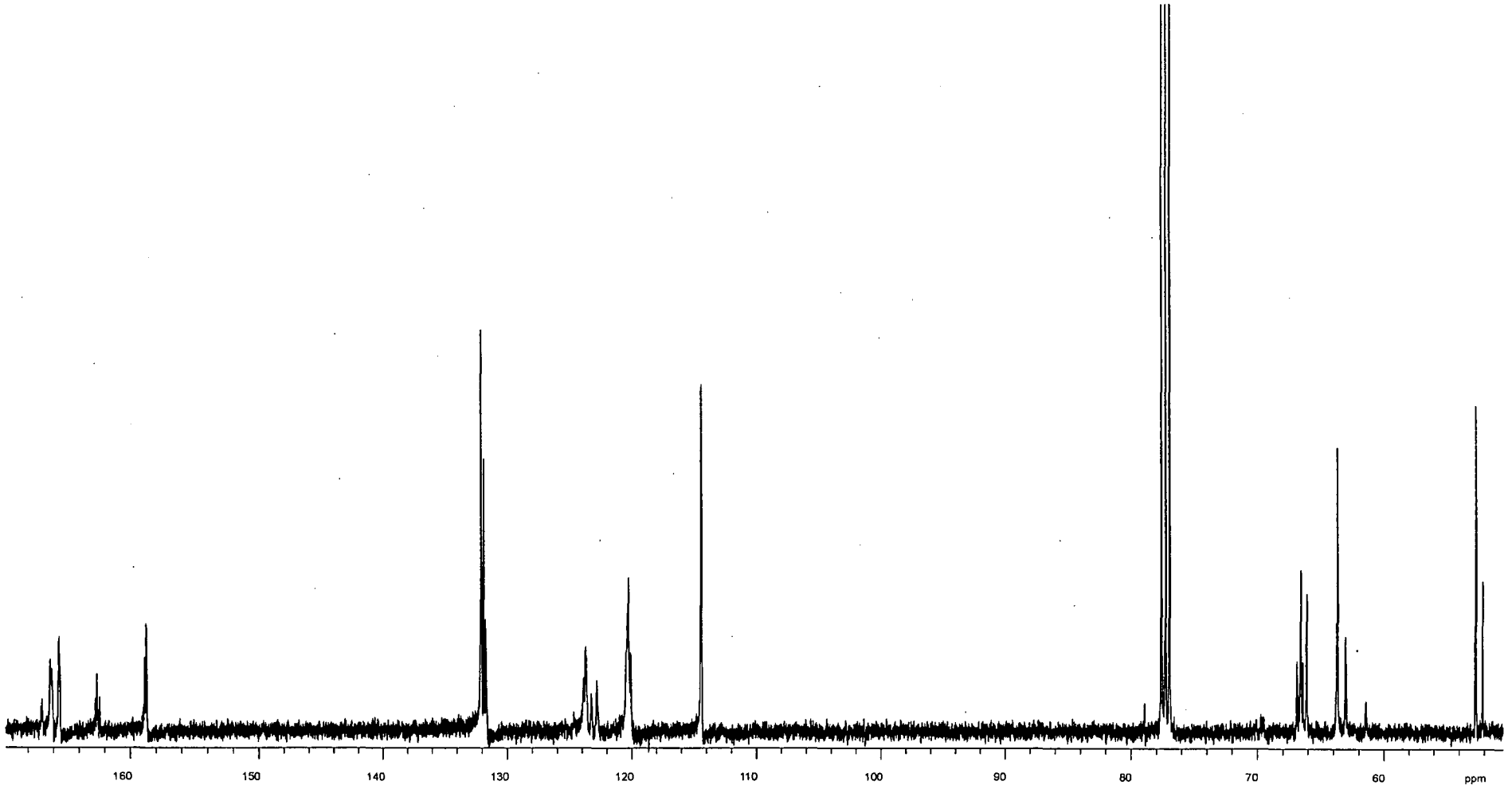

B06-5

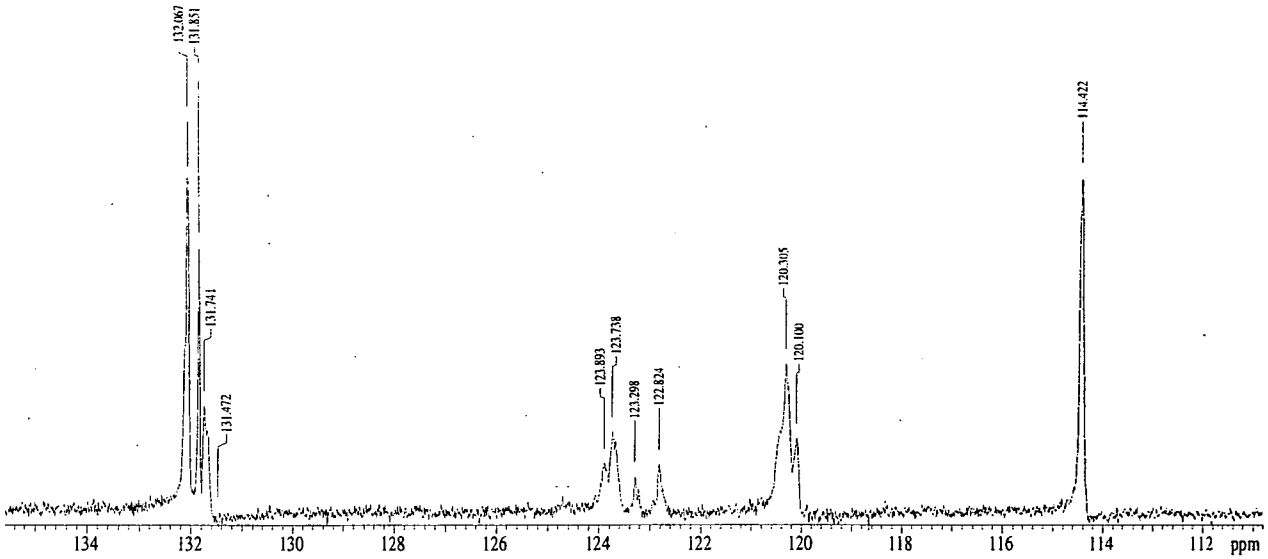
132.067
131.851
131.741
131.472
123.893
123.738
123.298
122.824
120.305
120.100
114.422
134
132
130
128
126
124
122
120
118
116
114
112
ppm

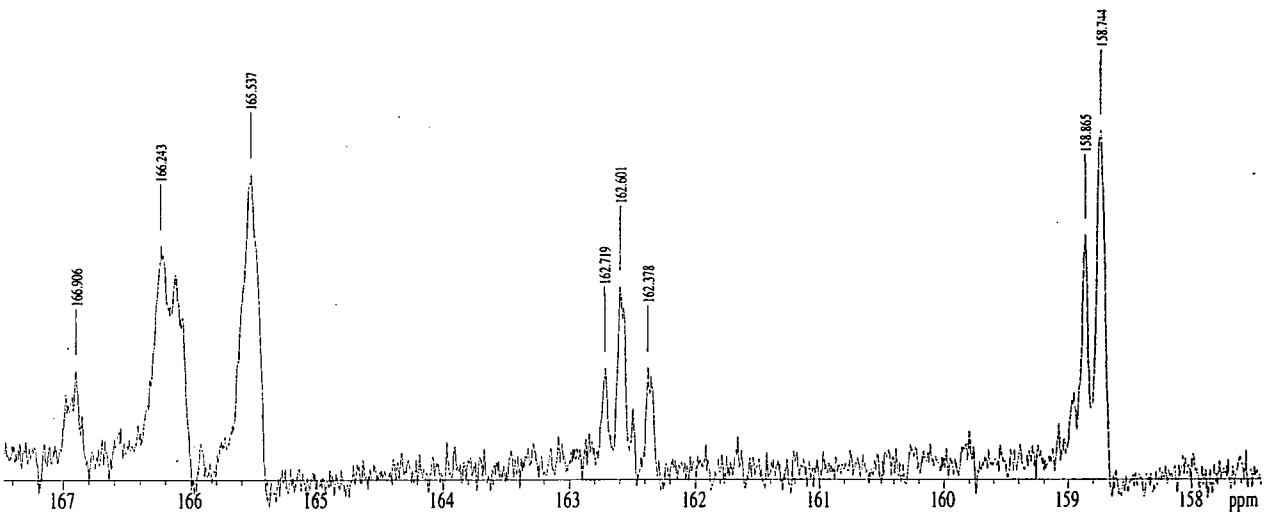
166.906
166.243
165.537
162.719
162.601
162.378
158.865
158.744
167
166
165
164
163
162
161
160
159
158
ppm

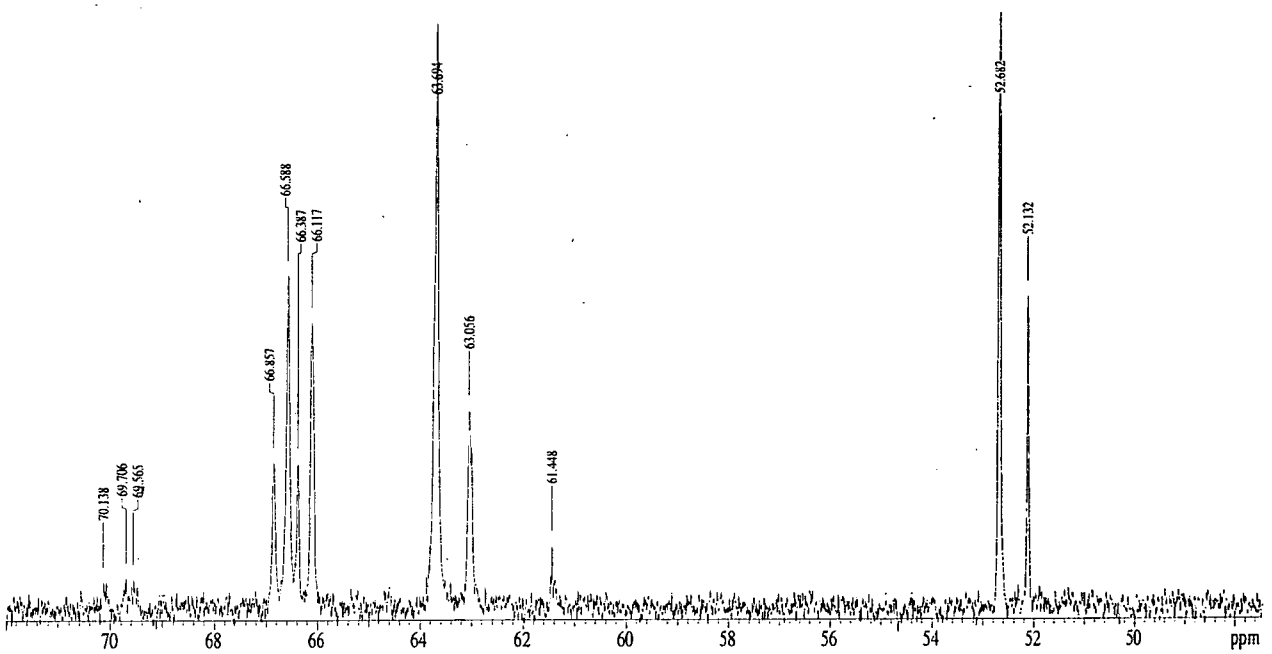
70.138
69.706
69.565
66.857
66.588
66.387
66.117
63.694
63.056
61.448
52.682
52.132
70
68
66
64
62
60
58
56
54
52
50
ppm

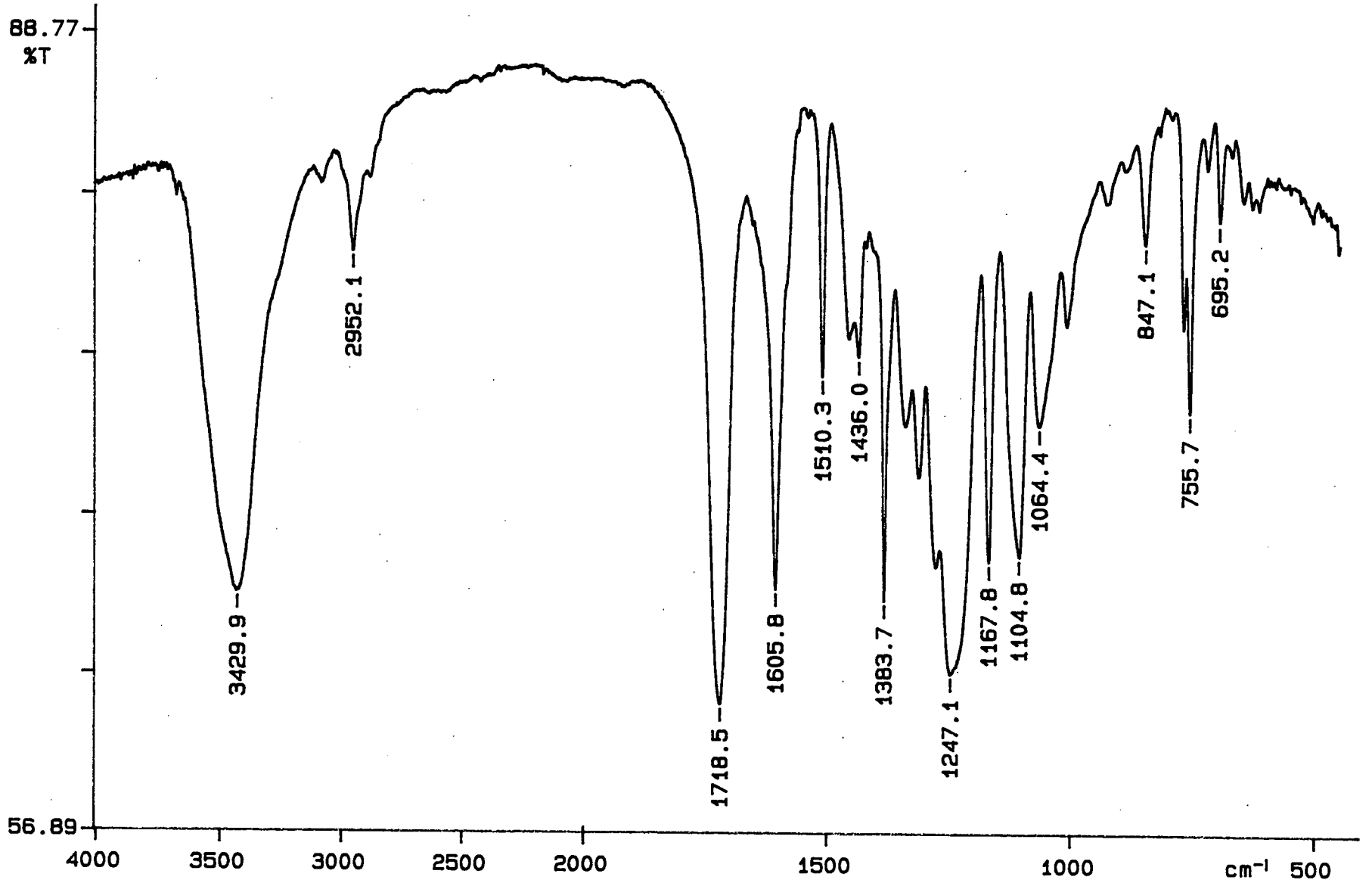

98/02/19 12: 15 s-373
ia72-7p: 16 scans, 4.0cm-1
40% branched

B07-1

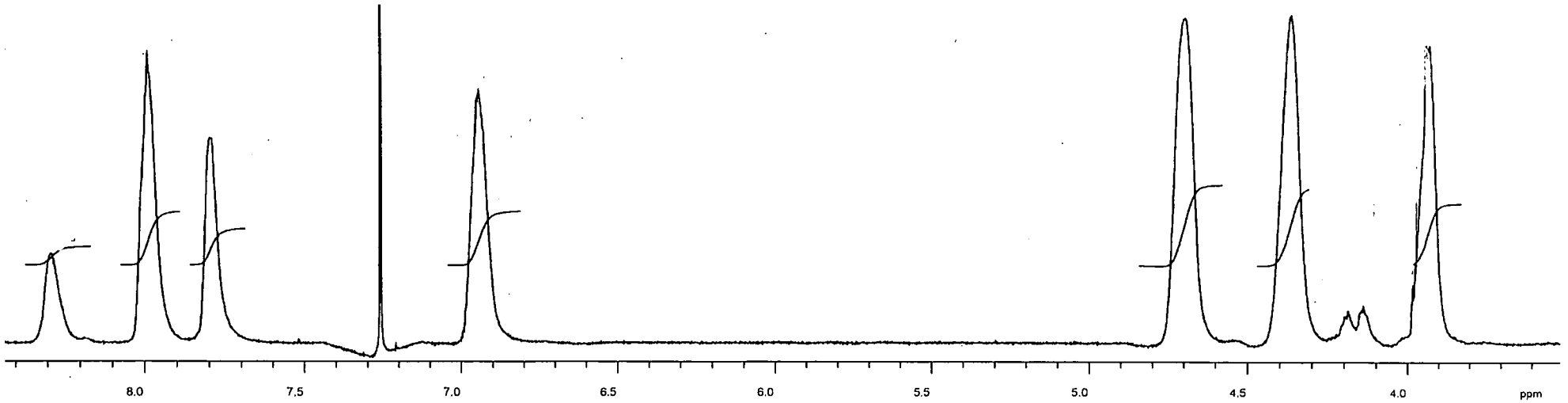

B07-2

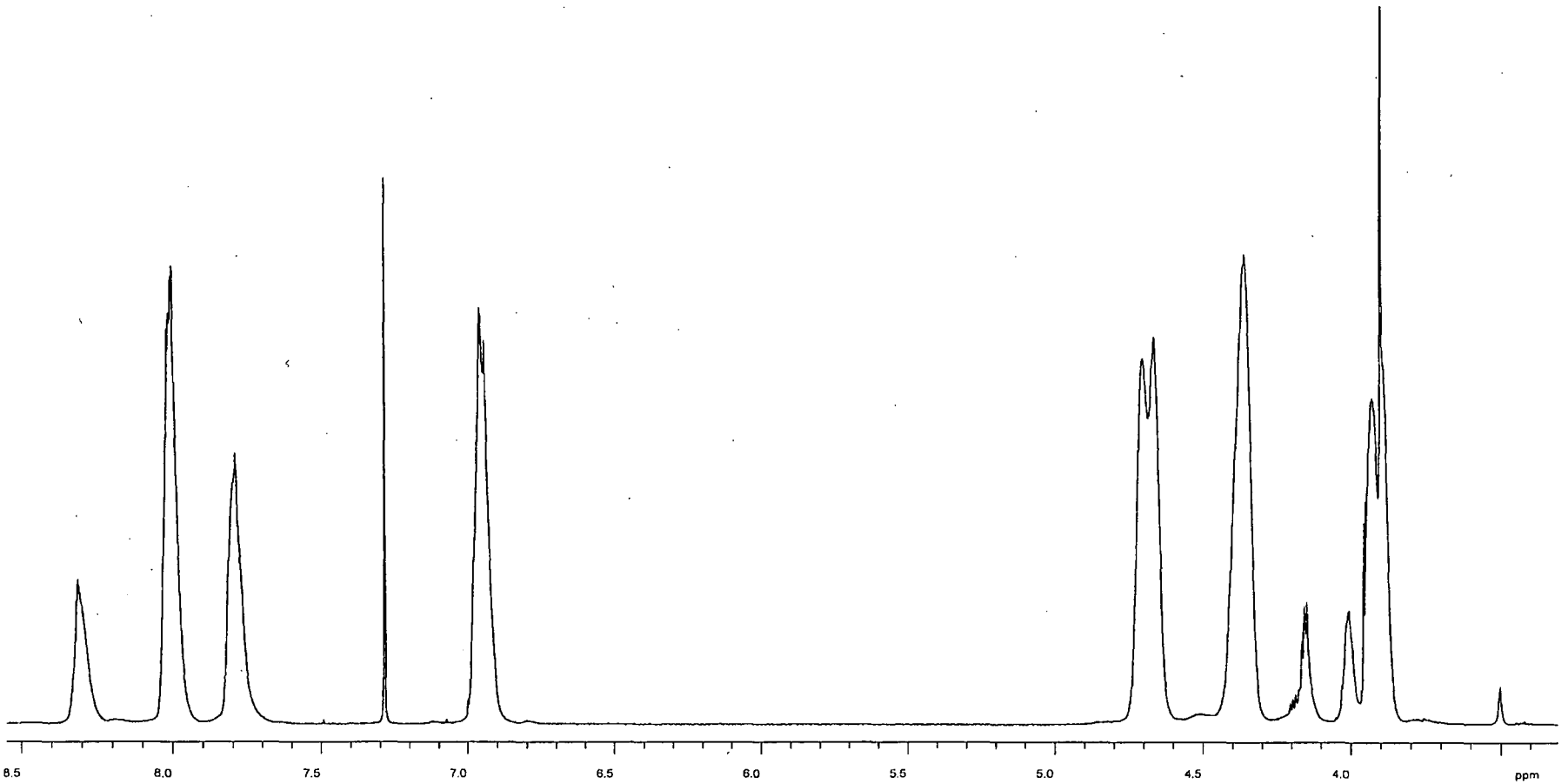

B07-3

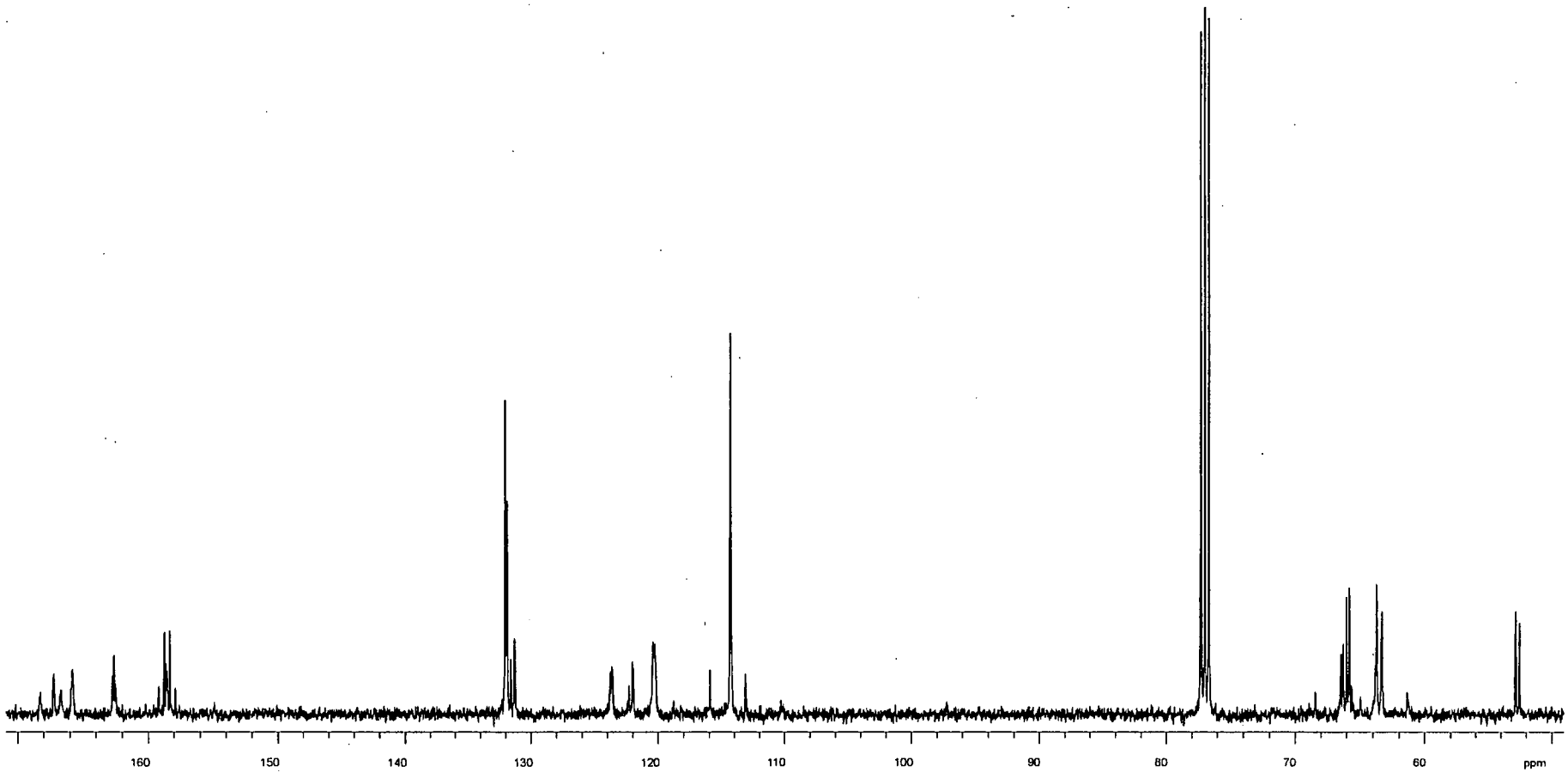

B07-4

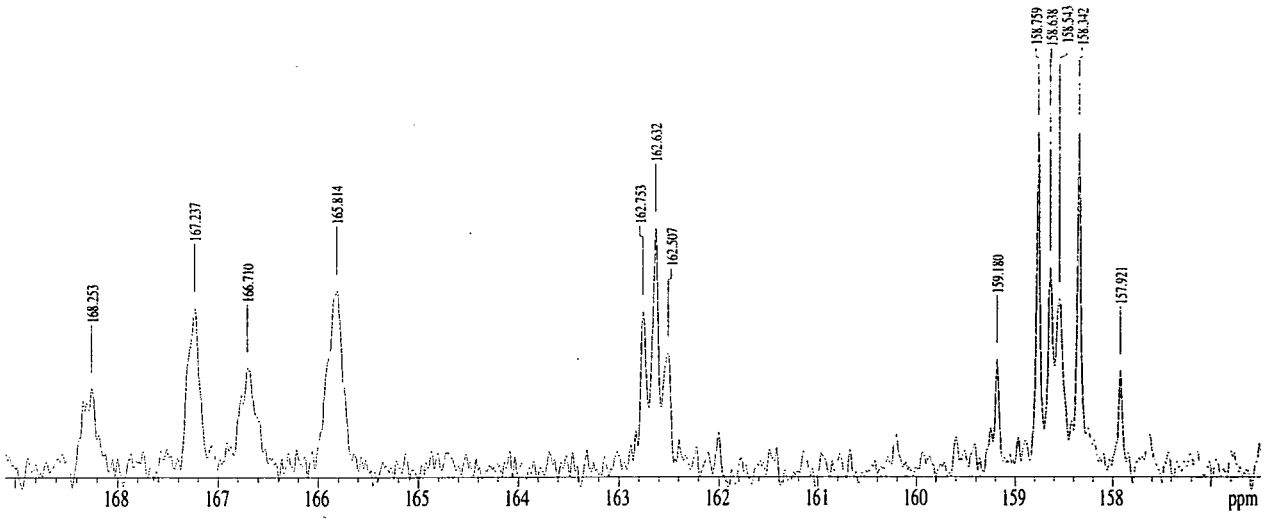
168.253
167.237
166.710
165.814
162.753
162.632
162.507
159.180
158.759
158.638
158.543
158.342
157.921
168
167
166
165
164
163
162
161
160
159
158
ppm

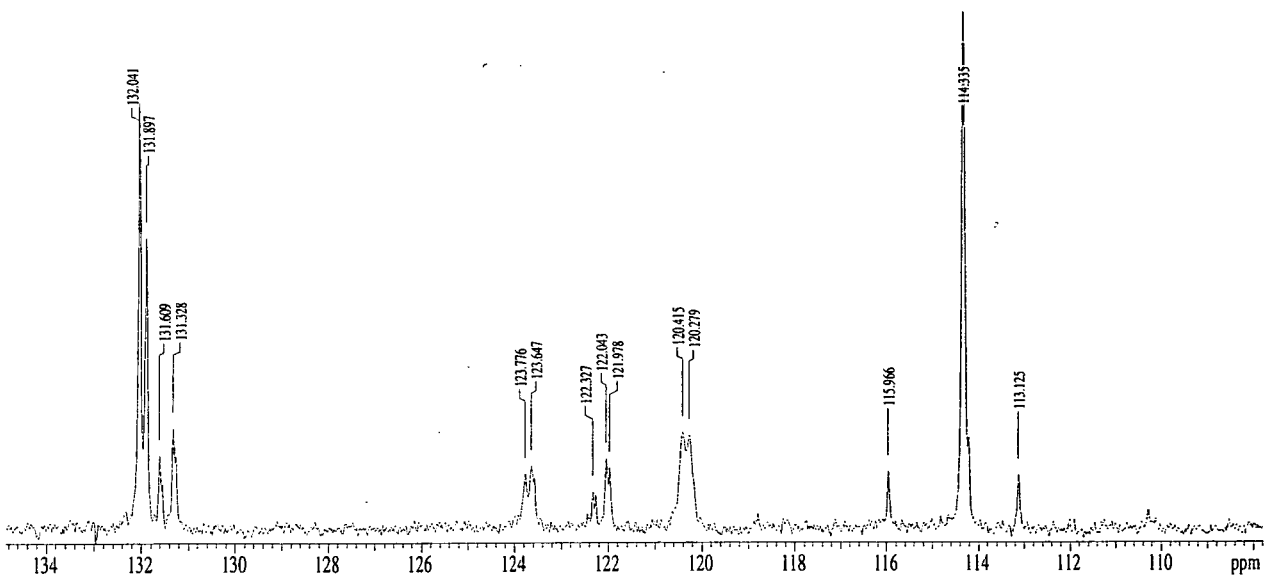
132.041
131.897
131.609
131.328
123.776
123.647
122.327
122.043
121.978
120.415
120.279
115.966
114.335
113.125
134
132
130
128
126
124
122
120
118
116
114
112
110
ppm

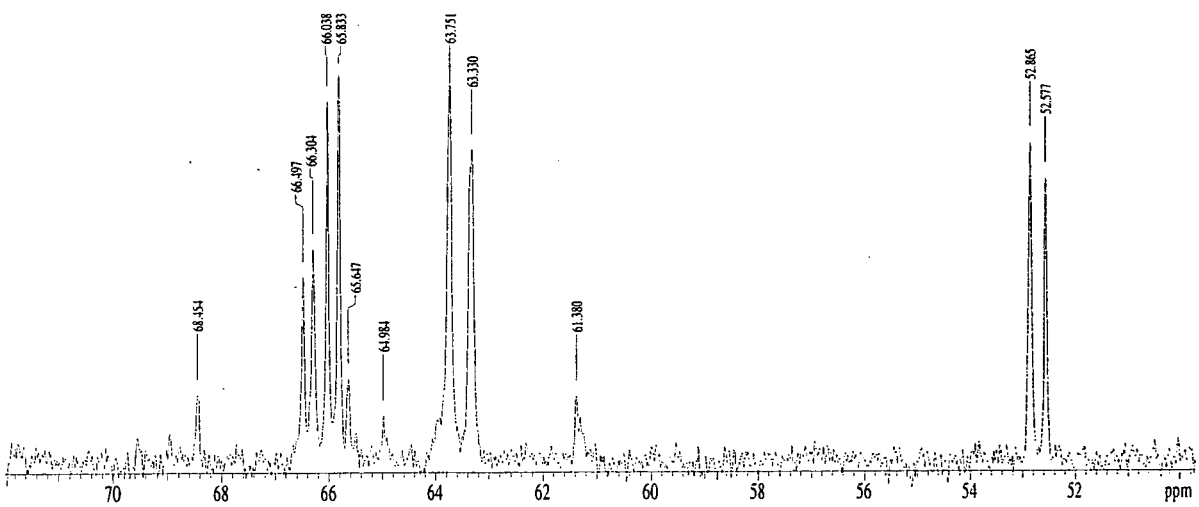
68.454
66.497
66.304
66.038
65.833
65.647
64.984
63.751
63.330
61.380
52.865
52.577
70
68
66
64
62
60
58
56
54
52
ppm

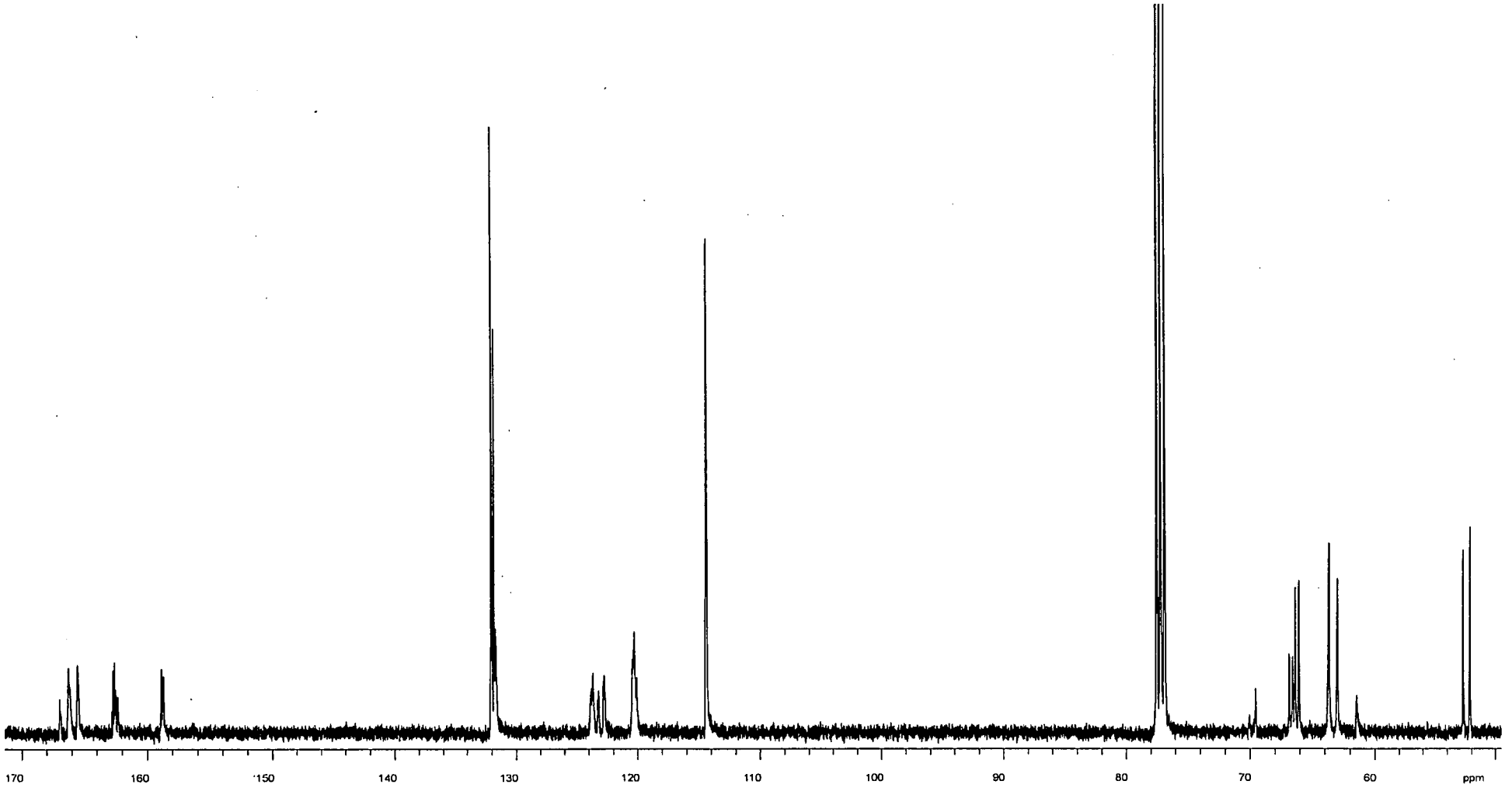

B07-5

B07-5

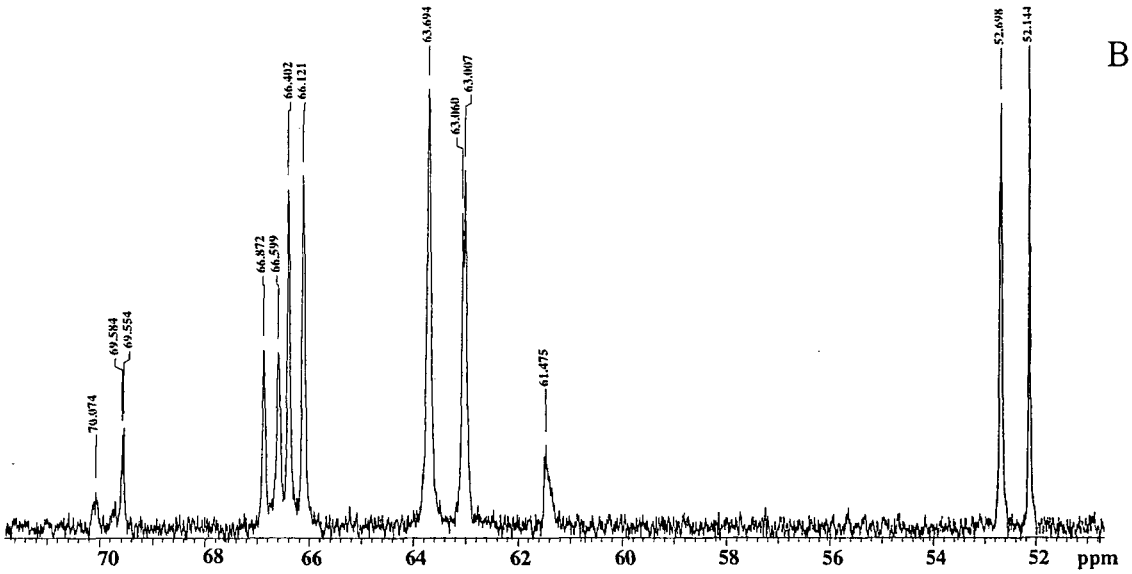
70.074
69.584
69.554
66.872
66.599
66.402
66.121
63.694
63.660
63.607
61.475
52.698
52.144
70
68
66
64
62
60
58
56
54
52
ppm

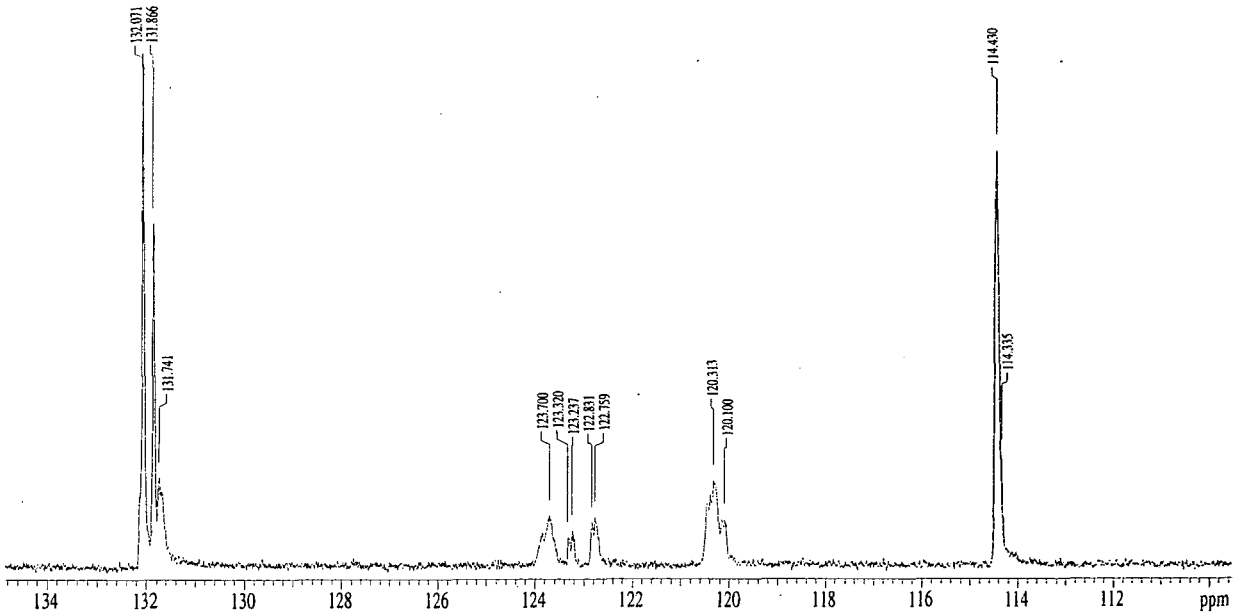
132.071
131.866
131.741
123.700
123.320
123.237
122.831
122.759
120.313
120.100
114.430
114.335
134
132
130
128
126
124
122
120
118
116
114
112
ppm

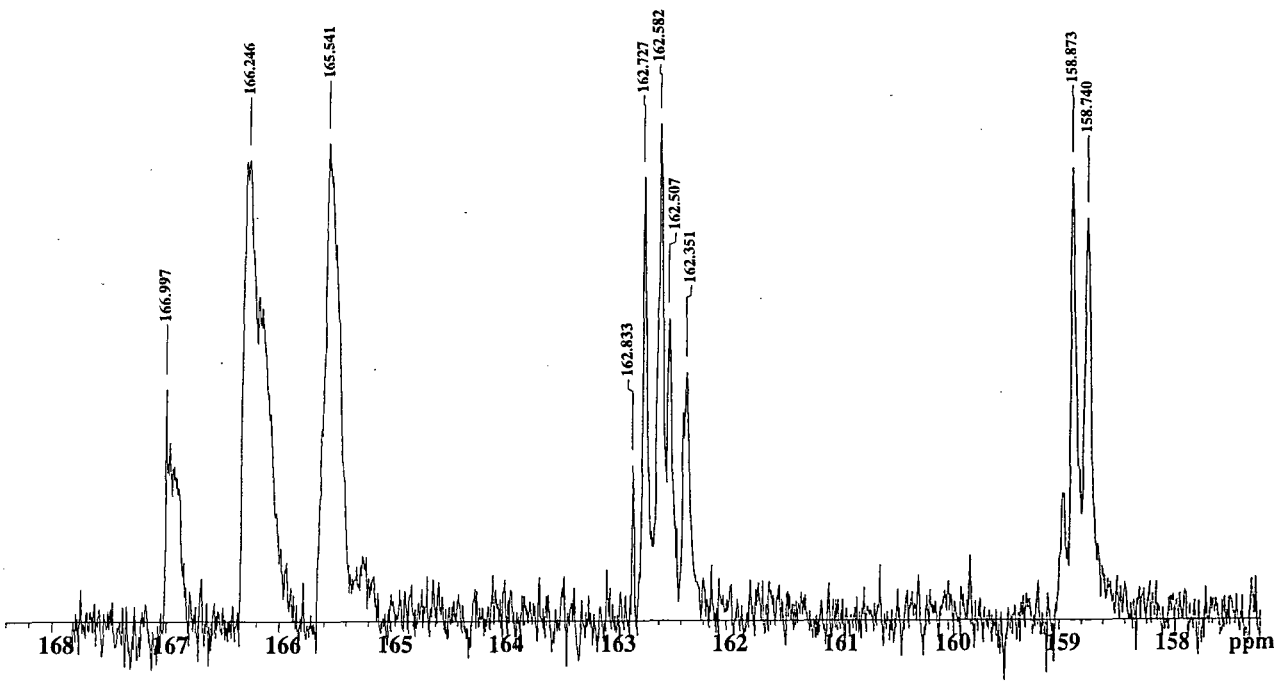
166.997
166.246
165.541
162.833
162.727
162.582
162.507
162.351
158.873
158.740
168
167
166
165
164
163
162
161
160
159
158
ppm

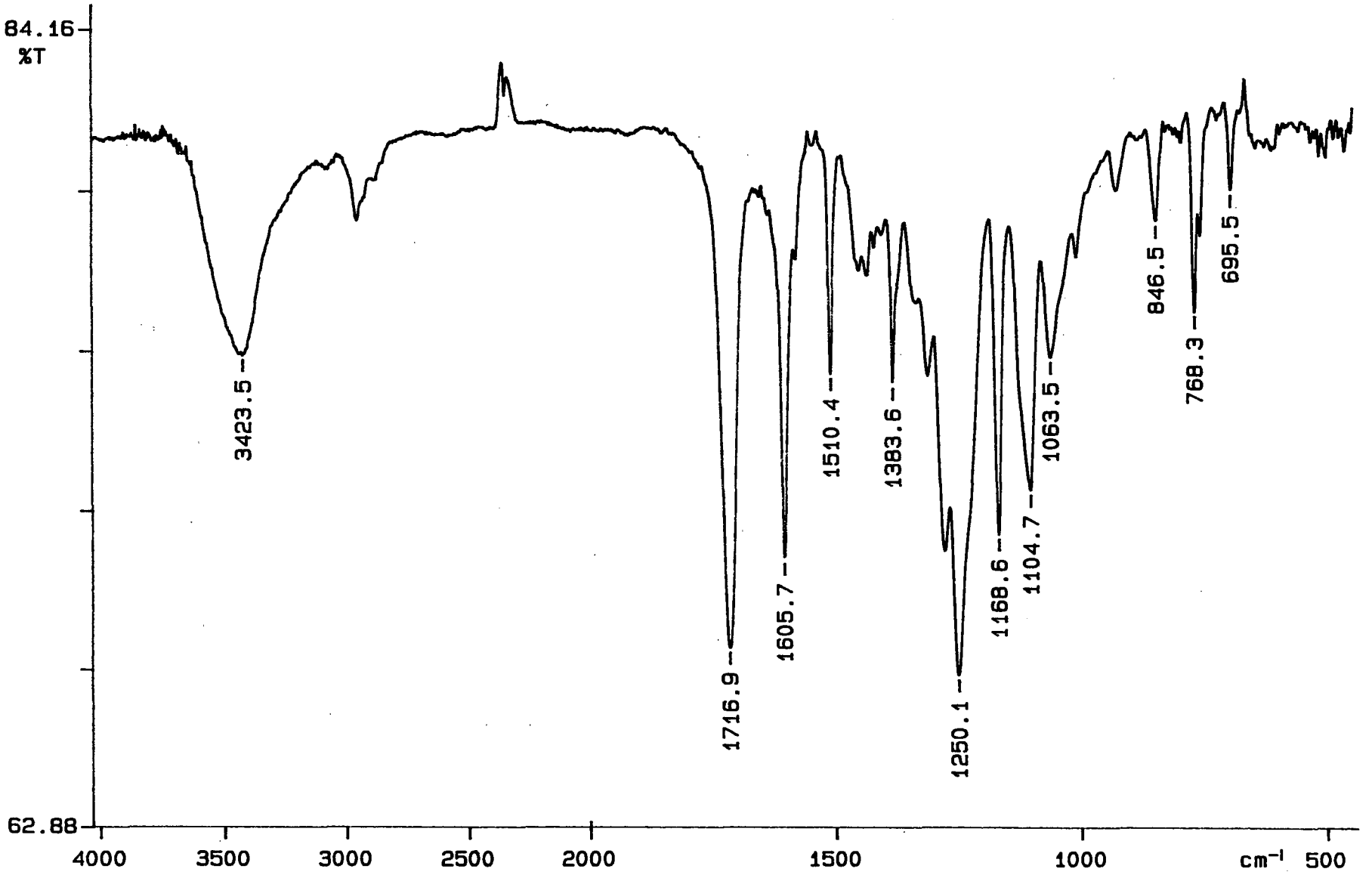

98/01/30 10:58 s-373
Y: 16 scans, 4.0cm-1, flat

B08-1

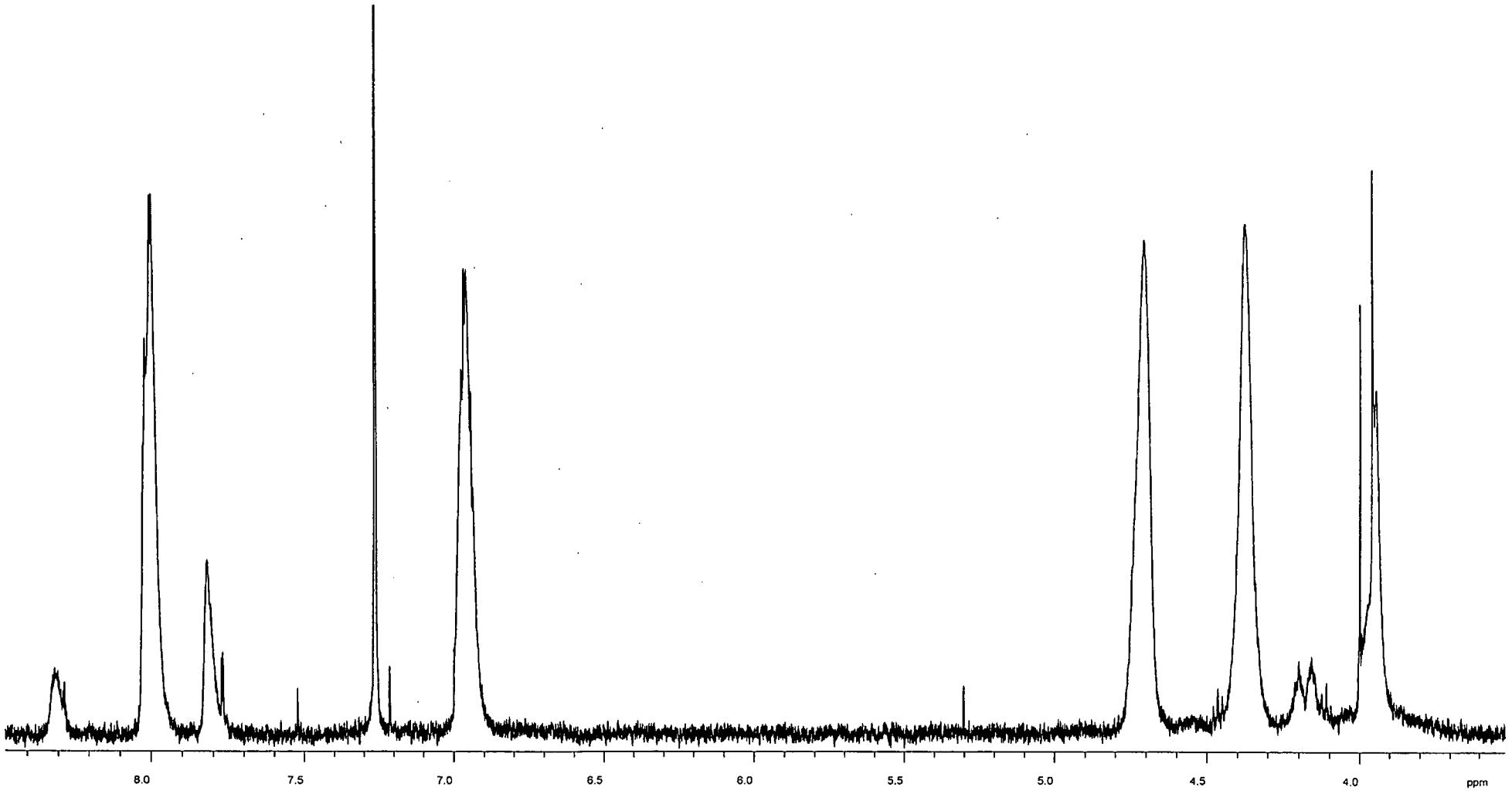

B08-2

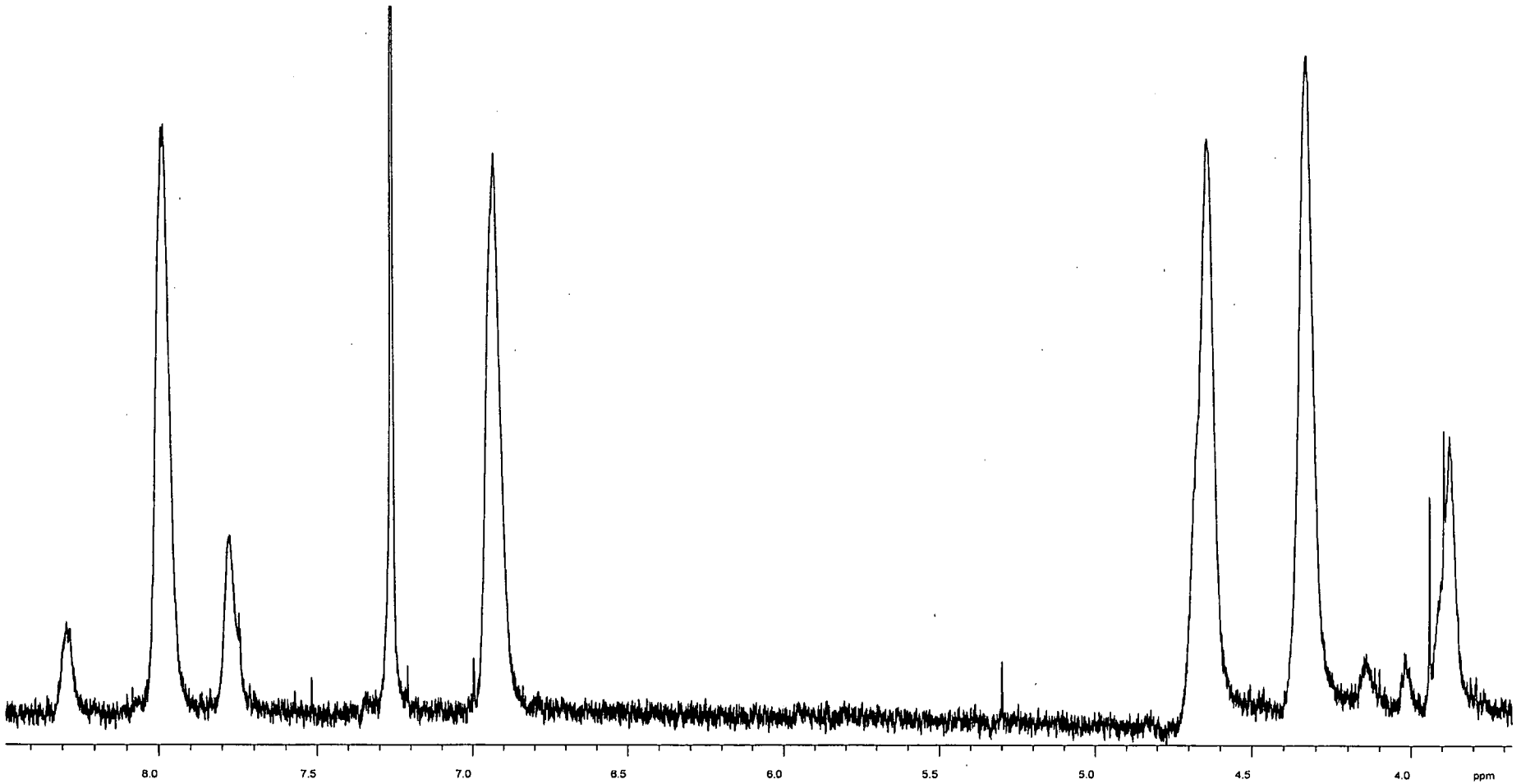

B08-3

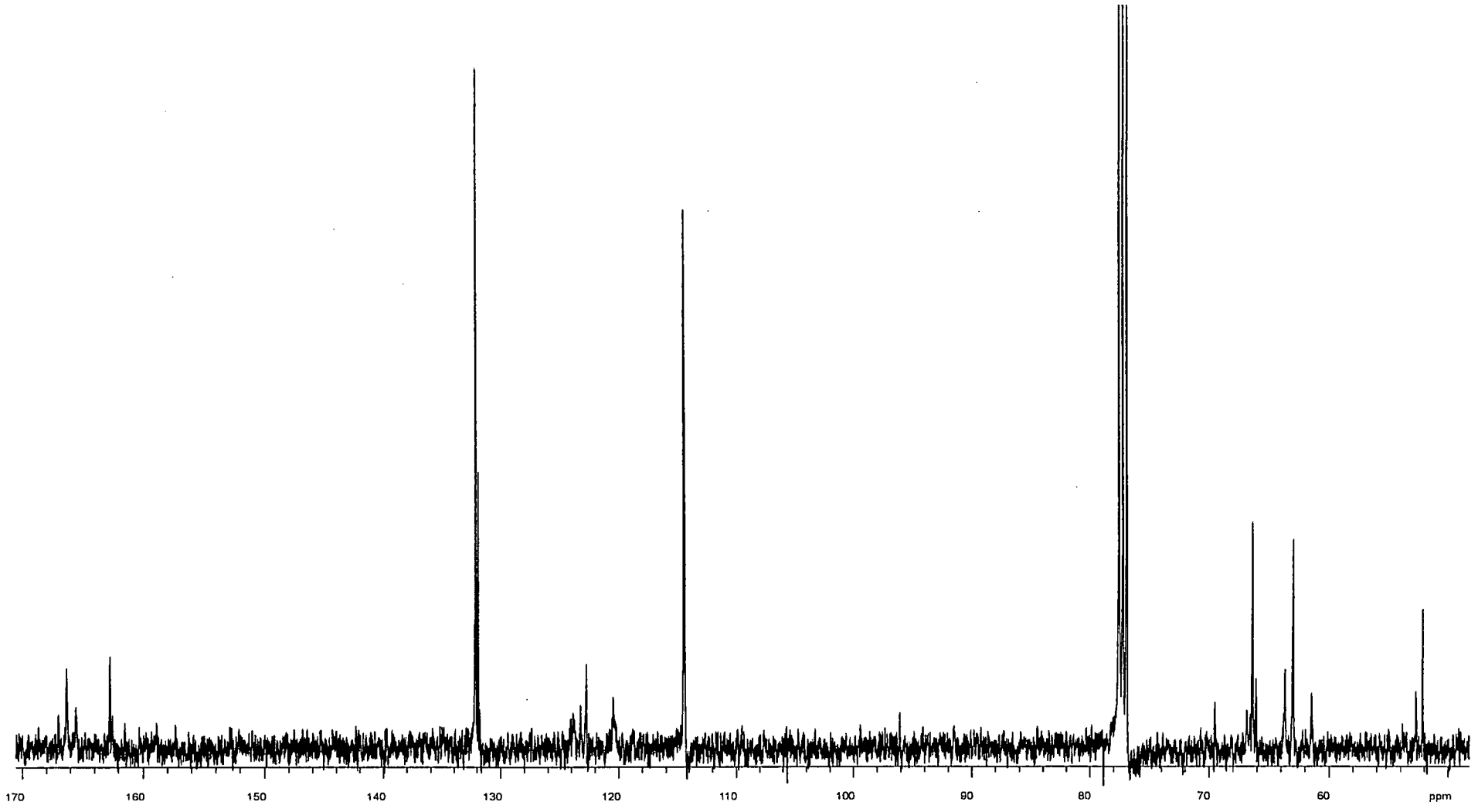

B08-5

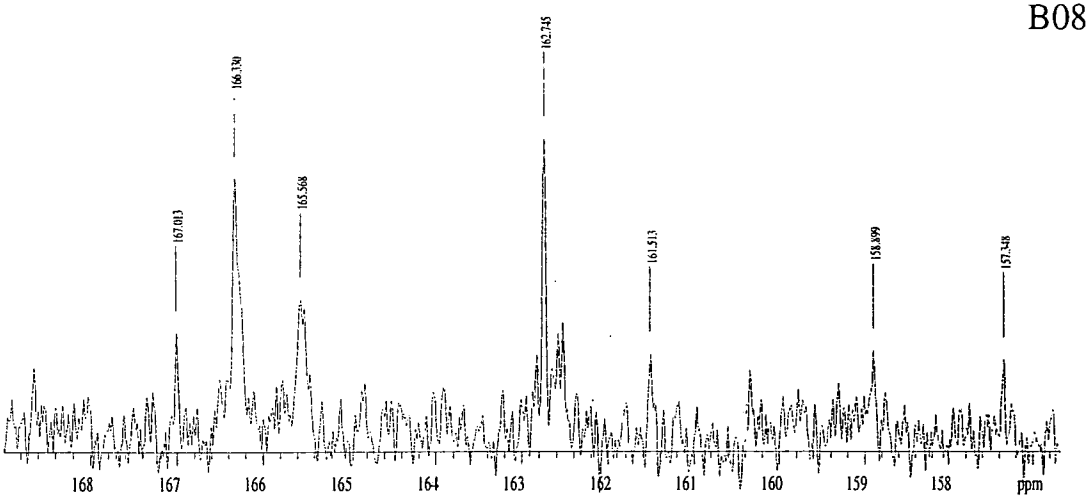
167.013
166.330
165.568
162.745
161.513
158.099
157.348
168
167
166
165
164
163
162
161
160
159
158
ppm

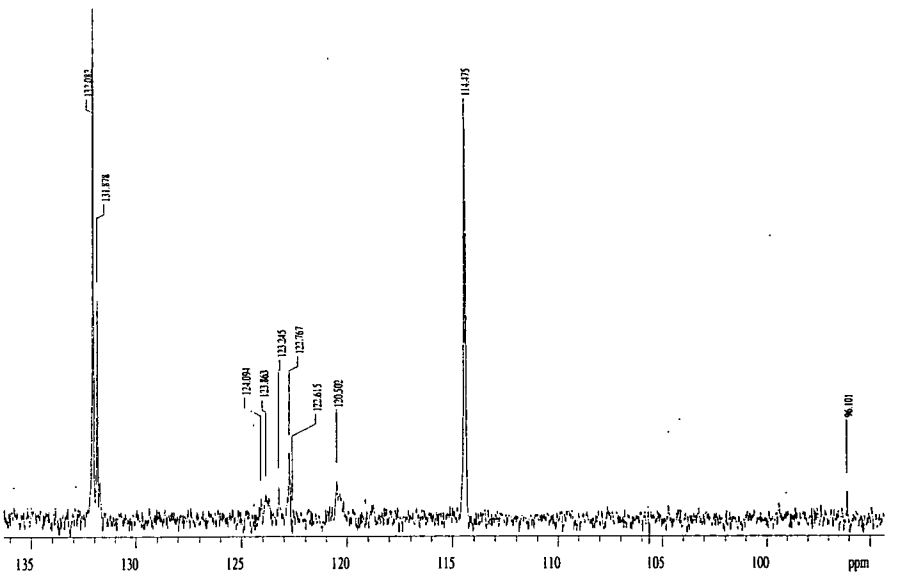
132.092
131.678
124.094
123.863
123.545
122.767
122.615
120.502
114.375
96.101
135
130
125
120
115
110
105
100
ppm

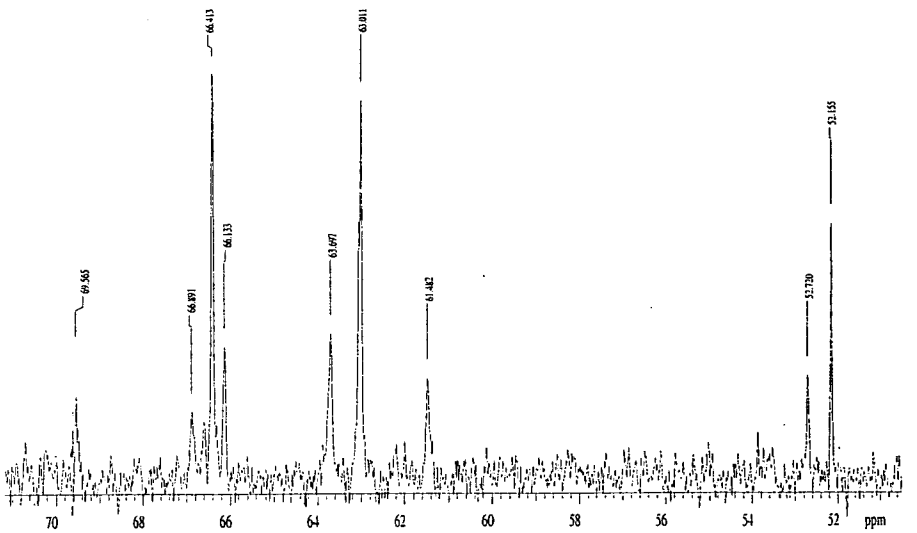
69.565
66.891
66.413
66.133
63.697
63.011
61.482
53.155
53.720
70
68
66
64
62
60
58
56
54
52
ppm

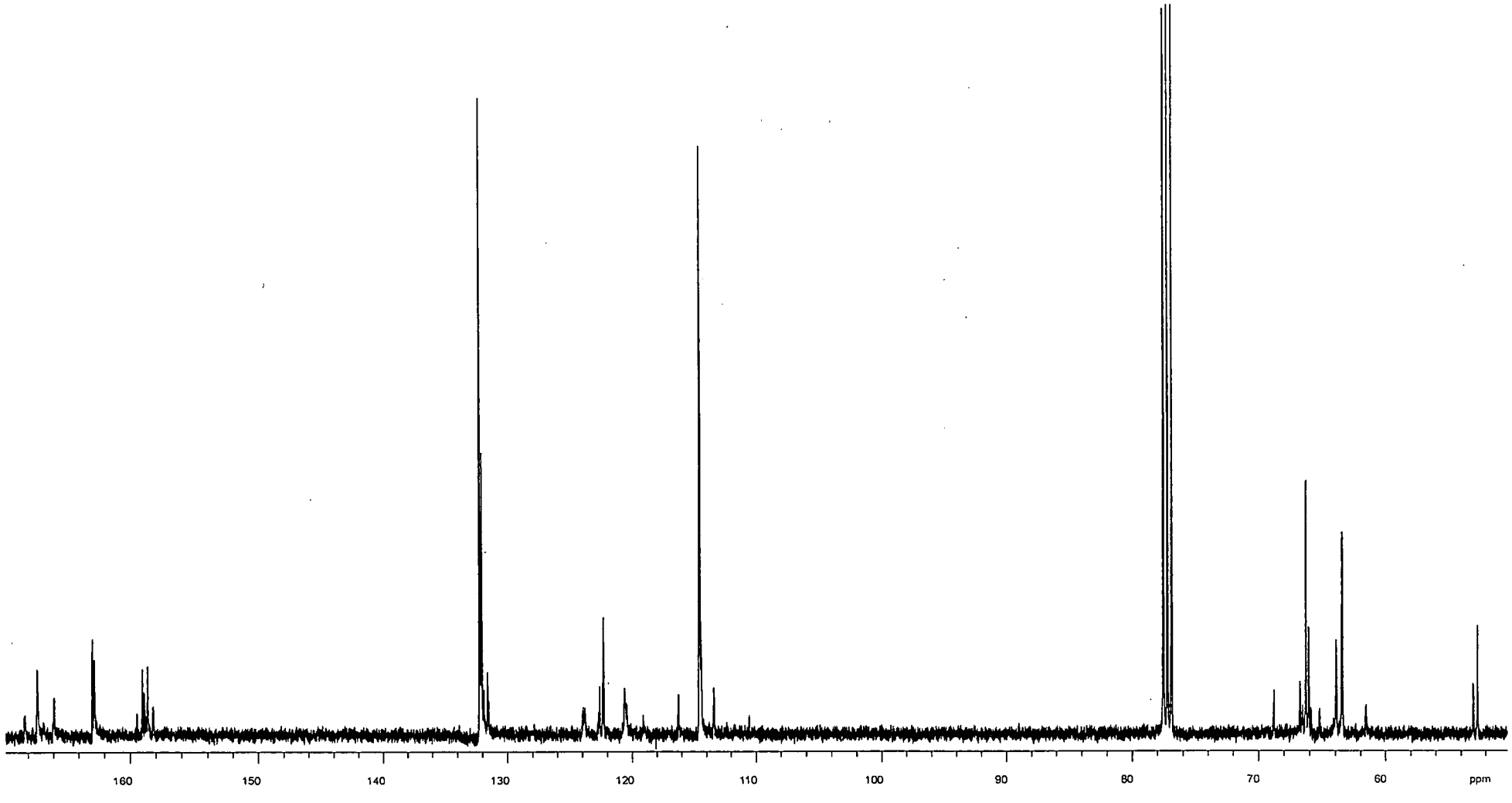

B08-4

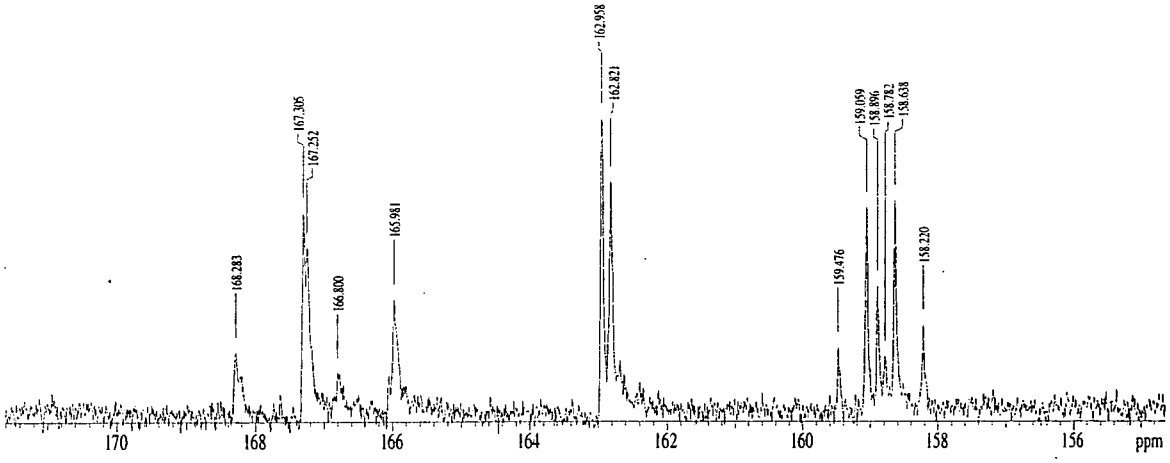
162.958
162.821
167.306
167.252
159.059
158.896
158.782
158.638
168.283
165.981
166.800
159.476
158.220
170
168
166
164
162
160
158
156
ppm

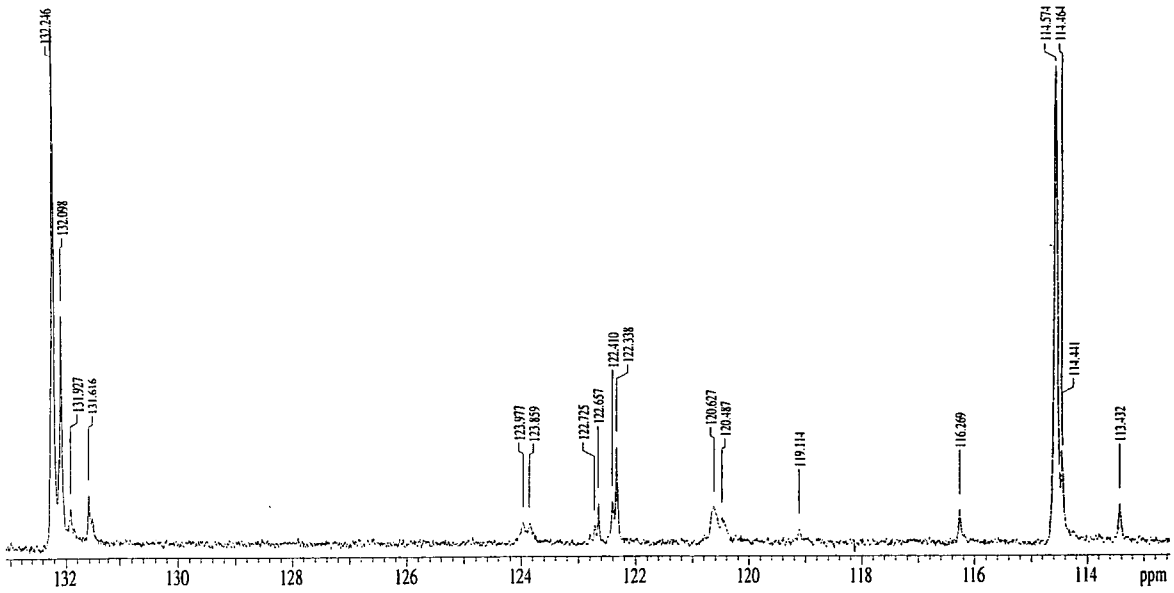
137.246
132.098
131.927
131.616
123.977
123.859
122.725
122.657
122.410
122.338
120.627
120.487
119.114
116.269
114.574
114.464
114.441
113.432
132
130
128
126
124
122
120
118
116
114
ppm

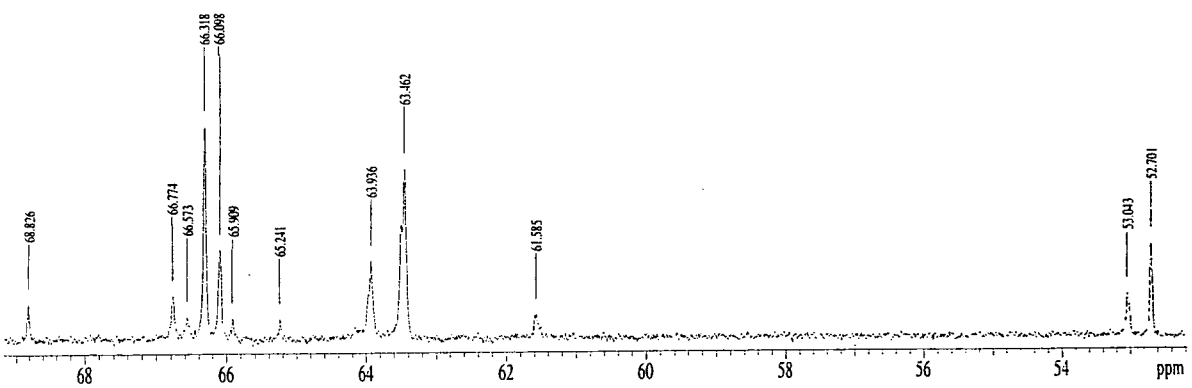
66.318
66.098
63.462
66.774
66.573
65.909
63.936
65.241
61.585
68.826
53.043
52.701
68
66
64
62
60
58
56
54
ppm

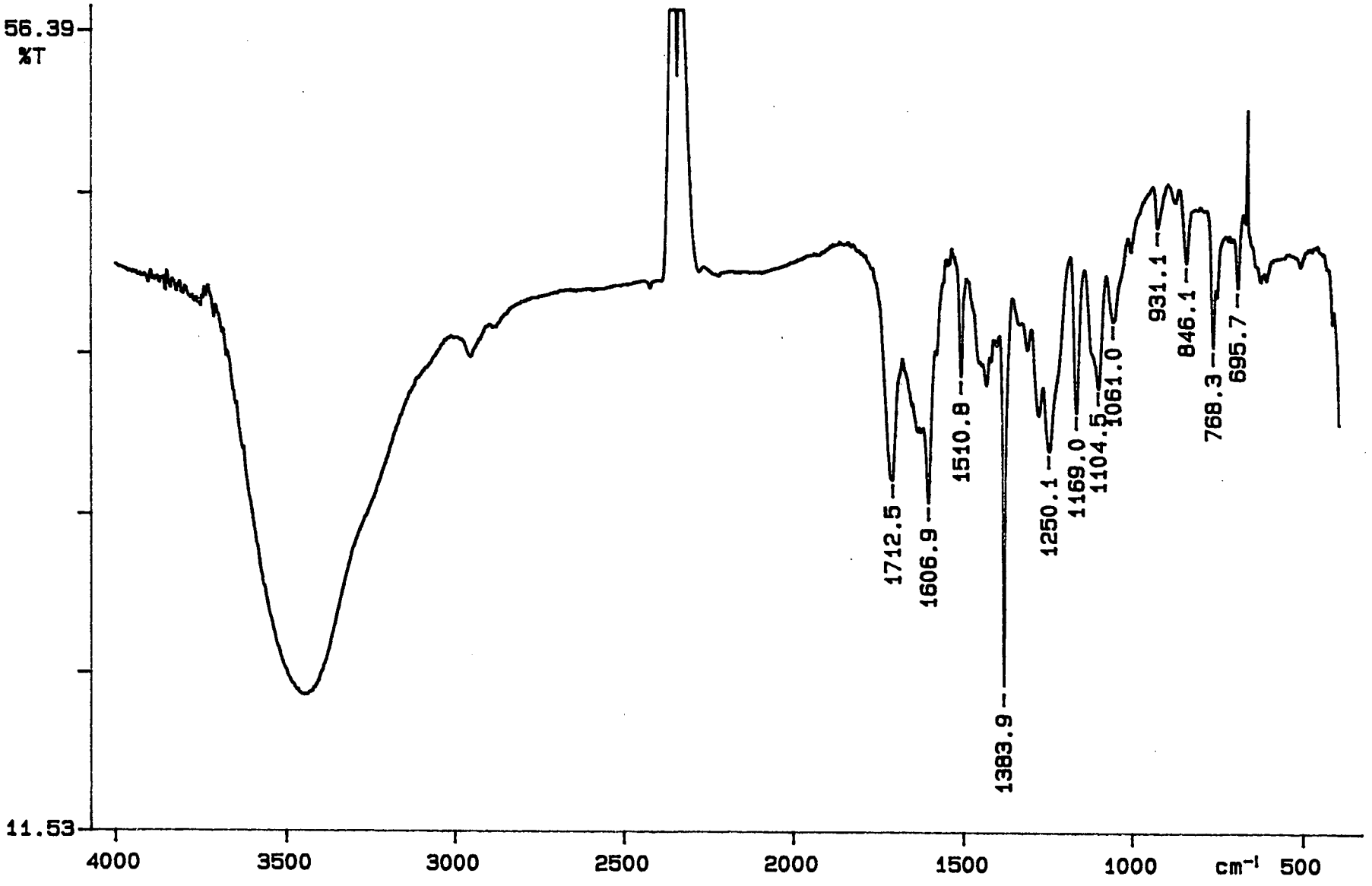

98/09/02 15:25
X: 16 scans, 4.0cm-1, flat

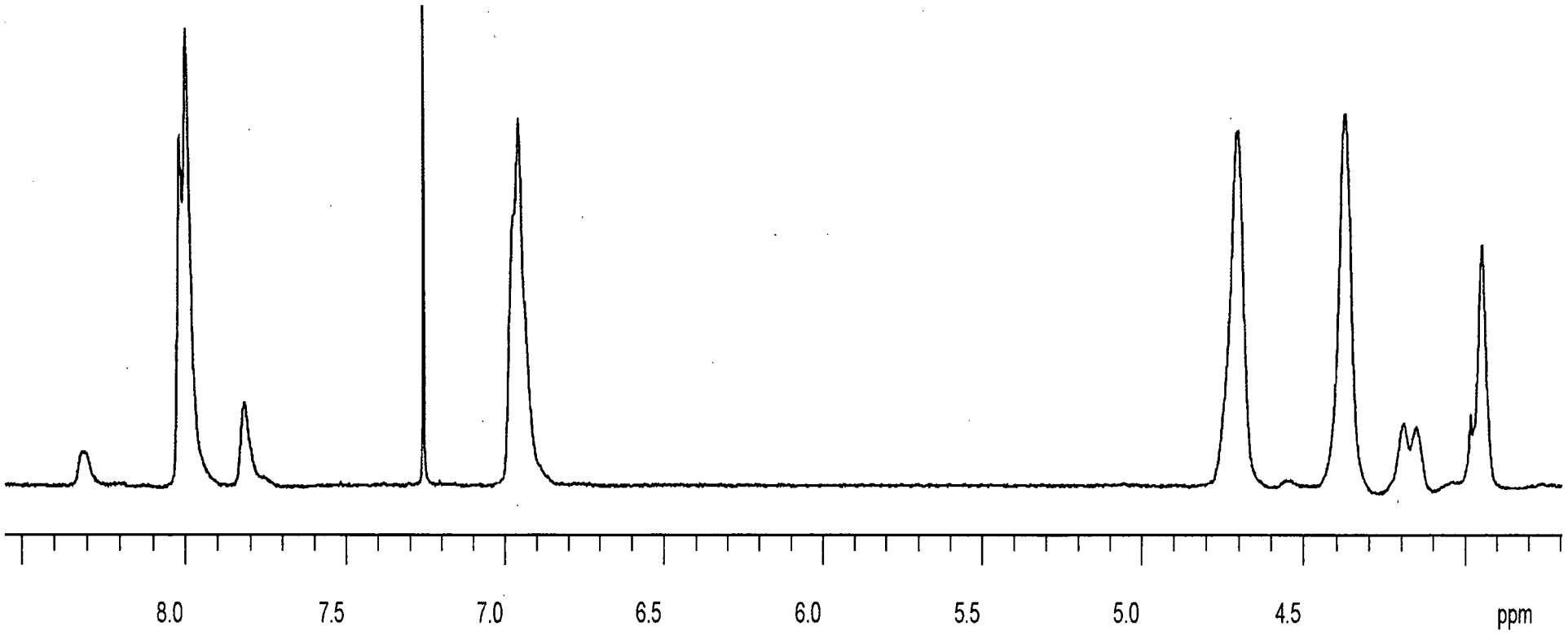

B09-2

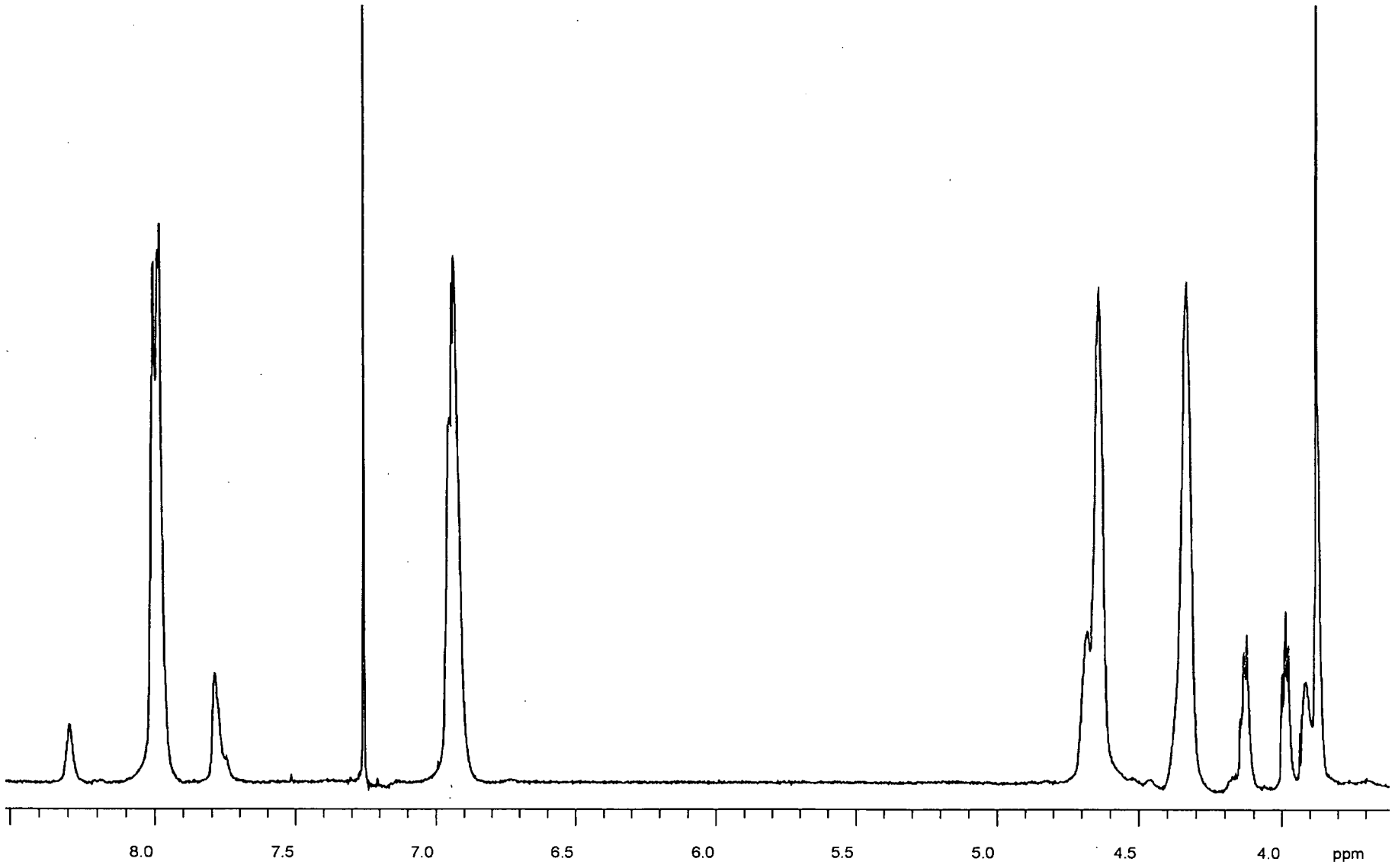

B09-3

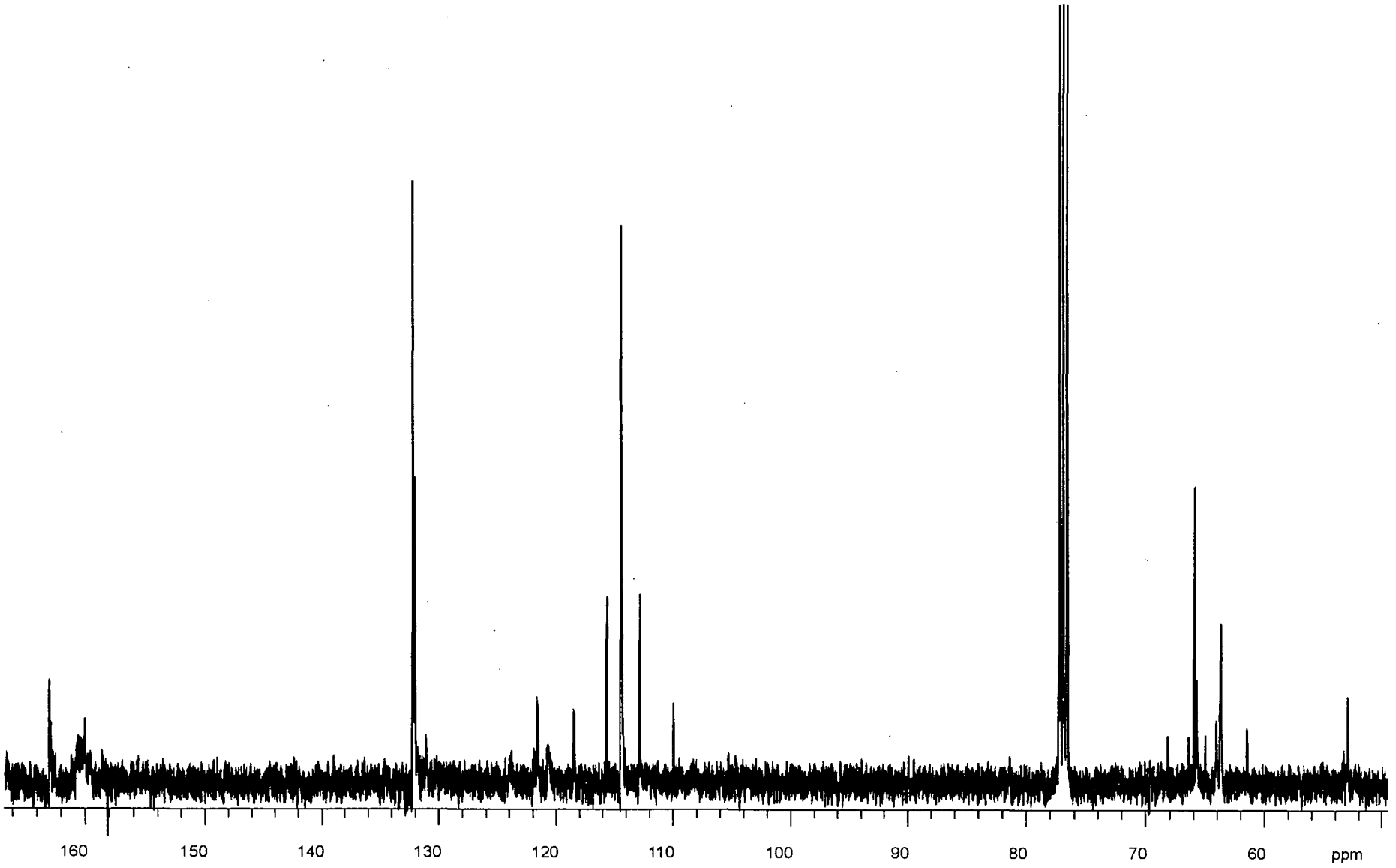

B09-4

B09-4

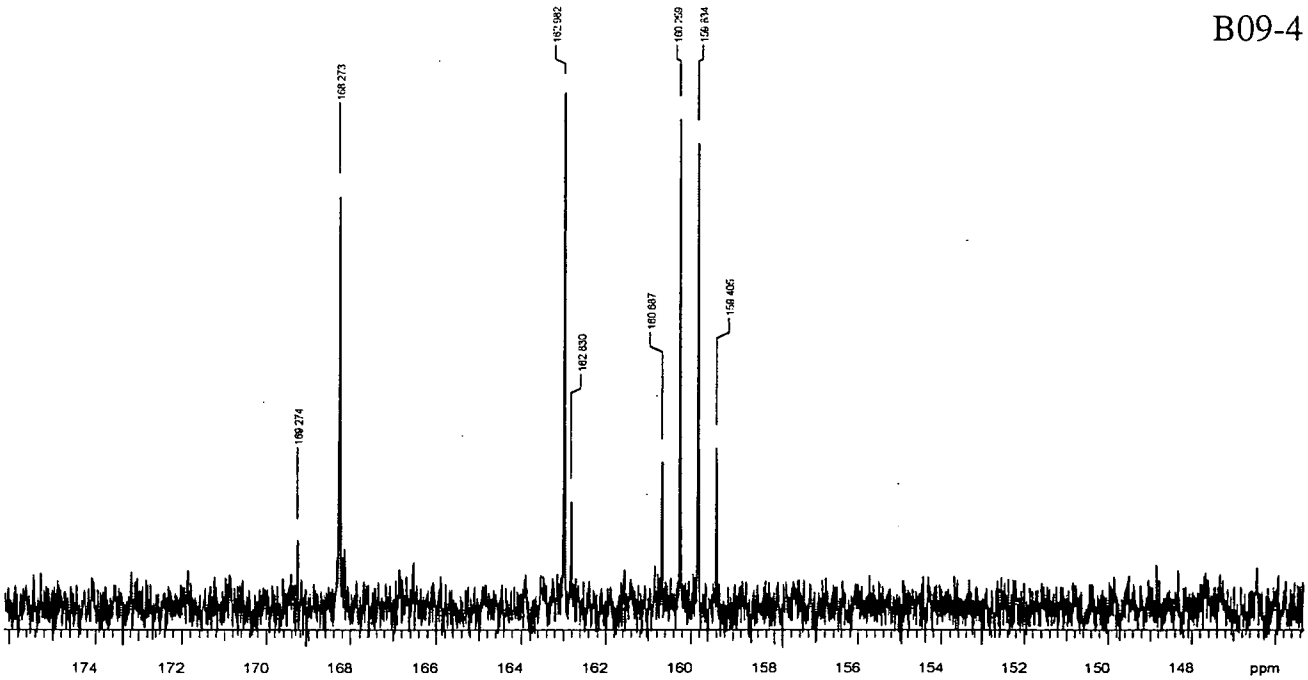
169.274
168.273
162.982
162.830
160.687
160.759
156.634
156.405
174
172
170
168
166
164
162
160
158
156
154
152
150
148
ppm

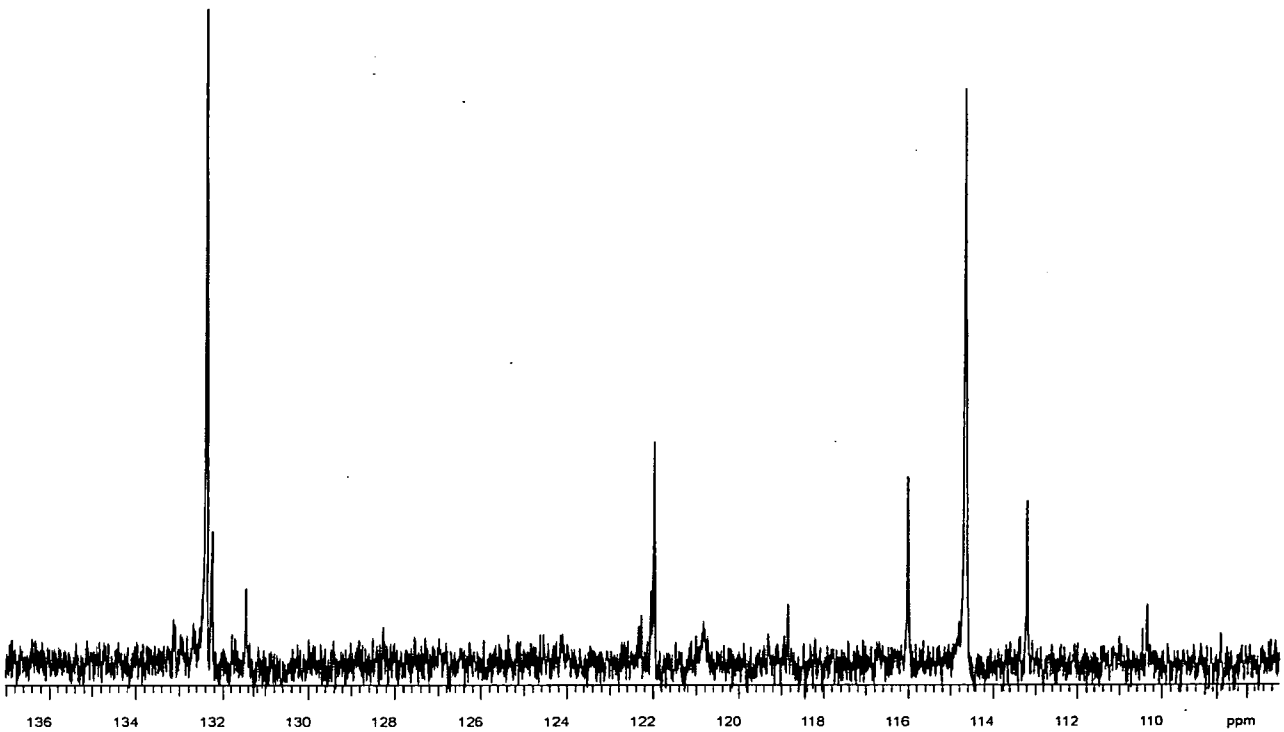
136
134
132
130
128
126
124
122
120
118
116
114
112
110
ppm

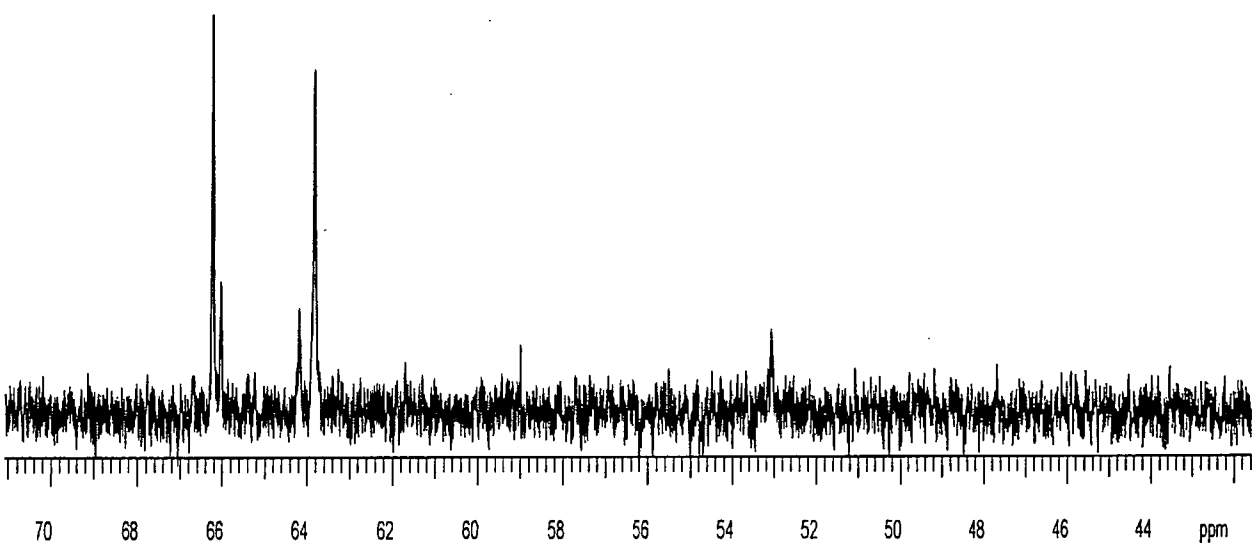
70
68
66
64
62
60
58
56
54
52
50
48
46
44
ppm

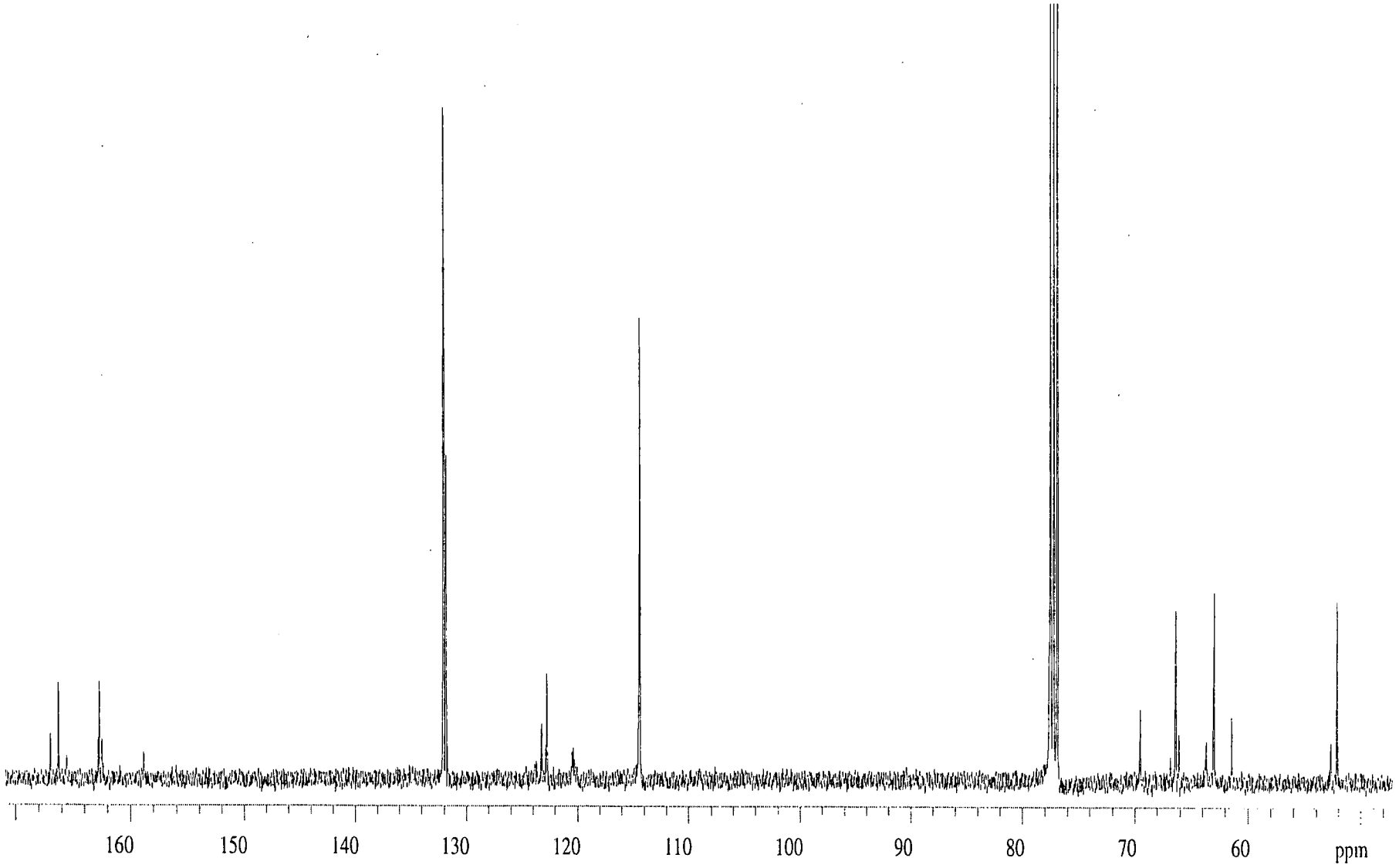

B09-5

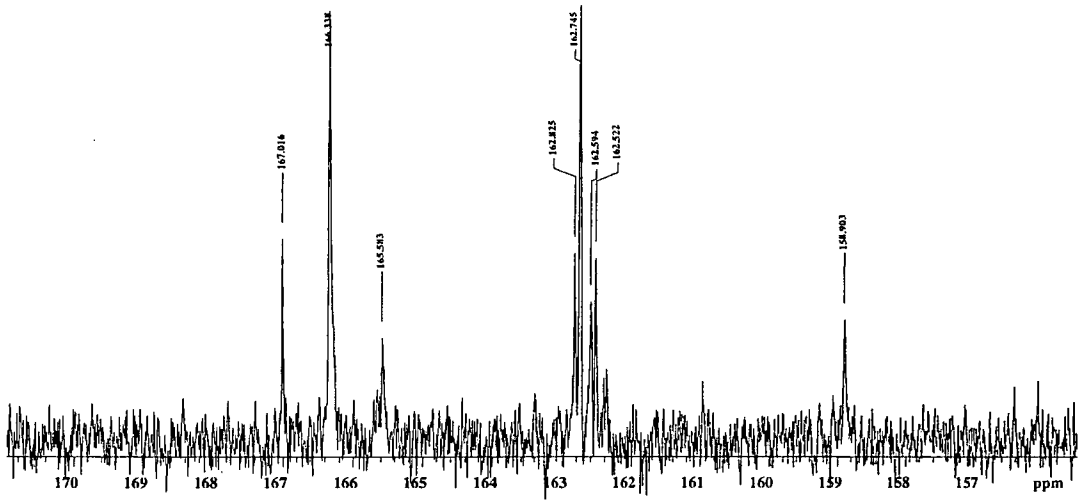
167.016
164.338
165.583
162.835
162.745
162.594
162.522
158.903
170
169
168
167
166
165
164
163
162
161
160
159
158
157
ppm

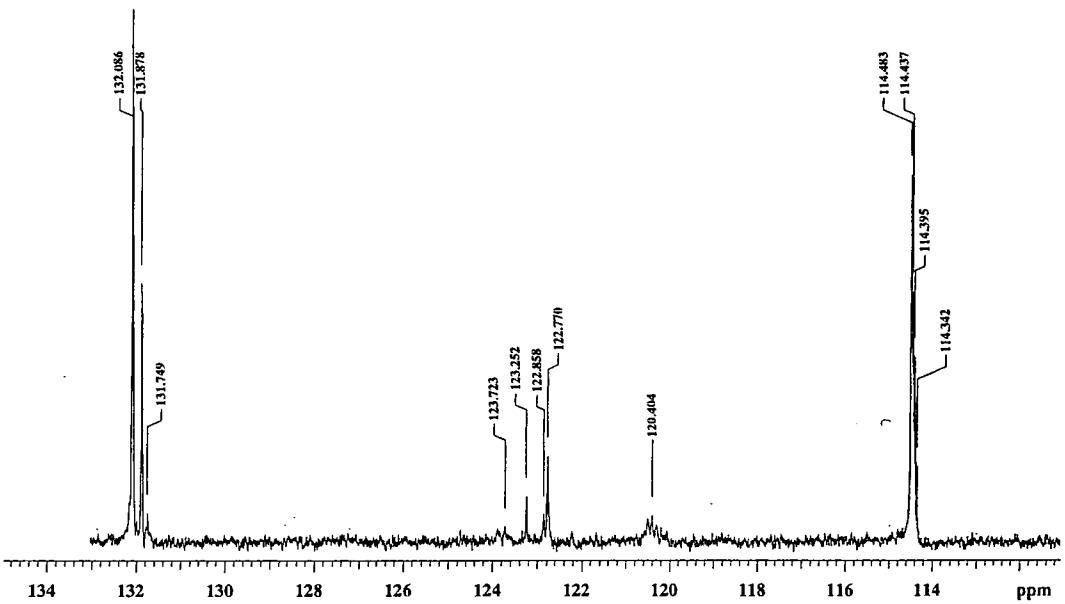
132.086
131.878
131.749
123.723
123.252
122.858
122.770
120.404
114.483
114.437
114.395
114.342
134
132
130
128
126
124
122
120
118
116
114
ppm

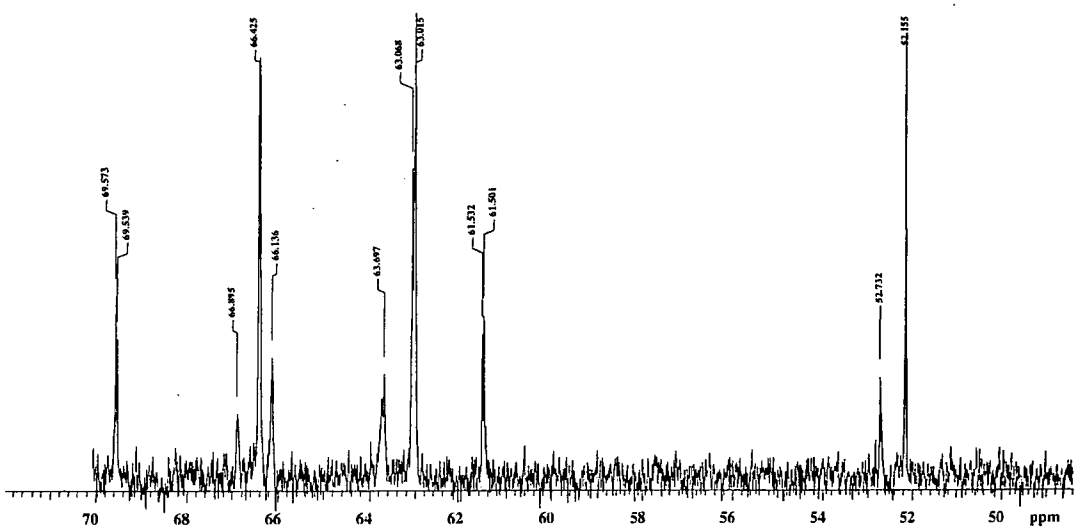
69.573
69.539
66.895
66.425
66.136
63.697
63.068
63.015
61.532
61.501
52.732
52.155
70
68
66
64
62
60
58
56
54
52
50
ppm

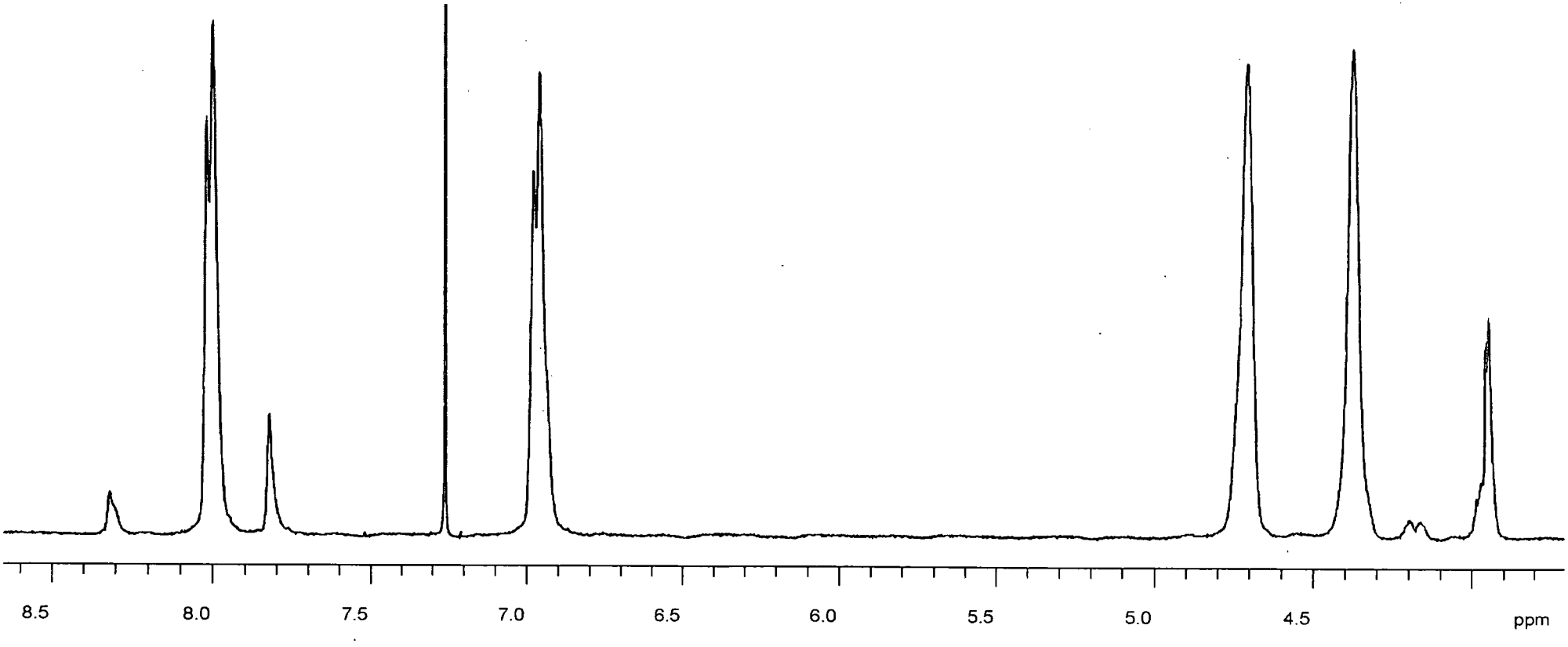

B09-b-2

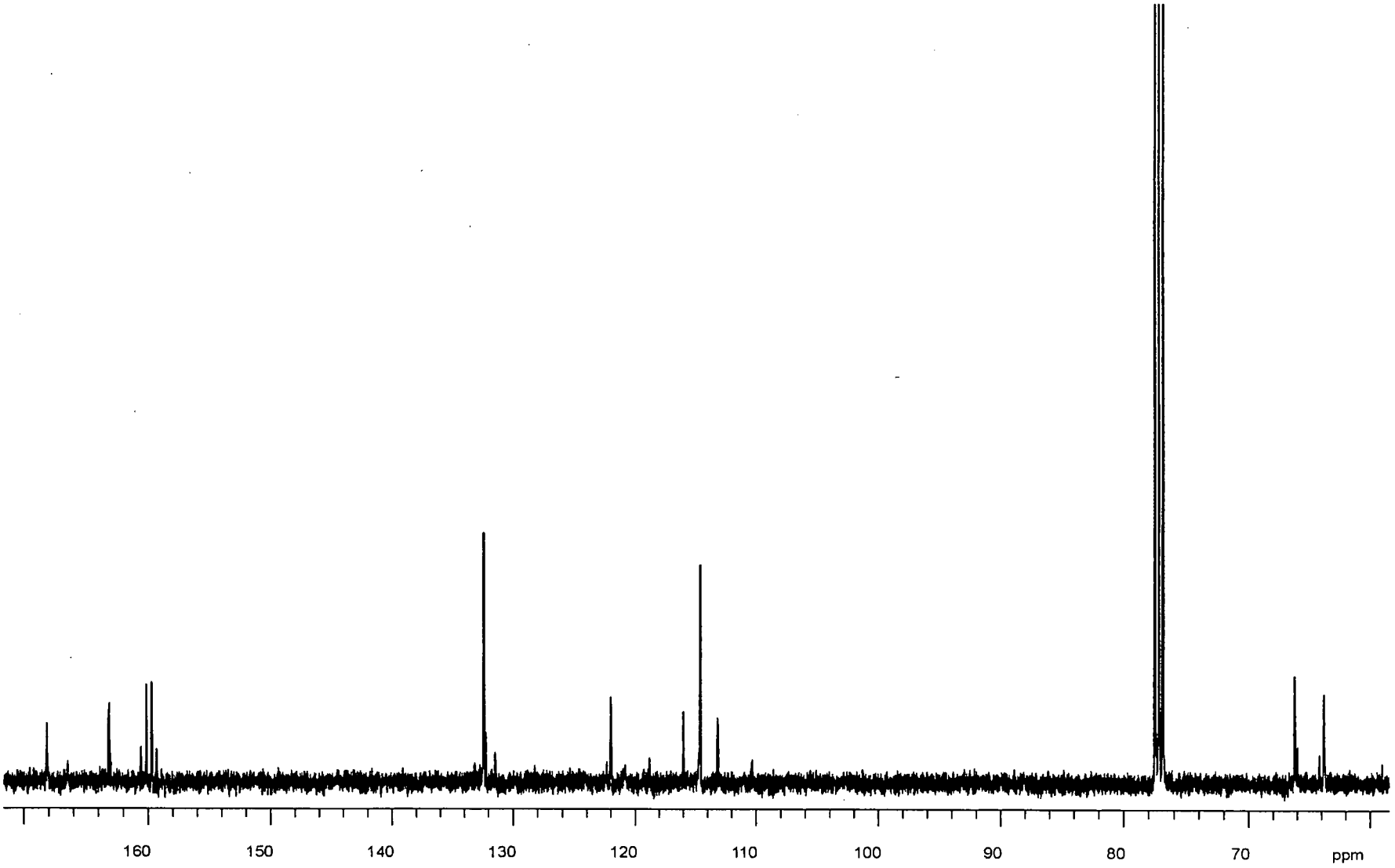

B09-b-4

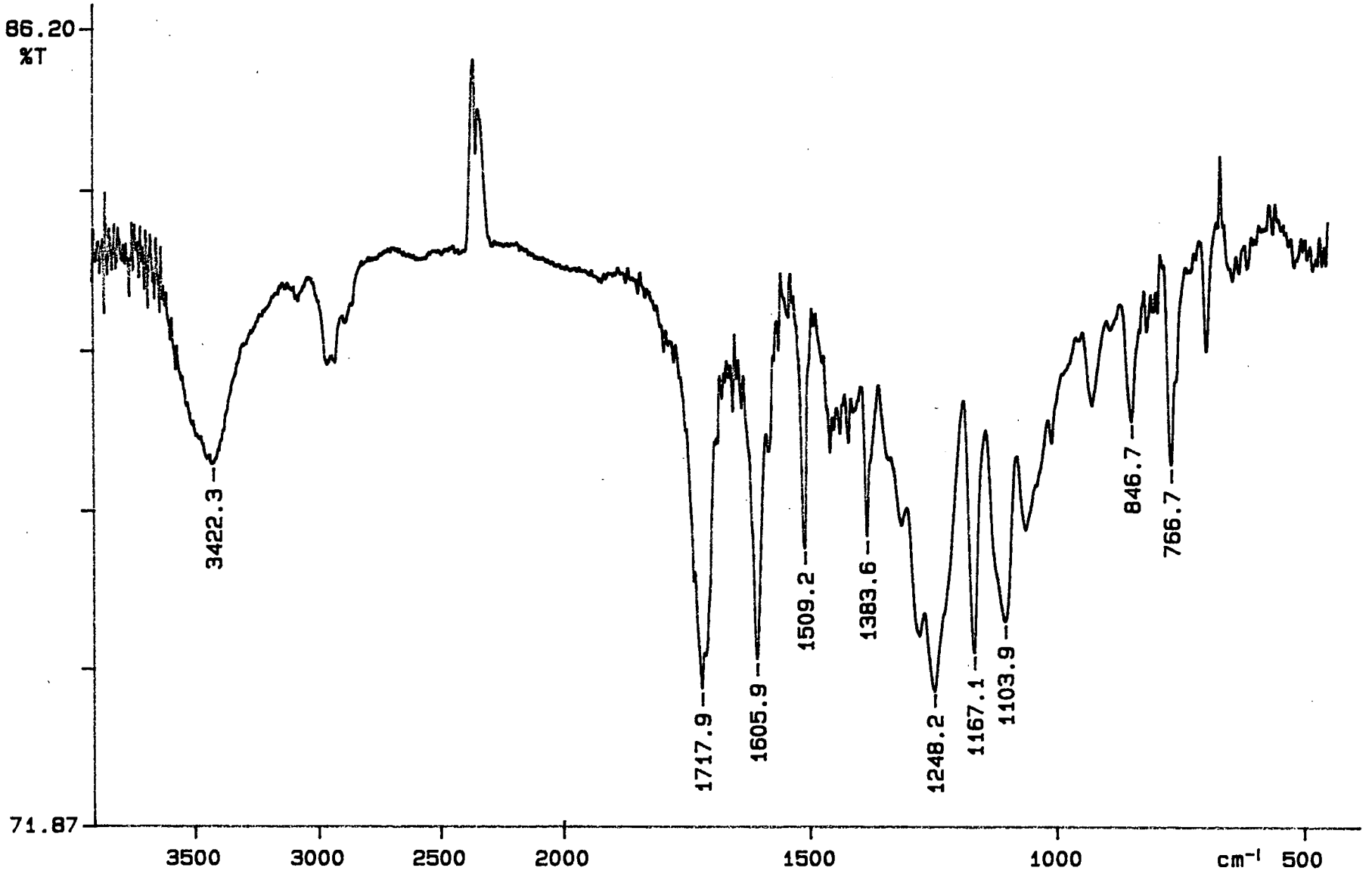

97/12/04 16:05 s-373
X: 16 scans, 4.0cm-1, flat

B10-1

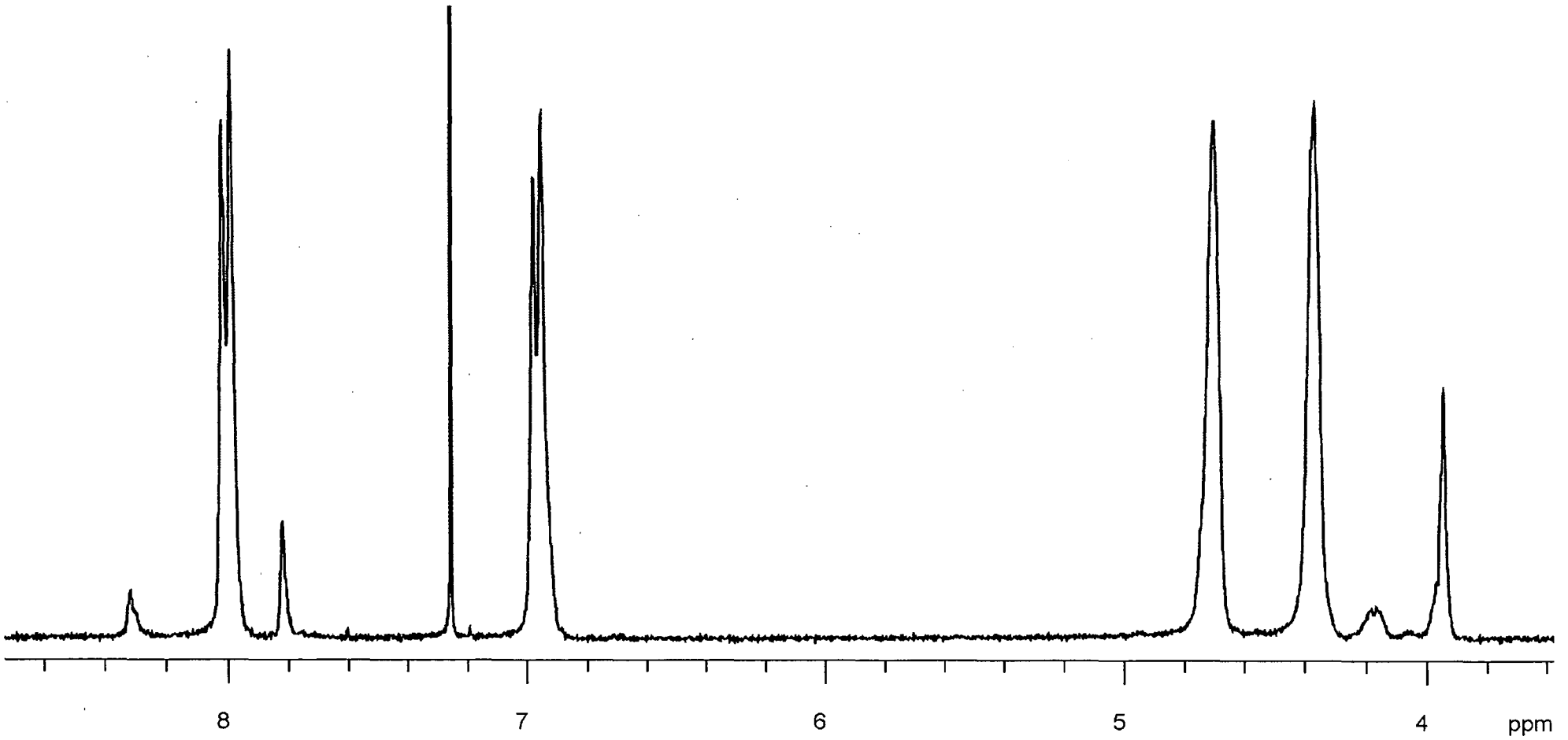

B10-2

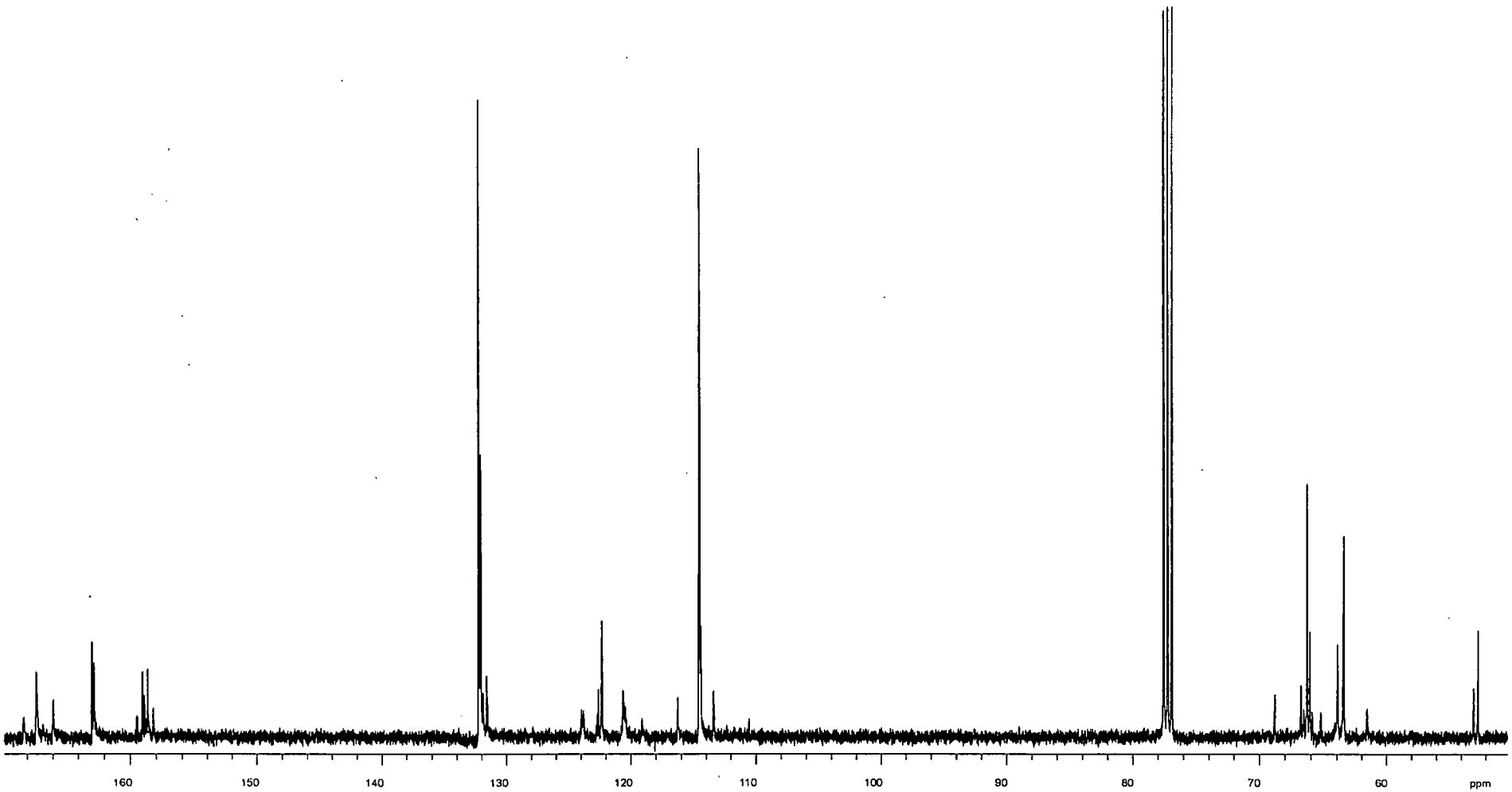

B10-4

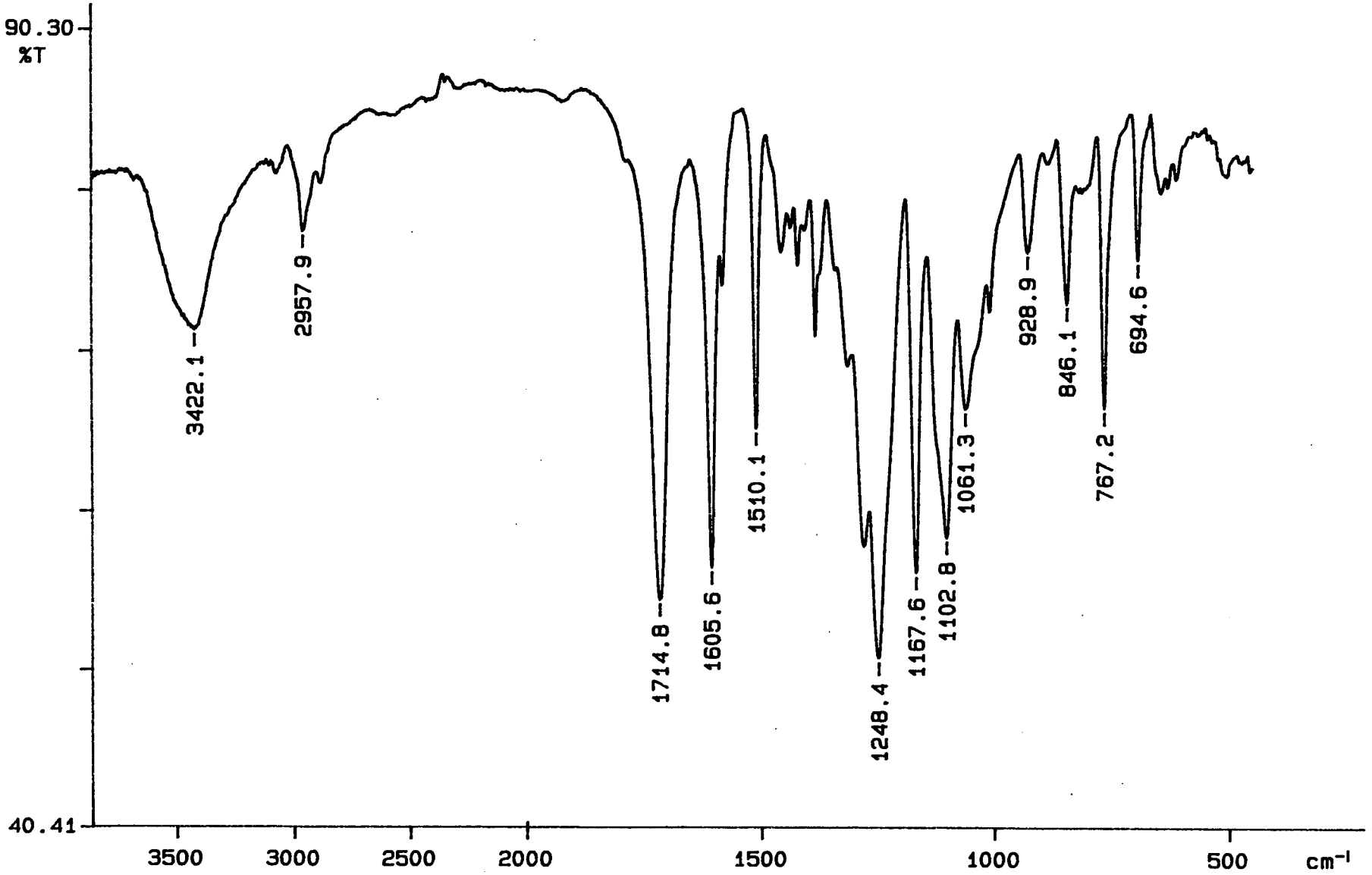

97/11/28 13:48 s-373
Y: 16 scans, 4.0cm-1

B11-1

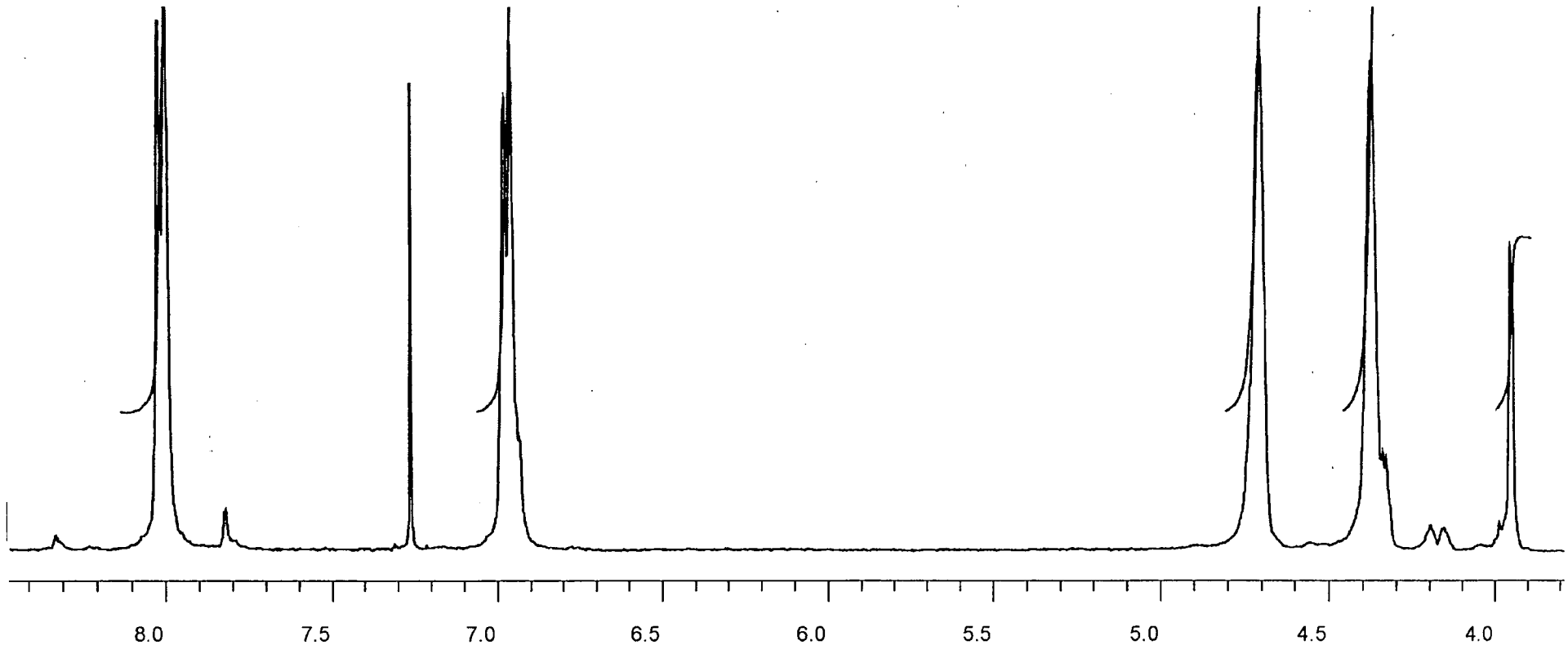

B11-2

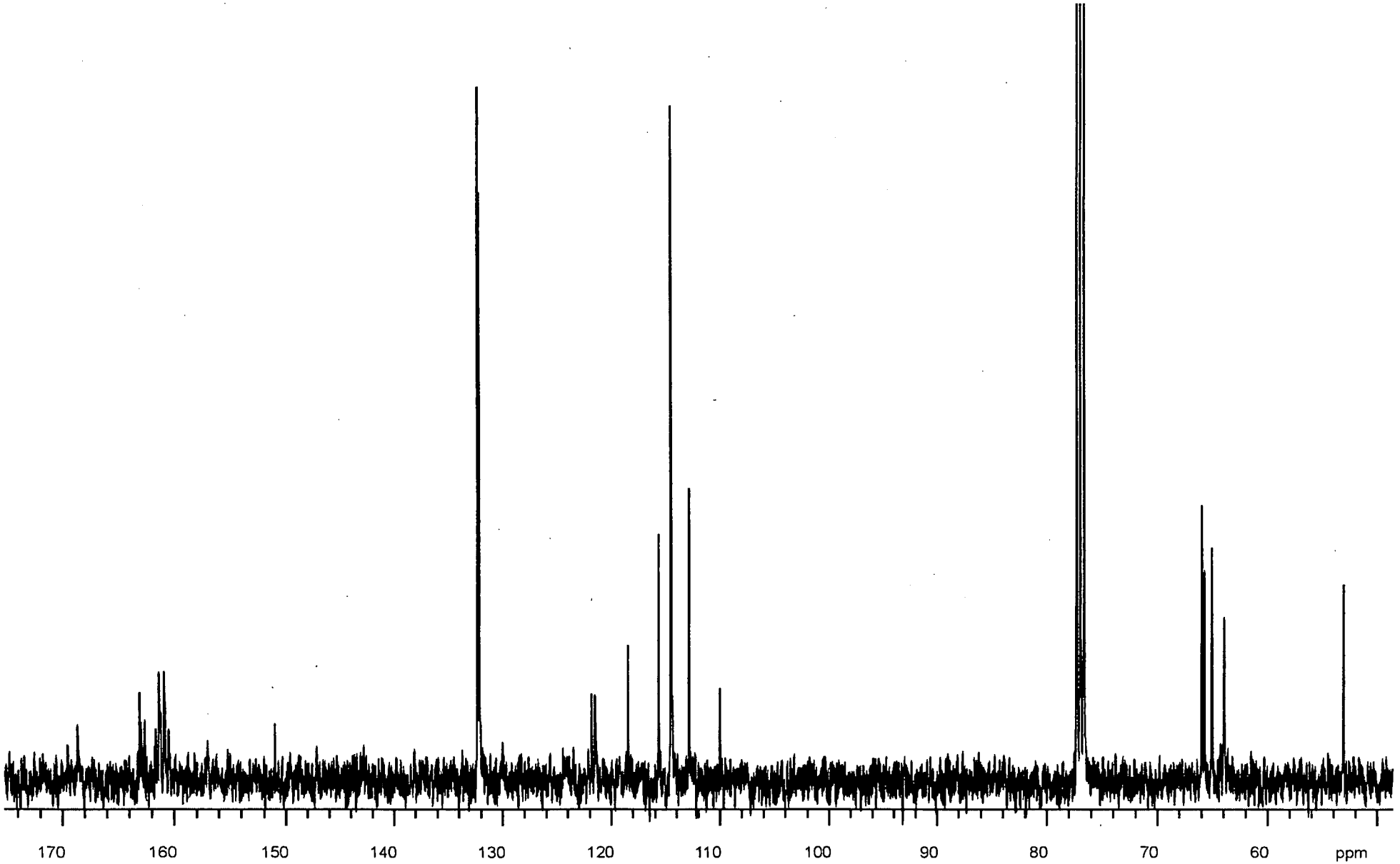

B11-4

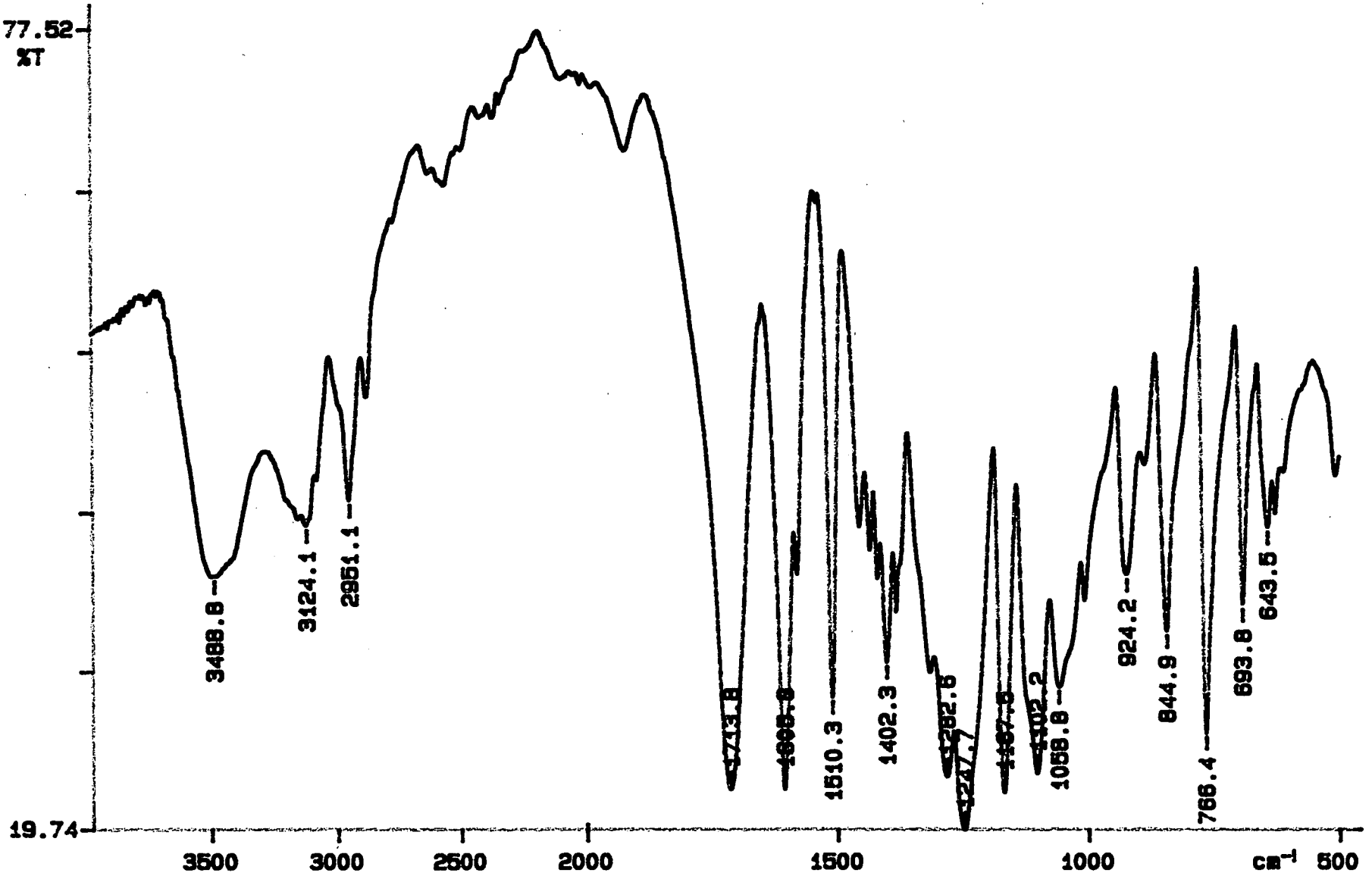

99/05/31 15: 47 s-373
Z: 16 scans, 4.0cm-1

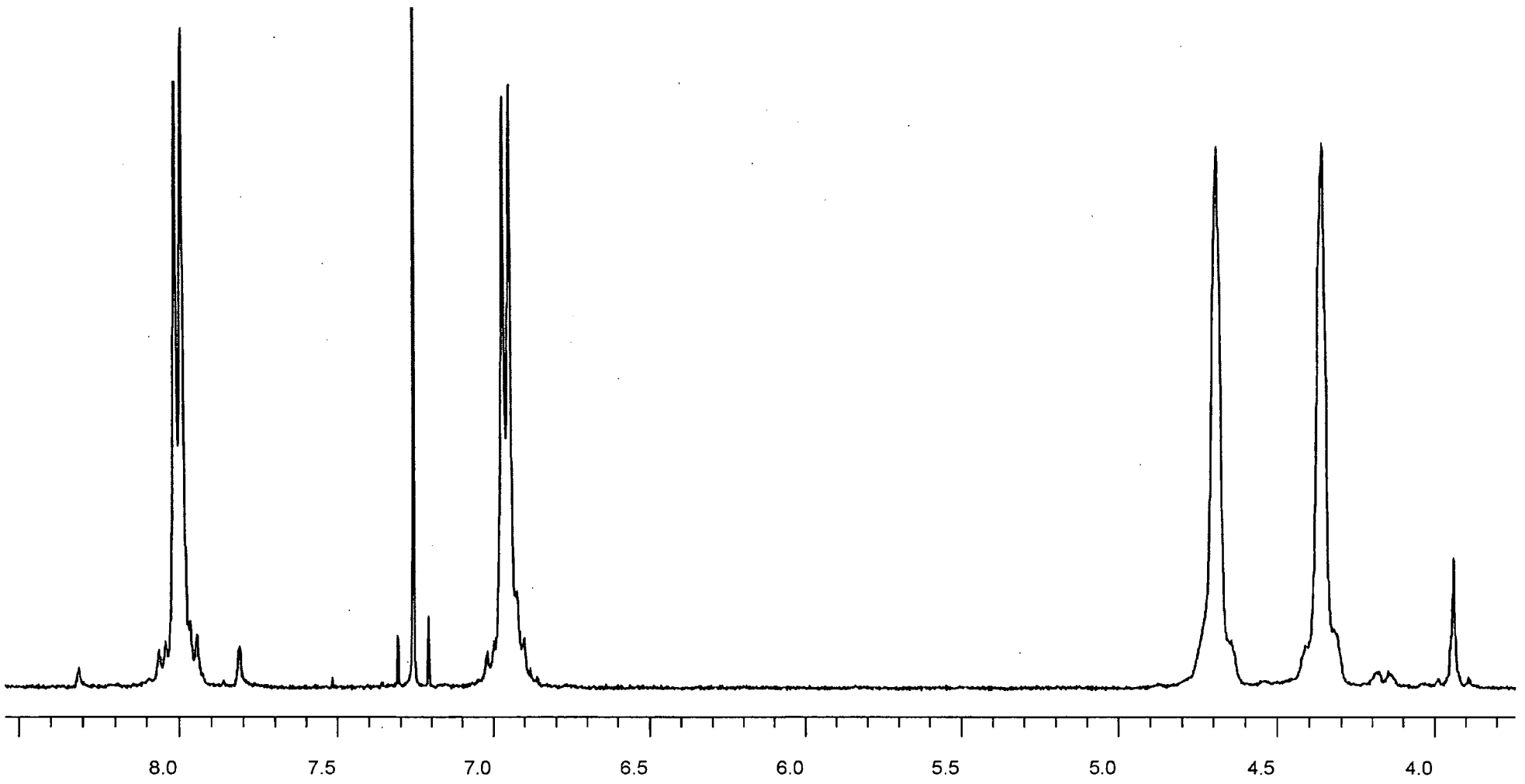

B12-2

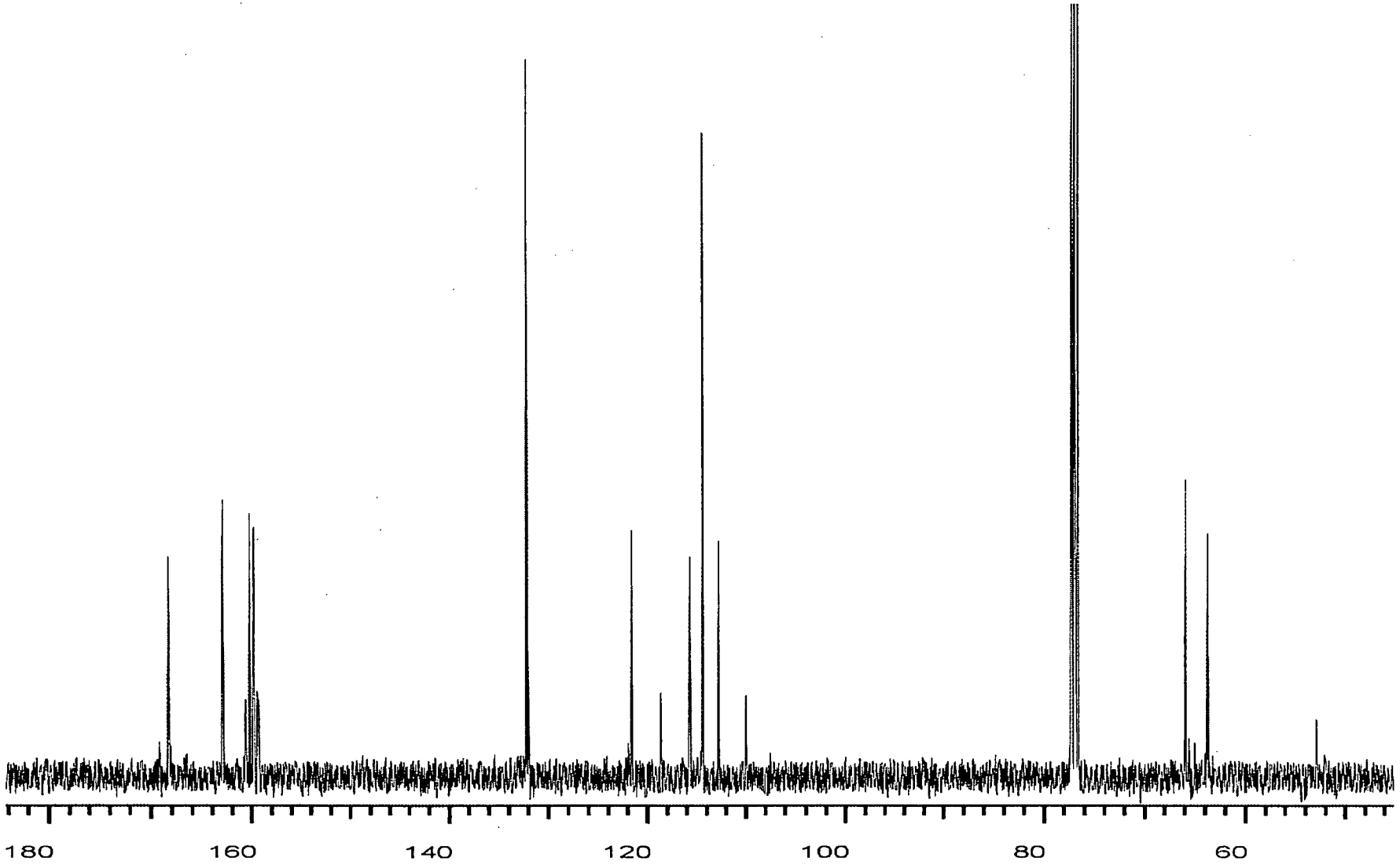

B12-4

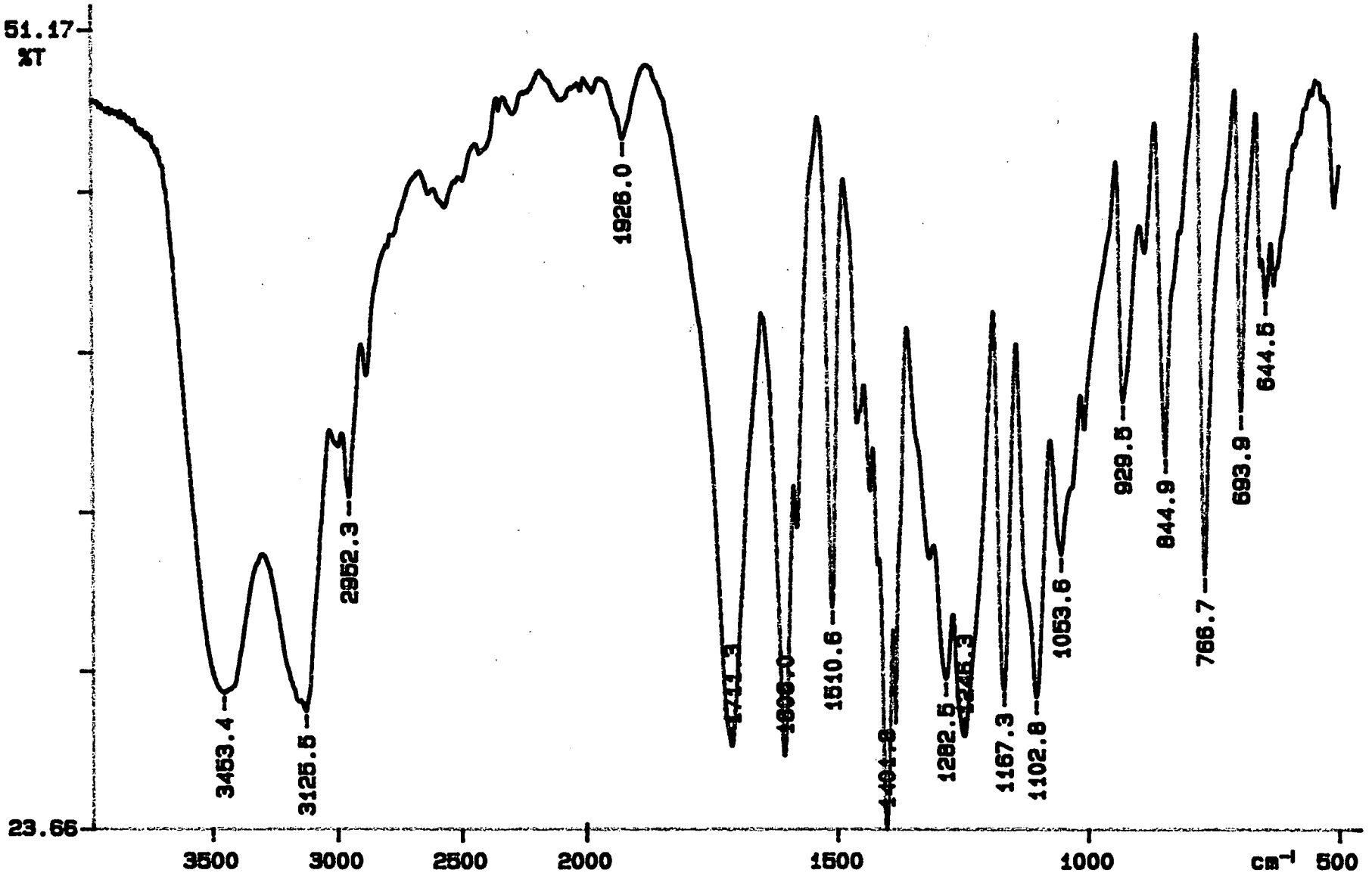

99/05/31 16:01 s-373
X: 16 scans, 4.0cm-1, flat

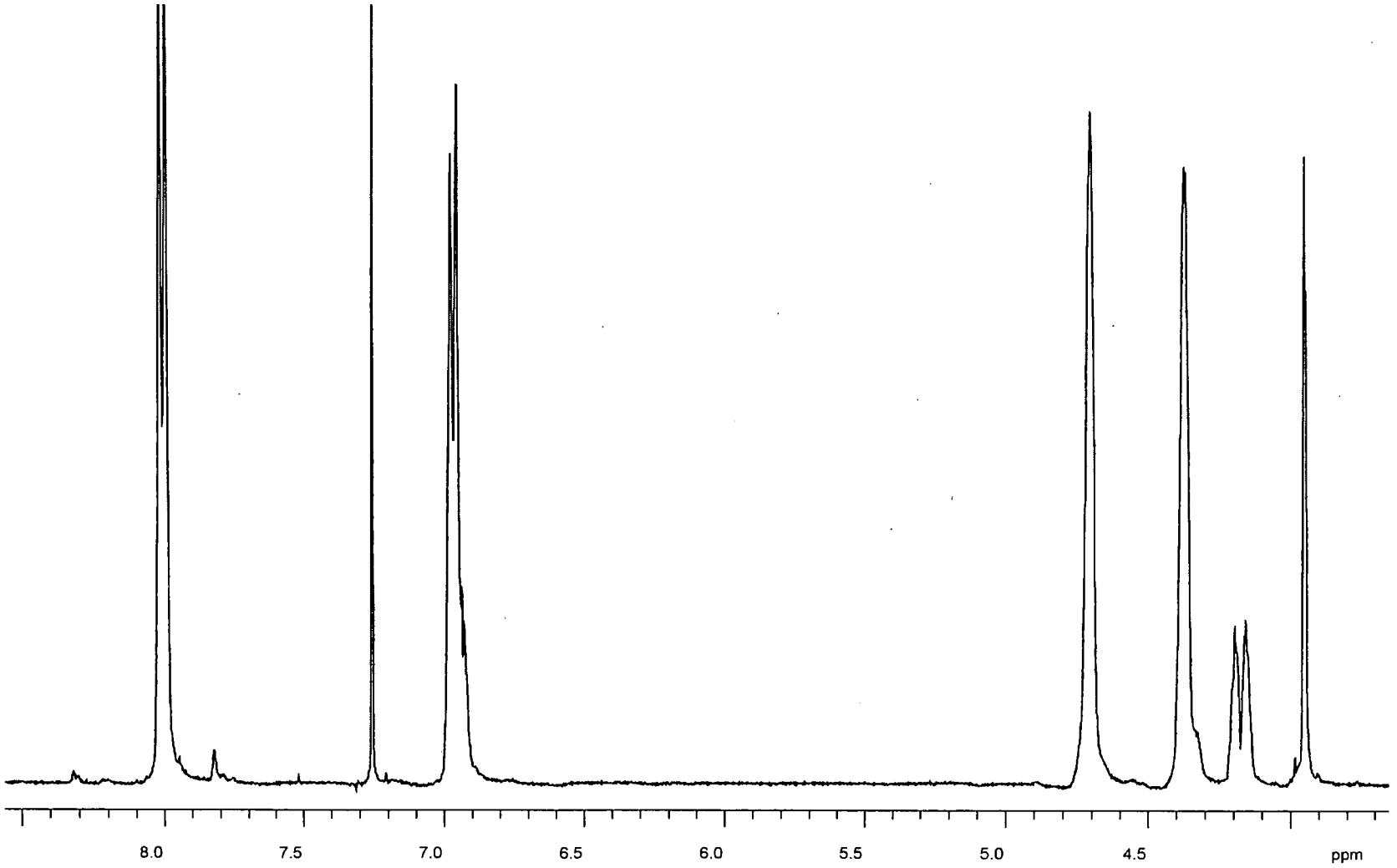

B13-2

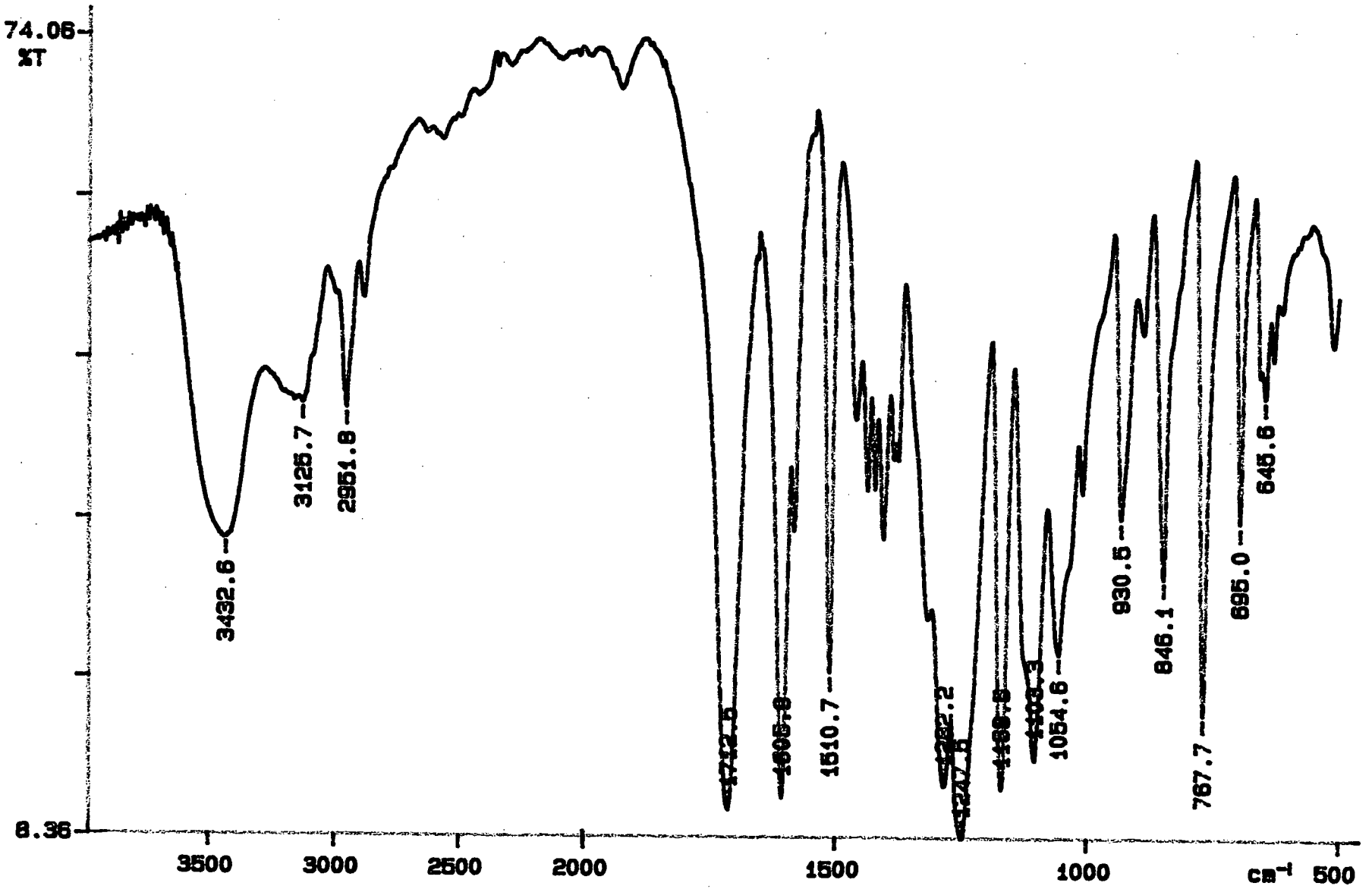

B14-1

99/05/31 16:33 s-373
Y: 16 scans, 4.0cm-1

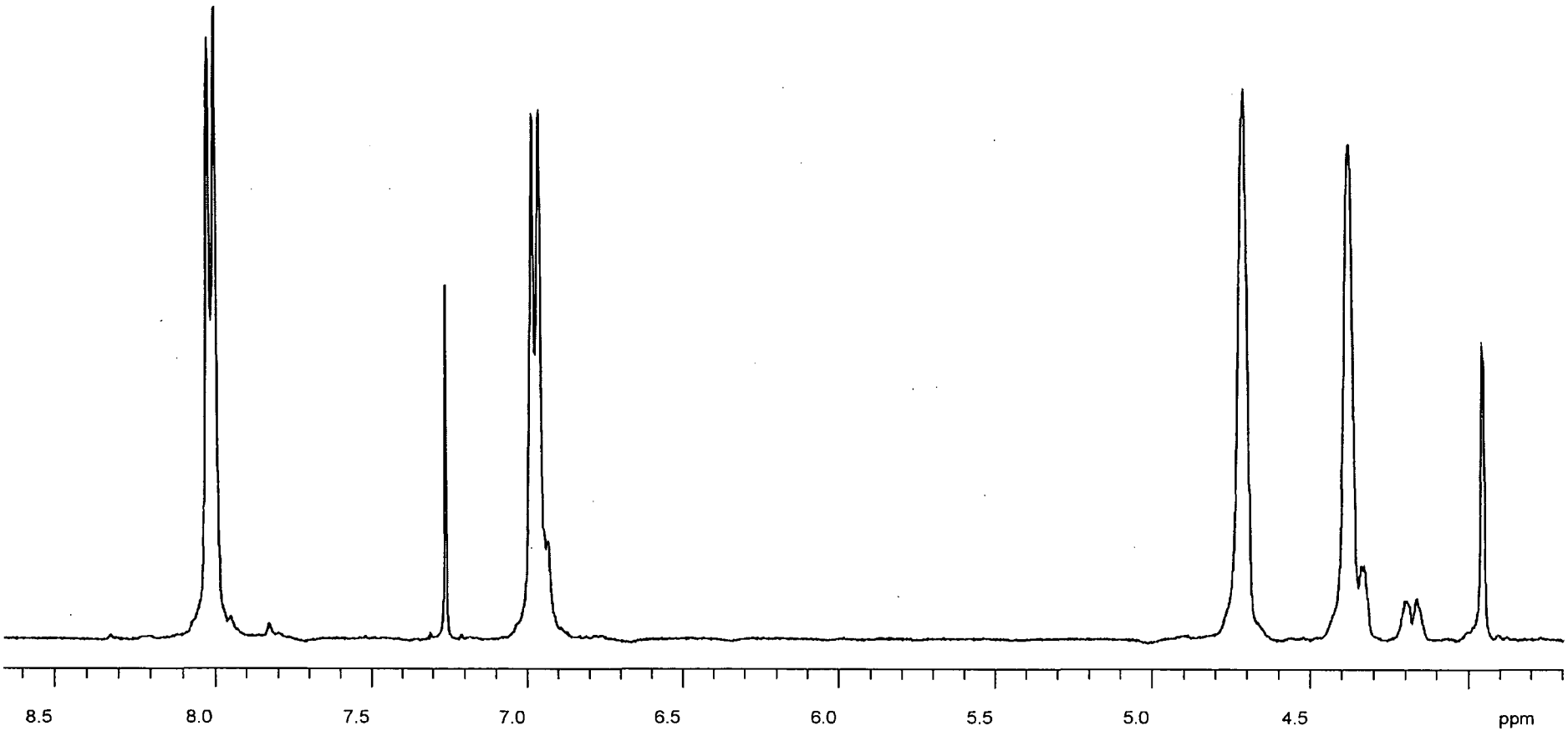

B14-2

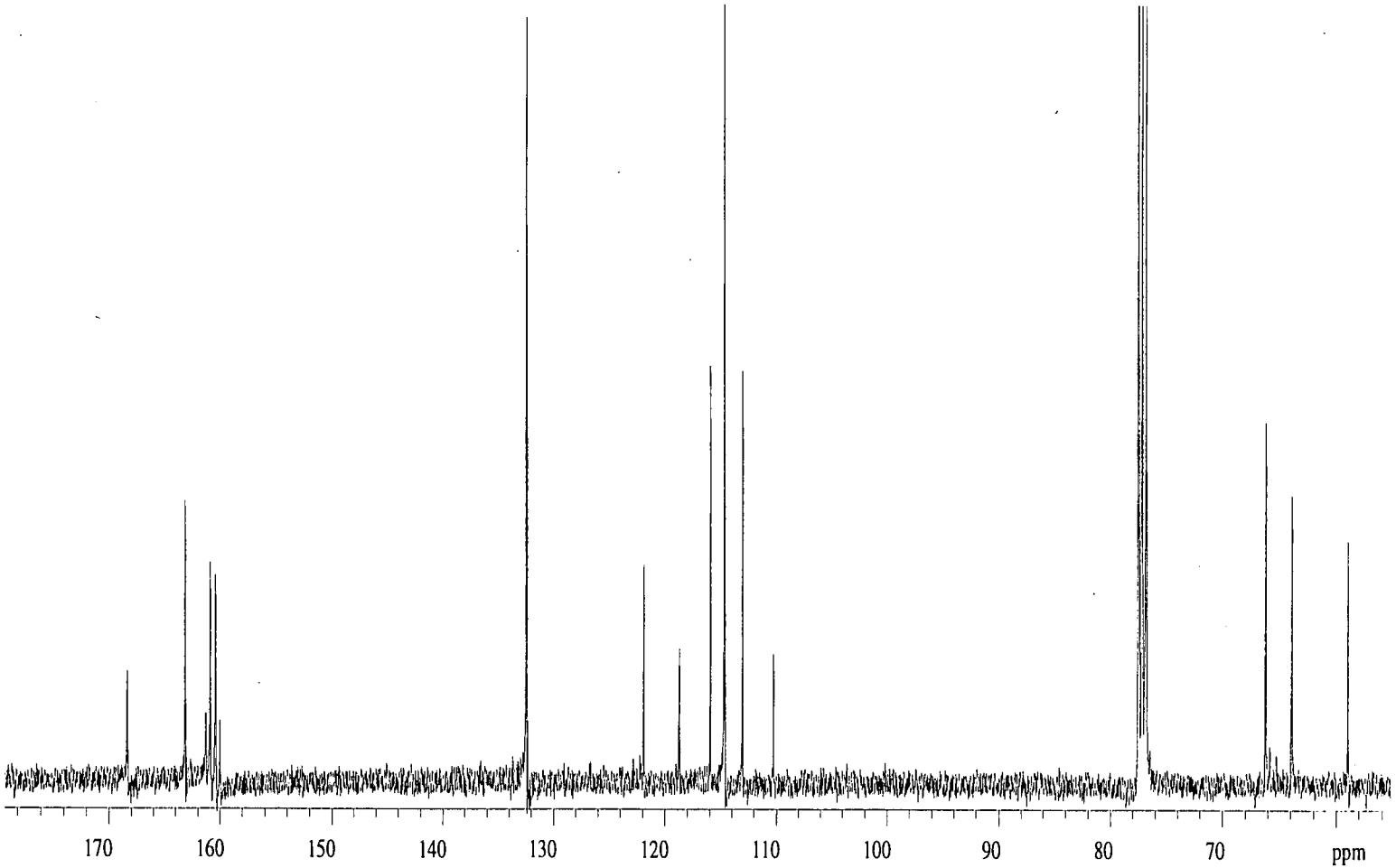

B14-4

APPENDIX (C)

Statistical Analysis

Linear Regression Analysis

Linear regression analysis has been used to calculate the statistics for all best-fit lines of the type y=mx+c. The least squares method of analysis is described as follows.

The slope **m**:

$$m = [n(\Sigma xy) - (\Sigma x).(\Sigma y)] / [n(\Sigma x^2) - (\Sigma x)^2] \quad \text{Eq. C.1}$$

where n is the population (number of data points), x is the x-value, y is the y-value

The intercept **c**:

$$c = [n(\Sigma y).(\Sigma x^2) - (\Sigma x).(\Sigma xy)] / [n(\Sigma x^2) - (\Sigma x)^2] \quad \text{Eq. C.2}$$

The Pearson product moment correlation coefficient **R**:

$$R = [n(\Sigma xy) - (\Sigma x).(\Sigma y)] / \{[n(\Sigma x^2) - (\Sigma x)^2].[n(\Sigma y^2) - (\Sigma y)^2]\}^{1/2} \quad \text{Eq. C.3}$$

The square of the Pearson product (R^2), or the coefficient of determination, compares estimated and actual data to produce a value of between 0 and 1. The closer this value is to 1 the more accurate is the fit.

Standard Deviation (s)

The standard deviation, **s**, is used to measure how significantly values deviate from their mean average. The calculation used throughout this thesis is based on the non-biased (n-1) method and assumes that the data is a sample of a larger population.

$$s = \{[n\Sigma x^2 - (\Sigma x)^2] / n(n-1)\}^{1/2} \quad \text{Eq. C.4}$$

where n is the population (number of data points), x is the x-value, y is the y-value

APPENDIX (D)

Conferences/Courses Attended

1997:

Macro Group Young Researchers Meeting, Queens Hotel, Leeds, 2-4 April.

IRC Industrial Club Meeting, Royal Armouries, Leeds, 17-19 September.

1998:

IRC courses in Polymer Physics & Engineering, Universities of Bradford & Leeds, 6-9 January.

Macro Group Young Researchers Meeting, University of Durham, 6-9 April.

37th IUPAC (Macromolecular Division), Gold Coast, Australia, 12-17 July.

Research Councils' Graduate School Programme, Brighton, 12-17 November.